Time-Resolved Measurements of Sugar-Binding-Induced Conformational Changes in the Melibiose Permease from *Escherichia Coli*

Co-tutelle de thèse

Dissertation	Présentée pour obtenir
zur Erlangung des Doktorgrades	le titre de Docteur
der Naturwissenschaften	en Sciences de la Vie
vorgelegt im Fachbereich	Université de Nice Sophia-Antipolis
Chemische und pharmazeutische Wissenschaften	École Doctorale des Sciences
der Johann Wolfgang Goethe-Universität	de la Vie et de la Santé
in Frankfurt am Main	
von	par
Kerstin Meyer-Lipp	Kerstin Meyer-Lipp
aus Hamburg	
Frankfurt am Main	Nice
Germany	France
2005	2005
(DF1)	

vom Fachbereich Chemische und
pharmazeutische Wissenschaften der
Johann Wolfgang Goethe-Universität als
Dissertation angenommen.

Dekan: Prof. Dr. Harald Schwalbe
Gutachter: Prof. Dr. Ernst Bamberg
            Dr. Gérard Leblanc

Datum der Disputation: 11. November 2005

soutenue le 11. Novembre 2005 devant le jury
composé de:
Professeur Dr. Ernst Bamberg, Rapporteur
Docteur Gérard Leblanc, Rapporteur
Professeur Dr. Laurent Counillon, Examinateur
Professeur Dr. Bernd Ludwig, Examinateur

Nothing in life is to be feared,

it is only to be understood.

Marie Curie

Für Jonas und Peter

Table of Contents

Table of Figures

Table of Tables

Abbreviations

A	acceptor
ATP	adenosine-triphosphate
biotin maleimide	3-(N-maleimidylpropionyl)biocytin
BLM	black lipid membranes
BSA	bovine serum albumin
C-less permease	permease devoid of all intrinsic cysteines
D	donor
dATP	2'-deoxyadenosine-triphosphate
dCTP	2'-deoxycytidine-triphosphate
DDM	n-dodecyl-β-D-maltoside
dGTP	2'-deoxyguanosine-5'-triphosphate
DMSO	dimethyl sulfoxide
Dns^2-S-Gal	2'-(N-dansyl) aminoethyl-1-thio-β-D-galactopyranoside
DTT	1,4-dithio-threitol
dTTP	2'-deoxythymidine-5'-triphosphate
EAAC	excitatory amino acid carrier
Eff	efflux
FRET	fluorescence resonance energy transfer
FTIR	fourier transform infrared spectroscopy
GalP	galactose/H^+ co-transporter
GAT	γ-aminobutyric acid-transporter
Glc	glucose
GlpT	glycerol-3-phosphate transporter
GPH	glycoside (or galactoside)-pentoside-hexuronide:cation symporter family
IMV	Inverted membrane vesicle
Inf	influx
ISO	inside- out
$K_{0.5}$	half saturation concentration
K_{Na}	Na^+ activation constant
KPi	potassium phosphate buffer (KH_2PO_4)
LacS	lactose permease of *S. thermophilus*
LacY	lactose permease of *E.coli*
LAPAO	3-(laurylamido)-N,N'-dimethylaminopropylamine oxide
LB	Luria Broth
MelB	melibiose permease

VIII

melibiose	α-D-galactopyranosyl-(1→6)- α-D-glucopyranose
MFS	major facilitator superfamily
MIANS	2-(4'-maleimidylanilino)naphthalene-6- sulfonic acid
MPB	3-(N-maleimidylpropionyl)biocytin
MTS	methanethiosulfonate reagents
MTSEA$^+$	(2-aminoethyl) methanethiosulfonate
MTSES$^-$	(2-sulfonatoethyl) methanethiosulfonate
NEM	*N*-ethyl maleimide
NIS	Na$^+$/I$^-$ co-transporter
NTA	nitrilotriacetic acid
OxlT	oxalate transporter
PAGE	polyacrylamide gel electrophoresis
PC	phosphatidyl choline
pCMBS	p-chloromercuribenzene sulfonate
PCR	polymerase chain reaction
PTS	phosphotransferase systeme
PutP	proline transporter
RSO	right-side-out
SDS	sodium dodecyl sulfate
SE	standard error
SGLT1	Na$^+$/glucose co-transporter
SOB	sodium binding
SSM	solid supported membrane
stilbene disulfonate	4-acetamido-4'-maleimidylstilbene-2,2'-disulfonate
TAE	tris-acetate-EDTA
TBS	tris-buffered saline
ThioGlo®	9-Acetoxy-2-(4-(2,5-dihydro-2,5-dioxo-1H-pyrrol-1-yl)-3-oxo-3-H-naphtho[2,1-b] pyran
TMG	methyl-1-thio-β-galactopyranoside
UV	ultraviolet
VCR	voltage clamp fluorometry
α-NPG	*p*-nitrophenyl- α -D-6-galactopyranoside

Amino acids

A	Ala	alanine		M	Met	methionine
C	Cys	cysteine		N	Asn	asparagine
D	Asp	aspartic acid		P	Pro	proline
E	Glu	glutamic acid		Q	Gln	glutamine
F	Phe	phenylalanine		R	Arg	arginine
G	gly	glycine		S	Ser	serine
H	His	histidine		T	Thr	threonine
I	Ile	isoleucine		V	val	valine
K	Lys	lysine		W	Trp	tryotophan
L	Leu	leucine		Y	Tyr	tyrosine

X

1   Introduction

1.1 Transporters Play Key Roles for the Life of Cells

Nutrient acquisition is an important function for all living organisms, and many cellular activities are directed towards this goal. A key aspect of this acquisition process is the transport of nutrients and ions from the external environment through the cell membrane into the cytoplasm. Composed of lipids, proteins, and carbohydrates, membranes are mostly arranged in lipid bilayer structures, but according to their function they have different compositions. Attached to or embedded in these membranes are proteins that carry out essential reactions, such as the import and export of various solutes and proteins, the transduction of signals, the generation of metabolic energy, and the communication with other cells. Statistical analysis of all known genome sequences predicts that 20 to 30% of all open reading frames encode integral membrane proteins [Wallin & von Heijne 1998]. Transporters are one group of integral membrane proteins allowing the uptake of essential nutrients and ions and the excretion of deleterious substances and end products of the metabolism [Mitchell 1967]. In the last years, transporters gained enormous interest, as many human diseases turned out to be associated to defects in transport. Furthermore, membrane transporters are involved in the processes of drug resistance and drug-targeting.

By definition, transporters facilitate vectorial rather than, or in addition to, chemical reactions [Saier 2000a]. According to their energy coupling mechanism, transporters can be classified into distinct groups [Saier 2000a] represented schematically in Figure 1-1. The simplest mechanism is the passive transport, a process that is not coupled to metabolic energy and can, therefore, not give rise to concentration gradients of the transported substrate across the membrane. The driving force of passive transport processes is the electrochemical potential gradient. Small lipophilic molecules may diffuse directly through the membrane, whereas water soluble or charged molecules require proteins embedded in the membrane (facilitated diffusion). These are the channels that open and close in response to specific signals, e.g., ligands or voltage. In contrast, the characteristics of active transport processes are the need of energy for the transport reaction and the ability to accumulate solutes against their electrochemical concentration gradients. Primary active transporters drive solute accumulation or extrusion at the expense of a primary energy source, such as ATP hydrolysis, photon

absorption, electron flow, substrate decarboxylation, or methyl transfer [Dimroth 1997]. Secondary active transporters couple the process of solute uptake to a secondary source of energy, i.e., an ion electrochemical gradient, termed in the case of protons proton motive force [Mitchell 1961] and sodium motive force in the case of Na^+ [Poolman & Konings 1993, Saier 2000a]. This class of transporters catalyzes uni-, anti-, and/or symport. Finally, group trans-locaters couple the transport of a solute to the chemical modification of the substrate, e.g., the bacterial phosphotransferase system (PTS), which phosphorylates its sugar substrates during uptake.
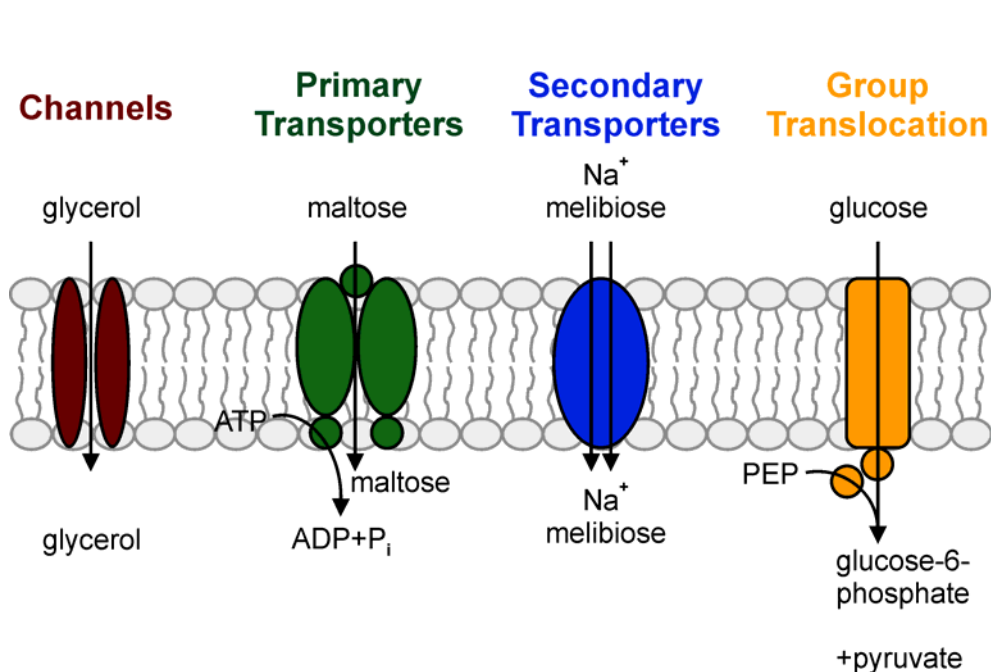
Figure 1-1. Representative examples of the four main classes of transporters of *E.coli*.

Channel proteins allow diffusion through a membrane pore, e.g., the glycerol channel (GlpF).

Primary transporters utilize chemical energy, typically in the form of ATP, to drive transport, e.g., the maltose ABC transporter (MalEFGK).

Secondary transporters utilize chemiosmotic energy, for instance in the form of a proton or sodium gradient, to drive transport, e.g., the melibiose permease (MelB).

Group translocation systems transport and concomitantly phosphorylate their substrates during transport, e.g., the glucose PTS system (PtsG/Crr).

Picture is modified after Paulsen *et al.* [Paulsen *et al.* 2000].

1.2 Classification of the Melibiose Permease

Carbohydrate metabolism has been studied extensively over the last decades of years and the major metabolic pathways are well established. Most bacterial cells have the capacity to utilize several carbohydrates as carbon and energy source and possess, therefore, various transport proteins and catabolic enzymes for their metabolism. One of these transporters is the melibiose permease (MelB) of *Escherichia coli*, which was one of the first active transport systems that was studied in bacterial species. First discovered by Pardee [Pardee 1957] and later investigated in more detail by Prestidge and Pardee [Prestidge & Pardee 1965], it was named methyl-1-thio-β-galactopyranoside (TMG) permease II (later termed MelB) differing from TMG permease I (or lactose permease) with respect to heat lability and the sugar selectivity profile. For a long time it was believed that in prokaryotes the co-transported cation used for substrate accumulation is the proton, while in animal cells it is exclusively Na^+. However, in the pioneer work of Stock and Roseman in 1971 it was shown that the TMG permease II of the analogous carrier of *Salmonella typhimurium* used Na^+ as co-transporting cation for TMG accumulation [Stock & Roseman 1971]. The observation was confirmed [Tokuda & Kaback 1977, 1978], and later also demonstrated for MelB of *E. coli* [Tsuchiya *et al.* 1977].

1.2.1 MelB Belongs to the GPH Transport Family

Transporters are classified according to the transporter classification system [Saier 2000a]. MelB belongs to the glycoside (or galactoside)-pentoside-hexuronide (GPH):cation symporter family (2.A.2) [Poolman *et al.* 1996, Saier 2000a]. Although proteins of the GPH family show only marginal sequence similarity with members of the major facilitator superfamily (MFS, 2.A.1), motif/matrix analyses clearly suggest that these proteins all arose from a common ancestor [Saier 2000b]. Also, the presence of the MFS characteristic motif (R K) X G (R K) (R K) in some members of this family including MelB has been noted. Therefore, it was suggested that the GPH family might be a member of the distantly related MFS superfamily [Saier 2000b, Saier *et al.* 1999], although at the moment they are depicted as two different families both belonging to the subclass 2A of porters (uniporters, symporters, and anti-porters). The GPH family has almost 50 members from bacteria, archaea, and eukaryotes (plants and animals) [Saier 2000a, Paulsen: www.membranetransport.org]. Members of this family share sequence identity with each other over their entire length. Sequence alignment identified subfamilies, the most important being 'MelB', 'LacS' and 'GusB'. The amphiphatic

nature of helix II and the high sequence conservation of interhelix loop 10-11 and helix XI are features shared by these proteins [Poolman *et al.* 1996]. The identity between the subfamily MelB and LacS varies between 19 and 27% and between 'MelB' and 'GusB' between 24-28% [Poolman *et al.* 1996]. A phylogenetic tree of some representative members of the GPH family is shown in Figure 1-2.
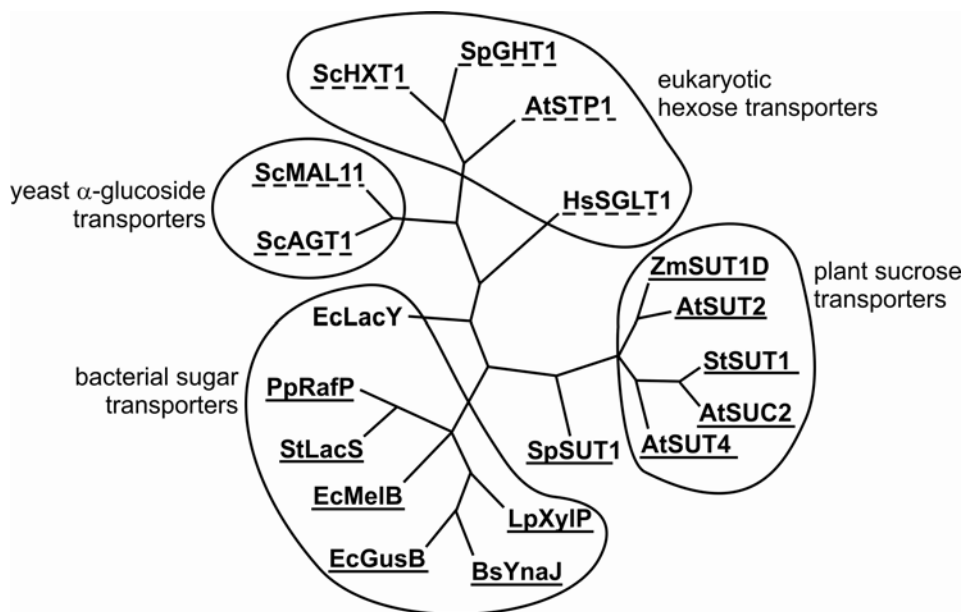
Figure 1-2. Phylogenetic tree of sugar transporters from bacteria, yeasts, humans, and plants.
Members of the GPH family are identified by a solid line, members of the sugar porter family (member of the MFS) by a dashed underline. E_CLacY is a member of the oligosaccharide:H$^+$ symporter family of the MFS [Saier 2000a].
Bootstrap analysis was performed on aligned amino acid sequences of the *Escherichia coli* lactose transporter (EcLacY), melibiose transporter (EcMelB), and glucuronide transporter (EcGusB); *Pediococcus pentosaceus* raffinose transporter (PpRafP); *Streptococcus thermophilus* lactose transporter (StLacS); *Bacillus subtilus* putative xyloside transporter (BsYnaJ); *Lactobacillus pentosus* xyloside transporter (LpXylP); *Schizo-saccharomyces pombe* maltose transporter (SpSUT1), and glucose transporter (SpGHT1); *Arabidopsis thaliana* sucrose transporters (AtSUT4, AtSUC2 and AtSUT2), and monosaccharide transporter (AtSTP1); *Saccharo-myces cerevisiae* hexose transporter (ScHXT1), maltose transporter (ScMAL11), and α-glucoside transporter (ScAGT1); *Solanum tuberosum* sucrose transporter (StSUT1); *Zea mays* sucrose transporter (ZmSUT1); *Homo sapiens* glucose transporter (HsSGLT1). The figure is taken from Reinders and Ward [Reinders & Ward 2001].

1.2.2 Cloning of MelB and Related Transporters

MelB is a transport system in charge of the accumulation of the disaccharide melibiose (α-D-galactopyranosyl-($1{\rightarrow}6$)-α-D-glucopyranose). It is found in members of the Enterobacteriaceae family, such as *Escherichia coli* [Yazyu *et al.* 1984], *Salmonella typhimurium* [Mizushima *et al.* 1992], *Klebsiella pneumoniae* [Hama & Wilson 1992], and *Enterobacter aerogenes* [Okazaki *et al.* 1997c]. The genes encoding these transporters have been cloned and sequenced and share between 78 and 98% identical residues [Okazaki *et al.* 1997b, Poolman *et al.* 1996]. The melibiose transporter of *Enterobacter cloacae* [Okazaki *et al.* 1997a, b] shows only 15% similarity with MelB of *E. coli*, but 85% with the lactose permease (LacY) of *E.coli*. *Citrobacter freundii* from this family has a cryptic melibiose transporter, but correction of a frameshift results in an expression of a functional active melibiose transporter [Shimamoto *et al.* 2001]. Ignoring the frameshift mutation at position 86, it has 86% identity with MelB of *S. typhimurium*, 84% with *E.coli*, 79% with *K. pneumoniae* and 78% with *E. aerogenes*. Phylogenecially it was placed to the group of *S. typhimurium* and *E. coli*, since they are all able to use Na^+ as co-transported cation.

The best studied melibiose permease is the one of *E. coli*, encoded by the *mel*B gene in the melibiose operon, which consists of at least two structural genes, *mel*A, and *mel*B, and is located at approximately 93 min on the revised genetic map [Hanatani *et al.* 1984]. *mel*B is intercalated between *mel*A, which encodes for the α-galactosidase, responsible for the hydrolysis of melibiose into glucose and galactose in the cytoplasm, and a putative third gene, *mel*C, the function of which is unknown [Hanatani *et al.* 1984] The amino-acid sequence [Yazyu *et al.* 1984] indicated a protein consisting of 469 amino acid residues with a molecular weight of 52 kDa. As with other membrane proteins, the apparent molecular mass of the melibiose carrier estimated by sodium dodecyl sulfate (SDS) polyacrylamide gel electrophoresis (PAGE) is significantly smaller (39 kDa [Botfield & Wilson 1989, Pourcher *et al.* 1990a]). This is essentially due to the high proportion of negatively charged SDS molecules associated to this highly hydrophobic protein (>64% apolar residues) in the solubilized state. Edman degradation of the purified MelB of *E. coli* showed that the amino-terminus of MelB does not correspond to MTTKL as it was deduced from the nucleotide sequence of MelB [Yazyu *et al.* 1984], but rather to MSISMTTKL [Pourcher *et al.* 1995]. A significant proportion of expressed transporters lacks an amino-terminal Met as a consequence of post-translational modification, thus in total the protein consists of 473 amino acids instead of 469.

1.3 Structure of the Melibiose Permease

1.3.1 MelB Contains 12 Transmembrane Segments

On the basis of hydropathy profiling of the primary amino acid sequence, a topology model of MelB was developed. Initially, 10 long hydrophobic segments traversing the membrane were suggested [Yazyu *et al.* 1984], but this model was altered and 11 helices proposed [Botfield & Wilson 1988]. Later, vectorial labeling with antibodies predicted that the C terminus lies also within the cytoplasm, thus making an even number of helices (10 or 12) necessary [Botfield & Wilson 1989]. The current model of MelB (Figure 1-3) suggests 12 transmembrane domains in an α- helical conformation crossing the membrane in zigzag fashion connected by hydrophilic loops with the N and C termini facing the cytoplasm [Pourcher *et al.* 1990a]. The model has received strong support from extensive *melB-phoA* fusion analysis [Botfield *et al.* 1992, Pourcher *et al.* 1996]. Proteolytic digestion experiments as well as the analysis of two dimensional crystals verified the existence of 12 transmembrane domains [Gwizdek *et al.* 1997, Hacksell *et al.* 2002]. Fourier transform infrared spectroscopy (FTIR) suggests that the secondary structure is dominated by α-helical components (up to 50%) and contains also β-structures (20%) [Dave *et al.* 2000].
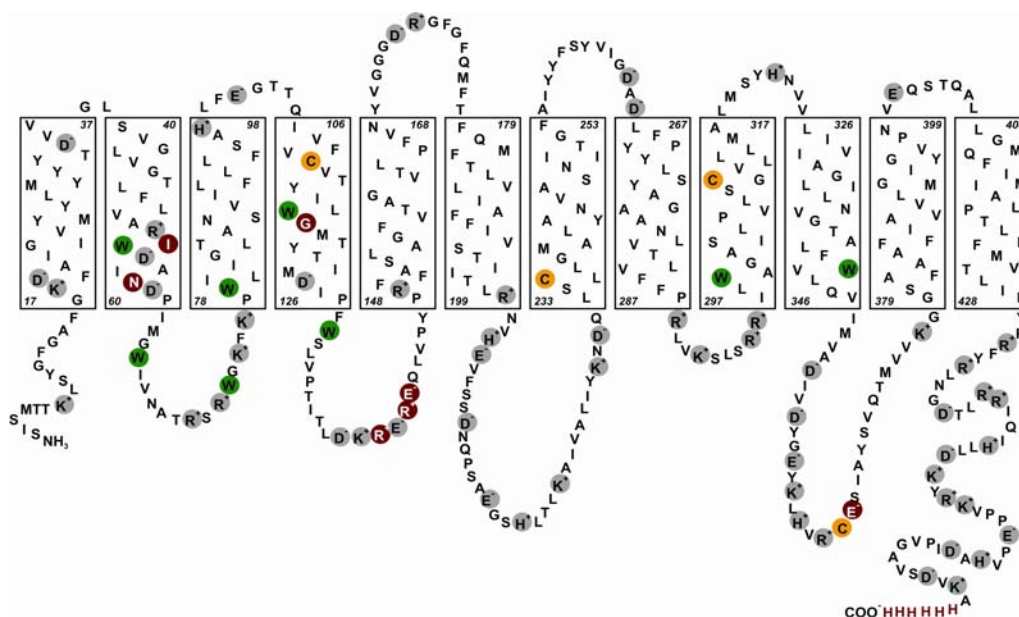
Figure 1-3. Predicted secondary structure of MelB.

Native cysteines are yellow. Amino acids mutated into cysteines in this work are red. Charged amino acids are colored in grey, and all tryptophans are green. The picture is taken from Pourcher *et al.* [Pourcher *et al.* 1996].

1.3.2 Towards the Two and Three Dimensional Structure

Although a significant number of secondary active transporters has been functionally studied in detail, little is known about their three-dimensional structure. The breakthrough was achieved with the crystallization of two members of the major facilitator superfamily, the lactose permease (LacY) and the glycerol-3-phosphate transporter (GlpT) from *E. coli* [Abramson *et al.* 2003b, Huang *et al.* 2003]. As predicted, these two proteins consist of 12 transmembrane helices arranged symmetrically in two 6-helix bundles, and reveal a large internal cavity, open towards the cytoplasm, but completely closed towards the periplasm.

The projection structure of MelB from two-dimensional crystals was determined at 8 Å resolution using electron crystallography [Hacksell *et al.* 2002]. This map shows an asymmetric protein unit composed of two domains lining a central cavity (Figure 1-4). The best resolved density peaks in the MelB projection structure (A, B, C, and J) were assigned to helices oriented nearly perpendicular with respect to the membrane plane, while helices D, E, F, H, L may predict the presence of tilted α-helices [Hacksell *et al.* 2002].
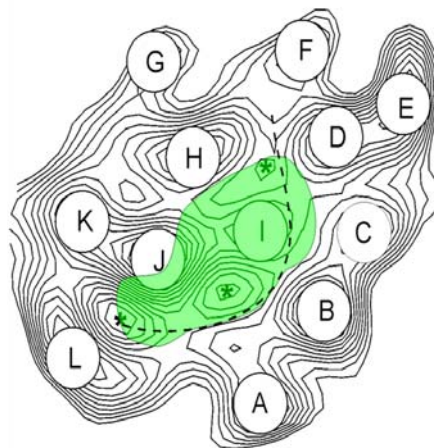
Figure 1-4. Structure of MelB.

 Helix Packing as deduced from 2-dimensional crystals. Picture is taken from Hacksell *et al.* [Hacksell *et al.* 2002].

1.3.3 Non-Crystallographic Approaches to Helix Packing

Since membrane protein crystallization progresses slowly, alternative techniques, such as cysteine-scanning mutagenesis, are also used to obtain useful and detailed information on the three-dimensional protein structure. Cysteine-scanning mutagenesis has already been successfully applied to MelB. A functional active permease devoid of the four native Cys residues with similar properties to the wild-type enzyme has been constructed (C-less permease) [Weissborn *et al.* 1997] with the purpose of delineating the putative aqueous channel and assessing helix proximity. Analysis of channel size by Zeng suggested that at least six helices are needed to create a channel large enough for disaccharides to pass through [Zeng *et al.* 1996]. In order to find and localize a putative aqueous channel in MelB, some helices were systematically studied by the approach of Cys-scanning mutagenesis and probed by the water soluble SH-reagent p-chloromercuribenzene sulfonate (pCMBS).

So far, only four helices of MelB are certainly identified to line the proposed aqueous channel. Thereby, especially the charged amino acids of helices II and XI (Arg-52, Asp-55, and Asp-59 of helix II [Matsuzaki *et al.* 1999], and Lys-377 of helix XI [Ding & Wilson 2000a]), and two non-charged amino acids of helix XI (Leu-391 and Phe-385) [Ding & Wilson 2000a] as well as helix IV [Wilson & Wilson 1998] seem to line directly this channel. Furthermore, whereas helix I was suggested to lie completely within the channel [Ding & Wilson 2001a], helix VI lies most likely completely in the membrane and is, therefore, placed outside the aqueous channel [Ding *et al.* 2001]. Recently, analysis of loop 10-11 suggested that most of this loop is not surface exposed consistent with a re-entrant loop structure [Ding 2004]. Such a re-entrant loop structure of loop 10-11 has also been proposed for the MelB homologue LacS [Poolman *et al.* 1996, Spooner *et al.* 1999]. A central, curve-shaped cleft, assigned to an intra-protein aqueous co-substrate pathway, was also derived from the two dimensional projection structure (see Figure 1-4 and [Hacksell *et al.* 2002]).

Charged amino acids are thermodynamically unfavorable in membrane-spanning regions, but as ion pair or salt bridge with a few additional hydrogen bonds extremely stable in the hydrophobic environment of a transmembrane α-helix [Honig & Hubbell 1984]. A survey of salt bridges in proteins suggests that one third of all salt bridges are of complex nature where more than two charged residues are joined [Musafia *et al.* 1995]. Salt-bridges also indicate close proximity of the helices that bear the bridged amino acids. Thus far, in MelB salt-bridges have been identified between Arg-52 (helix II) and Asp-55 (helix II), and between Arg-52 and Asp-19 (helix I) [Franco & Wilson 1999]. Furthermore, Asp-19 forms an

intrahelical salt-bridge with Lys-18 [Ding & Wilson 2001a]. Additionally, it was proposed that Lys-377 (helix XI) bridges with Asp-59 (helix II) [Ding & Wilson 2000a, Franco *et al.* 2001], Asp-55 and/or Asp-124 [Ding & Wilson 2001b, Wilson & Wilson 1998]. These studies, therefore, revealed proximities between helices XI and II, between helices XI and IV, and between helices I and II, and could provide information concerning the three-dimensional helical arrangement.

Additional evidence for helix proximity war inferred from analysis of second-site revertants, i.e., transporters in which a first mutation causes severe loss of the activity, while a second mutation at a different site restores partial or full activity. Double mutation sites in a restored active mutant may implicate proximity between the two helices in which the two mutations occur. Studies of such second-site revertants led to the following suggestions (see also Figure 1-5):

Helix I (cytoplasmic end) is close to **helix IV** (cytoplasmic end) (K18C/M123R) and to **helix VII** (Y31C/S234L; Y31C/L236F) [Ding & Wilson 2001a].

Helix II is close to **helix IV** (D55S/G117D; R52S/W116R) [Franco & Wilson 1999, Wilson *et al.* 1995] and also to **helix VII** (R52S/S247R) (D59C/S234Leu) [Franco & Wilson 1999; Zani 1994, unpublished results] and **helix X** (R52S/T338R) [Franco & Wilson 1999].

Helix IV was shown to be in close contact with **helix XI** (D124S/V375A or G) [Wilson & Wilson 1998].

Helix X was proposed to be closed to **helix V** or **loop 4-5** (R149C/V343G) [Abdel-Dayem 2003].

Loop 10-11 is close to the cytoplasmic part of **helix I** (A350C/I22N; A350C/I22S) and to the periplasmic part of **helix VIII** (A350C/F268L) [Ding 2004].

Helix XI is close to **helix I** (K377V/F20L; K377C/I22S; A383C/I22S or N or L; L391C/I22N or T; L391C/D19E; G395C/D19E; G395C/I22N) [Ding & Wilson 2000a, Franco *et al.* 2001], to **helix II** (K377C/D59A; K377V/D59V; K377V/D59N) [Ding & Wilson 2000a, Franco *et al.* 2001], to **helix V** or **loop 4-5** (L391C/A152S), and finally to the **C -terminal loop** (F385/R441) [Ding & Wilson 2000a].

Crosslinking studies confirmed the proximity between **helices I** and **XI** [Ding & Wilson 2001c].

Although an assignment of the helices in the 2-dimensional map to helix numbers was not performed, it is likely that helix I in Figure 1-4 corresponds to helix one (I) in MelB, since it has been shown that helix I is completely within an intraprotein aqueous channel [Ding & Wilson 2001a]. Interestingly, in the distantly related MFS family, the least conserved helices 3, 6, 9, and 12 lie at the periphery of the molecule facing the interior or lipid bilayer [Goswitz & Brooker 1995]. It is possible that the same holds true for MelB in particular for helices A, E, K, and G. Interestingly, biochemical studies combined with Cys-scanning mutagenesis suggest that helix VI might be one of these 4 peripheral helices in MelB [Ding *et al.* 2001]. More likely candidates for such helices being completely within the lipid bilayer are helices XII and III, as they have thus far not been implicated in any functioning of the transporter, e.g., substrate binding. For the oxalate transporter (OxlT) it was suggested that these 4 peripheral are perpendicular to the plane of the lipid bilayer [Hirai *et al.* 2002]. On ground of these considerations and the data obtained from proximity studies described above, the following assignment of the helices to the density map (Figure 1-5) can be proposed [Gérard Leblanc, unpublished results].
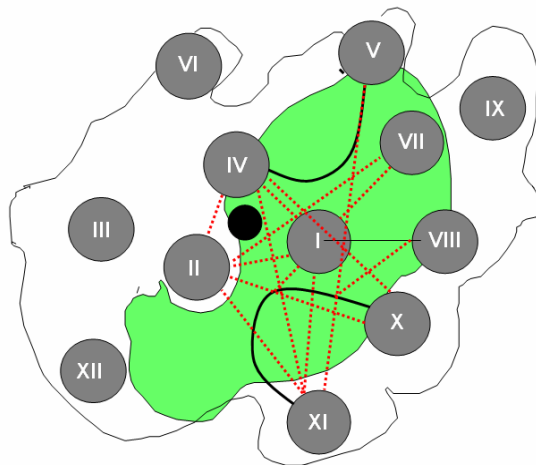
Figure 1-5. Proposed model for the arrangement of helices.

The model from Figure 1-4 was taken and the assignment made using the information given in the text. The red dashed lines indicate proximity between helices as described in the text. Loops 4-5 and 10-11, both believed to play a key role for the transport function, are also depicted (black lines). The black circle indicates the Na^+ bound to helices I, II, and IV [Gérard Leblanc, unpublished].

1.4 MelB Substrate Binding Sites

1.4.1 Cation and Sugar Selectivity Profile

MelB is most unusual in its ability to use Na^+, Li^+, or H^+ as coupling cation depending on the configuration of the transported sugar. Whereas sugars with *β*-configuration (e.g., TMG, methyl-*β*-galactoside, and lactose) are equally well transported with either Na^+ or Li^+, but not with H^+, sugars with α-configuration (e.g., melibiose or α-methyl-galactoside) are co-transported with H^+, Na^+, or Li^+ [Tsuchiya & Wilson 1978, Tsuchiya *et al.* 1977, 1978, 1980, Tsuchiya *et al.* 1983, Wilson & Wilson 1987, Wilson *et al.* 1986]. Further carbohydrates that are transported by MelB are *p*-nitrophenyl-α-D-6-galactopyranoside (α-NPG), galactose, thio-galactosyl- β-galactoside, L-arabinose-β-galactoside, D-fructose-β-galactoside, raffinose, *p*-nitrophenyl-β-galactopyranoside, 2-deoxy-2-amino-D-galactose, fucose, and arabinose. In contrast, xylose, glucose, galactinol, D-tagatose, and 2-deoxy-D-galactose are not transported with any ion [Wilson & Wilson 1987]. K^+, Cs^+, Rb^+, NH_4^+, Mg^{2+}, Mn^{2+}, Ca^{2+}, and $choline^+$ as well as chloride did not have any stimulating effect on sugar binding and/or transport [Lopilato *et al.* 1978, Stock & Roseman 1971, Tsuchiya *et al.* 1977,1980]. Melibiose is the only carbohydrate used in this thesis and, therefore, depicted in Figure 1-6. It is widely distributed in beans, legumes, seeds, roots, and soy-products.
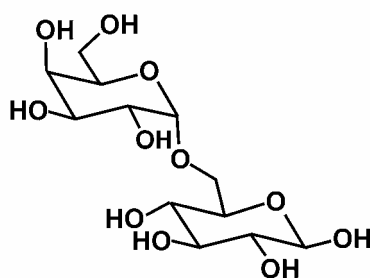
Figure 1-6. Structure of melibiose.

α-D-galactopyranosyl (1→6) α-D-glucopyranose

1.4.2 In Search of the Cation Binding Site

One common strategy to determine binding sites in proteins is the approach of site-directed mutagenesis, where amino acid residues of the protein are replaced and the effects on the activity of the transporter are investigated. Target amino acids are usually charged or hydrophilic residues, conserved amino acids within the same transport family, or amino acids that were shown to be important in other proteins.

Different amino acids have been considered to be part of a putative ion binding site. Likely candidates for residues involved in proton binding are His, Glu, and Asp [Henderson 1990] . Indeed, in LacY, which obligatory couples the transport of galactosides to protons, Glu-325 is essential for efficient substrate binding (review in [Abramson *et al.* 2003a]). The MelB homologue lactose permease (LacS) from *S. thermophilus*, which also uses only H^+ as coupling ion, lost the ability of H^+ coupling when Asp-71 was mutated to Asn [Poolman *et al.* 1996]. Adapted to the model of MelB (see below), Asp-22, Asp-71, and Asp-140 were proposed to be essential for H_3O-coordintation, whereas Asp-67 participates more in the structural organization of the cation binding site [Knol *et al.* 1999a].

For Na^+-coupling symporters a recognizable sodium binding (SOB) motif was suggested [Deguchi *et al.* 1990], which was also identified in a modified form in $MelB_{EC}$ (G X_{39} A X_4 L X_3 P R, present between Gly-236 and Arg-288 [Yamato & Anraku 1993]). However, since this motif is conserved in MelB from *E. coli*, *S. typhimurium*, and *K. pneumoniae*, and MelB of *K. pneumoniae* lacks the capacity to couple the symport of melibiose to Na^+, it appears that the occurrence of this motif does not always correlate with Na^+ symport activity. Therefore, it was concluded that the SOB sequence motif is neither universally necessary nor sufficient for Na^+ symport [Reizer *et al.* 1994]. The same conclusion was drawn for the proline transporter (PutP) from *E. coli*, namely that Arg-376, which is part of the SOB motif, is not involved in Na^+ recognition [Jung 2001]. His, Cys, or oxygen atoms in acids, amides, or hydroxyls (e.g., Asp and Glu) can be involved directly in Na^+ binding, e.g., in the case of PutP, Asp-55 has been proposed to participate in Na^+ binding, Arg-40 was thought to be located close to the site of ion binding, and Asp-187 may be involved in the release of Na^+ at the cytoplasmic side of the membrane (for a review see [Jung 2001]).

In the case of MelB, site-directed mutagenesis experiments suggested that none of the native seven histidines [Pourcher *et al.* 1990b, Pourcher *et al.* 1992] or of the four cysteines

[Botfield 1989, Weissborn *et al.* 1997] is essential for the interaction of the transport protein with the coupling cation and/or sugar or critical for the transport reaction.

With the aim of identifying the putative cation binding site of MelB, charged residues in helix I, II, III, and IV have been investigated. The suggestion that the carboxylate side chains of Asp-19 (helix I), 55, 59 (both helix II), and 124 (helix IV) participate in Na^+ coordination (Figure 1-7) is based on the observation that their independent replacement by a neutral residue prevented the utilization of Na^+ and Li^+ as coupling ions. Whereas the binding of α-NPG, melibiose, and TMG remained possible, it was no longer stimulated by Na^+ [Ding & Wilson 2001b, Ding *et al.* 2000, Leblanc *et al.* 1993, Poolman *et al.* 1996, Pourcher *et al.* 1991, 1993, Wilson & Wilson 1992, 1994, Zani *et al.* 1993, 1994]. When the polar residues aligned with Asp-35, 55, 59, and 124 were mutated, only Y28F, N87A, and Y120F exhibited reduction of affinity for Na^+ [Zani *et al.* 1994]. It was suggested that these mutants may either directly enhance MelB's affinity for the coupling ion, or may influence the position of the carboxyl moiety of Asp-55, 59, or 124. The initial assumption that Asp-35 participates in cation binding [Pourcher *et al.* 1993] was later rejected [Poolman *et al.* 1996]. Also the substitution of Glu-101 by Gln (loop 3-4) resulted in no change in transport activity [Wilson & Wilson 1992]. In agreement with the proposed structure of the binding site (Figure 1-7) these two residues are positioned out of the network.

Additional information concerning the cation binding site came from studies with chimeras of MelB from *E. coli* and *K. pneumoniae* indicating that, among the first 81 amino acid residues of the *E. coli* protein that are essential for coupling Na^+ to melibiose transport [Hama & Wilson 1993], only Asn-58 is important for Na^+ recognition [Franco & Wilson 1996, Hama & Wilson 1994]. In this context it is interesting to note that only those transporters of the GPH family having an Asn at this position can use Na^+ as coupling cation [Poolman *et al.* 1996]. Finally, some interesting mutants that might be involved in cation binding should be mentioned. Arg at position 52 is not absolutely required for transport, but a positive charge and even more the structure of the side chain are important for efficient cation coupling and transport [Ding & Wilson 2001b, Franco & Wilson 1999, Zani *et al.* 1994]. Arg-52 is, furthermore, ion-paired with Asp-55 [Franco & Wilson 1999] suggesting that this interaction may well be required to contribute to an optimal positioning of Asp-55 with Na^+. While the low expression level in some studies with the K377C mutant did not clarify the role of Lys-377 [Ding 2003, 2004, Ding & Wilson 2000a, b], substitutions with Val and especially Asp revealed its importance for efficient cation coupling [Franco *et al.* 2001]. It was suggested
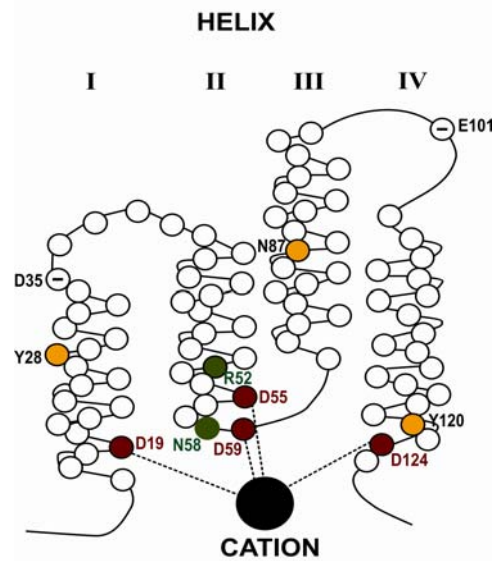
Figure 1-7. Putative cation binding site.

Asp, 19 (helix I) Asp 55 (helix II) Asp 59 (helix II), and Asp 124 (helix II) were suggested to form a cation coordination site (in red). Asn-58 and Arg-52 are important for Na^+ recognition (in green). Polar amino acids suggested to be important for the overall structure are yellow. Taken from Poolman *et al.* [Poolman *et al.* 1996].

that Lys-377 forms a salt bridge with amino acids from helix II implying a possible involvement of helix XI in cation-binding. Furthermore, the H^+-coupling was lost and an absolute requirement for Na^+ or Li^+ acquired, when Pro-126 [Botfield & Wilson 1988, Ding *et al.* 2000, Niiya *et al.* 1982, Yazyu *et al.* 1985] or Pro-146 was mutated [Kawakami *et al.* 1988]. However, although it is unlikely that Pro participates directly in H^+ binding, because it does not possess a dissociable group [Yazyu *et al.* 1985], one possible involvement could be over cis-trans isomerization of amino acid bonds with Pro residues, which has been implicated in dynamic processes of proteins [Brands *et al.* 1975].

Based on these observations it was suggested that the side chains of Asp-19, 55, 59, and 124 form at least part of a network involved in the coordination of the cation (Figure 1-7), and that Asn-58 and Asp-59 in addition to Asp-19, 55, and 124 are crucial for the co-ordination of Na^+. Most likely a hydronium ion H_3O^+ is used rather than H^+ [Boyer 1988]. Since H_3O^+ is complexed by three hydrogen bonds but Na^+ by five, both ions might use a different cluster of coordination atoms [Poolman *et al.* 1996].

Finally it should be stressed that studies of second site revertants and the existence of salt bridges is consistent with the structure of the proposed cation binding site. Thus, Arg-52 may

be salt-bridged with Asp-19 and Asp-55 bringing helix II in close contact with helix I [Franco & Wilson 1999]. Lys-377 (helix XI) is salt-bridged with Asp-59 (helix II) [Ding & Wilson 2000a, Franco *et al.* 2001], Asp-55, and Asp-124 [Ding & Wilson 2001a, Wilson & Wilson 1998]. Furthermore, it was suggested that Gly-117 from helix IV is close to Asp-55 in helix II [Wilson *et al.* 1995], Arg-52 close to Trp-116 (helix IV) [Franco & Wilson 1999], and Asp-124 close to Val-375 (helix XI, [Wilson & Wilson 1998]).

1.4.3 In Search of the Sugar Binding Site

A general scheme for the interaction between proteins and their carbohydrate substrates was derived from studies crystallizing the arabinose, maltose, and galactose binding proteins from *E.coli* [Quiocho 1986, 1988]. Not only extensive hydrogen bonding interactions of the OH groups in particular with Asp, Asn, Glu, and Gln residues, but also nonpolar interactions of the carbon backbone with aromatic residues in the initial binding of a ligand to a protein are important forms of interactions between the sugar and the protein. In complexing with the protein, the sugars exchange their solvation shell of water for hydrogen bonds with polar groups within the substrate binding site. Concomitantly, the previously bound water is displaced and often excluded from the binding site. Hydroxyl groups serve simultaneously as hydrogen bond donors and acceptors. [Quiocho 1986, 1988]. Similar interactions could be assumed to exist in transmembrane proteins, e.g., studies on LacY demonstrate that Glu-126 may interact with O4, O5, or O6 atoms of the galactopyranosyl ring [Kaback 1997].

Since individual point mutations of MelB often result in more than one change in the functional properties of the transporter, such as the concomitant modification of its ionic and sugar selectivity profile, a hypothetical model for the sugar binding site was thus far not proposed. Amino acids involved in sugar binding or lying close to the sugar binding site have, however, been identified.

Several mutations, identified when cells were grown on melibiose in the presence of a high concentration of the non-metabolizable competitive inhibitor TMG, were found to be in helices I, IV, VII, X, XI and loop 10-11. These helices, which are close to each other, might form a binding site for sugar and cation or line a channel through which these substrates could diffuse into the protein during the transport event [Botfield & Wilson 1988, Ding *et al.* 2000]. More detailed studies revealed that amino acids from helix IX (Trp-299) and helix X (Trp-342), although not directly involved in sugar binding, are close to or at the sugar binding site [Cordat *et al.* 1998, Mus-Veteau & Leblanc 1996]. pCMBS inhibition was blocked by

melibiose in single-Cys mutants from helix XI (S380C, A381C, A384C, I387C, A388C, and L391C) indicating that these residues might also be close to the sugar binding site [Ding & Wilson 2000b]. Systematic Cys-scanning analysis of the entire loop 10-11 revealed that melibiose protects also against pCMBS inhibition of T373C and V376C from the periplasm suggesting that these two residues are close to the substrate binding site [Ding 2003, 2004]. Also Asn-335 and Thr-338 from helix X seemed to be involved in sugar binding [Basquin 2001]. Additionally, active-site-directed labeling of MelB identified sequences in helix X and XI, respectively, as targets of the labeling reaction [Ambroise *et al.* 2000]. Taken together, all these data suggest that the sugar-binding site is preferentially located in the C-terminal part of the transporter, mainly in helix IX, X, and XI.

Further studies proposed also an involvement of some N-terminal domains in sugar binding. For example, fluorescence resonance energy transfer (FRET) measurements suggested that Trp-64, lying in the N-terminal loop 2-3 is close to the sugar-binding site [Cordat *et al.* 1998]. It was also suggested that the architecture of the side chain at position 59 influences sugar binding directly [Franco *et al.* 2001], and that Trp-116 and/or Trp-128 both may play a role in sugar selectivity by stabilizing binding and transport of sugars bearing a β-configuration [Cordat *et al.* 2000]. Recently, active-site-directed labeling of MelB was used as strategy of choice to identify domains or residues directly participating in the substrate-protein interaction. The target amino acid of photo labeling with *p*-azidophenyl-α-D-galacto-pyranoside was R141 [Ambroise *et al.* 2000]. Detailed analysis revealed that Arg-141 is not directly involved in sugar binding, but rather in the transport mechanism. On the other hand, Arg-149 lies directly at the sugar binding site [Abdel-Dayem *et al.* 2003]. Also S153C shows a strong decrease for α-NPG affinity and seems, therefore, to board the sugar binding site [Basquin 2001].

1.4.4 Overlap of Cation and Sugar Binding Sites

An overlap of cation and sugar binding site could account for the high frequency of single mutations producing simultaneous alteration of sugar and ionic recognition properties of MelB [Botfield & Wilson 1988, Wilson & Wilson 1994, Yazyu *et al.* 1985, Zani *et al.* 1994], and reflects also the cooperative interactions between cation and sugar binding processes. Helix IV could play a role in connecting cation- and sugar-binding sites [Cordat *et al.* 2000]. Moreover, the proximity between the cation- and sugar binding site with a distance of around 20 Å between the loop 2-3 and the sugar binding site was determined [Cordat *et al.* 1998].

1.5 Melibiose Transport: From Periplasm to Cytoplasm

1.5.1 Transport of Melibiose across the Outer Membrane

The gram[-] bacterium *E. coli* protects itself by an additional structure, the outer membrane, which presents the first barrier for a substance to enter. Embedded in this membrane are non-specific aqueous diffusion channels, or porins, which act as physical barrier restricting the diffusion of large molecules into the periplasm (molecular weight < 1000 kDa). They allow sugars to diffuse from the environment to the periplasm [Nikaido & Saier 1992]. Maltoporin of *E.coli* is one known channel permitting the diffusion of, e.g., melibiose [Wang *et al.* 1997]. However, in bacteria the major permeability barrier is the cytoplasmic membrane.

1.5.2 Transport Systems at the Cytoplasmic Membrane

According to the chemiosmotic theory [Mitchell 1961, 1966], the development of an electrochemical proton gradient $\Delta\mu_{H+}$ across the membrane is the immediate driving force for active transport. $\Delta\mu_{H+}$ is the result of the oxidation of substrates via the respiratory chain [Mitchell & Moyle 1967], (Figure 1-8). Whereas the co-transport of melibiose with protons is directly coupled to $\Delta\mu_{H+}$, the Na^+ co-transport mode requires an electrochemical Na^+ gradient $\Delta\mu_{Na+}$, which is generated through the action of a Na^+/H^+ exchanger [West & Mitchell 1974] and used to accumulate melibiose up to 200 fold into the cell [Tokuda & Kaback 1977].
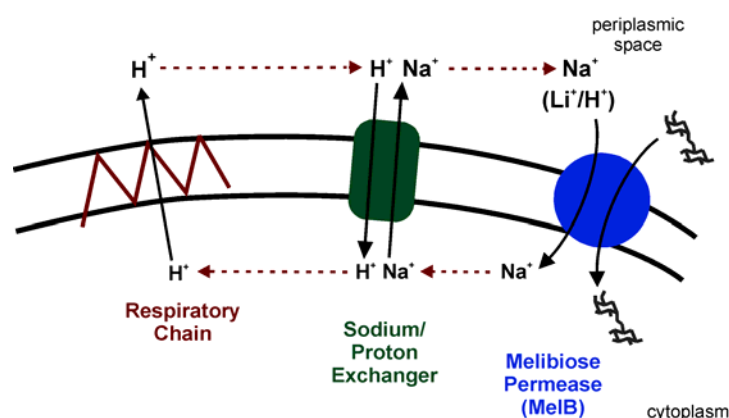
Figure 1-8. Transport systems at the cytoplasmic membrane.
The respiratory chain generates $\Delta\mu_{H+}$, which is either used directly by MelB to accumulate melibiose with protons, or by the Na^+/H^+ exchanger to generate $\Delta\mu_{Na+}$. $\Delta\mu_{Na+}$ is used by MelB to accumulate melibiose with Na^+.

1.5.3 Substrate Binding Activity on MelB

α-NPG is a suitable high affinity substrate to monitor sugar binding activity of MelB [Cohn & Kaback 1980], as it is co-transported with either H^+ or Na^+ [Wilson & Wilson 1987] and competitively displaced from the permease by melibiose [Damiano-Forano *et al.* 1986]. Studying the effects of Na^+, Li^+, and H^+ on the NPG binding constants revealed that substrate binding occurs in a 1:1 ratio [Damiano-Forano *et al.* 1986]. The initial suggestion that Li^+ and H^+ have the same recognition site or share a common domain, whereas the Na^+ recognition site lays on a distinct domain [Kawakami *et al.* 1988] was rejected, as competition of the cations for a common binding site was found [Damiano-Forano *et al.* 1986, Hama & Wilson 1994, Mus-Veteau *et al.* 1995]. Na^+ enhances the affinity of MelB for the co-transported sugar [Bassilana *et al.* 1985, Cohn & Kaback 1980, Damiano-Forano *et al.* 1986] and also the hydrophobicity of the sugar binding site [Maehrel *et al.* 1998]. Furthermore, H^+ is a less efficient activator than Na^+ or Li^+ for sugar binding [Bassilana *et al.* 1985]. It was also shown that melibiose enhances the affinity for Na^+ [Ganea *et al.* 2001].

1.5.4 Kinetic Transport Model of MelB

MelB works as ion-coupled sugar co-transporter facilitating the uptake of 1 mole sugar with 1 mole ion [Bassilana *et al.* 1987, Niiya *et al.* 1980, Tokuda & Kaback 1977]. Kinetic analysis of the co-transport of the physiological substrate melibiose with either H^+, Na^+, or Li^+ as coupling cation revealed significant differences in the kinetic parameters of transport rates depending on the chemical identity of the coupling ion [Bassilana *et al.* 1987, 1988, Tanaka *et al.* 1980]. In de-energized conditions, i.e., in the absence of a potential, and if Na^+ is the coupling cation, the V_{max} efflux (Eff) is higher than the V_{max} influx (Inf) (57 vs. 2 nmole per mg protein per minute). Under these conditions, not the return of the unloaded carrier [Bassilana *et al.* 1987, Cohn & Kaback 1980], but the release of Na^+ into the cytoplasm is the rate limiting step [Bassilana *et al.* 1987]. In contrast, efflux experiments suggested a rapid Na^+ release on the outside [Bassilana *et al.* 1988]. In the H^+ coupled mode, important influx is noted and sugar release is rate limiting for carrier turnover [Bassilana *et al.* 1988]. Furthermore, the V_{max}^{Inf} is 20 times higher when H^+ instead of Na^+ is the coupling cation (42 vs. 2 nmol per mg protein per minute). Such variability in the rate of co-substrates release in the cytoplasmic compartment depending on the chemical identity of the cation might reflect differences in stability of the ternary complex cation-sugar-carrier facing the intravesicular medium [Pourcher *et al.* 1990a].
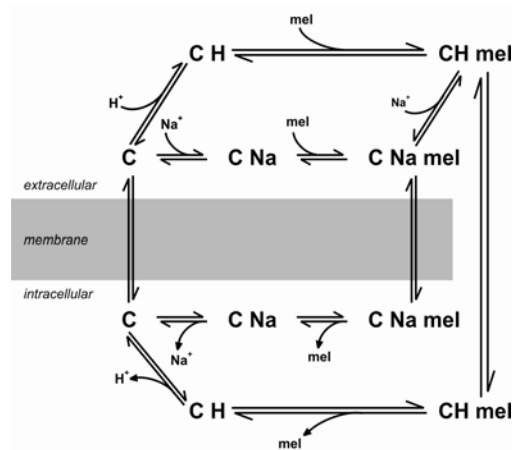
Figure 1-9. Kinetic model of MelB.

The transporter C, facing the extracellular space, binds Na^+ or H^+ and sequentially the sugar melibiose. The ternary complex (C-ion-sugar) reorients its binding sites to the intracellular site, releases first the sugar and then the ion. Finally, the empty carrier turns back to the extracellular side. An arrow from CHmel to CNamel indicates that melibiose can also enhance the carriers' affinity for Na^+ (after [Bassilana *et al.* 1987, 1988, Damiano-Forano *et al.* 1986, Ganea *et al.* 2001, Pourcher *et al.* 1990a])

The electrical potential $\Delta\Psi$ increases the rate of melibiose influx [Bassilana *et al.* 1985, Cohn & Kaback 1980, Lopilato *et al.* 1978]. This holds true only for the Na^+ coupled conditions, because if H^+ is the coupling ion, melibiose influx is almost insensitive to $\Delta\Psi$ [Bassilana *et al.* 1985, Leblanc *et al.* 1988]. In contrast, $\Delta\Psi$ increases the apparent affinity transport constant, K_t, in the H^+ mode, but has no effect in the Na^+ transport mode. Most likely, the major effect of the electrical membrane potential is to decrease the stability of the ternary complex facing the cytoplasmic compartment with a resulting increase of the rate of dissociation of the co-substrates in the inner compartment [Pourcher *et al.* 1990a]. Based on all these data, the mirror type kinetic model [Bassilana *et al.* 1987, 1988, Damiano-Forano *et al.* 1986, Ganea *et al.* 2001, Pourcher *et al.* 1990a] was proposed for the transport mechanism (Figure 1-9).

1.5.5 Substrate Induced Conformational Changes

Membrane transport proteins are proposed to catalyze transport by an "alternating access" mode [Jardettzky 1966, Jauch & Lauger 1986, Yan & Maloney 1995], i.e., they alternate between a minimum of two conformations, in which the binding site is made accessible from either side of the membrane. This concept agrees essentially with Mitchell's theory of a

mobile barrier [Mitchell 1990] and found recently support by structure determination of LacY and GltP [Abramson *et al.* 2003b, Huang *et al.* 2003]. An additional substrate-bound closed state was suggested from the analysis of two dimensional crystals of the oxalate exchanger OxlT [Heymann *et al.* 2001, 2003, Hirai & Subramaniam 2004].

As determined by intrinsic fluorescence spectroscopy and the analysis of H/D exchange kinetics, an ion-induced structural rearrangement of MelB takes place [Dave *et al.* 2000, Mus-Veteau *et al.* 1995]. Three Trp residues in the MelB N-terminal half (Trp-54, Trp-116, and Trp-128) were identified to be responsible for the Na^+-induced fluorescence changes, whereas neither Trp-299 nor Trp-342 from the C-terminal half of MelB participates to any extent to this signal variation [Cordat *et al.* 2000, Mus-Veteau & Leblanc 1996]. This conformational change involves probably a rearrangement of loop 4-5 [Gwizdek *et al.* 1997], but does not alter the orientation of helix I and XI with respect to each other [Ding & Wilson 2001c]. Upon subsequent melibiose binding, not only loop 4-5 undergoes further structural rearrangements [Gwizdek *et al.* 1997], but also loop 10-11 reflecting the dynamic aspects of this loop [Ding 2004]. The SH reagent N-ethyl maleimide (NEM), which does not block Na^+ dependent NPG binding [Damiano-Forano *et al.* 1986] but the melibiose transport activity [Lopilato *et al.* 1978] was found to have C364 from loop 10-11 as a target [Botfield 1988, Weissborn *et al.* 1997]. The binding of sugar significantly also reduces the accessibility of MelB to solvent [Dave *et al.* 2000] and induces a remarkable compactness of the carrier's structure, affecting mainly β-sheet domains of the transporter, which, may include cytoplasmic loops 4-5 and 10-11 according to secondary structure predictions [Dave *et al.* 2002]. Studies of the intrinsic Trp fluorescence properties also suggest a sugar-induced conformational change involving Trp-299 and Trp-342, which is not associated to transport, as the sugar-induced fluorescence variations still occur when the transport is blocked by NEM [Mus-Veteau & Leblanc 1996, Mus-Veteau *et al.* 1995].

1.5.6 Melibiose Metabolism

Carbohydrate metabolism has been studied extensively, and the major metabolic pathways are well established. Most bacterial cells have the capacity to utilize several carbohydrates as carbon and energy source and possess various transport proteins and catabolic enzymes for their metabolism. Melibiose, once entered in the cell, is cleaved by α-galactosidase into glucose and galactose [Webster *et al.* 1987]. Whether further metabolism of α-D-glucose and α-D-galactose proceeds by their initial export via sugar efflux transporters [Liu *et al.* 1999a,b]

followed by reentry, as proposed for the hydrolysis products of lactose [Huber *et al.* 1980], was not investigated. In the context of raffinose catabolism, it was suggested that the raffinose permease may facilitate the leakage of melibiose, when melibiose accumulates in the cell [Moniruzzaman *et al.* 1997]. Galactose is phosphorylated by galactokinase to galactose-1-phosphate and isomerized to glucose-1-phosphate [Lin 1987]. Glucose is either phosphorylated by the glucokinase or during the reentry in the cell by the PTS system to glucose-1-phosphate. The latter product is converted by phosphoglucomutase to glucose-6-phosphate, which enters the glycolytic pathway [Frankel 1987].

1.5.7 Regulation of MelB Activity

Bacteria species are capable of regulating their transport activities for selecting the preferred carbon sources when different substrates are present in the environment. This ability in part allows them to repress the synthesis of proteins, which are unnecessary for growth [Dills *et al.* 1980]. A dual regulation allows an instantaneous response of *E.coli* to the presence or absence of melibiose (inducer exclusion) and a slow response, which involves switching on/off gene expression (catabolite repression), i.e., in the absence of melibiose, the level of the MelB expression system will be low [Postma *et al.* 1993, Saier 1989]. The transcription initiation at the *melAB* promoter is completely dependent on MelR, a transcription activator that is triggered by melibiose and encoded by the *melR* gene located immediately upstream of the *melA* gene [Webster *et al.* 1989]. Thus, the expression of the *mel*AB operon is coupled to the availability of melibiose in the growth medium [Webster *et al.* 1988].

The PTS system is involved in the process of inducer exclusion occurring when the cell is metabolizing PTS sugars at a high rate (including glucose (Glc) and other monosaccharides) and results in the dephosphorylation of IIA^{Glc}, which inhibits melibiose transport via direct binding to MelB. In the absence of PTS sugars, IIA^{Glc} remains phosphorylated, which relieves inhibition of MelB. Analysis of inducer exclusion mutants revealed that Asp-438, Arg-441, and Ile-445, and Ala-368 conserved in the MelB proteins of *E. coli, S. typhimurium*, and K. *pneumoniae*, and probably loop 6-7 are interacting with IIA^{Glc} [Kuroda *et al.* 1992, 2001, Postma *et al.* 1993, Saier *et al.* 1983]. Thus, the COOH terminal portion of the melibiose carrier as well as the central loop are important for the interaction with the dephosphorylated IIA^{Glc}. In contrast, in the homolog LacS, the long carboxyl-terminal hydrophilic domain (about 160 amino acids) is homologous to IIA proteins/domains of various PTS systems and can be directly phosphorylated [Poolman & Konings 1993].

1.6 Time-Resolved Measurements

Biochemical reactions, such as substrate binding to enzymes, are usually very fast, and steady-state experiments are not capable of measuring time constants of individual reactions of the transport cycle. Therefore, relaxation or pre-steady-state techniques are applied, where the steady-state is perturbed by a sudden change of an external parameter, such as temperature, pressure, voltage, or substrate concentration, and the time course of the reaction approaching a new-steady state is followed. Such relaxation techniques have been extremely successful in the investigation soluble enzymes (see [Ferguson & Fersht 2003] for a review), but also of transport systems, e.g., transient (pre-steady-state) currents or fluorescence changes can be associated with relaxation processes and contain information on parameters of the transport cycle.

1.6.1 Measurements of Pre-Steady State Currents

Some problems need to be overcome in order to study directly charge translocation in transporters. They are, unlike channels, extremely slow systems with turnovers of only 1-100 s^{-1} [Bamberg *et al.* 1993], and single transporter recording would not be sufficient to measure significant charge translocation. The patch clamp technique [Hamil *et al.* 1981] in the whole-cell or giant-patch configuration opens the possibility to study directly charge translocation, as the synchronized performance by many electrogenic transporters generates measurable currents. A straightforward and commonly used technique to observe charge movements is to apply voltage steps across the membrane, which induce an alteration in the equilibrium charge distribution. The time-dependent redistribution of charges is then manifested as transient decaying currents. These so-called pre-steady-state relaxations have been documented for electrogenic co-transporters like the Na$^+$/glucose co-transporter SGLT1 [Hazama *et al.* 1997, Loo *et al.* 1993, Parent *et al.* 1992a], the Na$^+$/Pi co-transporter [Forster *et al.* 1998], the Na$^+$/I$^-$ co-transporter NIS [Eskandari *et al.* 1997], the human glutamate transporter [Wadiche *et al.* 1995], and the GABA/Na$^+$/Cl$^-$ co-transporter GAT 1 [Lu and Hilgemann 1999]. Furthermore, laser pulse-photolysis in combination with patch-clamp, allows to study substrate concentration jumps occurring on a sub-millisecond time scale. Thereby, a photolabile protecting group is covalently attached to the molecule of interest (caged compound) and released within microseconds upon irradiation with a short flash of UV laser light. By generating rapid light-activated concentration jumps, the kinetics of the transporter currents can then be studied, e.g., caged glutamate has been used to study the

excitatory amino acid carrier 1 EAAC1 [Grewer *et al*. 2001, Watzke et al 2001], caged GABA to study the γ-aminobutyric acid transporter GAT 1 [Bicho & Grewer 2005], and caged ATP to study the Na,K-ATPase [Friedrich *et al.* 1996].

Unfortunately, the path clamp technique is not applicable to bacterial transporters, as direct patching of *E. coli* cells is hampered by the small size of the cells. Furthermore, the expression of bacterial transporters in *Xenopus laevis* oocytes was not successful yet. Therefore, membrane fragments or liposomes containing the transporter of interest in a high density are adsorbed to a black lipid membrane (BLM) and used for the measurements of pre-steady state currents. For example, caged ATP and ADP were used to study charge translocation in the Na,K-ATPase [Bamberg *et al.* 2001, Fendler *et al.* 1985, 1987, 1993], the H,K-ATPase [Stengelin *et al*. 1993] , the Ca-ATPase [Hartung *et al.* 1987], and the ADP/ATP-exchanger [Gropp *et al.* 1999]. Furthermore, the time dependent photocurrent of the light-driven ion pump bacteriorhodopsin adsorbed to a BLM was studied after excitation with a short laser flash [Bamberg *et al.* 1979]. Although BLMs have many attractive properties and are useful for increasing the understanding of processes across membrane surfaces, they also have limitations, e.g., a BLM formed in the conventional manner is an extremely fragile structure with a limited lifetime. Also, caged compounds are not available for all substrates of interest. Therefore, BLMs on solid-supports [Florin & Gaub 1993, Seifert *et al.* 1993] have been developed in combination with a rapid solution exchange technique [Pintschovius & Fendler 1999]. With this technique, it is possible to combine the high sensitivity BLMs with the stable properties of solid supported membranes (SSM). Furthermore, the introduction of the rapid flow technique allows to measure pre-steady state currents with a high time resolution [Pintschovius & Fendler 1999].

Recently, the SSM method has proven to be useful for the investigation of electrogenic events associated to partial steps of the Na^+ melibiose symport reaction [Ganea *et al.* 2001]. A co-substrate concentration jump was found to give rise to a transient current corresponding to inward movements of positive charges. Transient signals with bi-exponential decays were observed by imposing either a simultaneous Na^+ and sugar concentration jump (ΔNaΔmel), a Na^+ concentration jump on liposomes already equilibrated with melibiose (ΔNa(mel)), or a melibiose concentration jump on liposomes already equilibrated with Na^+ (Δmel(Na)). The biphasic decay could be decomposed into a fast ($\tau_1 \sim$ 10-20 ms) and a slow component ($\tau_1 \sim$ 300-400 ms). Applying a melibiose concentration jump in the absence of Na^+ (Δmel), i.e., when the transporter functions in the H^+-transport mode, gave rise to a transient signal with a

biphasic decay, but the fast component was much slower ($\tau_1 \sim 100$ ms). In contrast, a simple Na^+ concentration jump (ΔNa), a situation in which no flow of substrates across the membrane is expected, resulted in mono-exponentially decaying signals ($\tau_1 \sim 10$ ms). This, and the fact that the slow component was suppressed by selective inactivation of cosubstrates translocation with NEM [Ganea *et al.* 2001, Lopilato *et al.* 1978] led to the conclusion that the fast component is associated to a substrate binding process, and the slow component, in the following also termed transport component, to the stationary transport activity of the permease.

1.6.2 Measurements of Fluorescence Changes

Changes in fluorescence can be measured on a millisecond time scale by the stopped-flow method (see also 2.6.1). This approach is especially interesting for studying the kinetics of ligand-binding, e.g., in the galactose/H^+ symporter (GalP) the binding kinetics of transport inhibitors were investigated [Martin *et al.* 1995]. The stopped-flow method was also applied to resolve reaction kinetics of different sugar transporters (review in [Walmsley *et al.* 1994]), the Ca-ATPase [Champeil *et al.* 1997], and of the Na^+,K^+-ATPase by using the voltage-sensitive fluorescent dye RH 421 [Clarke *et al.* 1998, 2003, Kane *et al.* 1997]. Voltage-clamp fluorometry (VCF), originally used to study conformational changes in potassium channels during the gating process [Mannuzzu *et al.* 1996], is an interesting approach to directly monitor real-time fluorescence changes at the same time as electrical changes. Recently, VCF was used to study SGLT1 [Meinild *et al.* 2002], GAT 1 [Li *et al.* 2000], the serotonin transporter [Li *et al.* 2002], and the Na,K-ATPase [Dempski *et al.* 2005, Geibel *et al.* 2003].

1.7 Why Study Transport by MelB? Objectives and Outline of the Thesis

Co-transporters catalyzing specifically the transfer of organic substrates and ions across membranes are of primary importance for the life of cells. One of these co-transporters, the melibiose permease (MelB) of *E.coli*, is a particularly interesting protein for studying the transport mechanism, as it uses several different cations and sugars as substrates. Furthermore, it is easily available in a purified and reconstituted form [Pourcher *et al.* 1995] and shares structural and functional features with other Na^+/solute co-transporters that play key functions in biological and medical relevant processes. Although such transport systems are very important, the knowledge about their reaction mechanism is limited and, thus, understanding the structure-function relationship remains an important challenge. The overall interest in the melibiose permease is of more fundamental nature, and understanding the transport mechanism in more detail would help to formulate general principles that could also be applied to eukaryotic transporters involved in pathophysiological processes.

So far, mainly steady-state measurements provided insights into the overall reaction mechanism of MelB (review in [Pourcher *et al.* 1990a]). Recently, the purified and reconstituted MelB, adsorbed onto solid supported membranes, proved to be a promising tool for its investigation by the electrophysiological approach [Ganea *et al.* 2001]. Several transition states of the reaction cycle remained, however, uncharacterized. Therefore, the global and primary objective of this thesis is to apply pre-steady state methods for the elucidation of reaction rates of individual steps in the cycle of MelB.

The orientation of the protein in the liposomes is a critical factor for its activity, as the kinetics of binding and translocation are different for the opposite directions of transport [Pourcher *et al.* 1990a]. However, the orientation of purified MelB in the liposomes was, so far, unknown, and the observed electrical behavior [Ganea *et al.* 2001] could not be assigned to a single population of the transporter. Therefore, the first issue of the thesis is to determine the orientation of the transporters in the liposomes, whereby the approach of site-directed labeling of single Cys-mutants should be applied. Furthermore, Ile-53, which could be selectively inhibited from one side [Matsuzaki *et al.* 1999], should be constructed, purified and reconstituted into liposomes allowing to study only one population of the transporters.

The electrical approach of pre-steady state measurements should help understanding an unexpected result of previous measurements [Ganea *et al.* 2001], i.e., a melibiose

concentration jump imposed on liposomes already equilibrated with Na^+ triggered transient electrical signals that also included a fast component. Since the sugar is an uncharged species, interpretation of the fast component is not straightforward. Therefore, the melibiose induced electrical signal in proteoliposomes equilibrated with Na^+ should be studied in detail.

For getting detailed understanding of the underlying molecular functioning of MelB, it is, furthermore, necessary to identify single amino acids, which play a role during substrate binding and/or translocation. Therefore, molecular biology methods, i.e., the approach of Cys-scanning mutagenesis, should be applied to MelB, and functionally important amino acids converted into Cys residues. Since in previous studies loop 4-5 of MelB was identified to play a crucial role in co-substrate translocation [Abdel-Dayem *et al.* 2003, Séry 2002], the functional consequences of mutating especially Arg-141 and Glu-142 into Cys should be studied by the SSM technique. E.g., dependencies of the concentration on the peak current indicate affinities of the substrates for the respective mutant, and modified charge translocation properties could provide information on altered steps in the reaction cycle. Further single Cys mutations of MelB should be made to clarify the role of two amino acids for MelB functioning, i.e., Asn-58, which was implied in the process of Na^+ recognition [Hama & Wilson 1994], and Gly-117, which might, as a member of helix IV, play a role in connecting the cation and sugar binding site [Cordat *et al.* 2000].

The stopped-flow technique, able to detect reactions even if they are electroneutral with a time resolution of up to 1 ms, should, furthermore, help to characterize the melibiose-induced conformational transition in more detail. Different fluorescence approaches should be followed to study the kinetics of the melibiose induces conformational change into more detail. First, the changes of the intrinsic Trp fluorescence of the protein, known to change upon addition of Na^+ and melibiose [Mus-Veteau *et al.* 1995], should be studied, and second, the changes of the fluorescent sugar analog dansyl galactoside monitoring events occurring at the sugar binding site [Maehrel *et al.* 1998]. Third, a mutant, which functions similar to the C-less mutant should be selectively labeled by fluorescence dyes and melibiose concentration jumps studied by pre-steady state fluorescence measurements.

Finally, it should be elucidated whether the application of two real time techniques used to study the same reaction allows the correlation of charge translocation with fluorescence changes.

2 Material and Methods

2.1 *Preparation of Proteoliposomes*

In the first part of this chapter, methods for gene mutagenesis and protein purification are described. Figure 2-1 shows the principle of the purification protocol including representative illustrations of protein analysis by sodium dodecyl sulfate polyacrylamide gel electrophoresis (SDS-PAGE) and gel filtration. If not otherwise stated, chemicals were obtained from commercial sources.

2.1.1 Bacterial Strain and Plasmids

E.coli DW2-R, a *recA*⁻ derivative of strain DW2 (*mel*A⁺, Δ*mel*B, Δ*lac*ZY) was used throughout the whole study [Botfield & Wilson 1988]. This strain is devoid of internal melibiose and lactose permease, but encodes for α-galactosidase. Preparation of competent cells was achieved by treating *E.coli* with calcium and rubidium chloride [Kushner 1978, Mandel & Higa 1970].

For transformation, the vector pK95ΔAHB, derived from pKK 223-3 (Pharmacia, Uppsala, Sweden) was purified by using the Qiagen Plasmid Maxi Kit (Qiagen, Hilden, Germany). pK95ΔAHB carries an ampicillin resistance and the wild-type or mutated *melB* gene under the control of the tac promoter [Mus-Veteau & Leblanc 1996, Pourcher *et al.* 1995]. *melB* is terminated by six successive triplets encoding His residues at its 3' extreme.

2.1.2 Bacterial Culture

E.coli DW2-R bacteria were transformed with the plasmid containing wild-type or any mutated *melB* (see 2.1.3) by using a heat-shock at 42°C [Mandel & Higa 1970]. Transformed cells were plated on MacConkey agar plates (containing 10 mM melibiose and 100 μg/mL ampicillin) and incubated overnight at 37°C. When melibiose was transported by the permease, it was hydrolyzed by α-galactosidase (encoded by the *melA* gene) into glucose and galactose. In response to the acidic by-products of sugar metabolism, the respective colonies turned red. In absence of melibiose transport, e.g., if a mutated transport-deficient *melB* gene was transformed into the bacteria, white colonies were observed.
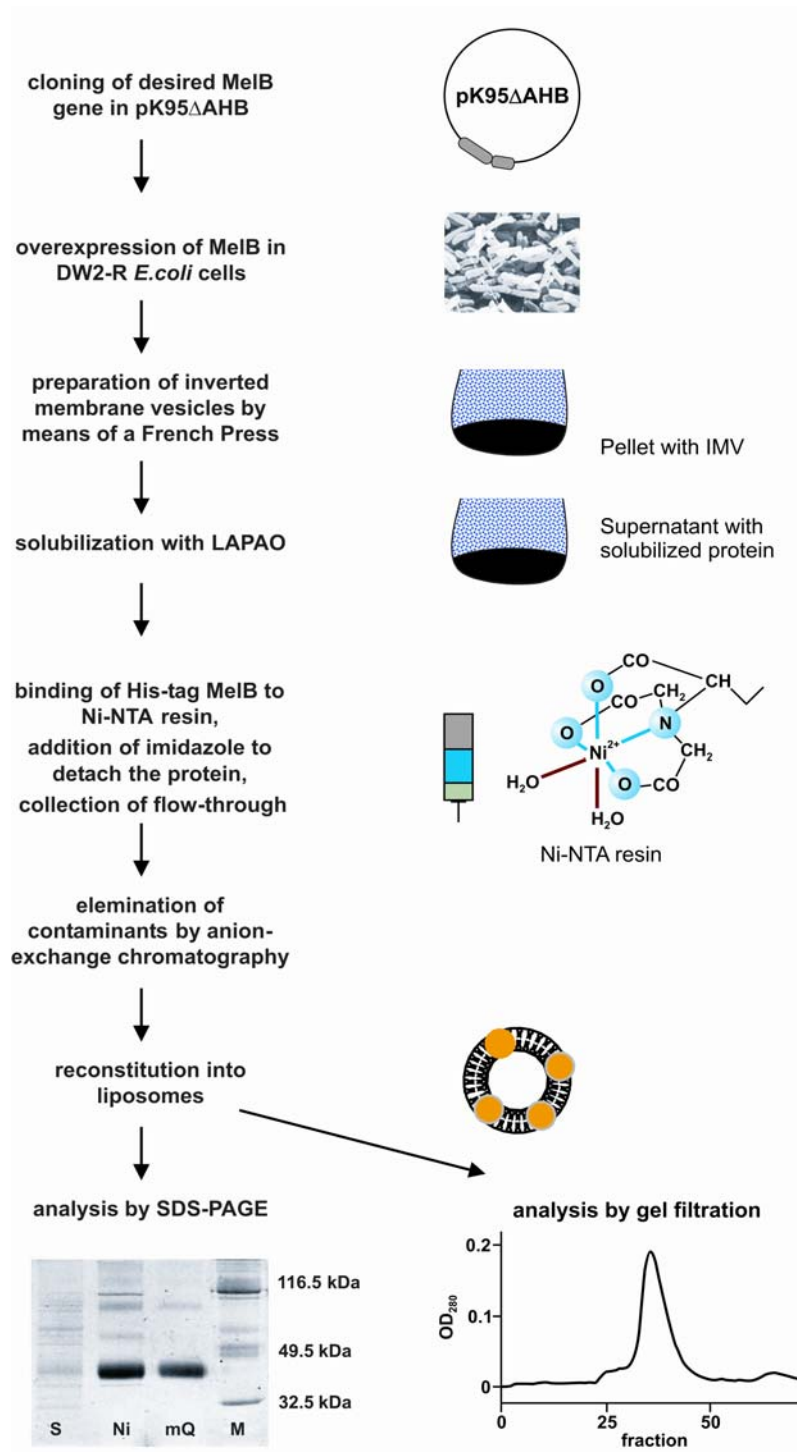
Figure 2-1. Flow chart of the protein purification procedure.

Consecutive steps of the protein purification procedure are shown on the left and the respective schematic image on the right. For the SDS-PAGE as well as for the gel filtration the mutant R139C was used.

For SDS-PAGE (12%), samples were denatured prior to the electrophoresis, and the gel was directly stained with SYPRO Orange. The bands were visualized with a UV detector. S: solubilized protein; Ni: protein after Ni-affinity chromatography; mQ: protein after anion-exchange chromatography; M: molecular weight marker.

The gel filtration was done on a Superdex^{TM} 200 column and the absorbance recorded at 280 nm.

Cells were selected and incubated at 30°C in Luria-Broth (LB) rich medium (10 g/L bacto tryptone, 5 g/L bacto yeast extract, 5 g/L NaCl). 100 µg/mL ampicillin were added to the medium in order to maintain the selection pressure. This pre-culture was used either to isolate plasmid DNA for sequencing or as inoculate for large scale cultures.

In the latter case, cells were incubated in 200 L (wild-type, C-less permease, and R141C) or 12 L (all other mutants) M9 minimal medium (6 g/L Na_2HPO_4, 3 g/L KH_2PO_4, 0.5 g/L NaCl, 1 g/L NH_4Cl) with the addition of 5 g/L glycerol, 1 mM $MgSO_4$, 0.1 mM $CaCl_2$, 1 mM thiamine, 2 g/L casamino acid, and 100 µg/mL ampicillin. Cells were grown at 30°C under continuous shaking until an OD_{600nm} of 1-1.2 was reached. Large scale cultures (200 L) were carried out at the Centre de Fermentation, Centre National de la Recherche Scientifique, Marseille, France. Cells were harvested, resuspended in 100 mM KH_2PO_4 (potassium phosphate buffer, KPi) buffer, pH 7.0, directly used, or stored in the presence of 15% glycerol at -80°C until further use.

2.1.3 Site-directed Mutagenesis

Base substitution mutations were introduced by the polymerase chain reaction (PCR) overlap extension method [Higuchi *et al.* 1988]. pK95ΔAHB with a cassette containing the *melB* gene [Mus-Veteau & Leblanc 1996, Pourcher *et al.* 1995] that encodes a permease devoid of its four native cysteines (C-less permease) was used as matrix. This C-less carrier contains a valine instead of Cys-235 and serines instead of Cys-110, Cys-310, and Cys-364 [Weissborn *et al.* 1997]. The *melB* gene sequence contains appropriately distributed unique restriction sites (about every 250 bp) that facilitate exchange of specific stretches of the MelB nucleotide sequence during mutagenesis.

Two separate PCRs were performed, each using a perfectly complementary primer at the end of the sequence, called external *melB* specific primer, and a mismatched primer (sense or antisense primer, respectively) designed to introduce a mutation at a specific point. Primers were 27 to 30 nucleotides in lengths (Sigma-Genosys Ltd, Havervill, UK). DNA was amplified in a final volume of 100 µL in a Hot Start® Storage and Reaction Tube (MolecularBio Products, San Diego, CA, USA) containing 1X reaction buffer (10 mM Tris-HCl (pH 8.85), 25 mM KCl, 5 mM $(NH_4)_2SO_4$, and 2 mM $MgSO_4$), 6% DMSO, 3% glycerol, 0.4 mM of each dATP, dCTP, dGTP, and dTTP, and 400 pmol of each primer. 2.5 units of PWO DNA Polymerase (Roche, Mannheim, Germany) were added directly before starting the PCR. Samples were subjected to the PCR in a RoboCycler® Gradient 40 Thermocycler (Stratagene,

La Jolla, CA, USA) following the temperature program as indicated: denaturation at 98°C for 1 minute, followed by five cycles at 98°C for 1 minute, 56°C for 1 minute, and 68°C for 1 minute, and 25 cycles at 95°C for 1 minute, 56°C for 1 minute, and 68°C for 1 minute, and a final extension step at 68°C for 7 minutes. These PCRs resulted in two overlapping fragments each containing the base substitution.

Amplification products were separated on 1% agarose gels in TAE-buffer (20 mM Tris-acetate and 0.5 mM EDTA, pH 8.3) (Life Technologies Inc., Rockville, MD, USA), and the desired fragments purified by using the QIAquick Gel Extraction Kit (Qiagen, Hilden, Germany). In a second PCR tour, the two purified fragments generated with the sense and antisense primers, respectively, were annealed together, and the two correspondent external primers were used to amplify the complete mutated gene. Conditions were as described for the first PCR. The desired products were separated on 1% agarose gels and purified as described above.

The final PCR product was subjected to restriction endonuclease digestion using adequate restriction enzymes (37°C for 2 h). The plasmid pK95ΔAHB was digested with the same restriction enzymes. Afterwards, the purified fragments were ligated with the plasmid overnight at 15°C using T4 DNA ligase (New England Biolabs Inc., Beverly, MA, USA).

The plasmid was transformed into *E.coli,* plated on MacConkey agar plates, the colonies were selected, a pre-culture done, and the plasmids afterwards purified with the QIAprep Spin Miniprep (Qiagen, Hilden, Germany).

Mutations were verified by dideoxy sequencing using ^{35}S-labeled dATP and the T7 Sequenase DNA sequencing kit, version 2.0 (USB Corporation, Cleveland, OH, USA) with appropriate *melB* specific primers [Sanger & Coulson 1978, Sanger *et al.* 1977].

Site-directed mutants are designated by the one-letter amino acid code followed by a number indicating the position of the residue in wild-type MelB and a second letter denoting the amino acid replacement at this position.

2.1.4 Protein Purification

Inverted membrane vesicles (IMVs) were prepared using a French-press procedure [Hertzberg & Hinkle 1974, Reenstra *et al.* 1980]. All steps were carried out at 0-4°C. Approximately 60 g (wet weight) of wild-type or mutated bacteria were rapidly thawed at 30°C and rinsed several times in a buffer containing 50 mM Tris-HCl (pH 8), 50 mM NaCl, and 5 mM β-mercapto-ethanol. Cells were resuspended at 5 mg/ml in the same buffer supplemented with 5 mM EDTA for destabilization of the external bacterial membranes. Directly before applying a pressure of 1200 psi by means of a French Press at 0-4°C (American Instruments Company, Silver Spring, Maryland, USA), 20 µg/mL of each DNAse and RNAse (Boehringer Mann-heim, Ingelheim, Germany) as well as 15 mM MgSO$_4$ were added to the cell suspensions. An excess of EDTA (15 mM) was then added to the product of the French Press and unbroken cells and large debris were eliminated by centrifugation at 4000 × g (Jouan CR 412, Saint-Herblain, France). The supernatant containing the IMVs was collected and washed several times with buffer (50 mM Tris-HCl (pH 8), 50 mM NaCl, and 5 mM β-mercaptoethanol) by centrifugation at approximately 500,000 × g at 4°C for 30 minutes (Beckmann Instruments XL-80 Ultracentrifuge, rotor 70Ti, Palo Alto, CA, USA). Finally, vesicles were resuspended in the same buffer and stored at -80°C until further use.

Protein purification was carried out mainly as described [Pourcher *et al.* 1995]. IMVs were thawed at 30°C and washed once in 600 mM NaCl, 20 mM Tris-HCl (pH 8), 5 mM β-mercaptoethanol, and 10 % glycerol. All following steps were performed at 0-4°C. After centrifugation at 500,000 × g for 20 minutes (Beckmann Instruments XL-80 Ultracentrifuge, rotor 70Ti, Palo Alto, CA, USA), the pellet was resuspended in a buffer of 10% glycerol, 600 mM NaCl, 20 mM Tris-HCl (pH 8), 5 mM β-mercaptoethanol, 10 mM imidazole, and 20 mM melibiose at a concentration of approximately 5 mg protein/mL and solubilized by the addition of 1% 3-(laurylamido)-*N,N'*-dimethylaminopropylamine oxide (LAPAO) [Brandolin *et al.* 1980] during 10 minutes on ice. In the following centrifugation for 30 minutes at 500,000 × g, the cell debris was eliminated. The supernatant (containing the solubilized protein) was incubated with Ni-nitrilotriacetic acid (NTA) resin (Qiagen, Hilden, Germany, pre-equilibrated with 10% glycerol, 600 mM NaCl, 20 mM Tris-HCl (pH 8), 5 mM β-mer-captoethanol, 10 mM imidazole, 0.2% LAPAO, and 20 mM melibiose) at a concentration of 25 mL resin/g membrane vesicle protein. After incubation for 1 hour under gentle agitation, the resin with the adsorbed material was centrifuged at 4000 × g (Jouan CR 412, Saint-

Herblain, France), washed once with the same medium, and loaded onto a fast protein liquid chromatography column (Waters 650E Advanced Protein Purification System, Millipore Corporation, Milford, MA, USA). Detergent exchange was carried out on the column by progressively replacing the buffer containing 0.2% LAPAO by 0.1% n-dodecyl-β-D-malto-side (DDM) (Boehringer Mannheim, Ingelheim, Germany) using the same background buffer by means of a linear gradient (50 mL), and terminated by an additional wash with the same buffer (50 mL). NaCl was progressively eliminated by means of a linear grading using the same buffer with a reduced NaCl concentration (50 mM) and DDM (0.1 %), respectively. A final wash of 40 mL was applied before rising the imidazole concentration to 100 mM to allow adsorbed proteins to detach from the column. For the purification of mutated MelB the final buffer contained additional 50 or 100 mM NaCl. When bacterial cultures of 12 L were done, protein purification was performed on columns with a volume of 10 mL (BioRad, Hercules, CA, USA) and buffer exchange done manually.

After evaluation of the flow-through by means of a D_2-lamp at 280 nm (Uvikon 820 Kontron®️ Spectrophotometer, Watford, UK), the fractions containing proteins were pooled and contaminating proteins were eliminated by applying it to a Macro-Prep-High-Q anion exchange support (Biorad, Hercules, CA, USA) pre-equilibrated with the elution buffer from the Ni-NTA column. Using the same buffer as for the elution of proteins after the Ni-column, high-purity MelB was obtained with the flow-through, whereas the contaminating proteins remained attached to the column.

2.1.5 Reconstitution

The pooled fractions containing the purified MelB were incubated for 15 minutes in the presence of a five-fold excess of total *E.coli* lipids (Avanti Polar Lipids Inc., Alabaster, AL, USA). Pre-washed Bio-beads SM-2 (BioRad, Hercules, CA, USA) were stepwise added at a concentration of 120 mg/mL solution to adsorb the detergent and the sample was incubated overnight at 4°C [Allen *et al.* 1980, Rigaud *et al.* 1988]. The proteoliposomes were washed twice in a 100 mM KPi buffer (pH 7), which was nominally Na^+ free (high purity grade, Suprapur, Merck, Darmstadt, Germany). Na^+ trapped in the vesicles was washed out by repeated freeze-thaw-sonication-wash cycles in 100 mM KPi buffer. Finally, proteoliposomes were collected by centrifugation at 500,000 × g for 30 minutes (Beckmann Instruments XL-80 Ultracentrifuge, rotor 70Ti, Palo Alto, CA, USA) and resuspended in the same buffer at a concentration of around 1 mg protein /mL. All steps were performed at 0-4°C.

2.1.6 Determination of Protein Purity

Purity and possible dimerization of proteins in the preparation were checked by gel filtration on a Superdex^{TM} 200 column (Amersham Pharmacia Biotech, Uppsala, Sweden) with a flow-through of 0.35 mL/min (see also Figure 2-1 for an example of the R139C mutant).

Additionally, proteins were separated by SDS-PAGE (12 %) [Laemmli 1970] and directly stained with SYPRO Orange protein gel stain in 7.5% acetic acid during 30 minutes in the dark (BioRad, Hercules, CA, USA). The bands were visualized by an ultraviolet (UV) detector and recorded with a digital camera (Figure 2-1).

Protein quantity was assayed according to Lowry [Lowry 1951] in the presence of 0.2% SDS using bovine serum albumin (BSA) as standard.

2.2 Transport Assay

Freshly grown bacteria were collected, washed several times with a Na$^+$ free buffer (100 mM KPi, pH 7.0), prepared with high purity salts (Merck, Darmstadt, Germany), resuspended in the same buffer and adjusted to an OD$_{600nm}$ of 2.2 – 2.4. According to the different transport modes of MelB, no salts, 10 mM NaCl, or 10 mM LiCl were added, respectively. 50 μL of bacteria were incubated at room temperature and the uptake reaction was initiated by adding 0.4 mM [^{3}H]melibiose (20 mCi/mmol, synthesis was carried out by Dr. B. Rousseau and Y. Ambroise from the Département de Biologie Joliot Curie/CEA Saclay, France) to the cells followed by vigorous mixing with a vortex mixer. Additional oxygen was provided to all cells during the assay. After 1, 3, 6, and 10 minutes the reaction was terminated by addition of a stop solution (100 mM Kpi, 100 mM KCl, pH 5.5) followed immediately by a rapid filtration through a pre-wetted Whatman GF/F filter (Whatman International Ltd. Maidstone, England) and an additional wash step of 2 mL stop solution. Radio-activity, accumulated by the cells and, thus, transported, was maintained in the filter whereas non-accumulated radioactivity passed through the filter. The filters were counted during 3 minutes in a Tri-Carb$^®$ 1900CA Liquid Scintillation Analyzer (Packard BioScience Company, Meriden, CT, USA). A blank value was obtained by adding the transport medium directly before filtration to the protein free reaction tube. The blank value was subtracted from measurements associated with membrane vesicles to determine uptake rates expressed as nmole/mg protein/time.

2.3 Orientation Assay

2.3.1 Semi-Quantitative Approach

Proteoliposome suspensions containing purified single Cys R139C or R141C MelB (0.25 mg of protein/mL, in 100 mM KPi, pH 7) were supplemented with 10 µM 3-(N-maleimidyl-propionyl)biocytin (biotin maleimide, MPB, Molecular Probes, Inc., Eugene, OR, USA [Bayer *et al.* 1995]), and incubated for 5 minutes at room temperature. MPB was added from a stock prepared in dimethyl sulfoxide (DMSO). The concentration of DMSO in the labeling medium did not exceed 1% (v/v). Some samples were afterwards subjected to three cycles of freeze-thaw-sonication in the presence of MPB. Where indicated, samples were pretreated with 200 µM of the membrane impermeant thiol reagent 4-acetamido-4'-maleimidylstilbene-2,2'-disulfonate (stilbene disulfonate, Molecular Probes, Inc., Eugene, OR, USA) for 10 min. at room temperature. Stilbene disulfonate was washed away by three cycles of centrifugation with 100 mM KPi, pH 7. As negative control, the C-less transporter was incubated with varying concentrations MPB (0 – 1000 µM) and subjected to three cycles of freeze-thaw-sonication. The MPB labeling reaction was stopped by the addition of 10 mM dithio-threitol (DTT) to the samples. All samples were solubilized in 1% SDS and subjected to SDS-PAGE (10%) [Laemmli 1970].

The amount of protein and the labeling-reaction of the protein with MPB were estimated by Western-Blot analysis [Gershoni & Palade 1982, Towbin *et al.* 1979]. A streptavidin-alkaline-phosphatase conjugate (Molecular Probes, Inc., Eugene, OR, USA) was used for the specific reaction with MPB and a MelB specific monoclonal antibody "21E4" (generated by Biocytex, Marseille, France), coupled directly to an alkaline phosphatase (Davids Biotechnologie, Regensburg, Germany) for the determination of the amount of protein. Antibodies were used in a 1:1000 dilution. An alkaline phosphatase conjugate substrate kit (BioRad, Hercules, CA, USA) was used to visualize the bands.

2.3.2 Quantitative Approach

The proteoliposomes (ca. 5 µg) were incubated with a His-biotin-antibody conjugate (Qiagen, Hilden, Germany) in a 1:1.5 molar ratio for 2 hours at 4°C in a 200 µL reaction volume (in 20 mM Tris-HCl, 500 mM NaCl, pH 7.4, 0.1% BSA, 0.05% Tween). The His-tag of the protein is located at the C-terminus of the transporter and is physiologically oriented to the cytoplasm of the bacterium, thus all inside-out orientated transporters were labeled. The

unbound antibody was removed by washing the liposomes three times by centrifugation (30 minutes, 4°C, 70,000 × g) with tris buffered saline (TBS) buffer. Afterwards, the proteoliposomes were solubilized during 10 minutes on ice by using 1% dodecyl-maltoside in TBS. The solubilized protein was divided into two portions: the reference (labeling of all transporters) was incubated again with the His-biotin antibody conjugate, to the inside-out labeled portion the same amount of buffer was added. Labeling was allowed to proceed for 2 hours at 4°C. Since the His-biotin antibody conjugate contains also a biotin-label, these mixtures could be bound to a NeutrAvidin™ coated plate (Pierce, Rockford, IL, USA). Binding was allowed to proceed for 2 hours at room temperature in the same buffer used for antibody binding. The MelB-specific antibody "21E4" (4 times molar as compared to the protein on the plate) was added and incubated during 2 hours at room temperature. The MelB antibody contains a coupled alkaline phosphatase, therefore, the 1-Step™pNPP (Pierce, Rockford, IL, USA) was used as substrate. The absorbance was measured after 15 minutes with a spectrophotometer (DU® 7500 spectrophotometer, Beckmann Instruments, Palo Alto, CA, USA) at 405 nm. As control, empty liposomes were incubated with the antibody and treated as the proteoliposomes.

2.4 Current Measurements with the SSM Technique

2.4.1 Theoretical Background of the SSM Method

One approach to generate stable lipid membranes on solid supports is the use of self-assembled long chain alkanethiol monolayers anchored to a gold surface via the sulfhydryl group. Addition of lipid to this monolayer results in the formation of a bilayer, on which either membrane fragments or proteoliposomes can be adsorbed. The SSM was characterized in detail [Florin & Gaub 1993, Seifert *et al.* 1993] and combined with a rapid solution exchange technique [Pintschovius & Fendler 1999] giving an interesting tool for the investigation of pre-steady state charge translocation of membrane transporters. It acts not only as carrier for proteoliposomes, but also as a high-capacitance, low conductance electrode. The flow technique allows one to generate virtually any substrate concentration jump on the surface of the SSM/proteoliposomes system evoking transient currents by the transporter, which can be recorded with a high time resolution.

Proteoliposomes adsorbed to the SSM can be depicted by an equivalent circuit (Figure 2-2). Simplified, the SSM can be represented by a capacitor (C_m) in parallel with a resistor (R_m).

SSM and proteoliposomes, together also called compound membrane [Seifert *et al.* 1993], are capacitively coupled and are connected in series. Since lipid layers are isolators, the SSM has, ideally, no conductance and carries, therefore, only capacitive currents. The charge translocation over the liposome membrane evoked by the proteins generates also charge translocation at the SSM by means of the mutual capacitance between the circuits and can be recorded as current response I(t). Because of the capacitive coupling of the liposome via the SSM, steady-state turnover does not generate a stationary current but rather results in a transient electrical signal decaying with the system time constant, which describes the charging of the compound membrane [Pintschovius & Fendler 1999].

The SSM technique as described was successfully used to investigate electrogenic reactions of the Na,K-ATPase [Pintschovius & Fendler 1999, Pintschovius *et al.* 1999, Tadini-Buoninsegni *et al.* 2003], the Ca-ATPase [Bartolommei *et al.* 2004, Buoninsegni *et al.* 2004], the melibiose permease [Ganea *et al.* 2001], the proline transporter [Zhou *et al.* 2004], the ADP/ATP carrier [Gropp *et al.* 1999], and the F_0/F_1 ATPase [Burzik *et al.* 2003]
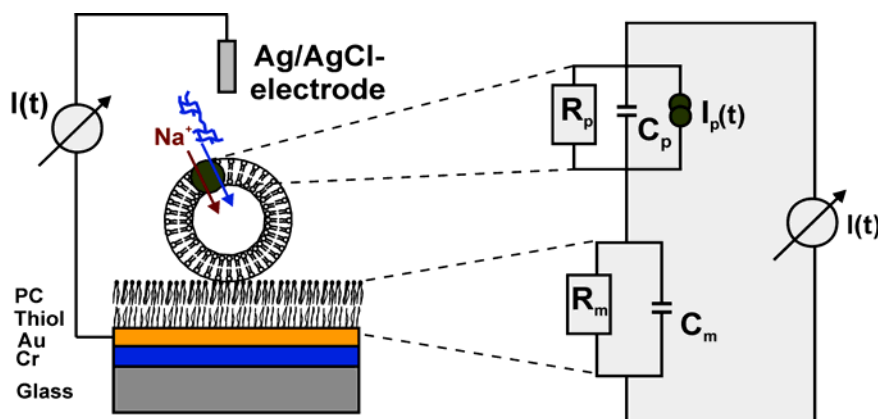
Figure 2-2. Structure and equivalent circuit of the solid supported membrane.

Left. The SSM consists of a glass support (1 mm), a chromium layer (Cr, 5 nm), a gold layer (Au, 150 nm), an octadecyl mercaptan monolayer (Thiol), a diphytanoyl phosphatidylcholine monolayer (PC), and the proteoliposomes.

Right. Equivalent circuit for the SSM with proteoliposomes adsorbed onto it. The SSM can be represented by a capacitor (C_m) in parallel with a resistor (R_m). Likewise, proteoliposomes are depicted as capacitor (C_p) in parallel with a resistor (R_p) and I_p, which represents the current generated by all transporters after their activation. I(t) is the current measured in the external device.

2.4.2 Material and Apparatus Used for the SSM Technique

Table 2-1. Apparatus Used for the SSM

Apparatus	Manufacturer
one-way valve, model 225T011, 12 VDC	NResearch, Mapelwood USA
3×3 valve, model 360T051, 12 VDC	NResearch, Mapelwood USA
simple 3-way valve, model 225T031, 12VDC	NResearch, Mapelwood USA
Current Amplifier, model 427	Keithly Instruments Inc., Cleveland Ohio, USA
Laboratory Power Supply PS-302A	Conrad Electronic GmbH, Hirschauonic, Germany
Power Supply FPS 4A, 13.8 V	Voltacraft GmbH, Germany
Valve driver	Self-made, Max-Planck-Institute for Biophysics, Frankfurt, Germany
Nitrogen, quality 4.0, UN 1066	Messer Griesheim GmbH, Germany
Digital Manometer GHD 14 AN	Greisinger-electronic GmbH, Regenstauf, Germany
Digital Oscilloscope, 3091	Nicolet, Madison, USA
Tygon and Teflon tubes	Reichelt, Heidelberg, Germany, and Cole Parmer Instruments Company, Vernon Hills, Illinois, USA
AD/DA card, AT-DIO-32-HS	National Instruments, Austin, TX, USA
Reference voltage generator	Self-made, Max-Planck-Institute for Biophysics, Frankfurt, Germany

If not otherwise stated, materials were obtained from commercial sources.

2.4.3 Preparation of Gold Electrodes

Gold electrodes were produced on cleaned glass plates in an evaporation device (MED 020, Balzers, Liechtenstein) at a pressure of $< 1*10^{-5}$ mbar. The glass surface was covered with a layer of 5 nm chromium before a gold layer (purity $> 99.9985\%$, Alfa Aesar, Karlsruhe, Germany) of 150 nm was deposited. The exact shape of the electrodes was obtained by positioning a 1 mm thick aluminium mask on the glass surface before starting the evaporation process. Finally, the electrodes were incubated in an ethanolic solution of 1 mM octadecyl mercaptan ($CH_3(CH_2)_{16}CH_2SH$, Aldrich, Steinheim, Germany) for 6 h at room temperature resulting in a monolayer of octadecyl mercaptan on the gold surface. The glass plates were stored in 10 µM octadecyl mercaptan until further need. Before use, they were cut into

individual electrodes, rinsed with ethanol, dried, and stored dust-free up to too weeks [Pintschovius & Fendler 1999, Seifert *et al.* 1993]. For experiments with E142C, ready-to-use gold electrodes were purchased (IonGate Biosciences GmbH, Frankfurt, Germany).

2.4.4 The Setup

The SSM, mounted in a flow-through cuvette, acted as working electrode, while an Ag/AgCl electrode was employed as reference electrode. The reference electrode was mechanically separated from the streaming solution by a polyacrylamide gel bridge and connected to the electrical circuit (see also Figure 2-3 for more details and [Pintschovius & Fendler 1999, Seifert *et al.* 1993]). Data acquisition and operation of the experimental setup were controlled via a computer using a homemade program based on LabView® (Version 4.1, National Instruments, Austin, TX, USA, the program was made by D. Zuber). If not otherwise stated, the experiments were carried out at room temperature (ca. 20-24 °C).
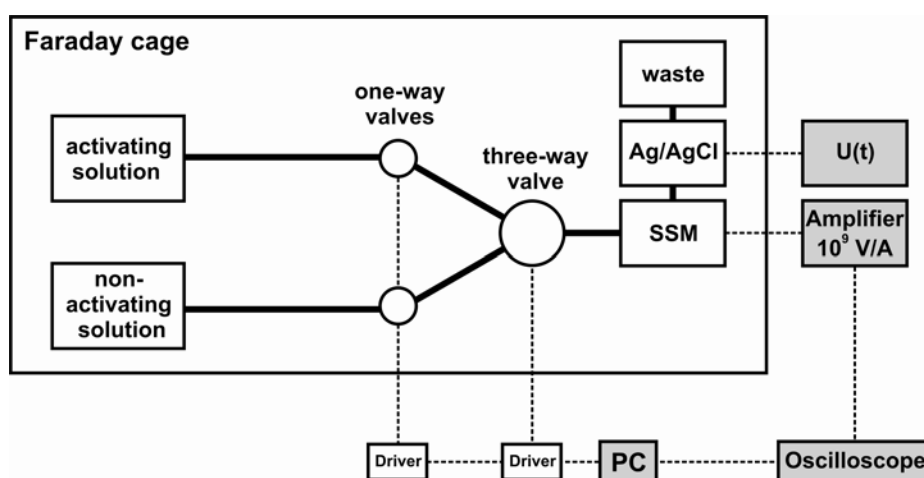
Figure 2-3. The SSM setup.

The solution containers, the electrical valves, and the SSM cuvette with the reference electrode are located in a Faraday cage. Solutions are driven through the cuvette by opening the one-way valves and applying a pressure of 0.6 bar to the containers [Ganea *et al.* 2001]. The flow of the solution starts, when the simple one-way flow-through valves are opened. A 3×3 valve [Pintschovius & Fendler 1999] or a simple three-way valve are used to switch the solution stream from the non-activating to the activating solution. The current signals, generated by the transporters, are amplified by an operational amplifier (10^9 V/A), filtered (low-pass, 1-10 ms), and visualized with an oscilloscope. Data recording, and electrical valves are controlled by the computer. Capacitance and conductance of the membrane are measured using the voltage source U(t) connected to the Ag/AgCl electrode.

2.4.5 Preparation and Characterization of the SSM

The lipid solution contained diphytanoyl phosphatidylcholine (PC, synthetic, Avanti Polar Lipids Inc., Pelham, AL, USA) and octadecylamine (60:1, wt/wt, 98%, Riedel-DeHaen AG, Seelze, Germany) in 1.5% n-decane [Bamberg *et al.* 1979]. To produce the bilayer, the mercaptan treated gold surface was covered with 3 μL of this lipid solution. The effective membrane had an area of around 1 mm^2. The electrode was afterwards mounted in a flow-through plexiglas cuvette with an inner volume of 17 μL. After the formation of the SSM, its capacitance and conductance were measured in order to ensure the correct preparation of the electrodes and the development of the SSM. The rectangular response to a triangular voltage (10 mV peak/peak, 0.5 Hz) and the current response to a 100 mV voltage jump after 1 s were monitored and the capacitance and conductance determined according to the following equations [Pintschovius & Fendler 1999, Seifert *et al.* 1993]:

$$G(1s) = \frac{I(1s)}{\Delta U} \qquad \text{[Equation 1]}$$

$$C = \frac{I_{cap}}{U_0} * \frac{T}{4} \qquad \text{[Equation 2]}$$

where I is the current measured after 1 s and ΔU the applied voltage jump (100 mV), U_0 is the amplitude of the triangular voltage (10 mV) with the period T of 2s, and I_{cap} the measured response current amplitude. 90 minutes after the formation of the SSM the values remained constant with $C = 200 - 400$ nF/cm^2 and $G_{1s} = 10 - 100$ nS/cm^2. The voltage jump and the triangular voltage were applied with a self-made reference current source via the Ag/AgCl electrode. Control experiments were performed on the protein-free SSM (either on the lipid membrane itself or after the addition of protein-free liposomes) in order to exclude solution exchange artifacts. 30 μL of the well-sonicated proteoliposome suspension (containing around 15 μg of purified protein) were added into the cuvette through the outlet channel and allowed to adsorb to the SSM for 45 minutes. After controlling the capacitance and conductance of the compound membrane, the experiments were started.

2.4.6 Measuring Protocol

The solution exchange protocols (Figure 2-4) consisted of three phases: (1) non-activating solution (1 s), (2) activating solution (1 s), (3) non-activating solution (1 s). The solutions contained 100 mM KPi buffer and the activating substrates NaCl and/or melibiose (see indications in the respective figure legends). To minimize ionic strength and osmotic effects, the non-activating solutions contained equimolar concentrations of KCl and/or glucose. Concentration jumps at the beginning of phase 2 (on-signal) and phase 3 (off-signal) caused electrical signals that were recorded via the computer. Only the on-signals will be used for analysis. For inhibition experiments, NEM (Sigma Aldrich, Deisenhofen, Germany) (100 mM stock solution in ethanol) was used at 1 mM in 100 mM KPi by adding it through the external channel to the compound membrane (incubation for 30 minutes). Methanethiosulfonate reagents (MTS, Toronto Research Chemical, Inc., Toronto, Canada) were solubilized in water and added to the proteoliposomes: $MTSEA^+$ ((2-aminoethyl) methanethiosulfonate) from a 100 mM stock solution at a final concentration of 2.5 mM, and $MTSES^-$ ((2-sulfonatoethyl) methanethiosulfonate) from a 500 mM stock at a final concentration of 10 mM.
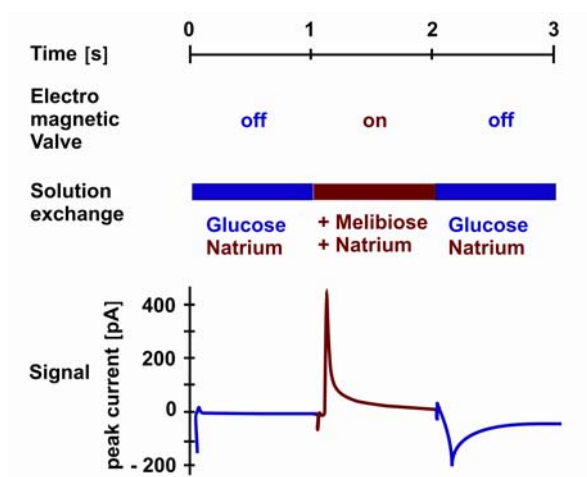
Figure 2-4. Typical Δmel(Na) solution exchange protocol.

The non-activating solution, containing 50 mM glucose and 10 mM Na^+ in 100 mM KPi buffer, pH 7, flowed for 1 s. When the three-way valve was switched (position "on"), the activating solution, where glucose is substituted by the same amount of melibiose, flowed for 1s. Finally, the non-activating solution flowed for 1 s again. The signal shows at 1, 2, and 3 s the artefact of the valve followed by the baseline (the first second), the on-signal (the second second), and the off-signal (the third second). In this thesis, only the on-signal was used for analysis.

2.4.7 Data Analysis

Data analysis was done with the Origin® program, Version 6 and 7 (OriginLab Corporation, Northampton, MA, USA).

Decaying phases of the electrical signals were fitted with a mono- or bi-exponential function as required

$$I(t) = A_1 e^{-(t-t_0)/\tau_1} + A_2 e^{-(t-t_0)/\tau_2}$$ [Equation 3]

where A_1 and A_2 are the amplitudes, t_0 is the x offset, and τ_1 and τ_2 are the time constants.

The dependence of the peak currents from the substrate concentration could be fitted with the function according to Michaelis-Menten

$$I(t) = \frac{I_{max} * [S]}{K_{0.5} + [S]}$$ [Equation 4]

where I_{max} is the maximal peak current at substrate saturation, $K_{0.5}$ the half saturation concentration, S the substrate and I(t) the peak current measured at time t.

The temperature dependency was analyzed by an Arrhenius plot (ln $1/\tau$ versus 1/T). The activation energy (E_a) can be calculated using the slope of the straight line according to

$$slope = -E_a / R$$ [Equation 5]

with the gas constant R of 8.314 J/mol*K.

Furthermore the Q_{10} was determined (with $k = 1/\tau$)

$$Q_{10} = k(T+10)/k(T)$$ [Equation 6]

Any parameters described in this work are, if not otherwise stated, mean values and the standard error (±S.E.) from at least three independent experiments.

2.5 Steady-State Fluorescence Spectroscopy

In the second part of the thesis, fluorescence techniques were used to investigate conformational changes related to ligand binding.

2.5.1 Introduction to Fluorescence Spectroscopic Methods

Fluorescence spectroscopy has been extensively used to study protein dynamics with exquisite sensitivity and selectivity. Generally, intrinsic and extrinsic reporter groups can be distinguished. The aromatic amino acids Phe, Trp, and Tyr, already present in the protein, belong to the intrinsic reporter groups. The advantages of Trp residues, namely that they can be preferentially excited at 297 nm and that the quantum yield and emission maximum are sensitive to the surrounding microenvironment, make it a potentially useful probe to study protein dynamics. When a Trp residue moves, evoked for example by the binding of a ligand, from a polar position, on the surface of the protein, to a more apolar position, buried within the protein interior, an increase in Trp fluorescence can occur. Changes in fluorescence can, therefore, be interpreted as conformational changes of the protein. However, interpretation of the molecular events involved in the conformational change of the protein is difficult when more than one Trp residue contributes to the fluorescence.

Extrinsic probes, attached to the protein, can be used when conformational changes should be detected at a specific site of interest. Extrinsic probes are very useful as long as the label does not significantly affect the structure or activity of the protein. For example, thiol-reactive fluorescent probes can, in combination with single-Cys mutants, modify proteins selectively at defined sites and report local conformational changes upon the addition of substrates. A fluorescence probe cannot only be attached to the protein of interest but also to its substrates, e.g., a dansyl group attached to a ligand can provide a means to assess the physicochemical properties of a potential substrate binding site.

2.5.2 Trp Fluorescence Spectroscopy

A LS50B spectrofluorometer (Perkin Elmer, Inc., Wellesley, MA, USA) was used to measure the intrinsic Trp fluorescence (λ_{ex} 297 ± 5 nm, λ_{em} 310-380 nm) arising from proteoliposomes (20 μg protein per assay in 1 mL KPi, pH 7) [Mus-Veteau *et al.* 1995]. Proteoliposomes were sonicated briefly before they were added to the cuvette. Each spectrum is the mean of three scans. All spectra were baseline-corrected using the fluorescence of the buffer as reference.

Spectra were recorded in the absence of substrates, in the presence of 10 mM NaCl, and in the presence of 10 mM NaCl and 30 mM melibiose. Additions of substrates were made under continuous stirring directly to the cuvette on the same proteoliposome preparation without removing the cuvette from the holder. The emitted fluorescence signal was integrated between 310-380 nm and the fluorescence changes expressed as $\Delta F/F_0$. Values are the mean and S.E. of at least three independent experiments.

2.5.3 FRET Measurements (Trp to Dansyl Galactoside)

Fluorescence resonance energy transfer (FRET) is a non-radiative process, by which the excitation energy can be passed from a fluorescent donor molecule (D) to an acceptor chromophore (A) over long distances, typically 10 – 100 Å. Overlap between the donor emission spectrum with the acceptor absorption spectrum is a prerequisite. For FRET measurements of MelB, a sugar analog carrying a dansyl group was chosen (2'-(N-dansyl) aminoethyl-1-thio-β-D-galactopyranoside (Dns^2-S-Gal)), as the dansyl fluorescence properties depend on solvent polarity providing a means to assess the physicochemical properties of the substrate binding site (or of its immediate proximity) and their variation during catalysis [Maehrel *et al.* 1998].

A LS50B spectrofluorometer (Perkin Elmer, Inc., Wellesley, MA, USA) was used to measure the Na^+-dependent FRET signals (λ_{ex} 297 ± 5 nm, λ_{em} 310-580 nm) arising from proteo-liposomes (20 μg protein per assay in 1 mL KPi, pH 7). Proteoliposomes were sonicated briefly before they were added to the cuvette. Each spectrum is the mean of 3 scans. All spectra were baseline-corrected using the fluorescence of the buffer as reference. The protein was incubated with the sugar fluorescent analog Dns^2-S-Gal at a final concentration of 10 μM. The FRET signal was recorded before and after the addition of 10 mM Na^+, and the Na^+-dependent signal was calculated by subtracting the spectra [Maehrel *et al.* 1998]. For comparison, the specific FRET signals were normalized for variation in the amount of permeases occupied by Dns^2-S-Gal molecules (according to [Cordat *et al.* 1998]). Dns^2-S-Gal synthesis was carried out by Dr. B. Rousseau and Y. Ambroise from the Département de Biologie Joliot Curie/CEA Saclay, France.

2.5.4 Labeling of Proteoliposomes with Extrinsic Probes

Proteoliposomes were thawed and sonicated directly before the fluorescence measurements were performed on a Hitachi F4500 fluorescence spectrophotometer (Tokyo, Japan). 9-Acetoxy-2-(4-(2,5-dihydro-2,5-dioxo-1H-pyrrol-1-yl)-3-oxo-3-H-naphtho[2,1-β] pyran (Thio-Glo3®) (Merck, Biosciences, Darmstadt, Germany) was added from a stock solution at a final concentration of 5 µM, and 2-(4'-maleimidylanilino)naphthalene-6- sulfonic acid (MIANS, Molecular Probes, Eugene, OR, USA) from a stock solution in DMSO at a final concentration of 5 µM. 15 µL proteoliposomes (around 1 mg/mL) in a total volume of 500 µL 100 mM KPi buffer, pH 7 were used (structure of the probes: see Figure 2-5). Both, ThioGlo3® and MIANS are essentially non-fluorescent until they react with Cys residues of the protein, therefore they do not have to be separated after the end of the labeling reaction. After labeling, emission and excitation spectra were recorded to determine maximal wavelengths (see Figure 3-21 for the spectra of the MIANS labeled mutant; for ThioGlo® labeled mutants, the data are not shown). For ThioGlo®, $\lambda_{ex(max)}$ was 365 nm and $\lambda_{em(max)}$ 440 nm. For MIANS, $\lambda_{ex(max)}$ was 328 nm and $\lambda_{em(max)}$ 415 nm. These wavelengths were used to excite (± 5 nm) the protein and record the emission. The baseline signal was recorded and the probe was added directly to the cuvette without removing it from the fluorometer. Fluorescence intensity development was followed during 20 minutes and recorded with the computer. The MIANS labeling reaction was also performed in the presence of substrates, i.e., the proteoliposomes were preincubated with 10 mM Na$^+$ and/or 50 mM melibiose for 10 minutes.
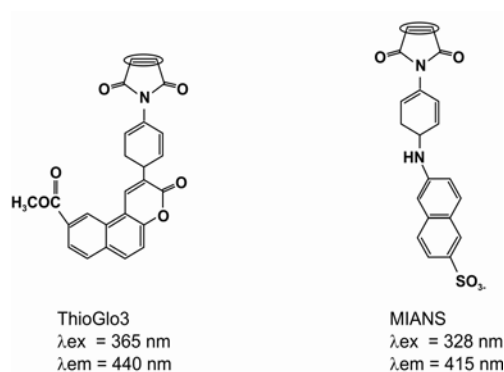
Figure 2-5. Structure and spectral properties of ThioGlo3® and MIANS.

Excitation and Emission maxima were determined from excitation and emission spectra. Formulas are adapted from Veenstra et al. [Veenstra et al. 2004].

After the fluorescence signal had reached a steady state (approximately 20 minutes), MelB substrates were added to the labeled protein and changes in fluorescence recorded. Either 10 mM Na$^+$ was added and then 30 mM melibiose or first the melibiose and then Na$^+$. 30 mM glucose was added as control.

To measure the dependency of the fluorescence signal from the concentration, the respective substrate was added from a 2 M stock solution (stepwise to the cuvette and the relative fluorescence change ($\Delta F/F_0$) plotted as a function of substrate concentration [S]. The data points were fitted with a hyperbolic function according to Michaelis-Menten, where ΔF_{max} is the maximal fluorescence change and $K_{0.5}$ the half saturation concentration:

$$\Delta F / F_0 = \frac{\Delta F_{max} * [S]}{K_{0.5} + [S]}$$

[Equation 7]

FRET measurements were performed on E365C MIANS-labeled proteoliposomes by exciting the tryptophans at 297 ± 5 nm. The emission spectrum was recorded between 310 and 500 nm. Subsequently, 10 mM Na$^+$ and 30 mM melibiose were added and the spectra recorded again.

2.6 Time-Resolved Fluorescence Measurements

2.6.1 Background of the Stopped-Flow Technique

A detailed investigation of the kinetic mechanism underlying the conformational change of a transporter, e.g., evoked by the binding of ligands, requires the use of rapid-mixing techniques such as stopped-flow fluorescence spectroscopy. Introduced in 1934 [Roughton 1934], the stopped-flow instrument allows the rapid mixing of the transporter with the ligand and enables one to time-resolve changes in the fluorescence on a millisecond timescale. Advantages of the stopped-flow technique are the high time resolution (1ms) and the possibility of monitoring real-time protein conformational changes at specific sites of interest, even if they are electroneutral.

2.6.2 The Stopped-Flow Apparatus

Stopped-flow experiments were carried out using an SF-61DX2 stopped-flow spectrofluorimeter (Hi-Tech Scientific Ltd, Salisbury, UK). Figure 2-6 shows a schematic diagram of the stopped-flow instrument.

The solutions in the observation chamber were excited by using a 100W short arc mercury lamp (Osram, München, Germany) to measure either the intrinsic Trp fluorescence (λ_{ex}=297 nm) of C-less or E365C proteoliposomes, the Dns^2-S-Gal fluorescence of C-less, or the fluorescence emitted from MIANS-labeled E365C (λ_{ex}=335 nm). The fluorescence was detected at right angles to the incident light beam at wavelengths > 320 nm (Trp emission), > 385 nm (MIANS emission), or > 400 nm (Dns^2-S-Gal emission) by using the glass cutoff filters WG320, GG385, and GG400 (Schott, Mainz, Germany) in front of the photomultiplier. The light intensities were recorded with a side-on photomultiplier, digitized via a high-speed analog-to-digital data acquisition board, and analyzed via the computer using the KinetAsyst2 program (Hi-Tech Scientific, Salisbury, UK). 1024 data points were recorded in a time window of 1s. The solutions were adjusted to the indicated temperatures for at least 20 minutes. The dead time of the instrument, i.e., the time required for the reactants, once mixed, to travel from the mixing chamber to the observation chamber, was 3 ms (C. Bamann, personal communication). The electrical time constant of the detection system was 1 ms.
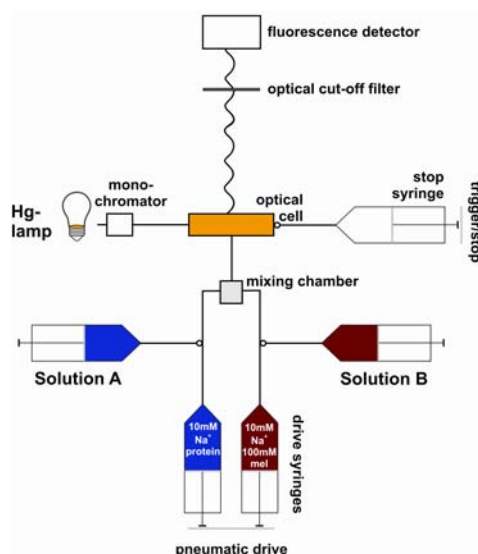
Figure 2-6. The stopped-flow method.
Reagent solutions A and B are transferred to the drive syringes via reservoir syringes. The two drive syringes are housed in a thermostatically controlled water bath. Activation of the pneumatic piston drives the solutions through a mixing chamber and optical cell to a stop syringe. The solution from the previous experiment is driven out of the observation chamber into the stop syringe. Data acquisition via the computer is started when the plunger of the stop-syringe activates the trigger and terminates the flow of the mixed solution. The fluorescence of the solution in the observation chamber can then be measured as a function of time.

2.6.3 Measuring Protocol

Kinetics of MelB conformational changes related to melibiose binding in the presence of Na^+ were investigated by mixing purified and reconstituted protein (ca. 20 µg/mL of C-less MelB, E365C, or MIANS-labeled E365C, respectively) in the presence of 10 mM Na^+ in 100 mM KPi buffer, pH7, with an equal volume (75 µL) of the same buffer containing 10 mM Na^+ and 100 mM melibiose, so that the melibiose concentration in the final solution was 50 mM. The concentration dependence was determined as described above for the steady-state measurements.

Each signal (MIANS signals) or averages of 3-6 traces (Trp signals) were fitted to bi-exponential functions:

$$\Delta F = F_{max} + A_1 e^{-(t-t_0)/\tau_1} + A_2 e^{-(t-t_0)/\tau_2} \qquad \text{[Equation 8]}$$

where ΔF is the change in fluorescence at time t, F_{max} is the maximal fluorescence intensity, A_1 and A_2 are the amplitudes, and τ_1 and τ_2 the time constants. t_0 was set to 16 or 17 ms. Average values for the Trp signal were calculated from two different fits from the averaged data and the MIANS signal from fits of individual data. The errors are expressed as S.E..

2.7 Proteolysis Experiments

Protease digestions were carried out on proteoliposomes (C-less or R141C) essentially as described [Gwizdek et al. 1997]. Briefly, proteoliposomes (25 µg protein in 100 mM KPi, pH 7) were sonicated and incubated with 0.75 µM monensin. Samples were incubated either in the absence of substrates, or in the presence of 20 mM Na^+, or 20 mM Na^+ and 30 mM melibiose for one hour at 25°C. The incubation was carried out in a total volume of 37.5 µL. 12.5 µL of a fresh stock solution of trypsin (100 µg/mL) were added to each tube and the mixture incubated for 10 minutes at 25°C. The reaction was quenched by the addition of 1µL phenylmethanesulfonyl-fluoride (200 mM stock solution in ethanol) and rapid cooling on ice. Samples were denatured during 10 minutes at 42°C in the presence of the 2X electrophoresis loading buffer and analyzed by 18% SDS-PAGE. A direct staining method of the gel was used with SYPRO Orange protein gel stain in 7.5% acetic acid during 30 minutes in the dark (BioRad, Hercules, CA, USA). The bands were visualized by a UV detector.

3 Results

Biological membranes have complex structures reflecting the wide range of functions they are required to perform. To study individually the properties of a protein, its purification is, therefore, a prerequisite. Since the content of, e.g., a transporter in the membrane is generally very low (about 0.15% of total proteins), the encoding gene must be overexpressed in order to obtain sufficient material for the purification. A strategy for the overproduction of MelB and the attachment of a His tag allowing the separation of the permease from other solubilized membrane proteins by Ni^{2+}-chelate affinity chromatography was developed [Pourcher *et al.* 1995]. Since many membrane proteins express their full activity only when they are correctly inserted into a lipid bilayer, MelB was, once purified, reconstituted into liposomes displaying H^+-, Na^+-, and Li^+-dependent sugar-binding and transport properties that were comparable to those of the wild-type MelB in its natural environment. In this thesis, wild-type and mutated MelBs were purified and reconstituted into liposomes according to the method of Pourcher *et al.* [Pourcher *et al.* 1995]. Such reconstituted proteins were then analyzed by different biochemical and biophysical approaches, whereby the focus was set to the time-resolved measurements of melibiose-induced conformational changes.

3.1 Orientation of the Proteins in the Liposomes

The orientation of the proteoliposomes, formed by mixing the purified, solubilized protein with lipids and adsorbing the detergent on polystyrene beads, remained, so far, unknown. To better relate electrical and fluorescence signals to a certain population of the transporters, the orientation of the proteins in the liposomes was determined.

3.1.1 Semi – Quantitative Approach

Single Cys R139C, located within loop 4-5 and physiologically oriented towards the inner compartment of the cell [Botfield *et al.* 1992, Pourcher *et al.* 1996], was selected to determine the orientation of the proteins in the liposomes, as its functional properties are similar to C-less and wild-type MelB [Abdel-Dayem *et al.* 2003]. In this way, orientation can be assessed under conditions, in which the protein functions and, presumably, protein structure and membrane insertion remain unaltered [Seal *et al.* 1998]. The thiol-specific compound 3-(*N'*-maleimidylpropionyl)biocytin (MPB), used to label the Cys of the protein, is a membrane-

impermeable maleimide [Bayer *et al.* 1985, Jung *et al.* 1998, Knol *et al.* 1996] or permeable at concentrations $\geq 100\ \mu M$ [Loo & Clarke 1995]. Thus, in order to ensure impermeability of MPB, it was used at $10\ \mu M$. Stilbene disulfonate, although considered membrane impermeable in intact cells [Loo & Clarke 1995], could also slowly cross the proteoliposomal membrane, when incubations were carried out for more than 30 minutes[Fang *et al.* 1999]. Therefore, the incubation time was set to 10 minutes.

MPB reacted with the inside-out (ISO) oriented transporters of R139C (Figure 3-1A). Repeated freeze-thaw-sonication cycles in the presence of MPB, which made both sides of the liposomes and, therefore, all transporters accessible to MPB, did not change the labeling reaction significantly (Figure 3-1A, ALL) suggesting that most of the proteins are ISO oriented. Stilbene disulfonate blocked the MPB labeling reaction completely (Figure 3-1A, NO). If freeze thaw sonication cycles were applied during MPB labeling and after the pre-incubation with stilbene disulfonate, a faint band was visible (Figure 3-1A, RSO) indicating that a small portion of the protein is right-side-out (RSO) oriented. This, furthermore, shows that neither MPB nor stilbene disulfonate crossed the liposomal membrane.

As negative control, C-less MelB was incubated with different concentrations of MPB (0-1000 μM) (Figure 3-1B). Only a minor non-specific reaction of the maleimide with the protein could be observed at $10\ \mu M$ MPB. Stronger bands were seen, if the MPB concentration was raised up to more than $100\ \mu M$. Therefore, the $10\ \mu M$ MBP used in this study is an appropriate concentration to label specifically the cysteines.

To ensure the same amount of protein in all lanes, Western-Blot analysis was performed using an antibody specific to MelB, which was directly coupled to an alkaline-phosphatase. The respective protein bands, displayed in the Figures 3-1A and B in the lanes "Protein", show that all lanes contained approximately the same amount of protein on the gel. Therefore, it is possible to compare the intensity of the bands. However, when the gels were scanned, the band (Figure 3-1A RSO) was too faint to be analyzed by intensity analysis with imaging programs, thus making it impossible to give semi-quantitative information.

Similar results were obtained for the non-transporting mutant R141C (Figure 3-1A) suggesting that functional as well as non-functional MelBs orient mainly in the ISO configuration in the liposomes. Consequently, the kinetic properties determined in this study refer to the backward running carrier.
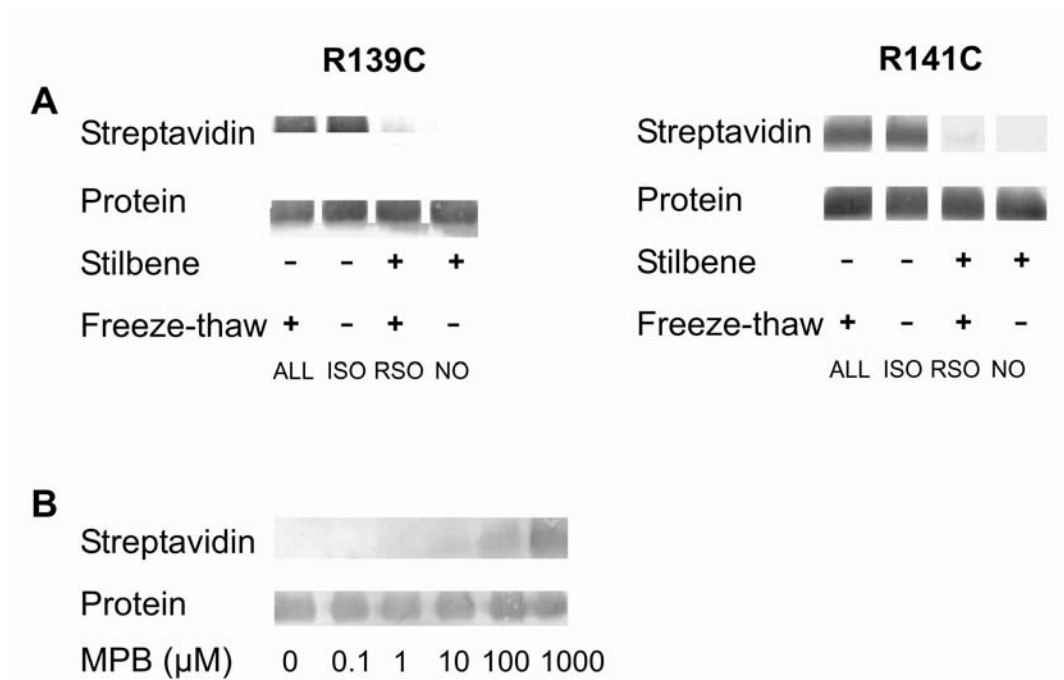
Figure 3-1. Orientation of the proteins in the liposomes.

A. Analysis of single Cys mutants. Single Cys R139C (left) and R141C (right) were treated with 10 μM MPB, some samples subjected to three freeze-thaw-sonication cycles, and incubated for 5 minutes at room temperature. The reaction was stopped by the addition of 10 mM DDT. Were indicated, samples were pretreated with 200 mM stilbene disulfonate. The samples were solubilized in 1% SDS, subjected to SDS-PAGE (10%), and analyzed by Western Blot analysis. Conditions for labeling were as follows: 1.) labeling of all transporters: proteoliposomes incubated with MPB were submitted to freeze-thaw-sonication to allow MPB to have access to both sides of the membrane (lane: ALL). 2.) Labeling of ISO oriented transporters: proteoliposomes incubated with MPB without subsequent freeze-thaw-sonication (lane: ISO). 3.) Labeling of RSO oriented transporters: pre-incubation of the proteoliposomes with the membrane-impermeable stilbene disulfonate to block all cysteines accessible from the outside followed by addition of MPB and freeze-thaw-sonication (lane: RSO). 4.) no labeling: pre-incubation with stilbene disulfonate before incubation with MPB (lane NO). A streptavidin-alkaline phosphatase conjugate was used for the specific reaction with MPB (lane "streptavidin") and a MelB specific monoclonal antibody "21E4" coupled directly to an alkaline phosphatase for the determination of the amount of protein (lane "protein"). An alkaline phosphatase conjugate substrate kit was used to analyze the amount of antibody bound to the proteins on the membrane.

B. Analysis of the C-less mutant. Proteoliposomes containing C-less MelB were supplemented with varying MPB concentrations (0-1000 μM), subjected to three freeze-thaw-sonication cycles, and incubated for 5 minutes at room temperatures. They were analyzed as described in A.

3.1.2 Quantitative Approach

Since the intensity of the bands (Figure 3-1A) yields only an estimation of the percentage of the transporters' orientation, a quantitative ELISA assay was developed. Proteoliposomes were labeled with his-antibodies conjugated to a biotin and adsorbed onto a streptavidin-analog coated plate. After binding of a melibiose specific antibody, which was coupled to an alkaline phosphatase, the absorbance of a color reagent was measured photometrically and compared with the one from proteoliposomes labeled with his-antibody after solubilization.

Unfortunately, the results showed large variations. In the majority of cases, the amount of ISO oriented transporters was detected to be larger than the total fraction (data not shown) indicating that the error of the assay was very large. Mainly two reasons could account for the observed problems: First, the initial amount of protein was too low. Therefore, the separation after the first labeling did not lead to an equal distribution of protein between the two fractions. Second, the labeling of the protein with his-antibody could be different in the presence and absence of detergent. Since performing the assay with a higher starting protein quantity would require a tremendous amount of the very expensive his-antibody, and since the results obtained from the semi-quantitative assay are sufficiently accurate for the analysis of the electrical and fluorescence data, I had to renounce a repetition.

3.2 Electrical Measurements

MelB proteoliposomes adsorbed onto a solid supported membrane have already been proven to be useful to investigate electrogenic events associated to partial steps of the Na^+/melibiose symport reaction (see chapter 1.6.1 and [Ganea *et al.* 2001]). This approach was also used in this work to study electrogenic events of MelB in more detail. MelB proteoliposomes, adsorbed onto the SSM, form a capacitively coupled system that enables measurements of transient electrical signals in response to different co-substrate concentration jumps: simultaneous concentration jumps of both cosubstrates (ΔmelΔNa), concentration jumps of Na^+ in the absence (ΔNa) or presence of melibiose (ΔNa(mel)), or concentration jumps of melibiose in the absence (Δmel) or presence of Na^+ (Δmel(Na)). To minimize ionic strength and osmotic effects, the non-activating solutions contained equimolar concentrations of KCl instead of NaCl and/or glucose instead of melibiose.

3.2.1 Control Measurements

In order to exclude the possibility of electrical signals originating from the solution exchange at the SSM surface, a series of control measurements was performed. A ΔmelΔNa or a sucrose concentration jump on the SSM without liposomes or with empty liposomes yielded no or only a negligible artifact (Figure 3-2A and [Ganea *et al.* 2001]). Furthermore, no signal could be recorded after a 50 mM melibiose concentration jump on liposomes (data not shown) or after a buffer solution exchange (Figure 3-2A). In contrast, Na^+ concentration jumps yielded electrical artifacts increasing linearly with Na^+ concentration (Figure 3-2B). These artifacts might originate from the slightly different interaction of the ions (Na^+ in the activating solution and K^+ in the non-activating solution) with the membrane surface causing a charge displacement upon exchange of K^+ by Na^+ [Zhou *et al.* 2004]. In order to minimize solution exchange artifacts, the Na^+ concentration was usually set to 10 mM when Na^+ was the activating ion.
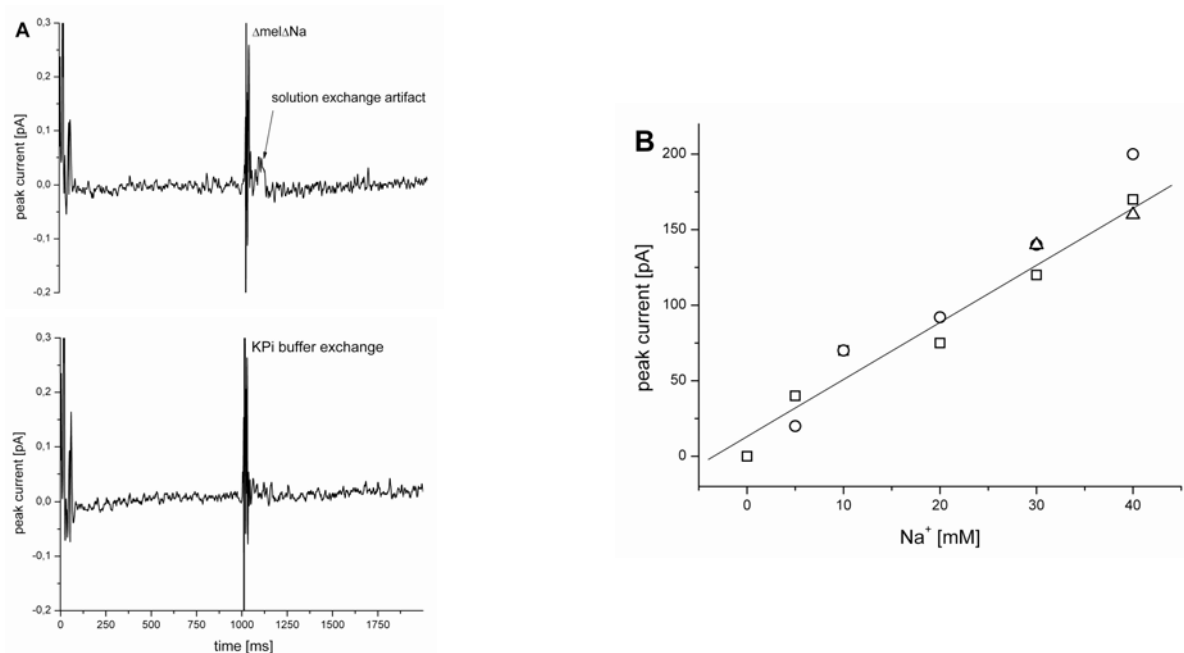
Figure 3-2. Control measurements.

A. Solution exchange on an empty membrane. The SSM was prepared and a ΔNaΔmel concentration jump (10 mM Na^+ and 20 mM melibiose) or a KPi/KPi buffer exchange performed and the transient signals recorded.

B: Na^+-solution exchange on the empty membrane. The SSM was prepared and ΔNa jumps at different Na^+ concentrations recorded. The figure shows a set of three experiments. The line is a linear fit to the data points.

3.2.2 Analysis of Wild-Type MelB

Transient electrical signals, generated by different concentration jumps by wild-type MelB were previously analyzed [Ganea *et al.* 2001]. Whereas substrate binding was associated to the fast component of the decay of the transient signal, substrate translocation was associated to the slow or so called transport component (see also 1.6.1). However, the finding that a Δmel(Na) concentration jump induced a transient signal with a fast decaying component was unexpected, because the sugar is an uncharged substrate, and, therefore, interpretation was not straightforward. In order to describe the underlying and/or related processes of melibiose binding better, the Δmel(Na) solution exchange was studied in more detail.

3.2.2.1 Melibiose Induced Electrical Signals

Typical currents and time constants recorded upon 20 mM melibiose concentration jumps on proteoliposomes are shown in Figure 3-3A. In the absence of Na^+ (trace 0 mM), the signal decays bi-exponentially (decay times 98 and 350 ms). In the presence of 3 mM Na^+, the resulting electrical signal is significantly bigger (687 vs. 406 pA) and faster (decay times 22.4 ms and 210 ms). Since melibiose carries no charge, one possible explanation for the sugar-induced fast component recorded on liposomes equilibrated with 3 mM Na^+ would be the binding of additional Na^+ to MelB due to the transporter's increased affinity for Na^+ in the presence of melibiose. If sugar-induced extra binding of Na^+ would exclusively account for the presence of the fast current component in the electrical response, this fast component should disappear on raising the concentration of Na^+ in the equilibrating solution. When the Na^+ concentration was increased to 100 mM (Figure 3-3A, trace 100 mM), a smaller electrical signal (464 pA) still including a significant fast phase, but a reduced transport component, was recorded (decay times 14.5 and 240 ms) suggesting that different processes than additional Na^+ binding must account for the fast component of the electrical signal at 100 mM Na^+. Whereas the time constants of Figure 3-3A come from fits of individual traces, average values are presented in Table 3-1.

The Na^+-concentration dependence of the peak currents of the sugar-induced response is shown in Figure 3-3B. The peak currents, normalized to the respective average value obtained at Na^+ concentrations between 1 and 10 mM, from 5 different sets of measurements are shown. The signal amplitude increases first with increasing Na^+ concentration up to ca. 1 mM. This phase is characterized by a half saturation concentration of $K_{0.5}^{Na} = 0.25$ mM. At Na^+

concentrations > 1 mM a plateau is reached and then the fast component amplitude declines steadily being reduced by ca. 30 % towards 100 mM Na$^+$. At Na$^+$ concentrations between 10 and 100 mM, the data displayed large variations among experiments.
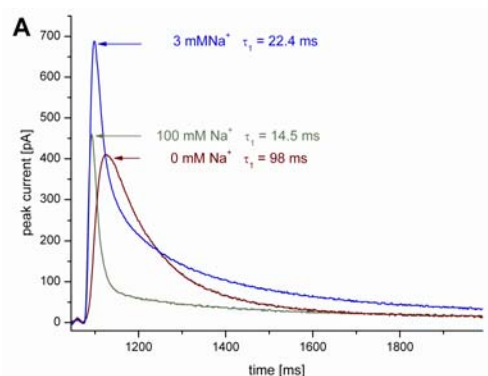
Table 3-1. τ_1 Average Values for Different Na$^+$ Concentrations

Na$^+$ [mM]	τ_1 [ms]	n
0	81.1 $\pm$ 9.7	4
3	18.1 $\pm$ 1.6	8
100	14.8 $\pm$ 1.5	6

Shown are the average values $\pm$ S.E.
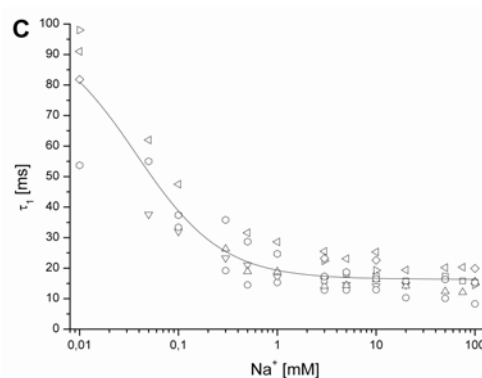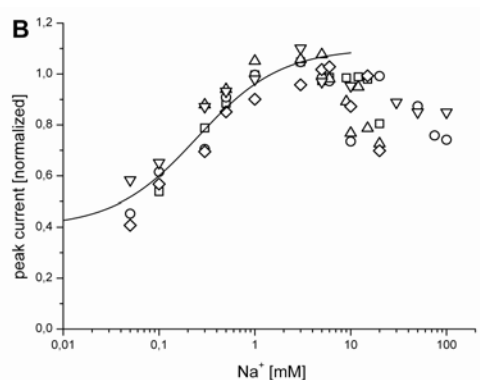
Figure 3-3. Electrical signals generated by MelB after different Δmel(Na) concentration jumps.

A. Typical electrical signals induced by Δmel(Na) concentration jumps. 20 mM melibiose concentration jumps in the absence (0 mM) and presence of 3 mM and 100 mM Na$^+$ were performed and recorded on the same SSM/proteoliposome preparation. The non-activating solution contained 20 mM glucose and the indicated Na$^+$ concentration, the activating solution the respective same amount of Na$^+$, but glucose was substituted by melibiose. The figure shows traces and time constants from a single representative experiment. The decaying signals were fitted with bi-exponential functions.

B. Dependence of the peak currents on the Na$^+$ concentration. Electrical signals were recorded after a 20 mM melibiose concentration jump in the presence of the indicated Na$^+$ concentration. The figure displays a compilation of 5 independent experiments (represented by the different symbols). The solid line is a hyperbolic function: $I_p = 0.4 + 0.7 * c / (c + K_{0.5}^{Na})$ with I_p = peak current, c = Na$^+$ concentration, and $K_{0.5}^{Na}$ = 0.25 mM.

C. Dependence of the fast decaying time constant on the Na$^+$ concentration. τ_1 was obtained by fitting the current traces with bi-exponential functions. The figure displays a compilation of 7 experiments.

Finally the time constants of the fast decay are plotted against the respective Na$^+$ concentration (Figure 3-3C). τ_1 decreases strongly between 0 and 0.5 mM and is approximately constant towards higher Na$^+$ concentrations. Since the decay of the signal is is constant, if a reaction is faster than 50 s^{-1} (τ_1=20 ms) [Ganea *et al.* 2001, Pintschovius & Fendler 1999], the relaxation time is limited by an instrumental parameter.

3.2.2.2 Inhibition by NEM

Inactivation of MelB turnover by NEM provides a means to better identify steps of the transport reaction associated with the melibiose-induced fast electrical event. A melibiose concentration jump was imposed in the presence of 100 mM Na$^+$ with and without 30 minutes pre-incubation with 2 mM NEM. The Na$^+$ concentration was set to 100 mM to exclude the possibility of extra Na$^+$ binding. Figure 3-4 shows that the melibiose induced transient signal is smaller (297 vs. 464 pA) and contains only a single fast component in the presence of NEM (τ_1 = 17.1 ms). In agreement with previous measurements [Ganea *et al.* 2001], the slow transport component of the signal disappeared completely in the presence of NEM. This demonstrates that the fast electrical component is associated to melibiose binding rather than to transport of the co-substrates. In particular, it excludes the contribution of additional electrogenic Na$^+$ binding during subsequent turnovers to the melibiose-induced signal.
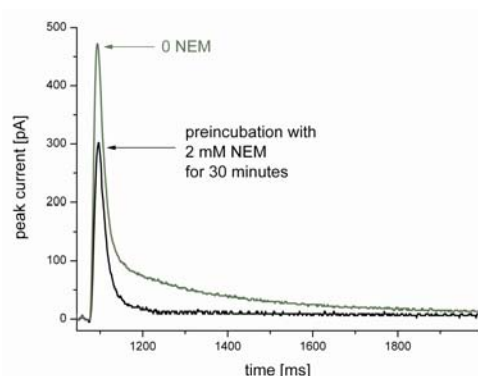
Figure 3-4. Inactivation of the Δmel(Na) signal by NEM.

Electrical signals generated by MelB were recorded after a 20 mM melibiose concentration jump in the presence of 100 mM Na$^+$. The SSM, including the adsorbed proteoliposomes, was incubated during 30 minutes with 2 mM NEM (in the absence of DDT), and the signal recorded again. One single representative experiment is shown. The experiment was repeated three times.

3.2.2.3 Effect of Internal and External Ions

To test whether the high ionic strength of the activating and non-activating solutions could be responsible for the decline of the peak current and the reduction of the transport component at high Na^+ concentrations, the signals after melibiose concentration jumps under different ionic conditions were compared. The electrical signals recorded after melibiose jumps were the same whether the protein was preincubated with 10 mM NaCl or 10 mM NaCl and 90 mM KCl (Figure 3-5A). In contrast, a melibiose jump in the presence of 100 mM NaCl caused a signal with a smaller peak current and a significantly smaller transport component (see also Figure 3-3A). This suggests that no factors other than Na^+ (e.g., ionic strength, chloride concentration, osmotic gradients) contribute to the decline of the signals observed at high Na^+ concentration.

Furthermore, the hypothesis that high internal Na^+ may be responsible for the decrease of the transient current was probed. In a first set of experiments, the SSM/proteoliposomes system was preincubated with 100 mM Na^+ to allow Na^+ to leak into the liposomes. Directly
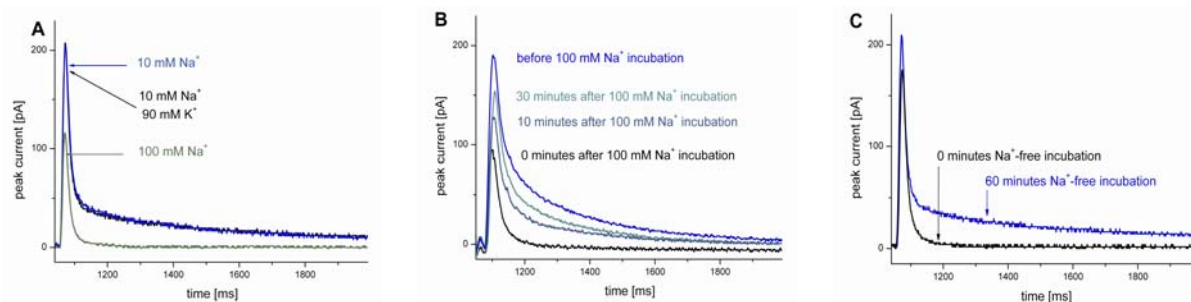
Figure 3-5. Effect of high external and internal ions on the Δmel(Na) signal.

A. Effect of high external ions. 20 mM melibiose concentration jumps were performed in the presence of either 10 mM NaCl, 10 mM NaCl plus 90 mM KCl, or 100 mM KCl, respectively.

B. Recovery of the transport component after the incubation with 100 mM Na^+. The incubation with buffer containing 100 mM Na^+ was performed after the absorption of the proteoliposomes to the SSM. Between the recordings of the signals, the SSM was incubated with Na^+ free buffer. Electrical signals were recorded after a 20 mM melibiose concentration jump in the presence of 5 mM Na^+.

C. Recovery of the transport component after preloading of the liposomes with 100 mM NaCl. The proteoliposomes were preloaded with 100 mM NaCl prior to the adsorption to the SSM. A 20 mM melibiose concentration jump was performed in the presence of 5 mM Na^+. Then, the SSM was incubated for one hour in Na^+-free buffer and the signal recorded again.

All Figures show traces from a single representative experiment. Each experiment was performed in triplicate.

afterwards, an electrical signal evoked by a 20 mM melibiose jump in the presence of 5 mM Na^+ was recorded. As can be seen (Figure 3-5B, trace 0 min), the slow transport component of the signal disappeared almost completely and the peak current decreased. After incubation of the SSM during 10 and 30 minutes with Na^+-free buffer, the same concentration jump yielded a signal with an increased peak current and a recovered slow transport component. In a second set of experiments, the proteoliposomes were preloaded with Na^+ prior to their adsorption onto the SSM membrane by three freeze-thaw-sonication cycles in 100 mM Na^+ buffer. After the liposomes were adsorbed to the SSM in a medium containing 100 mM Na^+ to prevent any loss of internal Na^+, a 20 mM melibiose concentration jump in the presence of 5 mM Na^+ was applied. Such a concentration jump induced an electrical signal with a strongly reduced slow component (Figure 3-5C). After one hour of incubation with Na^+-free buffer, the peak current increased and a significantly larger transport phase could be seen. These results clearly show that internal rather than external Na^+ is responsible for the decreased peak currents. It, furthermore, shows that the proteoliposomes are leaky and that Na^+ is able to cross the membrane either via a pathway provided by the transporter itself or by the lipid membrane. Once inside the liposome, Na^+ probably inhibits the electrical response.

3.2.2.4 pH Dependence

The decaying time constant τ_1 of the electrical signal after a Δmel(Na) concentration jump at intermediate Na^+ concentration (3 mM) has a value of $\sim$ 18 ms (Figure 3-3A) and is, therefore, similar to that after a Na^+ concentration jump in the absence of sugar (14 ms, [Ganea *et al.* 2001]). This relaxation time depends on the rate of substrate binding, but may in addition be significantly modulated by the rise time of the substrate concentration at the surface of the SSM. Since the concentration rise time is an instrumental parameter and, therefore, constant, a change in τ_1 would reflect a change in the binding properties of the substrate. In order to demarcate the Na^+ induced electrical signal from that induced by melibiose in the presence of saturating Na^+, two different concentration jumps at different pH values were applied (pH 5 to 8). Figure 3-6A and C illustrate the variation of τ_1 on pH. A pure Na^+ jump generated an electrical signal that slowed down at lower pH and, thereby, higher H^+ concentration (Figure 3-6A). A similar decrease towards lower pH was found for the peak currents (Figure 3-6B). Fitting the latter data to a Boltzmann equation yielded a pK of around pH 5.9. Remarkably, in proteoliposomes preincubated with 10 (Figure 3-6C, solid squares), or 100 mM Na^+ (Figure 3-6C, open squares) no or little dependence of the relaxation time from

pH was observed. Likewise, the peak currents are approximately constant for Δmel(Na) jumps in the range of pH 5.5 to 8 (Figure 3-6D). At pH 5, the very high proton concentration may have a direct effect on the protein and influence its function and/or stability accounting, thus, for the decreased peak current.
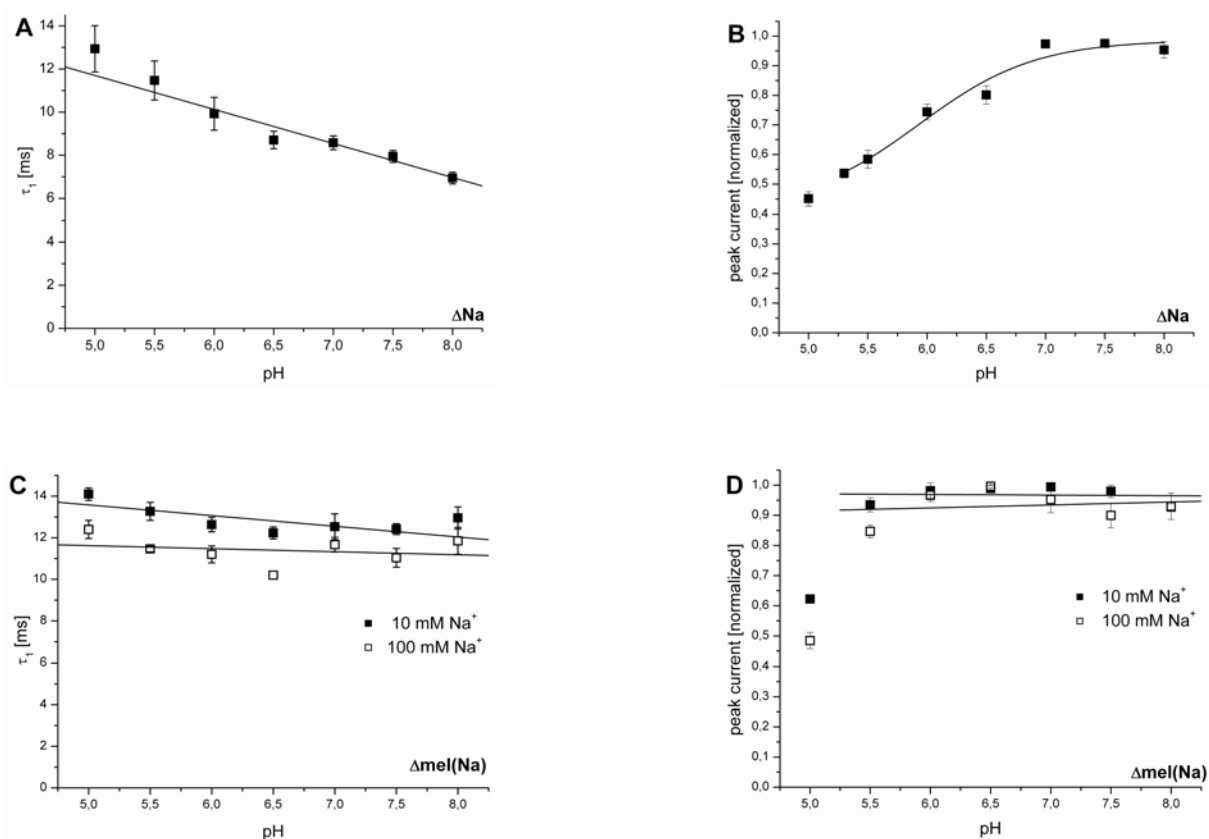
Figure 3-6. Effect of pH on the ΔNa and Δmel(Na) electrical signal.

A. ΔNa concentration jumps (10 mM Na$^+$) were performed and the decaying part of the signals fitted with a mono-exponential function. The resulting time constants were plotted against the respective pH. The solid line represents a linear fit to the data points.

B. ΔNa concentration jumps (10 mM Na$^+$) were performed and the peak currents plotted against the respective pH. The solid line is a fit according to the Boltzmann function: $y= ((I_{min}-I_{max})/(1+e^{(x-xo)/dx}))+I_{max}$, with $I_{min} = 0,42$, $I_{max} =0,99$, $x_0 = 5,93$, dx= 0,59. The fit was done between pH 5.5 and 8.

C. Δmel(Na) concentration jumps (20 mM melibiose) were performed, and the decaying part of the signals fitted with a mono- (100 mM Na$^+$) or bi-exponential (10 mM Na$^+$) function, respectively. solid squares: 10 mM Na$^+$: open squares: 100 mM Na$^+$. The solid lines represent linear fits to the data points.

D: Δmel(Na) concentration jumps were performed, the signals recorded and plotted against the respective pH. solid squares: in the presence of 10 mM Na$^+$: open squares: in the presence of 100 mM Na$^+$. The solid line represents linear fit to the data points.

Data points are mean values with S.E. from at least three individual experiments.

3.2.2.5 Temperature Dependence

To further characterize the molecular event underlying the melibiose induced electrical signal, the dependence of the Δmel(Na) signal on the temperature was measured. Increasing the temperature from 20 to 30°C not only increased the peak current by a factor of 2.5, but also the transport component (Figure 3-7A). At the same time, τ_1 decreased with increasing temperatures. The Arrhenius plots for 20 mM melibiose jumps in the presence of 10 and 100 mM Na^+ (Figure 3-7B) gave activation energies (E_a) of ca. 45 kJ/mole. The Q_{10} was determined to be 1.6 indicating a similar molecular mechanism underlying τ_1 at both Na^+ concentrations. However, it has to been taken into account that limitations hold also true here, i.e., τ_1 is possibly influences by time resolution of the method.
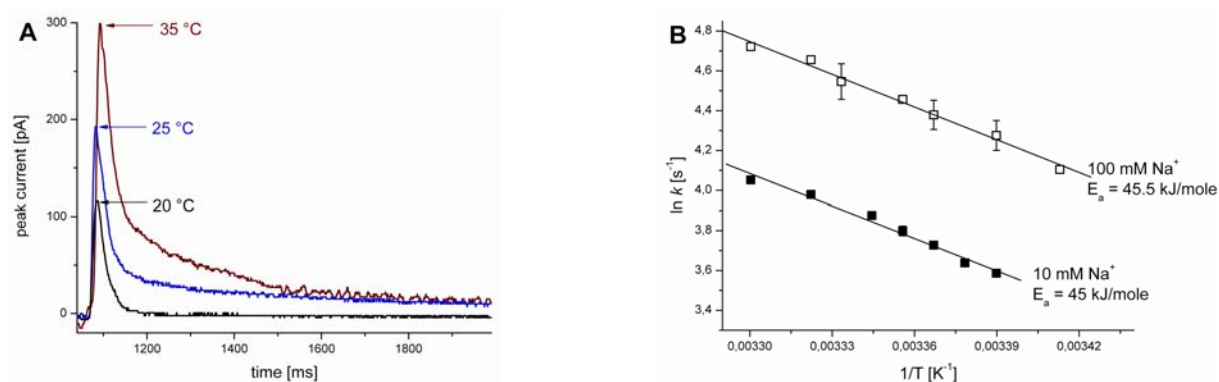
Figure 3-7. Dependence of the Δmel(Na) signal on the temperature.

A. Dependence of the peak current. The Faraday cage was isolated with styropor and equipped with a water-thermostated system allowing the solutions and the setup to be equilibrated at desired temperatures. Temperatures of the respective solution and the setup were set to the indicated temperature (from 20 to 35 °C). 20 mM melibiose concentration jumps were performed in the presence of 10 mM Na^+. Shown are three representative signals.

B. Arrhenius plot. The signals recorded as described in A were fitted with a mono- (100 mM Na^+, open squares) or bi-exponential function (10 mM Na^+, solid squares), respectively. $1/\tau_1$ ($=k$) was plotted against inverse temperature (in K). Shown is the average value and the S.E. (n=4 for 10 mM Na^+, n=2 for 100 mM Na^+).

3.2.2.6 Melibiose Concentration Dependence

10 mM Na$^+$ concentration jumps were performed on proteoliposomes in the presence of melibiose at varying concentrations (from 0.3 to 100 mM). The recorded transient signals had a bi-exponential decay. The magnitude of the peak currents increased as the melibiose concentration was raised from 0.3 to 20 mM and progressively decreased again. The charge displacement showed a similar dependency (Figure 3-8). The peak currents at 100 mM melibiose are comparable to those at low sugar concentrations.

A model function was generated, in which the Na$^+$ and melibiose-induced electrical responses correspond to distinct electrogenic events in the transporter.

$$\Delta Q = \Delta Q_{Na} + \Delta Q_{mel}\left(\frac{c}{c + K_{0.5}^{mel}(+Na^+)} - \frac{c}{c + K_{0.5}^{mel}(-Na^+)}\right) \qquad \text{[Equation 9]}$$

where ΔQ_{Na} and ΔQ_{mel} are distinct charge displacements triggered by Na$^+$ and melibiose binding, respectively, c is the melibiose concentration and $K_{0.5}^{mel}(+Na^+)$ and $K_{0.5}^{mel}(-Na^+)$ are the melibiose affinities of the transporter in the presence and absence of Na$^+$, respectively. $K_{0.5}^{mel}(+Na^+) = 3$ mM and $K_{0.5}^{mel}(-Na^+) = 22$ mM (taken from [Ganea *et al.* 2001]). ΔQ_{Na} and ΔQ_{mel} were the adjustable parameters of the fit to the normalized data. The model function used to fit the data points of Figure 3-8 is strictly valid only at saturating Na$^+$ concentration, a
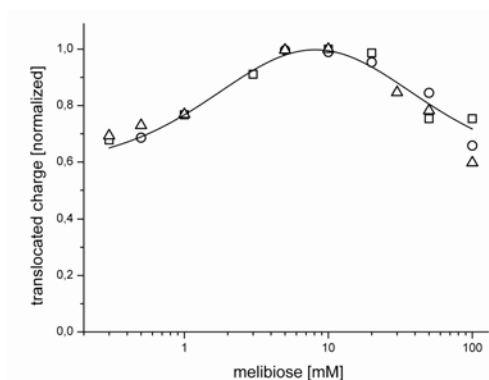
Figure 3-8. Dependence of the translocated charge on the melibiose concentration.

A 10 mM Na$^+$ concentration jump was performed in the presence of the indicated melibiose concentrations. The translocated charge was determined from the transient currents by numerical integration in the time range 1-60 ms. The results of three independent experiments (one measured by myself, two by Constanta Ganea) as indicated by different symbols are superimposed. The solid line is a fit to the data using the model function.

condition that is approximately obtained with 10 mM Na$^+$. This relatively low Na$^+$ concentration was chosen, because higher concentrations would have caused larger artifacts (see also Figure 3-2). When using this model function, a good quality fit could be obtained for the experimental data yielding $\Delta Q_{Na} = 0.58$ and $\Delta Q_{mel} = 0.91$. This fit, therefore, shows that Na$^+$ binding contributes $\sim$ 40% and melibiose binding $\sim$ 60% of the total displaced charge during binding of both substrates.

An independent confirmation that the charge displacement is similar after melibiose and Na$^+$ binding was obtained by comparing the translocated charge of the electrical signals in the presence of NEM. Integrating the signals obtained after a Δmel concentration jump yielded a total charge translocation of 51.5 $\pm$ 6.7 % (in % of the ΔNaΔmel signal, data not shown) and after a ΔNa concentration jump a charge translocation of 45.2 $\pm$ 1.9%.

3.2.3 Analysis of C-less, R141C, and E142C Mutants

Cysteine-scanning mutagenesis is an interesting approach to study systematically the structure and structure-function relationship of MelB. Thus, a fully functional active permease devoid of its four native cysteines (C-less permease) [Weissborn *et al.* 1997] has been used as genetic background and serves as control whenever single Cys mutants are investigated. When the charged amino acids of loop 4-5 were individually replaced by cysteines [Abdel-Dayem *et al.* 2003, Séry 2002], two interesting amino acid residues were identified. R141C is a transport-deficient mutant, although it is able to bind sugar with a three times reduced affinity as compared to C-less [Abdel-Dayem *et al.* 2003]. It was, thus, suggested that loop 4-5 is close to the sugar binding site, and may participate directly in co-substrate translocation. Changing the adjacent amino acid Glu-142 into Cys resulted in a mutant with a similar reduced sugar affinity and a ten fold reduction in the sugar accumulation level compared to C-less [Séry 2002]. The limited transport was completely abolished in the presence of NEM. In view of these results, the C-less mutant, R141C, and E142C were purified in this work by Ni^{2+}-affinity chromatography, reconstituted into liposomes, and analyzed in detail with the SSM method.

3.2.3.1 Control Experiments

To relate the electrical signals of R141C and E142C specifically to the mutation, control experiments with the C-less mutant were performed. The C-less transporter functions similar to wild-type MelB, i.e., it had no significant decrease in the ability to accumulate melibiose with co-transported Na^+ or H^+ and also similar substrate affinities as the wild-type [Abdel-Dayem *et al.* 2003, Weissborn *et al.* 1997]. Electrical measurements confirmed now the likewise functioning of C-less and wild-type MelB (upper line in each signal pair of Figure 3-9). The shape of the signals as well as the size of the peak currents (Figure 3-10) and the decaying time constants of the electrical signals (Table 3-2) were usually in the same order of magnitude of wild-type MelB. However, the peak current after a Δmel and after a ΔNa(mel) concentration jump was relatively larger in C-less than in wild-type MelB. The affinities for Na^+ in the presence and absence of melibiose resemble those of wild-type MelB, but the affinities of melibiose in the presence and absence of Na^+ are slightly lower compared to the wild-type (Table 3-3). In any instance, the C-less mutant works sufficiently similar to wild-type MelB, therefore, the variations of the electrical signals and the changes in affinity observed in all single Cys mutants can be assigned specifically to the introduced mutation.

MTSEA$^+$, MTSET$^+$, MTSES$^-$, or NEM added to the C-less transporter had no influence on the size of the peak currents and the shape of the signals (data not shown) suggesting that the functioning of the C-less transporter was not impaired under the influence of these sulfhydryl reagents. Thus, unspecific binding as shown for MPB at concentrations higher than 10 µM is not important for these maleimides. Previous results, where MTSEA$^+$ had a strong inhibitory effect on the C-less carrier [Ding 2003], could not be confirmed. In contrast, pCMBS reduced the size of the peak currents of the signals caused by Δmel, Δmel(Na), and ΔmelΔNa concentration jumps in the C-less mutant by ca. 50, 40, and 30%, respectively, and those peak currents caused by ΔNa and ΔNa(mel) concentration jumps by 10%. The stationary transport component was not suppressed (data not shown). The greater reduction of the peak currents after concentration jumps with melibiose suggests that the access of melibiose was blocked due to sterical reasons of the relatively big molecule pCMBS. Probably, pCMBS could act as non-specific inhibitor reacting with other residues than cysteines. Since in this work only MTSEA$^+$, MTSES$^-$, and NEM are employed, which did not have any influence on the C-less transporter, the reaction of these maleimides with the protein could be assigned specifically to the single introduced Cys.

3.2.3.2 Electrical Signals Generated by Different Concentration Jumps

Significant differences exist between the amplitudes and/or the time courses of decay of the transient electrical signals recorded on the one hand from R141C and E142C mutants and on the other hand from C-less MelB (Figure 3-9). The transient current generated in C-less MelB by a simple Na$^+$ concentration jump in the absence of sugar (ΔNa) decays, similar to the wild-type, mono-exponentially ($\tau_1 \sim 15$ ms, see also Table 3-2 for a comparison of all time constants). Likewise, R141C and E142C show mono-exponentially decaying signals with similar time constants ($\tau_1 \sim 9$ and 13 ms, respectively). On the other hand, a Na$^+$ concentration jump in the presence of melibiose (ΔNa(mel)) results in a signal that decays with a bi-exponential time course in wild-type and C-less MelB ($\tau_1 \sim 15$ and 13 ms, $\tau_2 \sim 330$ and 280 ms). In contrast, the signals evoked by ΔNa(mel) concentration jumps in both R141C and E142C decay only mono-exponentially ($\tau_1 \sim 14$ and 9 ms, respectively) indicating that the electrogenic event linked to Na$^+$ binding still occurs while that linked to transport activity is absent or severely reduced. In a third condition, a simple melibiose concentration jump was applied in the absence of Na$^+$ (Δmel), i.e., when the permease functions in the H$^+$/melibiose

transport mode. The resulting electrical signal decays with a bi-exponential time course in the wild-type and also in the C-less mutant ($\tau_1 \sim 100$ and 80 ms, $\tau_2 \sim 350$ and 260 ms). The fast decaying component is proportionally slower in the absence than in the presence of Na^+. In contrast, the R141C and E142C signals still include the relatively fast ($\tau_1 \sim 60$ and 52 ms), but lack the slowly decaying component. Similarly, after imposition of a melibiose concentration jump in the presence of Na^+ (Δmel(Na)) or after a simultaneous concentration jump of both substrates (ΔmelΔNa) the mutants retain a fast component (τ_1 R141C: ~ 19 or 15 ms, respectively, τ_1 E142C: ~ 19 or 8 ms, respectively), but did not exhibit the slow component observed in C-less MelB and wild-type (see Table 3-2 for the exact time constants). In summary, these data show that both R141C and E142C do only exhibit the fast decay component, but lack the slow transport component.

Table 3-2. Overview of the Decaying Time Constants of Different Solution Exchange Protocols.

		WT	C-less	R141C	R141C MTSEA	E142C
Δmel	τ_1 [ms]	98	82.5 ± 4.8	59.5 ± 7.9	$60,2 \pm 6,5$	51.8 ± 6.6
	τ_2 [ms]	350	258 ± 14		328 ± 80	
Δmel(Na)	τ_1 [ms]	17	15.4 ± 0.8	18.6 ± 1.0	27.5 ± 2.4	19.4 ± 2.3
	τ_2 [ms]	385	264 ± 25		368 ± 7	
ΔNa	τ_1 [ms]	14	14.8 ± 0.7	13.0 ± 1.0	10.5 ± 0.6	8.9 ± 0.7
	τ_2 [ms]					
ΔNa(mel)	τ_1 [ms]	15	11.5 ± 0.8	13.9 ± 1.3	12.8 ± 1.4	8.5 ± 0.4
	τ_2 [ms]	327	172 ± 10		131 ± 39	
ΔNaΔmel	τ_1 [ms]	15	19.2 ± 2.0	14.6 ± 0.5	12.1 ± 1.9	8.2 ± 0.3
	τ_2 [ms]	260	174 ± 10		282 ± 54	
n			5	4	3	4

The table shows the average value from n experiments and the S.E. Values for the wild-type were taken from [Ganea *et al.* 2001].
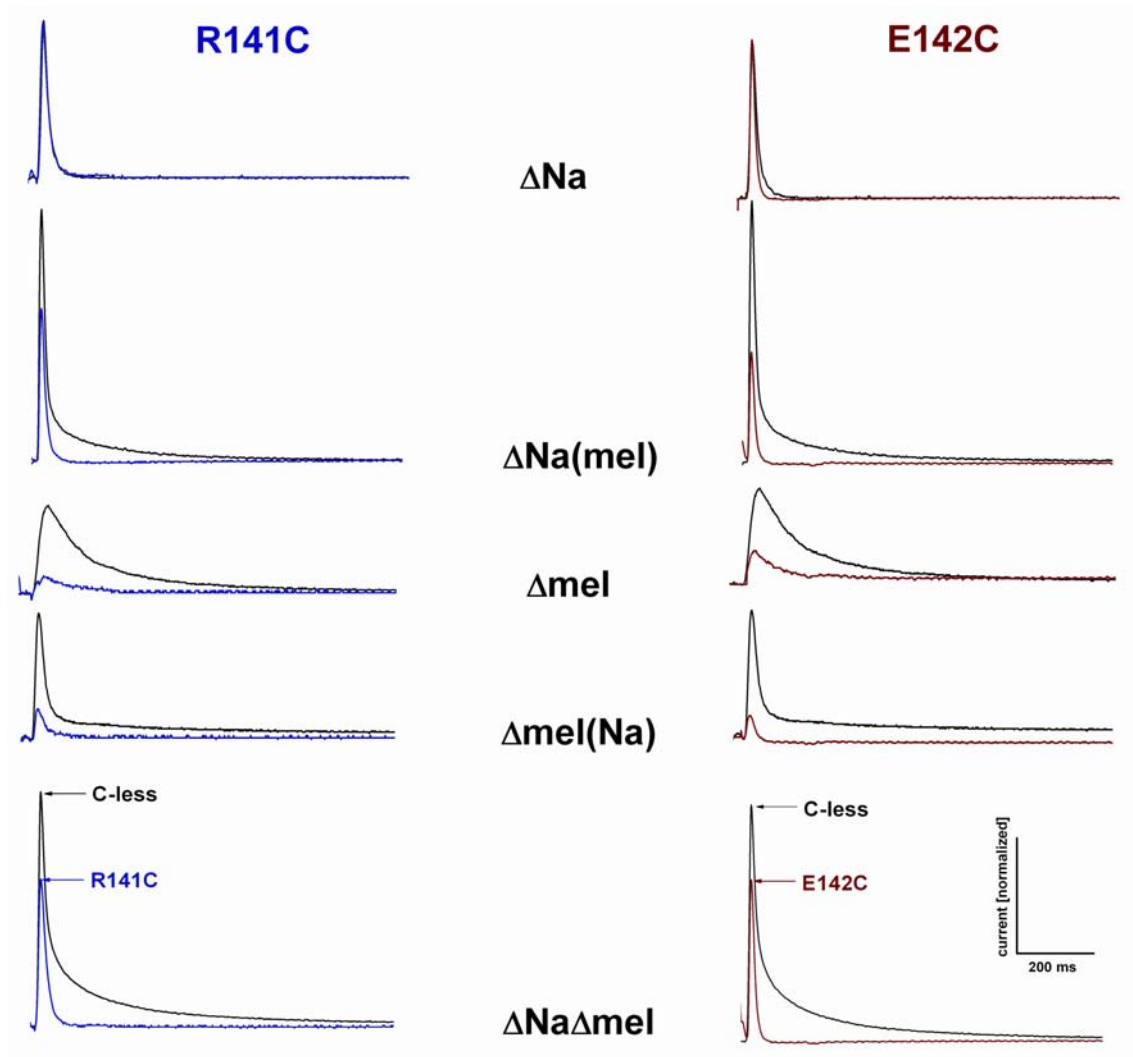
Figure 3-9. Comparison of the electrical signals recorded from R141C, E142C, and C-less MelB.
The solutions contained 50 mM melibiose and/or 10 mM NaCl in 0.1 M Kpi buffer, pH 7. The ionic strength in the activating and non-activating solutions was equilibrated with equimolar concentrations of the non-activating substances glucose and/or KCl. Either simple concentration jumps of one substrate were performed (Δmel, ΔNa), concentration jumps where the protein was already equilibrated with the sugar or salt, respectively (Δmel(Na) or ΔNa(mel)), or simultaneous concentration jumps of both substrates (ΔmelΔNa). The upper line in each signal-pair was recorded from the C-less mutant (black), the lower line from R141C (blue, left part) or E142 (red, right part). The data were normalized to the absolute peak current of the respective ΔNa signal (see also Figure 3-10).

Figure 3-9 not only shows that the shape of the decaying part of the electrical signal is modified by the mutations, but also indicates significant changes in the amplitudes of the peak currents. To better assess the mutant vs. C-less signal differences, the relative rather than absolute values of the various peak currents were considered. The peak currents elicited by a Na^+ concentration jump for each studied mutant or wild-type, respectively, were taken as reference (100% signal in Figure 3-10) and used to normalize the data, because the Na^+ partial reactions are not affected by the mutations, while the melibiose partial reactions are severely reduced (see below). When the electrogenic reaction becomes faster than 50 s^{-1} ($\tau_1 \sim 20$ ms), the peak current can be considered proportional to the translocated charge, since the decay of the signal is determined by an instrumental time constant that is approximately constant in most of the measurements (except for Δmel) [Ganea *et al.* 2001]. Several conclusions can be drawn from the diagram comparing the relative peak currents (Figure 3-10).
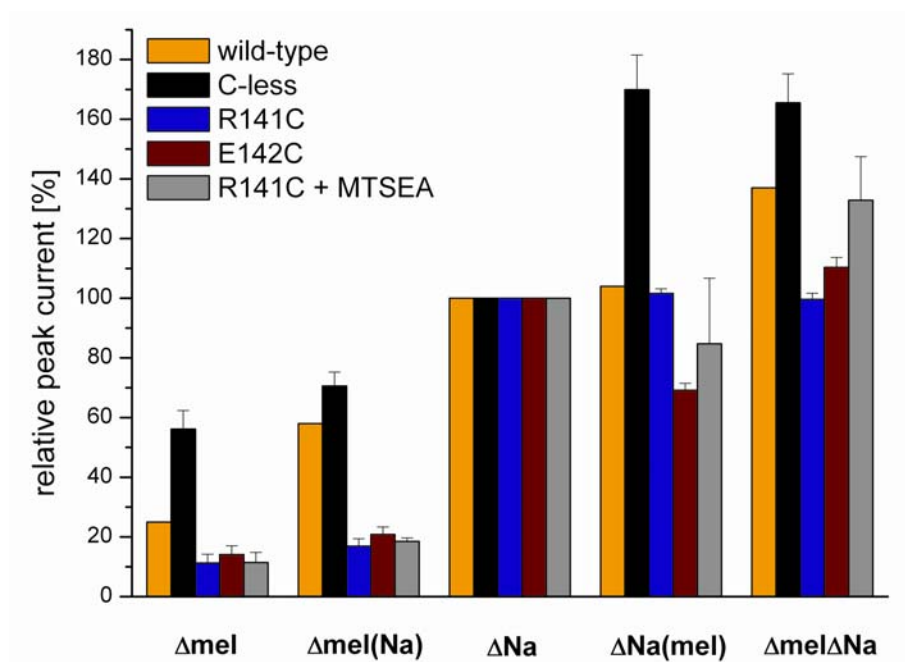
Figure 3-10. Comparison of the relative peak currents of the signals.

The relative peak currents of the electrical signals caused by different concentration jumps from at least three independent experiments were averaged. The conditions were as in Figure 3-9. Indicated are the mean values and the S.E. For normalization, the peak currents of the ΔNa signals were set to 100% and the sizes of all others signals expressed in relation to it. Wild-type (WT) data are taken from [Ganea *et al.* 2001].

First, the peak currents associated to melibiose binding in R141C and E142C in the presence of either H^+ (Δmel) or Na^+ (Δmel(Na)) are much smaller than the corresponding signals in C-less or wild-type. Secondly, C-less as well as wild type MelB show a comparatively larger peak current after a ΔNaΔmel challenge than after a ΔNa jump. This difference represents the additive contributions of the two distinct Na^+ and sugar electrogenic binding reactions (see discussion and [Meyer-Lipp *et al.* 2004]) to the signal during a ΔNaΔmel challenge, while only the Na^+ electrogenic binding makes up the signal during a ΔNa jump.. The fact that this difference is no longer observed in the two mutants may be accounted for, at least in part, by a severe reduction or loss of sugar-induced charge transfer. Third, it was observed that the Na^+-dependent increase of the melibiose-induced peak current in C-less (Δmel(Na) vs. Δmel) is barely seen in E142C and R141C. Also, the melibiose-dependent increase in the peak current observed after a Na^+ concentration jump (ΔNa(mel) vs. ΔNa) seen with C-less and wild-type MelB is not observed in the two mutants R141C and E142C. It is finally interesting to note that NEM added to R141C, or E142C proteoliposomes had no influence on the electrical signals (data not shown).

3.2.3.3 Re-introduction of a Positive Charge in R141C by MTSEA$^+$

It was previously shown by a transport assay that reintroducing the positive charge by reacting R141C with MTSEA$^+$ partly restored active substrate transport [Abdel-Dayem *et al.* 2003]. This is now confirmed by electrical measurements. Accordingly, Figure 3-11, illustrating a typical ΔNaΔmel concentration jump experiment, shows partial recovery of the slow electrical component after treatment of R141C with MTSEA$^+$. This is best appreciated in the inset of Figure 3-11, which illustrates how a bi-exponential fit matches better the time course of decay of the electrical signal than a mono-exponential fit. Although MTSEA$^+$ is able to restore part of the transport activity and the electrical slow decaying component, the relative peak currents evoked by melibiose and by Na^+ concentration jumps are similar in the absence and presence of MTSEA$^+$ (Figure 3-10). Only the ΔmelΔNa relative signal is slightly bigger in the presence of MTSEA$^+$. In contrast to this observation, any attempts to restore the slow electrical component with negatively charged SH reagent (e.g. MTSES$^-$) in the E142C mutants failed (data not shown).
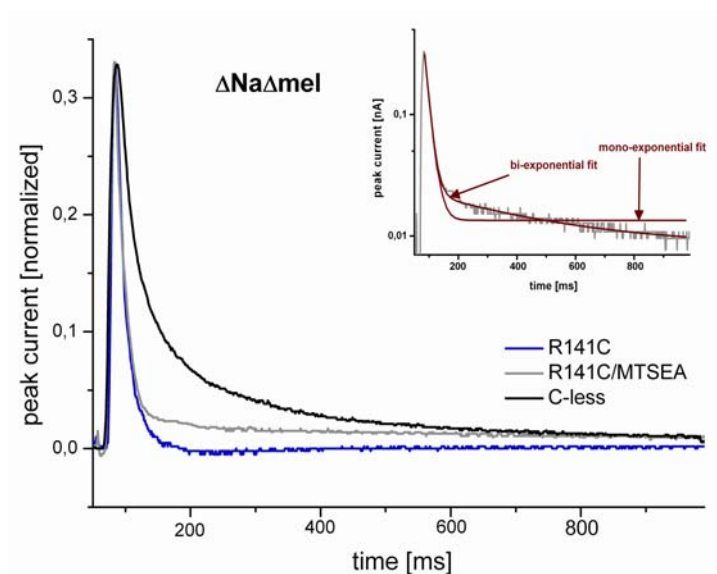
Figure 3-11. Recovery of the stationary charge transfer due to the addition of MTSEA$^+$.

2.5 mM MTSEA$^+$ were added to the proteoliposomes and incubation on the SSM performed for 45 minutes at room temperature. Signals were recorded with and without the addition of MTSEA$^+$. The signals, which are displayed here, come from a simultaneous concentration jump of 20 mM melibiose and 10 mM Na$^+$ (ΔmelΔNa). Shown are the signals of the C-less MelB (black line), R141C after the addition of 2.5 mM MTSEA$^+$ (grey line), and R141C without the addition of MTSEA$^+$ (blue line). For better comparison, all peak currents were normalized to the same value, i.e., the absolute peak current of the ΔmelΔNa jump of R141C after the addition of MTSEA$^+$.

The inset shows a mono- and a bi-exponential fit (red traces) on a half logarithmic scale of a ΔmelΔNa jump of the R141C signal after incubation with 2.5 mM MTSEA$^+$.

3.2.3.4 Na$^+$ and Melibiose Concentration Dependence

The dependence of the peak currents (I$_p$) on the substrate concentration was determined for different solution exchange protocols. Figure 3-12A depicts the variations of the peak currents recorded on imposing Na$^+$ concentration jumps in the presence or absence of saturating melibiose concentration for the C-less mutant. Both concentration dependencies were fitted using a hyperbolic function according to Michaelis-Menten. For the Figure 3-12, data points from three individual experiments were normalized to the respective maximal value (I$_{p(max)}$ determined from individual fits) and then averaged.
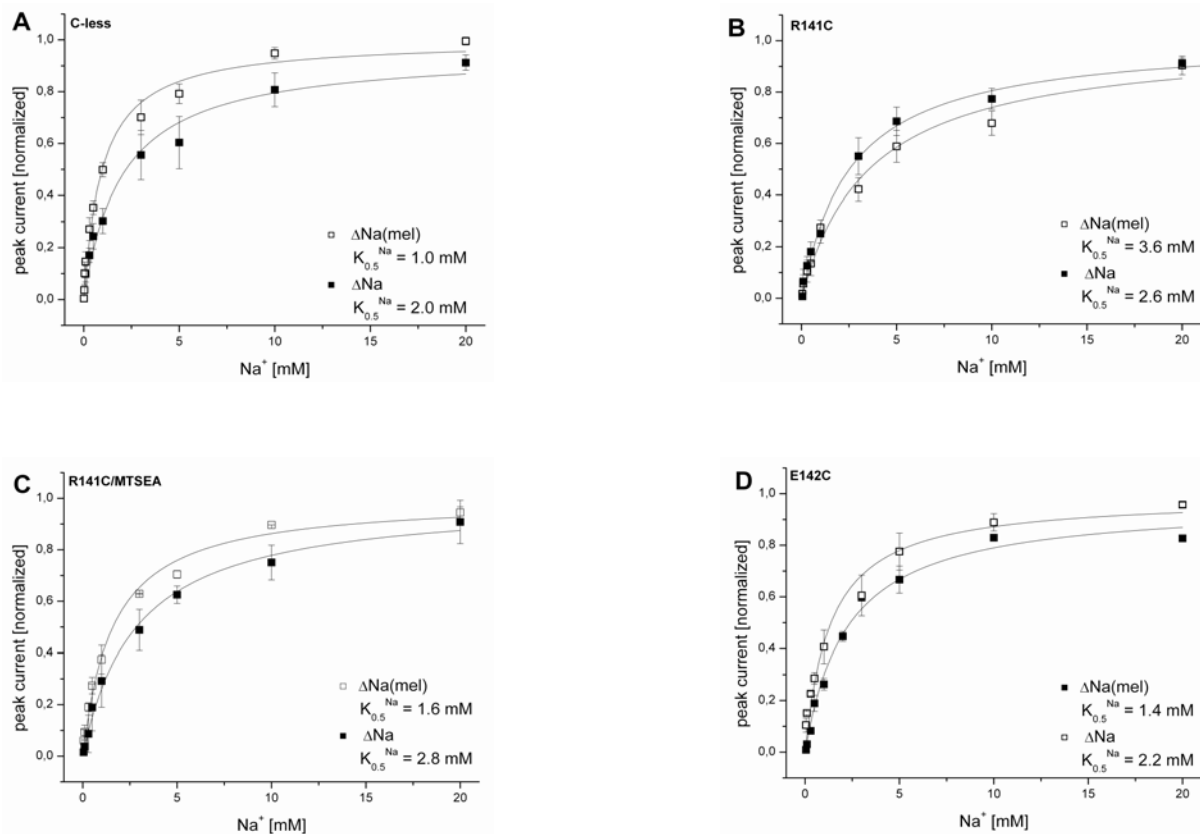
Figure 3-12. Half saturation concentrations (K$_{0.5}$) for Na$^+$ in the presence and absence of melibiose for C-less, R141C, and E142C.

The K$_{0.5}$ values were determined with the SSM for C-less (A), R141C (B), R141C in the presence of MTSEA$^+$ (C), and E142C (D). The variation of the peak currents (Ip) recorded on imposing different concentration jumps against increasing Na$^+$ were plotted and the resulting hyperbolic curves were fitted with the function according to Michaelis-Menten (I$_p$ = I$_{pmax}$ * c/(c+ K$_{0.5}$); c= substrate concentration). For the plots indicated here, measurements from at least three individual experiments were normalized and averaged. Normalization was done by dividing data points by the I$_{pmax}$ from the respective individual fit. Shown are the average values and S.E. The K$_{0.5}$ values that are indicated in the figure are the value from the fit of the averaged data points.

Whereas the figure shows the fits with the $K_{0.5}$ values to this averaged data, Table 3-3 presents the average values and S.E. from individual fits. In the absence of melibiose, the data yielded a half-saturation concentration ($K_{0.5}$) for Na^+ of 2.9 mM. In the presence of melibiose, $K_{0.5}$ decreased to 1.0 mM. These values are similar to the wild-type data and parallel the cooperative behavior of melibiose on Na^+ binding as also observed in the wild-type (see Table 3-3 and [Ganea *et al.* 2001]). In contrast, the cooperative effect of melibiose on Na^+ binding is reduced in R141C. The half-saturation concentration of Na^+ increases in the presence of melibiose from 2.7 mM to 3.6 mM in R141C. The half saturation concentration of E142C is similar to the C-less mutant (2.5 mM in the absence and 1.5 mM in the presence of melibiose) (Figure 3-12B and C, and Table 3-3). However, $MTSEA^+$ was able to increase the cooperative effect in R141C slightly as the $K_{0.5}^{Na}$ decreased in the presence of melibiose (Figure 3-12D and Table 3-3) indicating that probably the positive charge is important for the communication between the two binding sites.

Figure 3-13A shows that plotting the I_p dependence on the melibiose concentration shows also saturation behavior. The C-less mutant shows an increased $K_{0.5}^{mel}$ compared to the wild-type (50.4 mM vs. 22 mM, see also Table 3-3), but is likewise stimulated in the presence of Na^+ (4.5 mM in C-less vs. 3 mM mM in wild-type). Unfortunately, for R141C and E142C it was not possible to determine $K_{0.5}$ values for melibiose in the absence or presence of Na^+, since the melibiose signals for the two mutants were very unstable, constant over the whole titration series, or vanished completely after a few shots. Stable melibiose signals in R141C could be measured in the presence of $MTSEA^+$ (Figure 3.13B and Table 3-3) determining a $K_{0.5}^{mel}$ of 30.6 ± 17.1 mM. The large S.E. indicates that also here measurements were quite difficult to perform. The $K_{0.5}^{mel}$ was not significantly stimulated by Na^+ (21.5 ± 11.6 mM). This shows that, although a cooperative effect of Na^+ on the melibiose binding is visible, it is strongly reduced indicating a communication problem between the two binding sites.
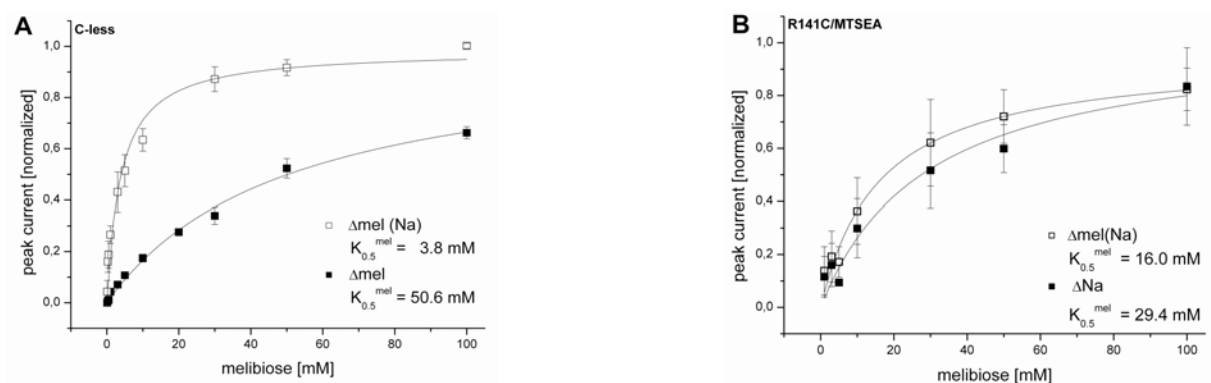
Figure 3-13. Half saturation concentrations (K$_{0.5}$) for melibiose in the presence and absence of Na$^+$ for C-less and R141C/MTSEA.

The K$_{0.5}$ values were determined as described for Figure 3-12.

Table 3-3. Half Saturation Constants of WT,C-less, R141C. and E142C MelB.

		WT [Ganea *et al.* 2001]	C-less	R141C	R141C + MTSEA	E142C
K$_{0.5}$^{Na} (mM)	without melibiose (ΔNa)	2.1	2.9 ± 0.8	2.7 ± 0.7	3.0 ± 1.2	2.5 ± 0.1
	in the presence of 50 mM melibiose (ΔNa(mel))	0.6	1.0 ± 0.1	3.6 ± 0.6	1.6 ± 0.1	1.5 ± 0.4
K$_{0.5}$^{mel} (mM)	without Na$^+$ (Δmel)	22	50.4 ± 1.8	n.m.	30.6±17.1	n.m.
	in the presence of 10 mM Na$^+$ (Δmel(Na))	3	4.5 ± 1.2	n.m.	21.5±11.6	n.m.

The K$_{0.5}$ values are averages and S.E. from at least three independent experiments. n.m. = non measurable.

3.2.4 Analysis of E365C Mutant

While carrier reorientation is severely impaired when Glu-365 is mutated into Gly, Asp, or Ala, binding of the sugar analog α-NPG remained similar to the wild-type [Pourcher *et al.* 1990]. Since these data implicated a participation of Glu-365 in the reorientation process, E365C was constructed in this thesis by site-directed mutagenesis to better study the role of this residue.

Initial characterization included the measurement of melibiose uptake in intact cells. Again, the C-less mutant served as control (Figure 3-14A). Although the overall level of sugar accumulation is limited reduced in E365C (Figure 3-14B), it is stimulated by Na^+ and Li^+ indicating that position 365 can tolerate at least some structural variation. A similar conclusion was drawn by Ding [Ding 2003, 2004]. Nevertheless, the E365C mutant was purified and reconstituted into liposomes to study its charge translocation properties.
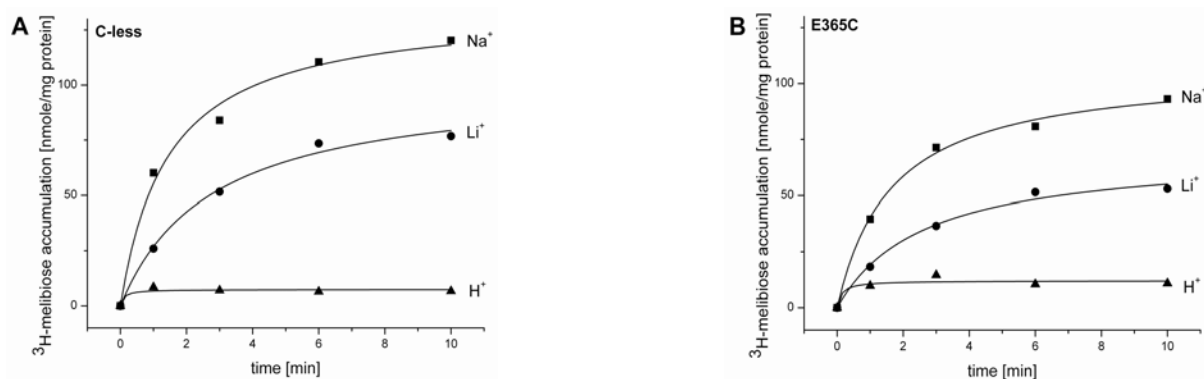
Figure 3-14. Cell sugar transport by C-less and E365C expressing *E.coli* cells.

Active transport was assayed on concentrated *E.coli* DW2-R cells bacteria expressing C-less (A) or E365C (B) permeases, respectively. Cell transport was assayed using cells (2 mg of protein/mL) equilibrated in 100 mM KPi, pH 7. Transport was started immediately after the addition of [^{3}H] melibiose (20 mCi/mmol) at a final concentration of 0.4 mM, respectively. According to the different transport modes of MelB, the cells were preincubated with 10 mM NaCl, 10 mM LiCl, or no salts, respectively. The reaction was terminated at the indicated time points by a rapid dilution followed by immediate filtration.

3.2.4.1 Electrical Signals Generated by Different Concentration Jumps

Large transient currents were observed on imposing different cosubstrate concentration jumps to the E365C mutant (Figure 3-15). Although the signals in Figure 3-15 look similar to those obtained for the C-less mutant, some differences between C-less and E365C should be noted. First, the relative peak currents of Δmel and Δmel(Na) concentration jumps are only half of the sizes of the C-less mutant (see also Table 3-4).
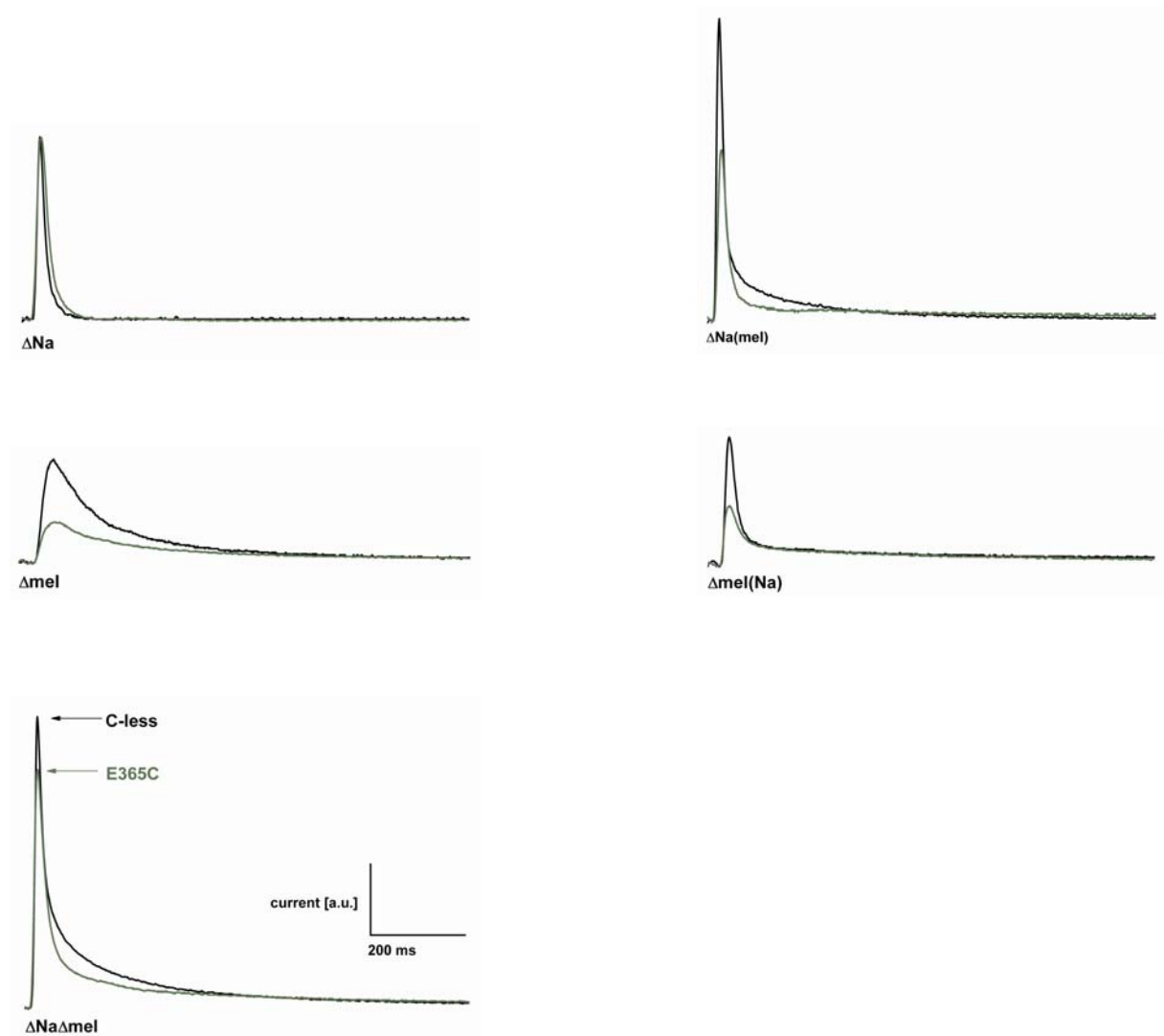
Figure 3-15. Comparison of the electrical signals recorded from E365C and C-less MelB.

The signals were recorded and normalized as described for Figure 3-9. The upper black line in each signal-pair was recorded from the C-less mutant and the lower green line from E365C.

74

Furthermore, the $\Delta Na(mel)$ concentration jump causes signals with peak currents smaller than that obtained after a ΔNa concentration jump. This is different from the behavior in the C-less mutant, where the peak current is enhanced after a Na^+ concentration jump in the presence of melibiose (see also Table 3-4). On the other hand, decaying time constants τ_1 and τ_2 from all signals recorded after different solution exchange protocols agree well with those from C-less MelB indicating that the mutation does not significantly influence the kinetic properties of the carrier. NEM, added to E365C on the SSM/proteoliposomes system, had no effect on the size and the stationary component of the electrical signal (data not shown).

Table 3-4. Characteristics of E365C Electrical Signals Compared to C-less MelB.

		C-less	E365C
Δmel	τ_1 [ms]	82.5 ± 4.8	97.4 ± 18.6
	τ_2 [ms]	258 ± 14.4	284 ± 21
	peak current [% of ΔNa]	56 ± 6.2	22.0 ± 4.1
Δmel(Na)	τ_1 [ms]	15.4 ± 0.8	16.9 ± 1.1
	τ_2 [ms]	264 ± 55	308 ± 22.3
	peak current [% of ΔNa]	70.6 ± 4.6	32.2 ± 5.2
ΔNa	τ_1 [ms]	14.8 ± 0.7	14.4 ± 1.1
	τ_2 [ms]		
	peak current [% of ΔNa]	100	100
ΔNa(mel)	τ_1 [ms]	11.5 ± 1.9	$15,1 \pm 1.3$
	τ_2 [ms]	172 ± 21.4	189 ± 57
	peak current [% of ΔNa]	169.9 ± 11.6	94 ± 5
ΔNaΔmel	τ_1 [ms]	19.2 ± 2.0	$18,1 \pm 1,9$
	τ_2 [ms]	174.1 ± 9.9	208 ± 20.6
	peak current [% of ΔNa]	165.5 ± 9.7	133 ± 3.5
n		5	4

For better comparison with the R141C and E142C data, the data from E365C were also normalized to the ΔNa signal. Indicated are the average values and the S.E.

3.2.4.2 Na⁺ and Melibiose Concentration Dependence

The $K_{0.5}^{Na}$ determined for Na^+ in the presence and absence of melibiose are similar to that of the C-less mutant (Figure 3-16 and Table 3-5). On the other hand, the $K_{0.5}^{mel}$ was around half of the value determined for C-less mutant, but similar to the wild-type. (Table 3-5). Although the $K_{0.5}^{mel}$ is smaller in the presence of Na^+, the cooperative effect of the ion on melibiose binding was reduced as compared to the C-less mutant.
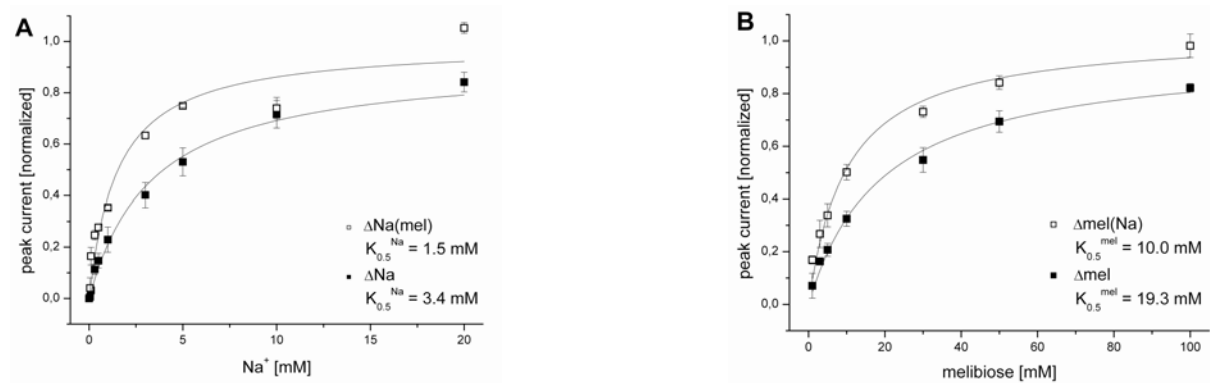
Figure 3-16. Half saturation concentrations for Na⁺ and melibiose for E365C.

The $K_{0.5}$ values were determined as described for Figure 3-12.

A. Na^+ concentration dependence in the presence and absence of melibiose.

B. Melibiose concentration dependence in the presence and absence of Na^+.

Table 3-5. Half Saturation Constants of WT, C-less, and E365C.

		WT	C-less	E365C
$K_{0.5}^{Na}$ [mM]	without melibiose (ΔNa)	2.1	2.9 ± 0.8	4.3 ± 1.0
	in the presence of 50 mM melibiose (ΔNa(mel))	0.6	1.0 ± 0.1	1.6 ± 0.2
$K_{0.5}^{mel}$ [mM]	without Na^+ (Δmel)	22	50.4 ± 1.8	22.3 ± 3.0
	in the presence of 10 mM Na^+ (Δmel(Na))	3	4.5 ± 1.2	9.4 ± 1.0

The $K_{0.5}$ values are averages and S.E. from at least three independent experiments.

3.3 Fluorescence Measurements

Fluorescence spectroscopy has been used extensively to study protein dynamics with exquisite sensitivity and selectivity. Since fluorescence probes sense their surrounding environment, which could differ in the absence and presence of ligands, changes in fluorescence can be interpreted as conformational changes of the protein.

3.3.1 Steady-State Intrinsic Tryptophan Fluorescence

Trp residues of MelB can be preferentially excited at 297 nm and serve, therefore, as intrinsic probe to monitor conformational changes of the protein upon substrate addition. While in wild-type MelB the addition of Na^+ induces a quenching of around 2%, subsequent melibiose addition enhances the steady-state fluorescence signal by ca. 17% [Mus-Veteau *et al.* 1995]. Since these variations in Trp fluorescence persisted in the presence of NEM, they were assigned to conformational changes in the early transport cycle of MelB.

In order to assess the implications of mutated amino acids in the Trp fluorescence properties of MelB, purified and reconstituted proteins (C-less, R141C, E142C, and E365C) were excited at 297 nm and the emission spectra recorded. A typical spectrum for C-less MelB is shown in Figure 3-17A. As in the wild-type, the fluorescence emission is slightly quenched by Na^+, and subsequent melibiose addition induces a large fluorescence increase indicating that the removal of the intrinsic cysteines did not significantly influence conformational changes associated to substrate binding. Figure 3-17B shows that, among the single Cys mutants, only R141C had a reduced fluorescence response elicited by Na^+. Both, E142C and E365C showed Trp quenching after Na^+ addition similar to the C-less mutant (3.1 ± 1.0 % and 4.1 ± 1.8%, respectively). Subsequent addition of melibiose enhanced the fluorescence signal by 10.9 ± 0.9 % in E365C, which is in the same order of magnitude as in the C-less mutant (17.8 ± 1 %). In contrast, these fluorescence signals were almost absent in R141C and E142C indicating a lack of conformational changes associated to melibiose binding. Upon addition of $MTSEA^+$ to R141C, the sugar-induced fluorescence signal did not return (data not shown). Also, NEM did not change the fluorescence properties of E142C (data not shown).
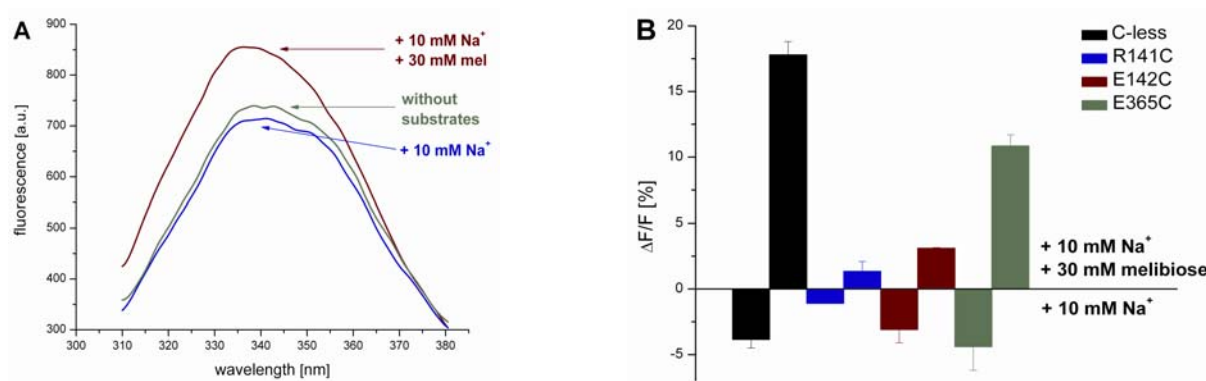
Figure 3-17. Trp fluorescence emission spectra of C-less, R141C, E142C, and E365C.

A. Typical fluorescence emission spectra for C-less MelB proteoliposomes. Approximately 20 μg of protein in 1 mL KPi (pH 7) were excited at 297 ± 5 nm and the emission spectrum recorded between 310 and 380 nm. Subsequently, 10 mM Na$^+$ and 30 mM melibiose were added, and after each addition the spectrum recorded again. Each spectrum is the mean of three scans.

B. ΔF/F variations for C-less, R141C, E142C, and E365C proteoliposomes. Measurements were the same as described in A. After excitation, the emitted fluorescence light (F) was integrated between 310 and 380 nm. Values are the means of three experiments and the S.E..

3.3.2 Steady-State Fluorescence Resonance Energy Transfer

Insights into co-substrate-induced structural changes of MelB can also be obtained from FRET spectroscopy measurements of proteoliposomes incubated in the presence of the β-galactoside fluorescent sugar analog 2'-(*N*-5-dimethylaminonaphthalene-1-sulfonyl)-aminoethyl-1-thio-β-D-galactopyranoside (Dns^2-S-Gal, [Maehrel *et al.* 1998]). The approach is interesting, since FRET occurs between the intrinsic tryptophans of MelB and the dansyl-sugar. Usually, FRET occurs if the emission spectrum of a donor, e.g. intrinsic tryptophans, overlaps with the excitation spectrum of an acceptor, e.g. Dns^2-S-Gal molecules, in close proximity (<50 Å of separation), and can be used to measure distances. In wild-type MelB the distance between Trp-299 and Dns^{2}S-Gal was estimated to 13.5 Å and that between Trp-64 and Dns^{2}S-Gal to 20 Å [Cordat *et al.* 1998].

A typical FRET measurement of C-less proteoliposomes, which is similar to that previously demonstrated for the wild-type [Maehrel *et al.* 1998], is shown in Figure 3-18A. When the protein was excited at 297 nm, the spectrum was typical for the transporter tryptophans (spectrum 1). Addition of 15 μM Dns$_2$-S-Gal gave rise to a small signal between 420 and 540

nm and a peak at 540 nm typical for dansylated sugars in an aqueous medium (spectrum 2). At the same time, the Trp fluorescence signal was quenched. Subsequent addition of 10 mM Na^+ induced a drastic increase in light emitted between 420 and 540 nm (spectrum 3), and a further quenching of the Trp fluorescence signal. The increase in the fluorescence emission signal was due to a FRET phenomenon between the MelB tryptophans and the Dns^2-S-Gal molecules bound specifically to the transporter and reflects a variation of MelB's structure close to the sugar binding site in the presence of Na^+ [Maehrel *et al.* 1998]. Finally, 30 mM melibiose addition reversed the spectral changes (spectrum 4).

Furthermore, the Na^+-difference spectra were calculated for R141C, E142C, and E365C proteoliposomes and compared to the C-less mutant. All three single Cys mutants retained a significant Na^+-dependent FRET signal similar to the C-less mutant (Figure 3-18B) indicating that Na^+ still induces a cooperative modification of the sugar binding site structure. The emission maximum of E142C, but not of R141C and E365C, was shifted from 460 nm in the C-less mutant to 480 nm in E142C meaning that the vicinity of the sugar environment is more polar in E142C than in the other mutants.
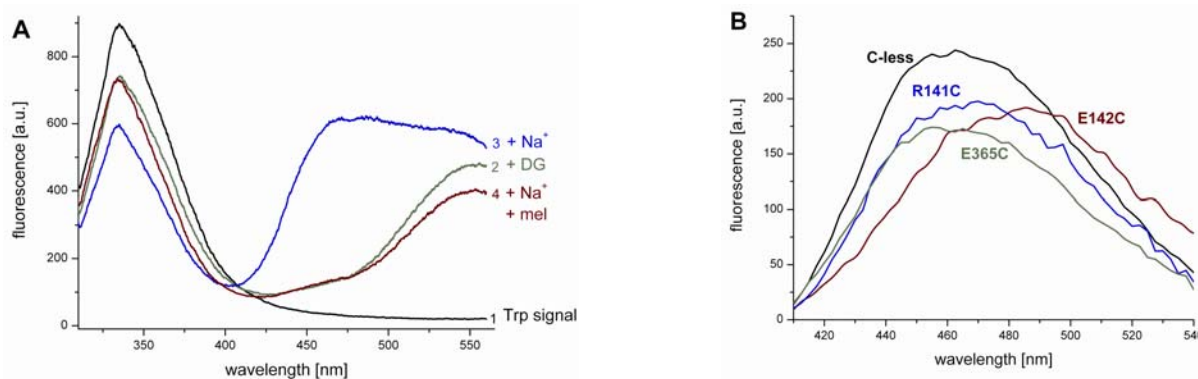
Figure 3-18. Fluorescence resonance energy transfer.

A. FRET between MelB Trp and Dns^2-S-Gal in C-less proteoliposomes. Conditions were as described for Figure 3-17A, except that the emission was recorded between 310 and 565 nm before any addition (spectrum 1, black) or after consecutive additions of 15 μM Dns^2-S-Gal (spectrum 2, green line), 10 mM Na^+ (spectrum 3, blue line), and 30 mM melibiose (spectrum 4, red line). Each spectrum is the mean of three scans.

B. Na^+-dependent variation of the FRET signal recorded from C-less MelB, R141C, E142C (bold spectrum), and E365C (dotted spectrum) proteoliposomes incubated in the presence of the fluorescence sugar analog Dns^2-S-Gal. The FRET signal (average of 3 scans) was recorded before and after the addition of 10 mM Na^+ as described in A. The Na^+- depending signals were calculated by subtracting the spectra (spectrum 3-spectrum 2).

3.3.3 Fluorescence Probes Attached to MelB

Whereas Trp fluorescence changes reflect more global conformational changes of the protein, Cys-scanning mutagenesis in combination with site-specific fluorescence labeling opens the possibility to study conformational changes at certain sites of interest. To follow this approach, single Cys mutants were purified, reconstituted into liposomes, and exposed to different fluorescent probes.

3.3.3.1 Labeling of Proteoliposomes with ThioGlo3 and MIANS

G117C (see chapter 3.5), R139C [Abdel-Dayem *et al.* 2003], and E365C (see above and [Ding 2003, 2004]) function similar to wild-type and were, therefore, chosen as targets for the attachment of the fluorescent probes. For the labeling reaction sulfhydryl reagents were used, which are essentially non-fluorescent until the maleimide group reacts with a thiol in the protein. Therefore, the non-reacted label did not need to be separated from the protein. The first probe, 9-acetoxy-2-(4-(2,5-dihydro- 2,5-dioxo-1*H*-pyrrol-1-yl)phenyl)-3-oxo-3*H*-naphtho[2,1-*b*]pyran (ThioGlo3), was tested because of its high quantum yield and fast reactivity. The second probe, 2-(4'-maleimidylanilino)naphthalene-6- sulfonic acid (MIANS), was chosen, because its fluorescence is very sensitive to the aqueous solvation state, and also because of the overlap of its absorbance spectrum with the emission spectrum of the tryptophans [Hogland 2002].

In general, the probes were added to the cuvette, which contained a proteoliposomes suspension, and fluorescence was recorded as a function of time. When ThioGlo3 was added to G117C, R139C, and E365C, fluorescence increased with a fast phase followed by a slower one (Figure 3-19A). Unexpected, also the C-less mutant and R139C in the presence of NEM showed an increase in fluorescence, although the fast phase was absent. This indicates that ThioGlo3 binds either non-specifically to the protein or that it partitions into the lipid bilayer giving, thereby, rise to a high fluorescence background signal. Since the fast signal is only observed when specific labeling is expected, it is most likely that it is linked to specific binding of the probe to the protein.

When MIANS was added to the cuvette, no increase in fluorescence could be observed for G117C and R139C proteoliposomes. Either, these two mutants are not accessible by the probe or the Cys residues have a too polar environment, as MIANS develops only an appreciable fluorescence when bound to cysteines located in hydrophobic sites [Hogland 2002]. More
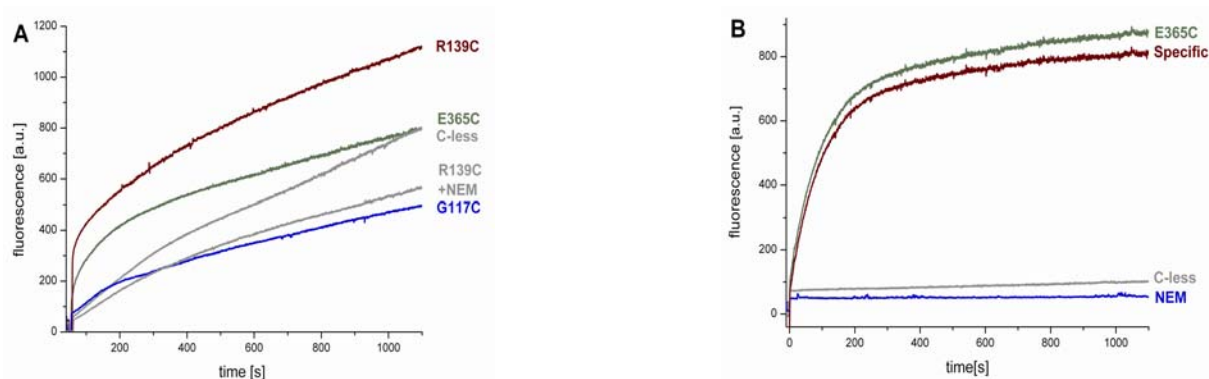
Figure 3-19. Time course of the labeling of single Cys mutants with ThioGlo and MIANS.

A. Labeling of single Cys proteoliposomes with ThioGlo3. 20 μL proteoliposomes of G117C, R139C, E365C, or C-less (around 1 mg/mL each) were suspended in Na^+-free, 100 mM KPi buffer (pH 7), and labeling was carried out in a total volume of 0.5 mL. R139C was also reacted in the presence of NEM. The reaction was started by adding 5 μM ThioGlo to the cuvette. Fluorescence was recorded over 20 minutes at 440 nm (λ_{ex}= 363 nm).

B. Labeling of E365C proteoliposomes with MIANS. The experiment was done as described in A except that 5 μM MIANS were added instead of ThioGlo. Fluorescence was recorded over 20 minutes at 415 nm with an excitation wavelength of 329 nm (total). E365C preincubated with 2 mM NEM for 30 minutes and C-less MelB are also depicted. The latter signal was used to correct the total spectrum for the nonspecific fraction. The difference is shown as specific labeling of E365C with MIANS.

interesting, a very important biphasic increase in MIANS fluorescence with a predominant fast ($\tau_1 \sim 85$ s) followed by a minor slower component ($\tau_2 \sim 700$ s) was observed in E365C (Figure 3-19B). The increase in fluorescence intensity with time proved that the Cys is readily accessible to the fluorescence probe. As control, the fluorescence labeling time course in the C-less mutant was tested. The small increase in fluorescence observed directly after the addition of MIANS to the C-less MelB did not further increase with time. This non-specific binding of the fluorophore to the protein and/or lipid membrane was subtracted from the recorded spectrum resulting in the specific fluorescence curve. Furthermore, when E365C was preincubated with 2 mM NEM for 10 minutes, MIANS addition did not result in any detectable fluorescence increase (Figure 3-19B). Therefore, the reaction between the probe and E365C can be considered to be specific. MIANS labeling of E365C in the presence of 10 mM Na^+ reduced the intensity of the fluorescence development slightly (data not shown). Furthermore, if the proteoliposomes were preincubated with 50 mM melibiose in the absence or presence of 10 mM Na^+, labeling proceeded faster ($\tau_1 \sim 50$ s and $\tau_2 \sim 210$ s, data not shown) suggesting that melibiose enhances the accessibility of the residue 365C to MIANS.

3.3.3.2 Effect of Na⁺ and Melibiose on the Steady-State Fluorescence

Na$^+$ and melibiose were added to the ThioGlo3 -labeled proteoliposomes for studying possible substrate induced conformational changes. In order to exclude the possibility that the non-specific binding of ThioGlo3 to the protein and/or lipid bilayer causes fluorescence changes, substrates were added to the C-less mutant after its incubation with ThioGlo3 (Figure 3-20A). Since no changes in fluorescence were observed, addition of substrates to the other labeled proteins could be considered to be specific for the respective mutan*t*. When Na$^+$ was added to the ThioGlo3 labeled G117C a quench in fluorescence was induced with a further quench upon consecutive melibiose addition (Figure 3-20B). On the other hand, glucose, which is not a MelB substrate, did not change the fluorescence emission. This result suggests that both Na$^+$ and melibiose induce local conformational changes around residue 117. The fluorescence changes after the addition of substrates to R139C or E365C gave results that were not reproducible and are not shown. For the following reasons, the analysis of theThioGlo3 labeled permeases was delayed: first, the main interest of this work was to investigate melibiose induced conformational changes, which were small in G117C; second, R139C and E365C mutants gave inconsistent results; and third, the labeling induced very high background fluorescence. For future work it is, therefore, recommended to label the solubilized protein with ThioGlo3, remove the unbound dye by dialysis and, and then reconstitute the protein. In this way, the high background fluorescence can be prevented and the results should be more reproducible.

In contrast to the above mentioned observations, very clear and reproducible results were obtained with the MIANS labeled E365C mutant showing that MIANS is appropriate to be used for fluorescence studies. Also, the labeling with MIANS was very specific to single Cys mutants. Addition of 10 mM Na$^+$ resulted in a 4.3 ± 0.6 % quench of the fluorescence signal (Figure 3-20C). Whereas subsequent glucose addition had no effect on the fluorescence signal, 50 mM melibiose in the presence of 10 mM Na$^+$ resulted in an enhancement of the initial signal of 19.8 ± 0.4 %. On the other hand, melibiose in the absence of Na$^+$ did only enhance the fluorescent signal by 4.6 ± 0.8 % (Figure 3-20D). Consecutive Na$^+$ addition enhanced the initial signal by 18.7 ± 1.4 %. This shows that the changes in fluorescence are specific to MelB substrates.

In order to better characterize the properties of the fluorophore MIANS, the excitation and emission spectra were recorded for the MIANS-labeled E365C. The excitation maximum, measured at a fixed emission wavelength of 415 nm, was determined to be 329 nm. The

maximum did not shift in the presence of Na^+ or Na^+ and melibiose (Figure 3-21A). This is in agreement with previous results suggesting that the polarity around the MIANS group attached to thiols does not significantly influence the absorption properties of the fluorophore [Hiratsuka 1992]. Na^+ induced a reduced excitation intensity and Na^+ and melibiose an increased excitation intensity.
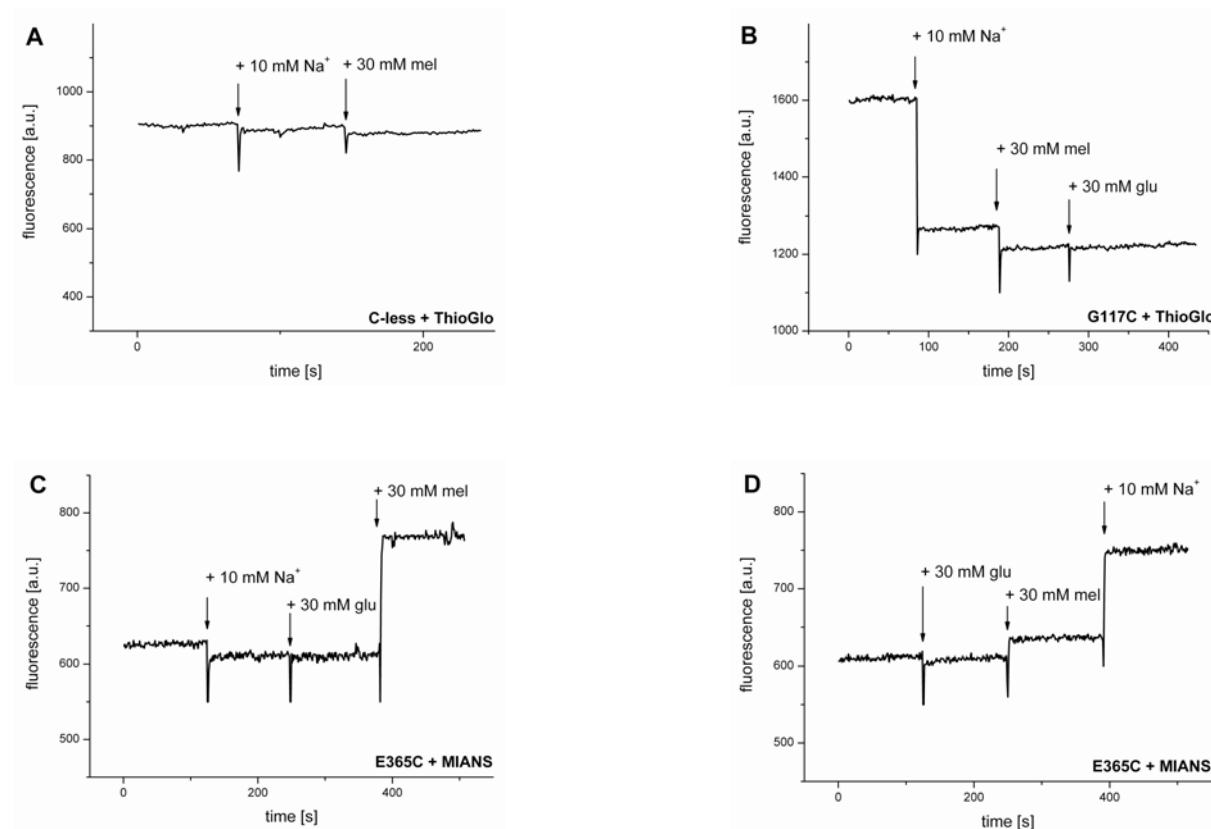
Figure 3-20. Fluorescence changes after substrates addition to labeled proteins.

A. Addition of substrates to the ThioGlo3-labeled C-less mutant. Experiments were performed as described for Figure 3-19A. After the fluorescence development had reached a steady state (approximately one hour), 10 mM Na^+ and 30 mM melibiose were consecutively added to the cuvette and the fluorescence changes recorded.

B. Addition of substrates to the ThioGlo3-labeled G117C mutant. Experiments were carried out as described for A except for that also 30 mM glucose were added as control.

C. Addition of substrates to the MIANS-labeled E365C mutant. Experiments were carried out as described for Figure 3-19B. After the fluorescence development had reached a steady state (approximately 20 minutes), 10 mM Na^+, 30 mM melibiose, and 30 mM glucose were consecutively added to the cuvette and the fluorescence changes recorded.

D. Addition of substrates to the MIANS-labeled E365C mutant. Experiments were carried out as described for C except that glucose was added first, then melibiose, and Na^+ last.

The emission maximum, measured at a fixed excitation wavelength of 328 nm, was determined to be 415 nm and did only red-shift by 1 nm upon Na^+ addition ($\lambda_{em(max)}$= 416 nm) and blue-shift by 1 nm upon Na^+ and melibiose addition ($\lambda_{em(max)}$= 414 nm, Figure 3-21B), which is not considered to be significant. At the same time, the emission maximum was quenched in the presence of Na^+ and enhanced in the presence of Na^+ and melibiose. From the environmental sensitive probe MIANS [Hogland 2002], one would have expected significant shifts in the emission maxima i.e., when MIANS was added to the model compound N-AcCys, the fluorescence intensity increased 13-fold in going from water to 99% ethanol, and at the same time the emission maximum blue-shifted by 21 nm [Hiratsuka 1992]. In any instance, the intensity changes are rather large allowing, thus, to measure substrate induced changes in the MIANS labeled E365C proteoliposomes in more detail (see next paragraphs).
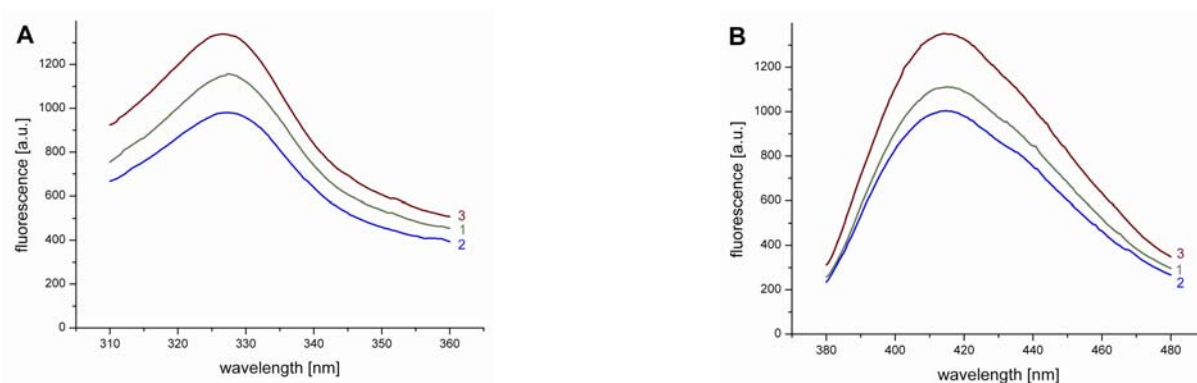
Figure 3-21. Excitation and emission spectra of MIANS-labeled E365C.

A: Excitation was recorded between 310 and 360 nm with a fixed emission wavelength of 415 nm. Spectra were recorded without any addition of substrates (spectrum 1, green), in the presence of 10 mM Na^+ (spectrum 2, blue) or in the presence of 10 mM Na^+ and 50 mM melibiose (spectrum 3, red).

B: Emission was recorded between 380 and 480 nm at a fixed excitation wavelength of 329 nm. Numbering and colors are as described for A.

3.3.3.3 Na$^+$ and Melibiose Concentration Dependence

The effects of different concentrations of the co-substrates on the fluorescence intensities of MIANS labeled E365C were studied in proteoliposomes preincubated with the respective other co-substrate. Plotting $\Delta F/F_0$ against increasing concentrations of melibiose or Na$^+$, respectively, resulted in hyperbolic curves that could be fitted with a function according to Michaelis-Menten (Figures 3-22). The half saturation concentration for Na$^+$ in the presence of 50 mM melibiose was determined with 0.17 ± 0.03 mM (average and S.E. of three individual experiments; in contrast, Figure 3-22A shows the $K_{0.5}$ obtained from the fit of the normalized data). It is possible that this value is lower compared to that obtained by SSM measurements (1.4 mM, see Table 3-4) because it is measured under steady-state conditions. The half saturation constant for melibiose in the presence of Na$^+$ was determined with 6.7 ± 1.0 mM (Figure 3-22B), a value which compares well with the one derived from electrical measurements (9.9 mM for E365C in the absence of the MIANS-label, Table 3-4). Thus, the label did not influence the affinity of the permease for melibiose.
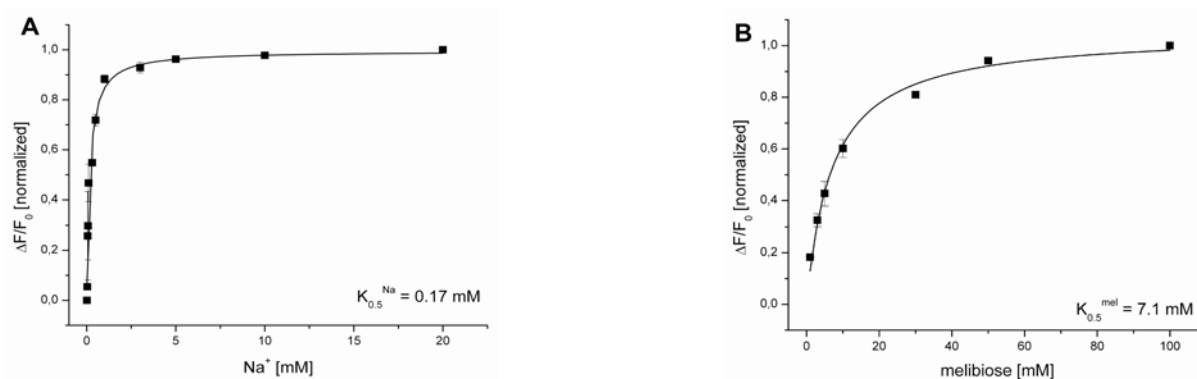
Figure 3-22. Effect of the concentration on the fluorescence intensity of MIANS-labeled E365C.
A. Concentration dependence of Na$^+$. The permease was labeled in the absence of ligands with MIANS as described for Figure 3-19B. 50 mM melibiose were added to the cuvette and the proteoliposomes incubated for around 5 minutes. Na$^+$ was added stepwise and the fluorescence change recorded. The relative fluorescence change was plotted against the respective concentration and normalized. Data points from three individual experiments were averaged ($\pm$ S.E.), and the points fitted with the function according to Michaelis-Menten. The $K_{0.5}^{Na}$ depicted in the Figure is the half saturation concentration of the fit to the normalized data.
B. Concentration dependence of melibiose. As described in A, except that the proteoliposomes were incubated with 10 mM Na$^+$ and melibiose was stepwise added. The $K_{0.5}^{mel}$ depicted in the Figure is the half saturation concentration of the fit to the normalized data.

3.3.3.4 MIANS Signal at 297 nm Excitation Wavelength

The fluorescence emission spectrum recorded from MIANS labeled E365C proteoliposomes was analyzed between 310 and 500 nm to assess the implication of permease tryptophans in the MIANS fluorescence signal upon illumination at 297 nm. In the absence of MIANS and MelB substrates, the fluorescence contribution in the 310-380 nm interval is typical of the transporter tryptophans (Figure 3-23, spectrum 1). In the presence of MIANS a strong reduction in the Trp emission intensity at 340 nm occurred with a concomitant increase in the MIANS emission intensity around 415 nm (spectrum 2). At first sight, this is indicative of a FRET phenomenon between the tryptophans of the permease and the MIANS dye. However, the following observations do not support this suggestion. Whereas subsequent addition of Na^+ did not significantly change the emission spectrum, except for a very small quench of the Trp signal at 340 nm (not shown), addition of both melibiose and Na^+ resulted in an small enhancement of the signal at 340 nm and 415 nm without a concomitant shift in the emission maximum (spectrum 3). If a FRET phenomenon were to occur, one would have expected a concomitant decrease in Trp fluorescence and increase in MIANS. On the other hand, melibiose enhances the Trp fluorescence emission, which could account for the enhanced fluorescence at 340 nm concomitant with the increase in MIANS fluorescence. Therefore, the FRET phenomenon is nevertheless a possible explanation for the observed spectra.
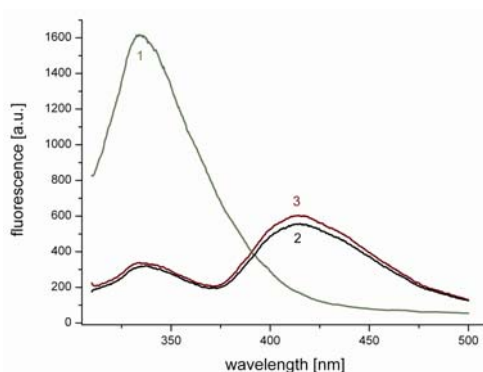
Figure 3-23. Emission spectra of MIANS-labeled E365C at 297 nm.

20 μg E365C proteoliposomes, resuspended in 480 μL KPi, pH 7, were added to the cuvette. MelB tryptophans were excited at 297 ± 5 nm and emission recorded between 310 and 500 nm (spectrum 1, green). Then, MIANS labeling was performed as described for Figure 3-19B and the tryptophans excited again (spectrum 2, blue). Addition of 10 mM Na^+ resulted in a spectrum similar to spectrum 2 except that a very small quench was observed in the Trp emission (not shown). Subsequently, 50 mM melibiose were added (spectrum 3, red). One representative experiment is shown.

3.3.3.5 Stopped-Flow Measurements

The data presented above show changes of the fluorescence emission intensity upon substrate addition, but they do, however, not resolve the kinetics of these changes. In order to unravel rate constants of individual reactions, especially the melibiose-induced conformational change, the stopped-flow technique was applied to C-less MelB, E365C, and the MIANS-labeled E365C mutant.

In a first set of stopped-flow experiments, the intrinsic Trp fluorescence of MelB was used to study the melibiose induced conformational change (see also Figure 3-17). Control measurements included a Δmel(Na) concentration jump without protein or in the presence of empty liposomes, a Δmel(K) concentration jump on C-less MelB, and a Δmel(Na) concentration jump on C-less MelB using a 360 cut-off filter. The control experiments did not result in any fluorescence signal (data not shown), thus, the conditions that were chosen are specific for the activity of MelB. C-less MelB proteoliposomes were preincubated with Na^+, and mixed with a solution containing Na^+ and melibiose (Δmel(Na) concentration jump). The enhancement of the fluorescence followed a bi-exponential time course with a τ_1 of ~14 ms and a τ_2 of ~300 ms (Figure 3-24A). A similar signal (τ_1 of ~15 ms, τ_2 of ~200 ms) was determined for the E365C mutant in the absence of any label (Figure 3-24B) indicating that the mutation from Glu to Cys at position 365 does not influence the rate of the melibiose-induced conformational changes as represented by the intrinsic Trp fluorescence. Interestingly, electrical signals elicited by a Δmel(Na) concentration jump decay with similar time courses both in C-less MelB and in the E365C mutant (τ_1 ~16-17 ms, τ_2 ~280 ms, see Figure 3-24C and D). Whereas the slow component of the electrical signal was linked to the stationary transport behavior of the permease, the meaning of the slow component in the Trp signal is, so far, unknown.
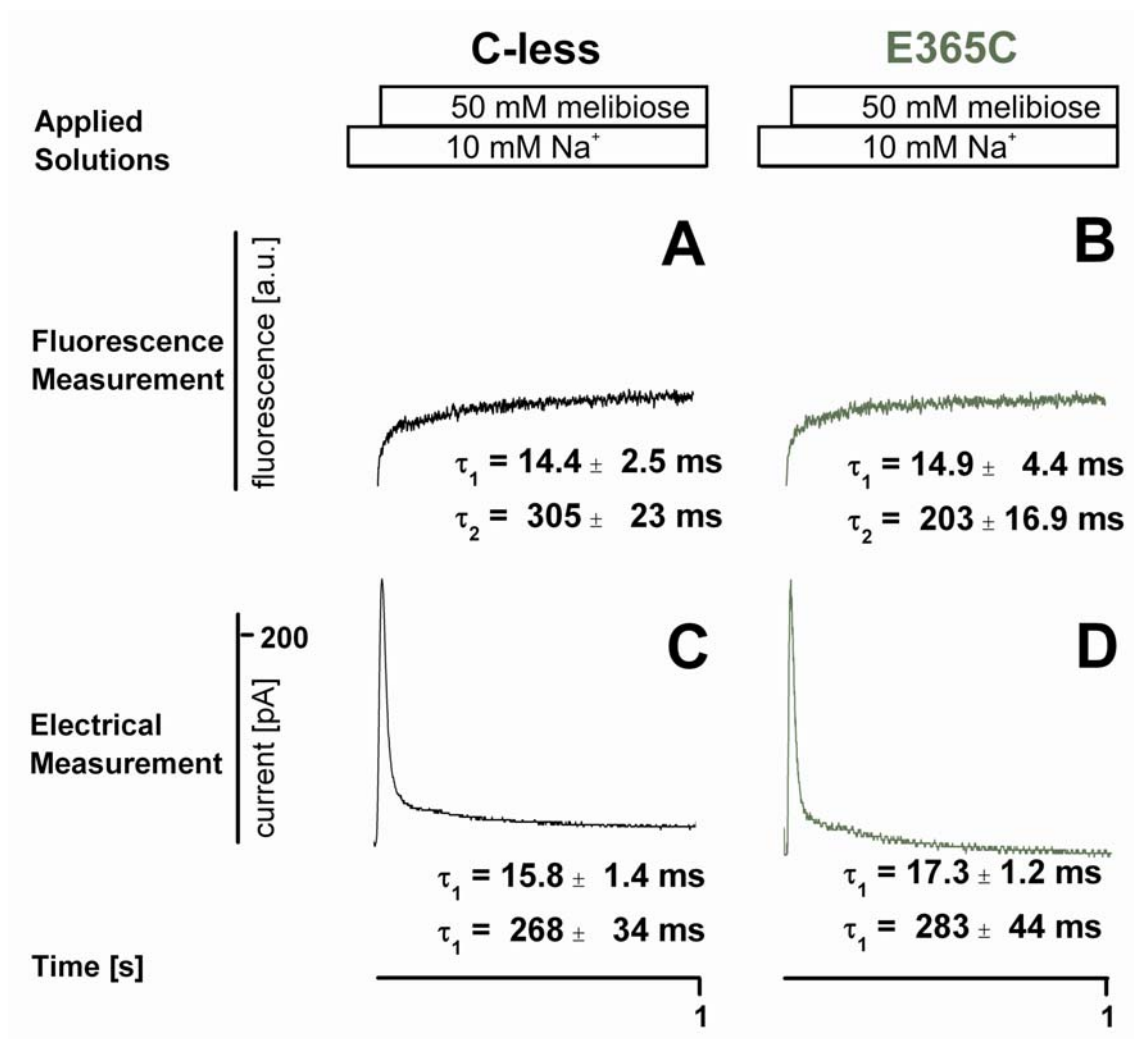
Figure 3-24. Trp fluorescence and electrical time-resolved Δmel(Na) experiment.

Fluorescence measurements: For fluorescence measurements, the protein (50 μL protein (1 mg/mL) in 1 mL KPi buffer) was equilibrated with 10 mM Na$^+$. As mixing solution 10 mM Na$^+$ and 100 mM melibiose were used (Δmel(Na) experiment) so that the final concentration in the reaction chamber was 50 mM melibiose. The excitation wavelength was set to 297 nm to excite the intrinsic tryptophans of the protein and a 320 nm cut-off filter used in front of the photomultiplier. All solutions were equilibrated at 24°C. Each trace shows the average of 6 or 9 spectra, respectively. A: C-less MelB, B: E365C.

Electrical measurements: For electrical measurements, the same conditions were used as described for Figure 3-3A except that a 50 mM melibiose concentration jump was applied. Individual, representative traces are shown. C: C-less MelB, D: E365C.

All time constants are averages and S.E. of 5-15 experiments.

In a second set of stopped-flow experiments, a Δmel(Na) concentration jump was applied to the MIANS labeled E365C protein. The resulting fluorescence signal showed an increase in amplitude (Figure 3-25A). Fitting the signal time course with a bi-exponential function revealed a τ_1 of ~43 ms and a τ_2 of ~230 ms. Plotting the relative fluorescence change as a function of the melibiose concentration resulted in a hyperbolic function with a half saturation concentration of 7.8 ± 1.1 mM (data not shown). This value is similar to that obtained from steady-state fluorescence measurements above (6.7 ± 1 mM, see also Figure 3-22B). As control, a glucose concentration jump was applied (Figure 3-25A) showing no change in fluorescence. Interestingly, the τ_1 determined with the MIANS fluorescence signal is around three times slower than that determined by the intrinsic Trp fluorescence suggesting that the two fluorescent signals monitor two different transitions in the reaction cycle.
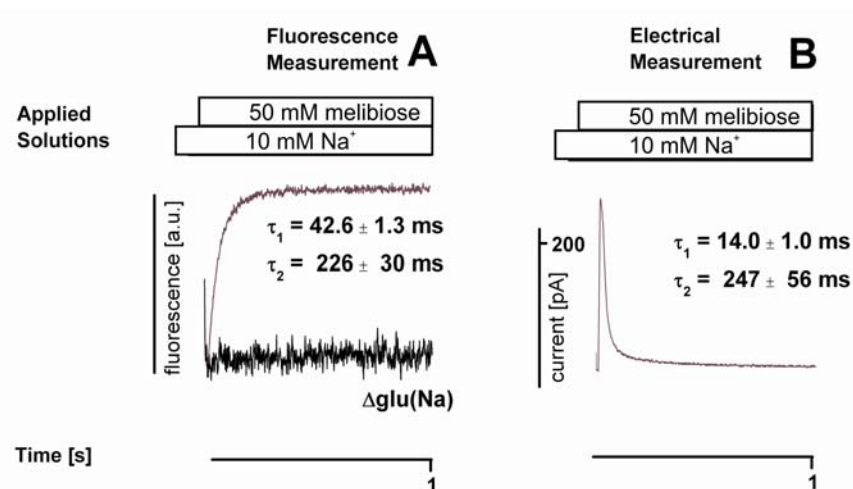
Figure 3-25. MIANS-labeled E365C fluorescence and electrical Δmel(Na) experiment.
A: E365C was labeled with MIANS for 30 minutes as described for Figure 3-19B. The excitation wavelength was set to 335 nm and a 385 nm cut-off filter was used in front of the photomultiplier. All solutions were equilibrated to 24°C. The trace shows the average of 15 measurements, the time constants are averages and S.E. of the same experiments. As control, a glucose concentration jump was applied to the MIANS-labeled E365C.
B: E365C was labeled with MIANS and adsorbed to the SSM. A Δmel(Na) concentration jump was recorded. Whereas the trace is recorded from a single experiment, the time constants are average and S.E. of three individual experiments.

Figure 3-25B displays, furthermore, the electrical signals from MIANS-labeled E365C evoked by a Δmel(Na) concentration jump. The electrical signal could be fitted with a bi-exponential function decaying with similar time constants ($\tau_1 \sim 14$ ms, $\tau_2 \sim 250$ ms) as the signal recorded from the MIANS unlabeled E365C, indicating that it is not the MIANS reaction with 365C that slows down the fluorescence signal. Overall, τ_1 determined by electrical measurements agrees, therefore, in all cases well with that determined with the intrinsic Trp fluorescence, while the process detected by the MIANS fluorescence is slower (τ_1 around 43 ms).

In a third stopped-flow experiment, the Na^+-induced Dns^2-S-Gal signal was analyzed in the C-less mutant (see also Figure 3-18). To this end, the proteoliposomes were preincubated with the fluorescence sugar analog Dns^2-S-Gal, and a Na^+ concentration jump performed ($\Delta Na(Dns^2$-S-Gal)). The resulting fluorescence signal in C-less MelB increased exponentially with a τ_1 of around 18 ms and a τ_2 of around 180 ms (Figure 3-26), thus demonstrating that the modification of the sugar binding site structure after the addition of Na^+ is fast proceeding with rate constant of around 55 s^{-1}.
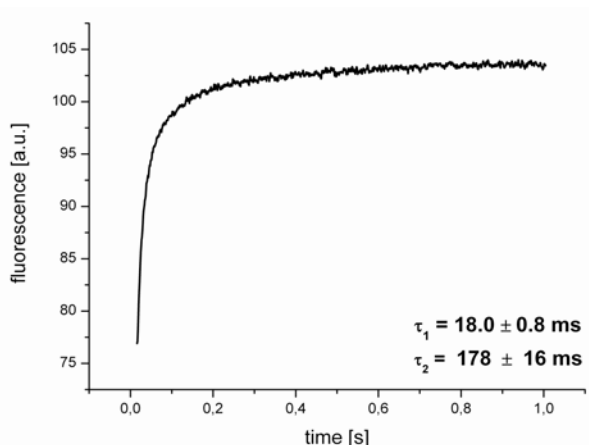
Figure 3-26. Na^+ induced fluorescence signal in the presence of Dns^2-S-Gal.

C-less MelB, resuspended in 100 mM KPi buffer, pH7, was equilibrated with 10 μM Dns^2-S-Gal. As mixing solution 20 mM Na^+ and 10 μM Dns^2-S-Gal were used in 100 mM KPi buffer, pH7. The excitation wavelength was set to 297 nm and a 400 nm cut-off filter was used in front of the photomultiplier. All solutions were equilibrated to 24°C. The trace shows the average of 5 measurements. Indicated time constants are the means and S.E. of five individual experiments.

3.3.3.6 Effects of Temperature on Pre-steady-state Fluorescence

The experiments with MelB have mainly been performed at room temperature (range 20 to 24°C), a situation that is certainly not physiological for *E.coli* transporters. In addition, studying the effects of temperature on the kinetics of the substrate-induced conformational changes is also a useful means to obtain more information on the nature of the process, since the temperature coefficient Q_{10} is related to the conformational changes involved. The stopped-flow technique provides a powerful tool to resolve kinetics up to 1 ms, therefore, it was used to acquire the activation energies for substrate-induced conformational changes in MelB.

Therefore, k $(1/\tau_1)$ was determined for the Na^+-induced Dns^2-S-Gal signal, the melibiose-induced Trp-signal, and the melibiose-induced MIANS signal at different temperatures. All fluorescence responses were fitted with double-exponential functions. Only τ_1 was used to calculate the activation energies, as the meaning of the slow decaying component is up to now uncertain.

Figure 3-27 shows that in all cases the reaction becomes faster at higher temperatures. Arrhenius plots gave similar slops in the C-less mutant for the processes induced by a Na^+ jump in the presence of Dns^2-S-Gal or by a melibiose jump (detected with the intrinsic Trp fluorescence) corresponding to activation energies of around 40 kJ/mole. The Q_{10}, calculated from the plots, was between 1.7 and 1.8. In contrast, the activation energy detected with the melibiose-induced signal in MIANS-labeled E365C mutant was around 2.5 times higher (~ 100 kJ/mole), and the corresponding Q_{10} was 3.7. As the conformational change after melibiose binding detected with the Trp fluorescence requires a significantly different activation energy as that detected with the MIANS-fluorescence, the results suggest that these two processes are different. Since E365C was found to function adequately similar to the C-less mutant having, especially, similar time constants in the melibiose-induced Trp signal (Figure 3-24), it is reasonable to assume that the activation energy measured with the Trp fluorescence in MIANS-unlabeled E365C would compare well with that of the C-less mutant. In any instance, it is mandatory to repeat the experiment with the unlabeled E365C mutant.
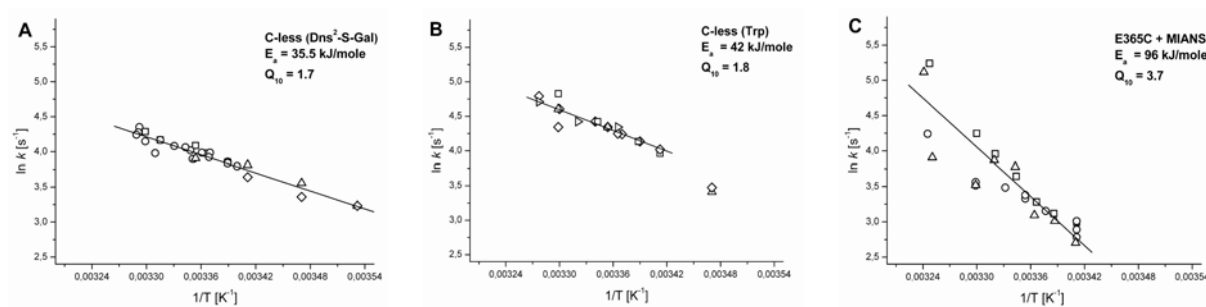
Figure 3-27. Arrhenius plots of the rate of substrate-induced fluorescence signals.

The temperature was varied between 15 and 32°C and plotted as 1/T (in K) against ln k. The activation energy was calculated as described for Figure 3-7. 3-5 individual experiments as represented by different symbols are shown in each figure.

A: ΔNa concentration jump in C-less MelB in the presence of Dns^2-S-Gal (as described for Figure 3-26).

B: Δmel(Na) concentration jump in C-less MelB at 297 nm excitation (as described for Figure 3-24).

C. Δmel(Na) concentration jump in MIANS-labeled E365C (as described for Figure 3-25).

3.4 Proteolysis Experiments

Substrate induced conformational transitions can also be studied by conformation dependent proteolysis patterns. For wild-type MelB it was shown that Na^+ alone reduces the rate of Trypsin digestion of loop 4-5 approximately 3-fold, while the simultaneous presence of melibiose and Na^+ reduces the rate up to 9 fold [Gwizdek *et al.* 1997]. On ground of these data, at least two conformational changes during the transport cycle of MelB were suggested, one occurring upon interaction of the coupling ion with the transporter, a second one triggered by sugar binding on the binary complex Na^+-permease.

In order to reveal, whether specifically R141 of loop 4-5 is involved in such substrate induced conformational changes, proteolysis experiments were performed on the R141C mutant. Therefore, purified MelB was incubated without substrates, with Na^+, or with Na^+ and melibiose before trypsin was added. The optimal enzyme concentration was determined with 10 μg/mL (data not shown) and used to digest the protein. Up to the present, protein digestion patterns were analyzed only after 10 minutes incubation with the protease, and no time course of the reaction was recorded. The proteolysis fragments should have sizes of 8, 17, 28, 36, and 45 kDa [Gwizdek *et al.* 1997].

First, the proteolysis experiments showed that the full length wild-type MelB in proteoliposomes disappears very rapidly (60% after 10 min of incubation) with the concomitant appearance of the cleavage fragments (Figure 3-28). As only cytoplasmic domains of MelB are processed by the protease, this result reinforces the conclusion of a predominant inside-out orientation of MelB in proteoliposomes.

For comparison between wild-type, C-less, and R141C, the band of 28 kDa was chosen, because it was usually strong and very well visible. For wild-type MelB (Figure 3-28), the intensity of this 28 kDa band was 92% when the protein was preincubated with Na^+ and 48% when the protein was preincubated with Na^+ and melibiose (compared to the band intensity when the protein was digested without substrates). This agrees with a protection of the cleavage sides in the presence of Na^+, which is more pronounced in the presence of both substrates. The C-less mutant showed an intensity of 73% in the presence of Na^+ alone and 54 % in the presence of both substrates, which is in good agreement with the value from the wild-type (Figure 3-28). In contrast, the intensity of this band in R141C was 76% in the presence of Na^+, but not further reduced in the presence of melibiose and Na^+ (Figure 3-28). Although semi-qualitative, the data suggest that the conformational change after melibiose

binding in R141C, which is in C-less responsible for the protection of the cleavage site, is either absent or different from the one in wild-type or C-less. However, the number of measured data points was too low to present statistical values.
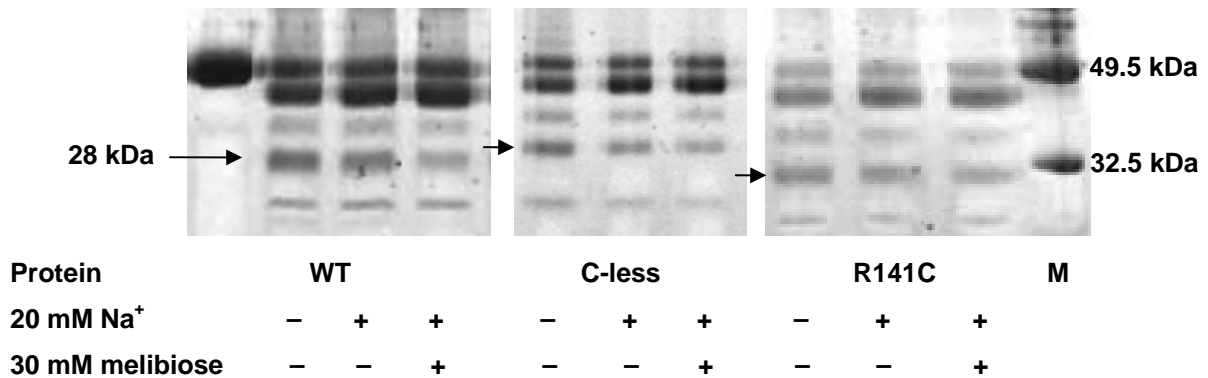
Figure 3-28. Proteolysis digestion patterns of wild-type, C-less, and R141C.

25 µg Proteoliposomes were preincubated without substrates or with 20 mM Na$^+$ or 20 mM Na$^+$ and 30 mM melibiose. Trypsin was added at 10 µg/mL and the reaction was carried out during 10 minutes at 25°C. The reaction was quenched by the addition of phenylmethanesulfonyl-fluoride and rapid cooling on ice. Analysis was done by 18% SDS-PAGE. WT means wild-type MelB, M is the molecular weight marker. The first line represents WT protein without the addition of trypsin. The figures are from different gels, therefore, the bands are not on exactly the same places.

3.5 Screening of Mutants I53C, N58C, G117C

Finally, three different mutants were constructed by PCR, overexpressed in *E.coli*, purified, and reconstituted into liposomes to investigate in more detail the transport mechanism of MelB, and to attempt better to assign the electrical signals to partial reactions of the transport cycle. Mainly, two questions should be answered:

1.) Is the observed electrical behavior of MelB [Ganea *et al.* 2001] the average of the inside-out and RSO oriented transporters?

In the beginning of the work, the orientation of the transporters in the liposomes was unknown, and, thus, the observed electrical behavior could not be assigned to a single population. To approach this problem, the I53C mutant was constructed, which could be selectively inhibited by the membrane-impermeable p-chloromercuribenzenesulfonic acid (pCMBS) from the intracellular side in inside-out vesicles [Matsuzaki *et al.* 1999]. Consequently, in proteoliposomes adsorbed to the SSM, only the RSO oriented transporters would remain active after pCMBS incubation and contribute to the electrical signal. However, although melibiose accumulation was probed to be similar to C-less (Figure 3-29 for I53C and 3-14 for C-less), the sugar transport in ISO membrane vesicles could only be inhibited with pCMBS by 50% (data not shown). The proteoliposomes did neither give any electrical signal on the SSM, nor showed significant changes in the intrinsic Trp fluorescence changes or Dns^2-S-Gal emission upon Na^+ addition (data not shown). Different reasons could account for this unexpected behavior of the proteoliposomes preparation. The content of the protein in the preparation was very low (data not shown), thus, not enough material was present. Also, instability of the mutant protein during purification may account for a decreased protein activity and/or quantity. Thus, this mutant could at this stage not be investigated any further.

2.) Which amino acid residues are involved in the process of cation and melibiose binding, or transport, and what are the implications in the electrical signal?

In order to investigate the cation-binding site in more detail, Asn-58, implicated in the Na^+ recognition process [Hama & Wilson 1993, 1994], was mutated into Cys. The transport rate of this mutant was only 9% of the Cys-less control and was not stimulated by Na^+ (Figure 3-29) confirming that Asn-58 is necessary for Na^+ recognition. Similar problems as observed with the I53C mutant may also account in this case for the missing electrical and Trp and FRET signals (data not shown). Problems in protein stability during the purification of mutants close to the cation binding site, e.g. D55C, have been observed frequently.
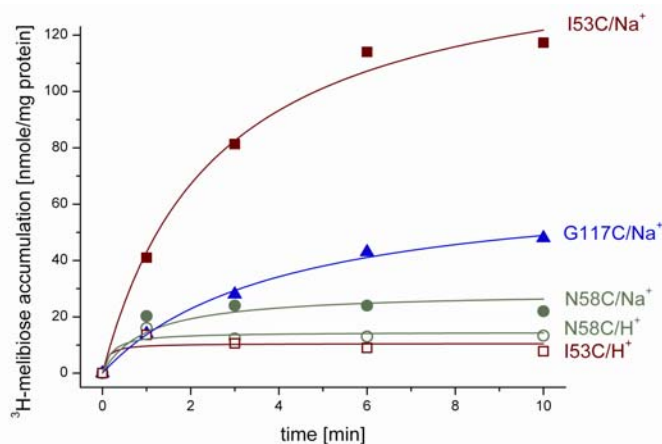
Figure 3-29. Cell sugar transport by I53C, N58C, and G117C expressing *E.coli* cells.

The experiment was performed as described for Figure 3-14. The data for the G117C mutant were generated by Manal Abdel-Dayem (not published).

Finally, Gly-117 of helix IV, which is believed to connect the cation and sugar binding site [Cordat *et al.* 2000], was changed into Cys. This mutation transported melibiose at a significant rate (Figure 3-29), but showed neither a Trp nor a significant FRET signal in proteoliposomes (data not shown). In contrast, it was possible to measure electrical signals using the different solution exchange protocols (Figure 3-30). The transient signals show characteristics similar to those recorded from the C-less mutant (Figure 3-9), although τ_1 of ΔNa and Δmel(Na) concentration jumps are significantly slower (23.5 and 27.8 ms vs. 14.8 and 15.4 ms in C-less mutant, respectively). Whereas NEM added to G117C had no effect on the electrical signals, MTSEA$^+$ reduced the peak current size and suppressed the slow decaying component (data not shown). Thus, a positive charge at position 117 is able to inhibit substrate translocation.

Finally, the half saturations for Na$^+$ in the absence and presence of melibiose were determined to be similar to C-less MelB with 3.8 and 1.6 mM, respectively (data not shown). The $K_{0.5}^{mel}$ were measured in the presence and absence of Na$^+$ with 33 and 9 mM, respectively, thus, the cooperative effect of Na$^+$ on melibiose binding is slightly reduced in this mutant. Since my involvement in the electrical measurements of this mutant was limited the purification of the protein and an initial screening, no statistical values can be represented here. The $K_{0.5}^{Na}$ in the absence of melibiose and the $K_{0.5}^{mel}$ in the presence of Na$^+$ are taken for comparison from Constanta Ganea (unpublished results).

Although the first question could not be sufficiently answered by constructing the I53C mutant, this has to be ascribed to problems in the purification procedure rather than to the general approach. Also N58C remains interesting for future studies, but for the investigation of these two mutants, problems in protein stability during purification have to be overcome.

ΔNa $\tau_1 = 23.5$ ms

ΔNa(mel) $\tau_1 = 17.7$ ms, $\tau_2 = 299$ ms

Δmel $\tau_1 = 89.5$ ms, $\tau_2 = 1469$ ms

Δmel(Na) $\tau_1 = 27.8$ ms, $\tau_2 = 339$ ms

50 pA

100 ms

ΔmelΔNa $\tau_1 = 21.5$ ms, $\tau_2 = 273$ ms
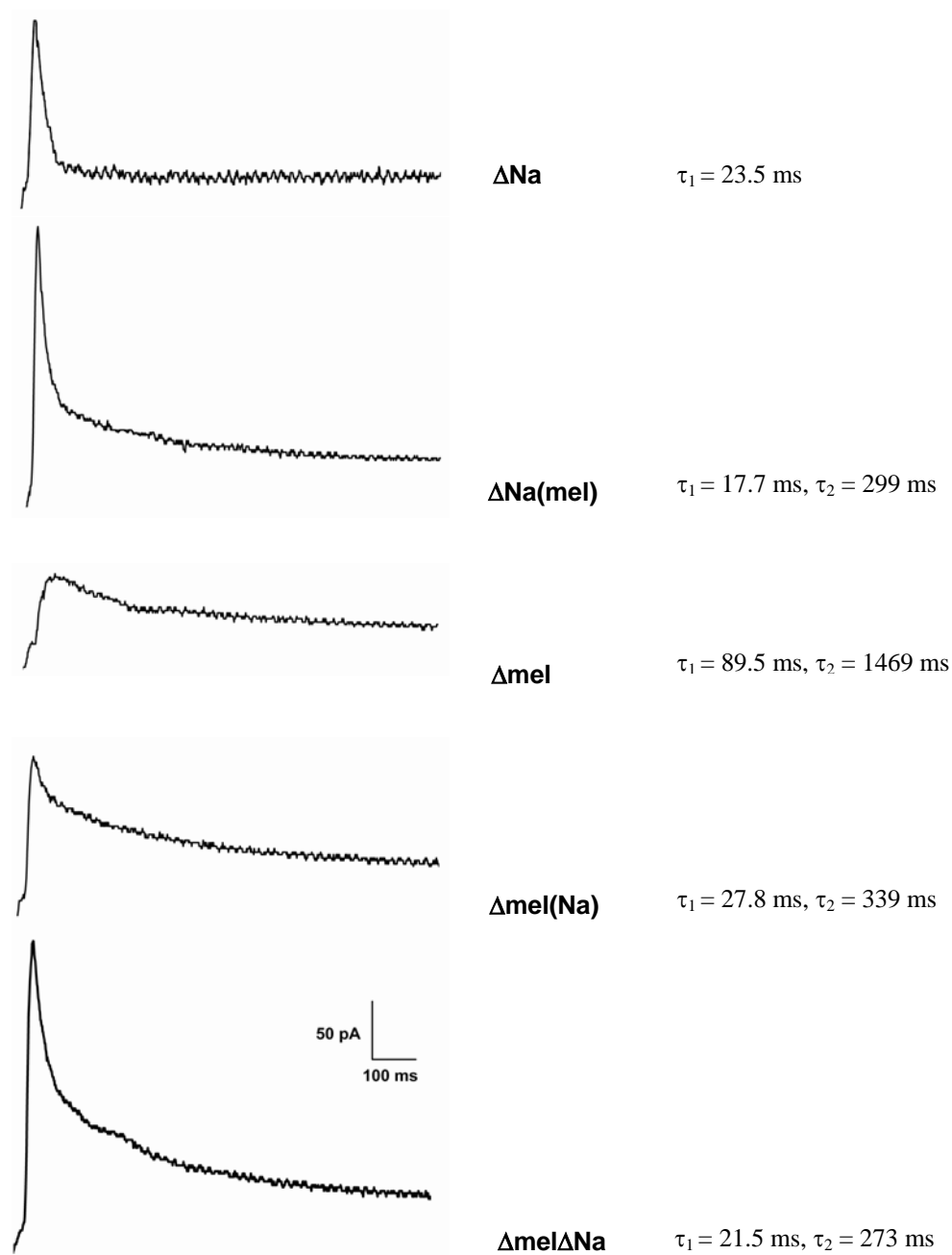
Figure 3-30. Electrical signals recorded from G117C proteoliposomes.

Conditions are as described for Figure 3-9 except that the signals were not normalized. The time constants, obtained from mono- or bi-exponential fits, respectively, are indicated on the right side for each signal and correspond to fits from individual traces.

97

4   Discussion

For a better understanding of the reaction kinetics of the melibiose permease (MelB), it is mandatory to study pre-steady state relaxations. For that purpose, wild-type or mutated MelB were purified and reconstituted into liposomes allowing, therefore, to study its properties without the interference with other membrane proteins. However, the orientation of the protein in the liposomes is a critical factor for its activity, as the kinetics of binding and translocation are different for the opposite directions of transport [Pourcher *et al.* 1990a]. Therefore, the orientation of MelB in the liposomes was determined in this thesis permitting now the relation of the pre-steady state electrical and fluorescence signals especially to the intracellular activity of MelB.

The main objective of this thesis was to characterize the kinetics and the underlying mechanism of the melibiose binding induced transition in MelB by an electrical and a fluorescence approach. The solid supported membrane technique in combination with fast solution exchanges is a direct method for studying pre-steady state charge translocation of MelB [Ganea *et al.* 2001]. The question was addressed why an uncharged substrate, namely the sugar melibiose, could trigger a transient electrical signal. Therefore, the transient signals induced by melibiose binding in the presence of saturating Na^+ concentration were analyzed, and different scenarios to explain this finding considered. Furthermore, investigation of the properties of the transport deficient mutants R141C and E142C of loop 4-5 [Abdel-Dayem *et al.* 2002, Séry 2002] complemented the knowledge about MelB functioning especially with respect to the melibiose induced charge translocation. Such mutant analysis could, therefore, help to elucidate the participation of individual amino acids in substrate binding and/or translocation. Finally, the melibiose-induced conformational change was studied by time-resolved fluorescence measurements providing, thereby, a direct tool to measure conformational changes at a certain site of interest. In the end, it was possible to correlate the electrical and fluorescence signals to partial reactions of the transport cycle, and a new kinetic model for MelB was developed.

4.1 MelB is Uniformly Oriented in the Liposomes

The orientation of the protein in the liposomes is a critical factor for its activity, as the kinetics of binding and translocation are different for the opposite directions of transport [Pourcher *et al.* 1990a]. The outcome of the orientation assay, which was performed by the use of the impermeable thiol-specific compound MPB, suggests that MelB is uniformly ISO oriented in the proteoliposome preparations (Figure 3-1). The observed extensive rate of cleavage of MelB cytoplasmic domains in the proteoliposomes by trypsin supports this contention (Figure 3-28). The knowledge about the orientation permits now the relation of the pre-steady state electrical and fluorescence signals to the intracellular activity of MelB.

The finding of the ISO configuration was unexpected, because the reconstitution method that was used, i.e., lipid addition to the detergent-protein micelle and subsequent detergent removal from ternary phospholipid-detergent-protein, was predicted to lead to a scrambled orientation of the protein [Rigaud *et al.* 1995]. Furthermore, repeated freeze-thaw sonication cycles, applied to the proteoliposomes, were expected to cause disruptions of the liposomes membranes resulting, theoretically, in a random orientation of the protein in the membrane. In contrast, reconstituting a membrane protein into detergent-saturated preformed liposomes, i.e., when the detergent concentration is at R_{sat} (= onset of solubilization), ensures a uni-directional insertion [Rigaud *et al.* 1995]. In this case, the protein inserts with its most hydrophobic moiety first [Rigaud *et al.* 1995] as it is unfavorable for a hydrophilic domain to penetrate the lipid bilayer once a closed vesicular structure is formed [Knol *et al.* 1999a]. Thus, when this latter method was applied to the reconstitution process, a unidirectional inside-out orientation was determined for transporters like PutP, the MelB homologue LacS, DtpT [Fang *et al.* 1999, Jung *et al.* 1998, Knol *et al.* 1996], and for the H^+-ATPase, the Ca^{2+}-ATPase, and the F_0F_1-ATPase [Levy *et al.* 1992, Richard *et al.* 1990, Rigaud *et al.* 1995].

Since MelB was not reconstituted into preformed liposomes, but was nevertheless uniformly oriented, it seems likely that more parameters play a role in deciding of how a protein inserts into liposomes. One possible explanation for the uniform orientation might be the structure of MelB. In the physiological orientation, MelB possesses long hydrophilic, partially charged loops directed towards the cytoplasm and a 45 amino acids long hydrophilic C-terminus at the cytoplasmic part of the protein, whereas the loops on the outside are very short. The large intracellular domains might prevent a scrambled or RSO out orientation due to sterical reasons and/or due to their hydrophilic character and charges. A similar explanation was

given for LacS [Knol *et al.* 1996] and bacteriorhodopsin [Rigaud *et al.* 1995]. Furthermore, a slow rate of detergent removal, in particular during progressive addition of SM2 Biobeads as it was done also for MelB, gives rise to a mixture of small detergent-saturated liposomes, lipid-protein-detergent, and protein-detergent micelles [Rigaud *et al.* 1995]. This situation mimics to some extent the use of preformed, detergent-saturated liposomes, and may provide an explanation for the unidirectional orientation. It was also suggested that liposomes small in diameter, which induce a strong curvature of the membrane and a lipid asymmetry, might favor the unidirectional insertion [Huang & Mason 1978]. Finally, it should be mentioned that also the choice of detergent could influence the orientation of the protein. Thus, for LacS a unidirectional orientation was obtained when Triton X-100 was used, and a random orientation when DDM was used [Knol *et al.* 1998]. For the reconstitution, the liposomes were saturated with detergent at R_{sat}. Further increase of the detergent concentration would favour liposome solubilization and the formation of micelles. Whereas in the case of Triton-X100 the liposomes are still closed at R_{sat}, open bilayer structures in the presence of DDM are formed at R_{sat}, which could explain the random orientation of the proteins in the liposomes when the reconstitution was done with DDM. However, different from our reconstitution method, a much higher lipid to protein ratio (100:1 vs. 5:1), and also a higher detergent concentration, which favors the formation of open structures, was used.

Although, the data obtained from MelB proteoliposomes can now be assigned to the backward running carrier reaction, some limits of this orientation assay have to be noted. First, MPB was claimed to be permeable only at concentrations $\geq 100\ \mu M$ [Loo & Clarke 1995]. Nevertheless, permeability at $10\ \mu M$, which was used in this work, could not be completely excluded, especially since the very low protein to lipid ratio of 1:5 could favor leakiness of the proteoliposomes and, therefore, permeability for MPB. Furthermore, a small non-specific reaction of the MPB with the C-less transporter was also visible at $10\ \mu M$ (Figure 3-1B) indicating that MPB can bind also non-specifically to the transporter and/or lipid membrane. Finally, also stilbene disulfonate was considered to be membrane permeable in proteoliposomes [Fang *et al.* 1999], which was avoided by setting the incubation time to 10 minutes. Nevertheless, this factor was not controllable. If only one of the two reagents that were used was membrane permeable instead of, as assumed, membrane impermeable, the assay would be difficult to analyze. It is, therefore, recommended for the future, to perform the quantitative assay with a higher amount of starting material. Also, the determination of the orientation of R139C or R141C in ISO and RSO vesicles could help to validate the method.

4.2 Melibiose Binding to Wild-Type MelB is Electrogenic

MelB transports one Na^+ per cycle across the membrane and is, therefore, considered to be an electrogenic transporter, i.e., it translocates net charge across the membrane. This overall electrogenic reaction may be subdivided into contributions of single reaction steps [Läuger 1991], e.g., Na^+ binding to MelB is an obvious electrogenic reaction triggering a monophasic transient current response decaying with a time constant of ~15 ms ($k \geq 50$ s^{-1}, [Ganea *et al.* 2001]. Since slippage or leak of Na^+, a common feature of many characterized electrogenic co-transporters (e.g., for SGLT1 [Chen *et al.* 1997] and the thyroid Na^+/I co-transporter NIS [Eskandari *et al.* 1997]) had not been documented for MelB yet, the Na^+ electrical signal was assigned only to a binding step and not to substrate translocation [Ganea *et al.* 2001].The knowledge about the ISO orientation of the protein allows now the assignment of this signal to an electrogenic intracellular Na^+ binding process. It can, however, not be excluded that an electrogenic reaction preceding Na^+ binding, e.g., the reorientation of a potentially charged empty carrier, could explain at least part of the observed charge translocation after a ΔNa jump. However, this is unlikely, since a ΔNa(mel) concentration jump, where the transporter is in a well-defined state before the Na^+ concentration jump takes place, causes a similar transient current [Ganea *et al.* 2001]. A likewise explanation was given for PutP [Zhou *et al.* 2004]. On the other hand, for SGLT1 Na^+ binding as well as the return of the negatively charged empty carrier were found to be electrogenic steps, thus both reactions contribute to the Na^+ electrical signal [Hazama *et al.* 1997, Loo *et al.* 1993]. Similar to MelB, charge movements caused by Na^+ binding were characterized in Na^+-coupled transporters of different families, e.g., EAAT2 [Wadiche *et al.* 1995], EAAC1 [Watzke *et al.* 2000], the GABA-transporter [Lu & Hilgemann 1999], the phosphate transporter [Forster *et al.* 1998], and PutP [Zhou *et al.* 2004]. In summary, it appears that electrogenic Na^+ binding is a general feature of Na^+-driven secondary transporters.

Although in general it is believed that association of Na^+ with a binding site localized within the transmembrane electric field is the major source of electrogenicity of Na^+-driven transport systems, it was also found that the substrate melibiose in the presence and absence of Na^+ could trigger an electrical signal upon binding to the MelB transporter [Ganea *et al.* 2001]. Since melibiose is an uncharged species, the explanation for the signal is not straightforward. Therefore, different scenarios are considered to explain this finding. Finally, a model function is used to describe that Na^+ and melibiose are distinct electrogenic processes displacing approximately an equal amount of charge.

4.2.1 Extra Na⁺ Binding is not Responsible for the Melibiose-Induced Electrical Signal

SSM experiments revealed that not only Na^+ binding causes an electrical signal, but also a melibiose concentration jump in the presence of Na^+. Different mechanistic scenarios to explain the finding that the non-charged substrate melibiose triggers an electrical signal will be discussed below in detail. However, the initial conditions yield further possibilities for variability. Since MelB accepts also H^+ as substrate, the cation binding sites are occupied with H^+ in the absence of Na^+. At the pH value used in this study (pH 7), the H^+ concentration is at saturating level so that all binding sites are occupied by H^+ [Bassilana *et al.* 1988, Damiano-Forano *et al.* 1986]. Consequently, at low concentrations of Na^+, the cation binding site can exist in a mixture of H^+ -bound and Na^+ -bound sites. Thus, the Δmel(Na) signal at low Na^+ concentration can come from melibiose binding to the H^+-bound transporter and to the Na^+-bound transporter. Furthermore, due to the increased affinity of the transporter for Na^+ in the presence of melibiose, the signal can be caused by additional electrogenic Na^+ binding. This makes the interpretation of the measurements rather difficult. Therefore, melibiose binding was studied at saturating Na^+ concentrations where only a single state of the carrier exists with all cation binding sites occupied by Na^+ [Bassilana *et al.* 1988, Damiano-Forano *et al.* 1986]. The data demonstrate that a sugar-induced fast electrical signal is still observed under the described conditions, i.e., Na^+ is bound to all MelB transporters and, thus, additional Na^+ binding is excluded as cause for the electrical signal (a Δmel(Na) jump at saturating 100 mM Na^+, Figure 3-3). Also, the fast sugar-induced transient current persists after inactivation of substrate transport by NEM treatment indicating that it is not linked to steady state co-substrate transport (Figure 3-4). Additional Na^+ binding in a second turnover of the transporter is also excluded on grounds of the low turnover of the carrier ($\sim 4s^{-1}$, [Pourcher *et al.* 1990a]). All these data support the contention that the fast phase of the electrical signal after a Δmel(Na) jump is neither linked to Na^+ binding nor to steady-state substrate transport.

Further support for the hypothesis that the melibiose-induced electrical signal does not come from Na^+ binding came from studying the dependence of the electrical signal on pH. The fast relaxation time constant (τ_1) of the decaying part of the transient signal was used to demarcate Na^+ binding from melibiose binding (Figure 3-6). τ_1 depends strongly on the pH in the case of ΔNa, but not in the case of Δmel(Na) experiments. This suggests that the molecular processes underlying the electrical responses observed in these two experiments are different. In the ΔNa solution exchange, Na^+ binding is the current-generating process and accounts for the pH

dependence. Since H^+ and Na^+ compete for a common binding site [Damiano-Forano *et al.* 1986], increasing H^+ inhibits Na^+ binding, thus τ_1 becomes slower. If the electrical signal of the Δmel(Na) concentration jump was kinetically controlled by binding of additional Na^+, a similar dependency would have been observed. This was, however, not the case. In contrast, no dependency of the Δmel(Na) signal from pH has been observed. A similar observation has been made previously [Damiano-Forano *et al.* 1986], i.e., increasing H^+ concentrations inhibited the Na^+-dependent sugar binding, but the inhibitory effect of H^+ disappeared as the Na^+ concentration increased. Together with the persistence of a fast electrical signal in transporters fully occupied by Na^+, these experiments, therefore, support the notion that the electrical signal observed during melibiose binding in the presence of Na^+ is not caused by extra Na^+ binding.

Consequently, the underlying molecular event must correspond to a movement of charges within MelB, most likely dependent upon conformational changes triggered by melibiose. Co-substrate-triggered conformational changes has been documented by analysis of the intrinsic MelB Trp fluorescence properties [Mus-Veteau & Leblanc 1996, Mus-Veteau *et al.* 1995], by FRET measurements with a fluorescence sugar analog [Maehrel *et al.* 1998], or finally by FTIR spectroscopy [Dave *et al.* 2000, Dave *et al.* 2002].

4.2.2 Charge Movement Observed during Melibiose Binding is not Linked to Intra- Protein Displacement of Already Bound Na^+

According to the arguments given above, melibiose binding results in an electrogenic conformational change. Now the question remains, which charges are displaced during this structural rearrangement of the protein. Two different schemes can be envisioned for melibiose binding in the presence of Na^+ (see Figure 4-1, left part). In scheme (a) the charge displaced during binding of melibiose corresponds to the co-substrate Na^+ that is moved deeper into the protein. In scheme (b) melibiose binding induces a charge movement not related to further displacement of bound Na^+. From the polarity of the transient currents it is inferred that either positive charges are moved inward (into the liposomes) or negative charges are moved outward during this process. For simplicity, this is arbitrarily represented in Figure 4-1 as positive charge moving into the liposome with melibiose. Fortunately, the two schemes predict distinct dependencies of the amount of displaced charge induced by a given Na^+ concentration jump at increasing melibiose concentrations.

In mechanism (a) in Figure 4-1 the hypothesis of a deeper migration of filled Na^+ binding sites in the presence of melibiose predicts that for a $\Delta Na(mel)$ jump the displaced charge during Na^+ binding should increase monotonically until saturation with increasing melibiose concentration (Figure 4-1a, $\Delta Na(mel)$ curve on the right). In mechanism (b), the Na^+ binding site remains at the same position whether or not melibiose is bound to MelB. If a Na^+ concentration jump is performed in the absence of melibiose, the resulting charge translocation will result only from Na^+ binding to MelB. If melibiose is present at saturating concentration, a Na^+ concentration jump will yield a charge translocation coming likewise only from Na^+ binding. Consequently, the Na^+-induced translocated charge is the same at zero and at saturating melibiose concentration. At intermediate melibiose concentrations, not all of the melibiose binding sites are saturated with the sugar when the Na^+ concentration jump is applied. Therefore, a Na^+ concentration jump causes additional melibiose binding to the protein due to the cooperative interaction of the two binding sites. Since melibiose binding was found to be electrogenic, this results in an extra charge translocation. Therefore, at rising melibiose concentration the displaced charge rises to a maximum at intermediate sugar concentration (Figure 4-1b, $\Delta Na(mel)$). This behavior as predicted by mechanism b) is indeed
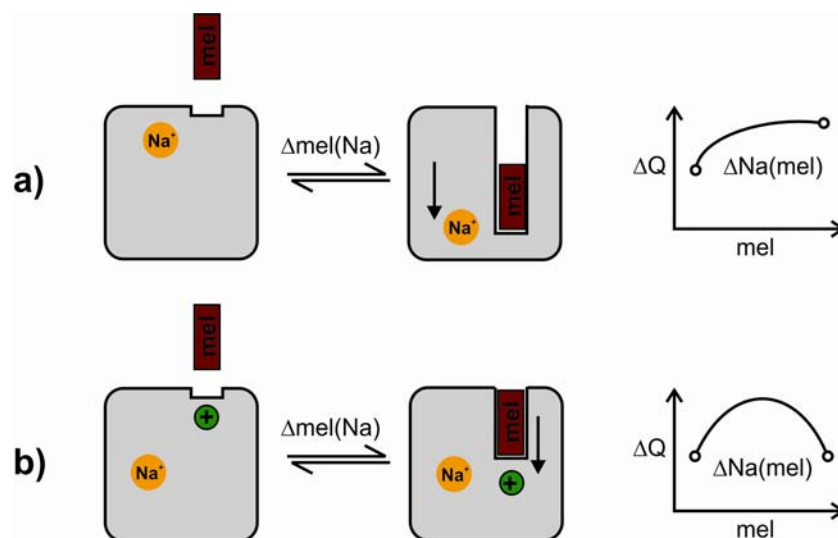
Figure 4-1. Mechanisms for the charge displacement during melibiose binding.

Two different mechanisms (a and b) for the charge displacement during melibiose binding in the presence of Na^+ ($\Delta mel(Na)$) are shown. For the two different mechanisms the respective predicted melibiose concentration dependence of the translocated charge during a $\Delta Na(mel)$ experiment is shown on the right.

experimentally observed (Figure 3-8). Consequently, the data demonstrate that upon binding, melibiose induces a charge translocation that does not represent the displacement of the co-substrate Na^+. It can, however, not be excluded that a high internal melibiose concentration inhibits the electrical signal as it is reported for high Na^+ concentration (Figure 3-3B). The following experiment could help understanding the effects at high melibiose concentration. A $\Delta Na(mel)$ concentration jump at 20 mM melibiose should be applied to proteoliposomes, preloaded with 100 mM melibiose and adsorbed to the SSM in the presence of 100 mM melibiose. If incubating the proteoliposomes/SSM system with melibiose-free buffer and repeating the $\Delta Na(mel)$ concentration jump after different time intervals would not increase the peak current, then it would indeed not be an inhibitory effect of the high internal melibiose concentration. In any instance, the arguments given above favor the hypothesis that Na^+ is not displaced during or after melibiose binding.

4.2.3 An Electrogenic Conformational Changes is Associated to the Melibiose-Induced Electrical Signal

Since the possibilities of extra Na^+ binding and displacement of already bound Na^+ were excluded as cause for the electrical signal after a $\Delta Mel(Na)$ concentration jump at saturating Na^+, this charge displacement has to be assigned to a movement of charged amino acid residues and/or electrical dipoles of the protein itself [Läuger 1991]. Likewise, this explanation, i.e., the movement of charged residues and/or electrical dipoles could also, at least in part, account for the electrogenic Na^+ binding signal discussed above (see 4.2.1). Speculating on the actual charged amino acids that are moved during this conformational change is rather difficult, since MelB has 63 charged amino acids. However, mutating charged into neutral amino acids and analyzing charge translocation properties of such mutants could help in the future to identify amino acids probably involved in such an electrogenic conformational change (see also in the discussion chapter 4.3 about the electrogenic properties of the two mutants R141C and E142C).

In this context, the temperature dependence of the electrical signal following a $\Delta mel(Na)$ jump was investigated in the wild-type by means of the SSM technique (Figure 3-7). Studying the effects of temperature on the kinetics of the transport characteristics is a useful means to obtain information on the nature of the underlying mechanism. Diffusion-controlled processes have usually Q_{10} values of 1.03 to 1.3 and, accordingly, activation energies seldom exceeding 17 kJ/mole, and carrier transport processes commonly have activation energies between 29 to

105 kJ/mole [Höfer 1981, p.97]. However, it is also been reported that certain values of Q_{10} can not be quoted as "proof" that a process is energy requiring (active) rather than passive. Such arguments are not supported by the facts, and activation energies for active and passive processes overlap extensively [Phair 2001]. The determined activation energy of 45 kJ/mole between 20 and 30°C for the Δmel(Na) jump supports in any instance more a conformational change as underlying mechanism. However, when interpreting the Arrhenius plot, it has to be noted that the rate constants were derived from time constants of the electrical signals, which are limited by the solution exchange and the filtering. Thus, processes faster than 10-20 ms cannot be resolved with the SSM technique. Accordingly, the underlying process might as well be faster and, probably depend stronger on the temperature. The differentiation between diffusional controlled processes and conformational changes is particularly interesting, since in the recent years different models for the functioning of transporters have been proposed, some of which are based on rather simple diffusional mechanisms, i.e., that co-transporters are single-file ion channels, in which multiple-substrates can permeate without conformational changes [Su *et al.* 1996]. However, the activation energy measured here could rather be used as declining than as supporting argument for such a model for MelB.

Anyway, based on the arguments given above, the most attractive explanation for the electrical signal after a Δmel(Na) jump is a conformational change. Interestingly, ATR-FTIR studies showed recently that melibiose binding to Na^+-bound MelB induces a remarkable compactness of the carrier's structure affecting mainly β-sheet domains of the transporter [Dave *et al.* 2002]. Conformational changes after sugar binding are a well known feature of soluble enzymes [Quiocho 1986]. A conformational change upon sugar binding at close to saturating Na^+, also associated with a charge movement, has been reported for the human Na^+/glucose co-transporter (hSGLT1) [Meinild *et al.* 2002]. As the measurements with hSGLT1 were done with a transport-deficient mutant (Q457C), it was postulated that the observed reaction is the final step of sugar binding preceding the sugar translocation step, although the authors did not specify which partial step is defective in this mutant. It could as well be that the reorientation still takes place, but a missing release of the substrate accounts for the transport defect. In any instance, it is tempting to propose a similar interpretation as for hSGLT1 also for MelB, as the electrical signal is also still observed under conditions, in which the transport is blocked by NEM (Figure 3-4). However, the partial reaction step, inhibited by NEM, was yet never defined. Also in PutP, an electrical signal was observed after a proline concentration jump in the absence of Na^+. As proline transport requires Na^+

and is, thus, excluded, the electrical signal was also assigned to an electrogenic conformational transition preceding the carrier's reorientation [Zhou *et al.* 2004]. Summarizing these studies, it is tempting to speculate that conformational changes associated to charge translocation can occur in electrogenic co-transporters at a step preceding the carrier's reorientation. In contrast to the results obtained with MelB, the fast phase of the glutamate-induced charge movement in EAAC1 was assigned to a voltage-dependent Na^+-binding reaction [Watzke *et al.* 2000]. But different from MelB, EAAC1 co-transports its substrate together with three Na^+ instead of one, thus glutamate bindings opens the way for further Na^+ binding.

4.2.4 Melibiose and Na^+ Binding are Distinct Electrogenic Processes

The dependence of the charge translocation caused by a Na^+ jump as a function of the sugar concentration in the medium is described by a model (see Figure 3-8), in which the Na^+- and the sugar-induced electrical responses correspond to distinct electrogenic events. The fit, furthermore, shows that Na^+ binding contributes ~ 40% and melibiose binding contributes ~ 60% of the total displaced charge during binding of both substrates. The model agrees well with the result obtained by integrating the signals in the presence of NEM, which showed that melibiose and Na^+ binding displace an equal amount of charge (each ca. 50% of the total translocated charge), and that both electrical processes are additive when simultaneous concentration jumps are performed (see text comment in 3.2.2.6). Likewise, in the absence of NEM integration of the current responses were performed, yielding total displaced charges after a Na^+ concentration jump or a melibiose concentration jump in the presence of Na^+ in the time range of 0 – 150 ms of equal amount (12 to 13 pC). On the other hand, a simultaneous concentration jump of Na^+ and melibiose gave approximately twice that value (24 pC, using the signals of Figure 1 from Ganea [Ganea *et al.* 2001]). This suggests that the final position of the binding site of a substrate is the same independent of whether the respective co-substrate is present or not and that cooperativity only comes in at the level of the speed or affinity of the binding process. Similar, in PutP the translocated charge is about the same for Na^+ and proline binding [Zhou *et al.* 2004]. In contrast, electrogenic Na^+ binding in EAAC1 has been found to be responsible for only 20% of the total charge movement [Wadiche *et al.* 1995].

4.3 R141C and E142C of Loop 4-5 Take Part in Conformational Transitions after Sugar Binding

Cys-scanning mutagenesis of the charged residues of loop 4-5 indicated that only the two adjacent residues R141 and E142 play significant roles in MelB functioning [Abdel-Dayem *et al.* 2003, Séry 2002]. In order to elucidate the defects caused by these two mutations into more detail, electrophysiological and spectroscopic data (see result section) are evaluated and related to previous biochemical measurements [Abdel-Dayem *et al.* 2003, Séry 2002]. C-less MelB was taken for comparison, since this mutant was used as background for genetic engineering, and its functional properties are alike to the wild-type [Abdel-Dayem *et al.* 2003, Weissborn *et al.* 1997]. Adequate similarity of the C-less mutant with the wild-type was confirmed by electrical (Figure 3-10, Table 3-2, Table 3-3) and fluorescence measurements (Figure 3-17 and Figure 3-18).

4.3.1 Substrate Translocation Rather than Binding is Impaired

Several lines of evidence support the contention that the major defect introduced by R141C and E142C is to impair translocation rather than binding of the co-substrates. It was demonstrated that both R141C and E142C retained the capacity to bind sugar including the high affinity sugar α-[^{3}H]NPG [Abdel-Dayem *et al.* 2003, Séry 2002] or the fluorescent sugar analog Dns^2-S-Gal (Figure 3-18B). Only the affinity for α-NPG was reduced slightly (around three times) in both mutants. Furthermore, the interaction of the cation with the mutated transporters remains comparable to that in wild- type or C-less MelB, as Na$^+$ still activates sugar binding (α–[^{3}H]NPG), enhances Dns^2-S-Gal fluorescence emission (Figure 3-18), and induces fast electrical signals in R141C and E142C proteoliposomes comparable to those recorded for WT and C-less transporters (Figure 3-9). Furthermore, the corresponding Na$^+$ activation constant (K_{Na}) for α-NPG binding [Abdel-Dayem *et al.* 2003, Séry 2002], and the $K_{0.5}^{Na}$ of the Na$^+$-induced electrical transients are not altered (Table 3-3). These data make a direct participation of R141 or E142 both in the cation coordination network in the N-terminal domain of MelB and in the sugar binding site, respectively, unlikely.

In contrast to these findings, a translocation defect in the carrier functioning easily accounts for the lack of transport activity of R141C and E142C mutants [Abdel-Dayem *et al.* 2003, Séry 2002]. It also explains the total (R141C [Abdel-Dayem *et al.* 2003]) or almost complete reduction (E142C [Séry 2002]) of melibiose counterflow activity. This exchange process only

involves sugar loading/release at each membrane surface and shuttling of the loaded complex (see steps 2 ↔ 3 ↔ 4 ↔ 5 in Figure 4-5, and [Kaback *et al.* 2001, Pourcher *et al.* 1990a]). It was demonstrated before that melibiose can displace bound α–[^{3}H]NPG or Dns^2-S-Gal from the sugar binding site irrespective of whether the transporters are outward facing (in RSO vesicles) or inward facing (in ISO vesicles or proteoliposomes) [Damiano-Forano *et al.* 1986, Maehrel *et al.* 1998]. Therefore, as α–[^{3}H]NPG or Dns^2-S-Gal are not affected, melibiose binding to R141C and E142C is also not impaired. Consequently, impediment of the melibiose exchange process in the two mutants must result from defective shuttling of the loaded carrier or possibly also from a defective substrate release. Furthermore, the lack of the transport electrical component, linked to co-substrate transmembrane flow and typically observed in wild-type or C-less MelB for all concentration jumps except ΔNa, is absent both in R141C and E142C (Figure 3-9). Consistently, R141C reacted with the positive sulfhydryl reagent MTSEA$^+$, concomitantly restores in part substrate translocation across the membrane [Abdel-Dayem *et al.* 2003] and a small transport component of the electrical signal (Figure 3-11). Thus, the electrical measurements serve as independent argument that the defect of the two mutants is linked to co-substrate transmembrane flow. It furthermore supports the contention of the importance of a positive charge at position 141 for the transport function. Although up to now no intraprotein salt-bridges with R141 were identified in MelB, such interactions, essential for the transport function, cannot be excluded. In contrast, a negative charge added at position 142 in the E142C mutant failed to recover a transport component indicating that either this negative charge is not essential for the transport function or that the negatively charged MTS reagent could not substitute sufficiently the structure of the Glu residue. Although MTSES$^-$ is not able to cross the lipid membrane, 142C should be accessible by the reagent, as the transporters are ISO oriented in the proteoliposomes.

As already mentioned, a small stationary phase was recovered (Figure 3-9) upon return of around 20% of the transport activity by the addition of MTSEA$^+$ to R141C. Unexpectedly, even if a very small transport of melibiose in the presence of Na$^+$ with a rate around 10 times lower compared to C-less was detectable in E142C [Séry 2002], the transport component of the decaying electrical signal was absent in the SSM measurements. The transport could be too low to lead to a detectable slow phase indicating that a given transport must exist in order to lead to a detectable transport component in electrical measurements.

4.3.2 Conformational Changes after Melibiose Binding are Defective

Other electrical properties and spectroscopic features of R141C and E142C provide complementary information useful for explaining the defects of the mutants. In contrast to C-less, R141C and E142C loose the capacity to generate fast transient electrical responses after melibiose concentration jumps in the absence (Δmel(H)) or presence of Na^+ (Δmel(Na)) at saturating levels (50 mM). As Na^+-dependent binding of melibiose (α-NPG or Dns^2-S-Gal) is retained in the mutants, the missing sugar-induced charge transfer reaction has to be due to modified properties of the ternary Na^+-melibiose-MelB complex. As outlined above, electrogenic conformational changes account for the fast phase of the Δmel(Na) signal, which is almost completely absent in the two mutants. The lack of the signal could not be caused by slower binding, as the affinity towards melibiose is only around three times lower in R141C and E142C compared to C-less. The affinity decrease would slow down the binding reaction at most by a factor of 3, which would have been observed in SSM experiments.. It is attractive to speculate that the positive charge at position 141 and/or the negative charge at position 142 might be among the charges moved during this conformational transition. Interestingly, the NEM inhibited wild-type shows the same phenotype as R141C and E142C, i.e., substrate binding is possible, while substrate translocation is disturbed. Although NEM-inhibited wild-type and mutants have a similar phenotype, they show different charge translocating properties, i.e., Na^+ and melibiose binding induce approximately an equal amount of charge translocation in the NEM-inhibited wild-type, but in R141C and E142C only Na^+ binding is the current generating process, while melibiose binding does not contribute significantly to the charge translocation. This suggests that, although the phenotypes are similar, wild-type with NEM and the two mutants must have defects that lead to different inhibited steps in the transport cycle.

An additional key finding of both R141C and E142C is the absence of any detectable Na^+-dependent increase in Trp signal upon sugar addition to the proteoliposomes (Figure 3-17B) indicating that conformational changes after melibiose binding are defective. Previous spectroscopic studies showed that the melibiose induced Trp fluorescence signal arises from a light emission increase of W299 and W342 in helices IX and X, respectively, that represents cooperative conformational changes elicited by the binding of MelB substrates [Mus-Veteau & Leblanc 1996, Mus-Veteau et al. 1995]. It must be recalled here that helices X and XI are among the different helices putatively lining the sugar binding site and/or the sugar pathway [Ambroise et al. 2000, Cordat et al. 1998, Cordat et al. 2000, Ding & Wilson 2000a, Mus-

Veteau & Leblanc 1996]. It appears, therefore, likely that the translocation defect of R141C or E142C may be cause by either incorrect structural organization of their respective ternary complex and/or to an impaired interaction between the substrate binding sites necessary for the obligatory coupled translocation process of the substrates, thereby preventing (R141C) or severely reducing (E142C) subsequent cycling of the mutated transporters. Analysis of Trp fluorescence is another means to demarcate the NEM inhibited wild-type, which shows fluorescence enhancement after melibiose binding. In contrast, R141C and E142C failed to show this fluorescence enhancement. Thus again, NEM inhibits the transporter cycle at a different step than the defects introduced by the mutations. Interestingly, MTSEA$^+$ addition did neither return the melibiose induced charge translocation nor the Trp fluorescence properties suggesting that, although a limited transport function is regained, MTSEA$^+$ cannot efficiently substitute the original function of the transporter.

Finally, preliminary proteolysis experiments (Figure 3-28) point also out that conformational changes after melibiose binding are defective in R141C, while those after Na$^+$ binding still occur. This was derived from the fact that MelB substrates afford cooperative protection against loop 4-5 digestion by trypsin in wild-type [Gwizdek *et al.* 1997] and C-less MelB, but in R141C, only Na$^+$ addition protects loop 4-5 from cleavage, while subsequent melibiose addition does not increase this protection. Thus, structural rearrangement upon Na$^+$ binding still occur in this mutant, but those after melibiose binding are defective.

4.3.3 Cooperative Interactions between the Binding sites are Affected

It should, finally, be mentioned that the FRET emission maximum of Dns^2-S-Gal bound to the sugar site of E142C is red shifted as compared to that in wild type or C-less MelB (Figure 3-18B), indicating that the sugar binding site environment after binding of Na$^+$ becomes proportionally less apolar as compared to C-less MelB. Because at the same time the disappearance of the Na$^+$-dependent sugar induced Trp fluorescence signal in E142C essentially implies a loss of fluorescence contribution of W299 (helix IX) and of W342 (helix X), one possible explanation is that the mutated E142C in loop 4-5 no longer exercises its normal positional (and/or tilt) influence on these two helices of the C-terminal half of MelB. It is likely to assume disrupted interactions between the loop 4-5 structural domain harboring E142C and these 2 C-terminal helices IX and X. MelB transport activity of E142C is restored in a revertant that has a serine in place of the isoleucine at position 22 in helix I [Séry 2002]. Strikingly, similar replacements of I22 by polar residues (Ser, Asn) also promote recovery of

several defective MelB transporters with initial point mutations on helix XI [Ding 2004, Ding & Wilson 2000a, b]. These findings lead to the attractive idea that an interaction of loop 4-5 with the inner half of helix I is important for stabilizing the interaction of helix I with one or several helices of the C-terminal domain lining the sugar binding site. As the cytoplasmic extremity of helix I contains D19, which is critical for Na^+-recognition, and thus belongs to the cationic binding site, it may be proposed that coordinated interactions between helix I, helices X and XI, and loop 4-5 are structural features essential for the MelB cooperative properties and for Na^+- sugar translocation. Proximity between helices I, IV, X, and XI was already suggested before [Ding & Wilson 2000b, Ding *et al.* 2000].

At variance with the observation on E142C, the emission maximum of FRET signal recorded from Dns^2-S-Gal bound to R141C is the same as in wild type or Cys-less MelB (Figure 3-18B) excluding any significant change in the structural organization of its sugar binding site. In contrast, the activating effect of melibiose on the half saturation concentration for Na^+ $(K_{0.5}^{Na})$ is lost in this mutant, pointing to an alteration of the cooperative interaction between the sugar and cation binding sites. Because the R141C mutation more selectively prevents cooperative or charge transfer phenomena linked to sugar binding, one may suspect R141 to be directly interacting with one domain lining the sugar binding site. One of the possible targets is helix X, since proximity between the local loop 4-5 domain harboring R141C and this helix is suggested by the observation that a second site revertant in the inner cytoplasmic half of helix X is found (V343G), which promotes recovery of activity of a defective mutant with a mutation at position 149 (R149C) located at the interface loop 4-5-helix V [Abdel-Dayem *et al.* 2003]. An alternative possibility is that by interacting with the reentrant loop 10-11 located in the C-terminal half of MelB [Ding 2004], R141 could favor the cooperative interactions between the co-substrates binding sites that are required for the obligatory coupled translocation of the two substrates. In fact, several point mutations in this loop have been reported to produce concomitant alteration of the ionic and sugar selectivity and/or drastic reduction of sugar transport [Botfield & Wilson 1988, Ding 2003, 2004].

4.3.4 Charged Amino Acids in Loop 4-5 Play Important Roles for Transporter Functions in Different Families

Among the charged amino acids of loop 4-5, Arg-141 and Glu-142 play a role in substrate translocation, while Arg-149 at the helix-loop interface is important for sugar binding [Abdel-Dayem *et al.* 2003]. These amino acids are highly conserved within the MelB subfamily

(Figure 4-2), and Arg-141 also within the GPH transport family indicating that they could play a role in transport function. Charged amino acids have also been implied to play crucial roles in the translocation process of other transporters. E.g., Arg-144 of helix V from LacY of *E. coli* is ion-paired during the turnover with Glu-126 of helix IV. Both amino acids are also important for sugar binding [Frillingos *et al.* 1997]. Although sequence alignement of MelB with LacY showed only marginal similarity, it is interesting to note that Arg-144 of LacY corresponds to Arg-141 of MelB, and Glu-126 of LacY to Trp-128 of MelB (Figure 4-2). The latter amino acid has been found to be important for the transport activity [Cordat *et al.* 2000]. When comparing sequences of individual helices, Arg-149 of MelB would correspond to Arg-144 of LacY, both of which are implied in the sugar recognition process. In contrast, amino acids, important for the transport function, were thus far not identified in this region in PutP. The only similarity in the primary amino acid structure is Arg-151 of PutP, which corresponds to Arg-149 in MelB. In PutP, only Asp-187 of loop 5-6 has been found to be important for active proline transport [Quick & Jung 1998].

```
MelB_Escherichia coli               PFWS-LVPTITLD-----KREREQLVPYPR 149
MelB_Shigella flexneri              PFWS-LVPTITLD-----KREREQLVPYPR 157
MelB_Salmonella typhimurium         PFWS-LVPTITLD-----KREREQLVPFPR 149
MelB_Klebsiella pneumoniae          PFWS-LVPTITLD-----KREREQLVPYPR 149
MelB_Enterobacter aerogenes         PFWS-LVPTITLD-----KREREQLVPYPR 149
MelB_Vibrio vulnificus              PYWS-MIPALSSS-----RQEREKLVVWPR 151
GusB_Escherichia coli               PYGS-LATAMTQQ-----PQSRARLGAARG 152
XylP_Lactobacillus pentosus         PITS-ILPSLTSN-----PQERVTLSTIRQ 173
LacS_Streptococcusthermophilus      GFWS-MIPALSLD-----SHEREKMATFAR 165
RafP_Pediococcus pentosaceus        GFWS-MLPSLTTD-----SREREKTATFAR 167
MelB_Synechocystis sp.              PYTA-LTPELTQN-----YNERTRLNSFR- 172
MelB_Fusobacterium nucleatum        PYNA-LIPEIGRT-----PEERLNLSTWQS 155


LacY_Escherichia coli               AVEA-FIEKVSRRSNFEFGRARMFGCVGWA 152
PutP_Escherichia coli               RIISALVILLFFT-----IYCASGIVAGAR 151
```

Figure 4-2. Sequence alignment of loop 4-5 of different members of the GPH transport family and LacY and PutP of the major-facilitator superfamily.

The alignment was done with ClustalW, v. 1.82 [Chenna *et al.* 2003]. Bold residues indicate amino acids changed into cysteine in this work in MelB of *E.coli* and the corresponding amino acids in the other transporters. MelB: melibiose permease, GusB: glucuronide transporter, XylP: xyloside permease, RafP: raffinose permease, LacS: lactose permease, LacY: lactose permease, PutP: proline transporter

4.4 Are Fluorescence and Charge Translocation Properties Related Processes?

Both, the SSM and the stopped-flow method are able to monitor pre-steady state kinetics of Na^+ and melibiose induced reactions, but different from the voltage clamp fluorometry (VCR) approach [Mannuzzu et al. 1995], they do not detect the two processes at the same time in parallel. The question now arises, whether it is, nevertheless, feasible to relate the kinetic constants determined by these two real-time methods, since the two measurements are made under the same conditions.

4.4.1 Melibiose Binding Induces a Fast Conformational Change, which is Kinetically Similar in Electrical and Trp-Fluorescence Measurements

Melibiose binding in the presence of Na^+ induces a fast electrogenic conformational change proceeding with a rate constant $> 50 \ s^{-1}$ in wild-type MelB both in the presence and absence of NEM. A similar rate constant was found with the SSM method for the C-less mutant as well as for E365C in the absence and presence of the MIANS label (Figure 3-24 and 3-25). This step was assigned to a conformational change preceding the carrier's reorientation (see also Figure 4-5). Stopped-flow measurements revealed, by using the intrinsic Trp fluorescence, a Na^+-dependent melibiose-induced conformational change proceeding with a rate constant in the same order of magnitude (~65 s^{-1}, see also Figure 4-5) for C-less MelB and E365C. Because of the kinetic similarity, it is tempting to suggest that these two measurements monitor the same process occurring after melibiose binding. Further evidence for this contention came from measuring activation energies for these two processes. Whereas measurements with the SSM yielded an activation energy of 45 kJ/mole (Q_{10} = 1.6), the stopped-flow measurements revealed an E_a of 42 kJ/mole (Q_{10} = 1.8). Although certain limits have to be taken into account for this comparison, i.e., data from the wild-type (SSM measurement) were compared to data with the C-less mutant (stopped-flow measurement), similar activation energies could, nevertheless, suggest that the underlying processes are also similar. In contrast, both R141C and E142C did neither give a significant electrical melibiose-induced signal nor a Trp fluorescence signal. On the other hand, the NEM-inhibited wild-type gave both melibiose induced electrical and Trp fluorescence signals. This comparison further supports the view that the processes detected by electrical and Trp fluorescence measurements after melibiose binding in the presence of Na^+ are kinetically and mechanistically the same, as

they are both not observed in the two mutants. Although simultaneous measurements of electrogenic activity and changes in Trp fluorescence are not possible with the SSM and stopped-flow technique, relating the results determined by these two real-time techniques offers considerable potential for correlating charge movements with conformational changes. It is, however, for future measurements advisable to improve the time resolution of the SSM, since the charge translocation measurements were done at the limit of detection.

4.4.2 Na$^+$ Binding induces a Fast Conformational Change at the Sugar Binding Site

The Na$^+$-induced Dns^2-S-Gal fluorescence change, monitoring a conformational change occurring at the sugar binding site, was investigated by means of the stopped-flow technique. This change takes place with a $k \sim 55$ s^{-1}. Now the question arises, to which partial reaction this time constant could correspond. It is interesting to note that a ΔNa(mel) jump on the SSM induces a signal decaying with a similar time constant ($k \geq 65$ s^{-1}). This could lead to the suggestion that the Na$^+$ induced charge translocation (in the presence of melibiose) is also accompanied by a conformational change represented by the Dns^2-S-Gal signal. This view is also consistent with the fact that Na$^+$ modifies the affinity of the transporter for melibiose. On the other hand, the rate constant as well as the activation energies of the ΔNa(Dns^2-S-Gal) jump are also similar to those obtained from Trp fluorescence and electrical measurements after a Δmel(Na) jump. With the experimental data presented here, it is, thus, difficult to relate the time constants to a specific partial reaction in the transport cycle. It can only be suggested, on grounds of mechanistic considerations, that the Dns^2-S-Gal signal monitors an event that is induced by Na$^+$ binding, but takes place at the sugar binding site by setting the sugar binding site to a conformation for high affinity binding. The following consideration suggest that the Dns^2-S-Gal signal monitors a transition from CHsugar to C'Nasugar ($3' \leftrightarrow 3*$ in Figure 4-5): Na$^+$ and melibiose binding induce similar charge translocation, but in the ΔNa(mel) signal almost only the Na$^+$ induced charge translocation accounts for the total charge translocation. The reason is that melibiose binds already in the absence of Na$^+$, therefore, the melibiose-induced charge translocation already took place before the Na$^+$ jump was applied. Since the final state after Na$^+$ and melibiose binding should be the same independent of what substrate was added first and since the $3' \leftrightarrow 3*$ transition corresponds to the electrogenic melibiose induced conformational change, the ΔNa(sugar) jump should induce a direct transition from CHsugar to C'Nasugar (as illustrated in Figure 4-5). It has to

be noted that the experiment was only done with the C-less mutant and has to be repeated also for the E365C mutant.

What is the reason that R141C and E142C both show the Dns^2-S-Gal FRET signal, but not the Trp fluorescence signal, if these two transitions lead to the same final state, i.e. the 3* conformation? Both signals most likely report on the structural organization of the sugar binding site. However, sugar binding is probably accompanied by multiple and coordinated interactions between different domains of the protein. Since such interactions are needed for efficient binding and cooperativity, it is reasonable to assume that mutants might exist, in which these two signals are dissipated. Probably, the mutations R141C and E142C modify only one of these multiple interactions reflected by the Trp signal, whereas the other interaction still exist. Furthermore, it would be interesting to see, whether R141C and E142C have similar activation energies and time constants as the C-less mutant.

4.5 E365C is Involved in the Translocation Reaction

4.5.1 Glutamate 365 is not Essential for Transport Function

When Glu-365 was replaced by Gly or Asp, a selective decrease of the maximal rate of the energy-dependent Na^+/TMG and H^+/melibiose transport was observed [Kaback 1988, Pourcher *et al.* 1990a]. Detailed analysis suggested that, while sugar binding was similar to the wild-type, reorientation of the loaded carrier was strongly and selectively impaired [Pourcher *et al.* 1990a]. On the other hand, mutating Glu-365 into Ala resulted in a protein with 50% of the TMG transport rate of wild-type, but transport was severely reduced when the temperature was raised from 25 to 37°C [Pourcher *et al.* 1990b]. It was, therefore, concluded that the local protein structure of the carrier and the proper location of the negative charge is required for optimal transport function. Changing Glu-365 into Cys contradicts this contention, as Na^+/melibiose co-transport was found to be only slightly reduced compared to the C-less mutant (Figure 3-14). Furthermore, the fluorescence (Figure 3-17 and 3-18) and electrical properties (Figures 3-15 and 3-24) of E365C resemble those of C-less MelB. These results indicate that neither the negative charge at position E365C nor the specific structure of Glu-365 is essential for the transport function.

A similar conclusion was drawn recently, as it was suggested that E365C, besides E357C and K359C, are charged amino acids of loop 10-11 that are not essential for transport function and can tolerate structural variations [Ding 2003, 2004]. In this context it is interesting to note that TMG resistant mutants were isolated in loop 10-11, which were able to transport melibiose quite well, but showed extremely poor transport of TMG. In addition, while melibiose-stimulated Na^+ uptake was observed, melibiose-stimulated H^+ uptake was completely lost in all mutants [Ding *et al.* 2000] indicating that loop 10-11 plays in general also an important role in sugar/cation recognition. However, as E365C could transport TMG equally well as melibiose (data not shown), it seems that E365 does not take part in this recognition process. Possible explanations for the strong reduction of transport activity in E365G/D could be a reduced level of protein expression or a reduced stability of the ternary complex Na^+/melibiose/MelB.

4.5.2 Does E365C of Loop 10-11 Participate in Na$^+$- and Melibiose-Induced Local Conformational Changes?

Although at position 365 MelB can tolerate structural variations, this does not exclude the possibility of an involvement of this local domain in substrate translocation and/or carrier reorientation. Evidence that loop 10-11 might play a crucial role for MelB transport function was suggested on grounds of inhibition experiments. First, C364 of loop 10-11 is the target of the transport inhibiting sulfhydryl reagent NEM [Botfield 1988, Weissborn *et al.* 1997], and second, IIA^{Glc}, which inhibits transport activity of MelB, binds among other residues to Ala-368 of loop 10-11 [Kuroda *et al.* 2001]. It is well established that conformational changes of MelB are involved in the coupling of Na$^+$-sugar translocation (as extensively reviewed in the introduction (1.5.5)). Conformational changes are not only important for the coordinated interaction between the two binding sites, but also for substrate translocation. However, the relation between such conformational changes and transporter functioning is poorly understood and remains an important challenge in current transporter investigation. Furthermore, information on single domains of MelB participating in such conformational transitions is limited, as most techniques used so far, i.e., analysis of intrinsic Trp fluorescence or charge translocation, allow only to assign conformational transitions to global rearrangements of the protein. In contrast, attaching a fluorescence probe to a defined site of interest opens the possibility to study local conformational changes occurring upon substrate binding.

Since neither the mutation E365C nor the attachment of the fluorescence probe MIANS to E365C influenced the transport (Figure 3-14), fluorescence (Figures 3-17 and 3-18), or electrical properties (Figures 3-15, 3-24, and 3-25) of MelB significantly, E365C proteoliposomes were used to study site-specific conformational changes in MIANS-labeled E365C. Although Na$^+$ binding occurs in the N-terminal half of the protein in helices I, II, and IV (review in [Poolman *et al.* 1996]), Na$^+$ binding induced a quench in MIANS fluorescence emission (Figure 3-20C). Whereas melibiose alone induced an increase in MIANS fluorescence intensity, this effect was much more pronounced in the presence of Na$^+$ (Figure 3-20C and D). However, from the environmental sensitive probe MIANS one would have expected red or blue-shifts in the emission maximum concomitantly with a change fluorescence emission intensity, respectively. In the following, two different explanations are given to account for the missing shift in the emission maximum.

First, experiments with MIANS-N-AcCys clearly showed that decreasing the polarity of a solvent increases the fluorescence intensity of the fluorophore accompanied by a blue shift in the emission maximum [Hiratsuka 1992] making MIANS a useful probe for studying environmental changes. However, when the experiment was carried out in a solvent containing 80% ethanol and 20% H_2O, the emission maximum was around 415 nm. This is the same maximum as that measured with the MIANS-labeled E365C indicating that this residue is already in a high apolar environment. When the polarity of the solvent in the model experiment was further increased (up to 99% ethanol), the fluorescence emission also increased, but was not accompanied by a significant shift of the emission maximum. Since it is reasonable to assume that without substrates E365C is already in a relatively hydrophobic environment, melibiose addition, although bringing the residue to an even more hydrophobic environment accompanied by an increase in fluorescence emission, would not lead to a shift in the emission maximum. Consequently, fluorescence changes of MIANS initiated by binding of melibiose may be explained by movements of the labeled amino acid to a less hydrophobic protein surface from a more hydrophobic protein interior.

Second, it cannot be excluded that Trp residues play a role in the intramolecular quenching of MIANS as it has been recently reported for other organic dyes [Marmé et al. 2003]. Such quenching, also called static quenching, requires the formation of a complex between the fluorophore and the tryptophan. Assuming that the tryptophans of helices X and XI, which are possibly in close proximity to loop 10-11, move away from the dye upon melibiose binding or that the dye moves away from the tryptophans, this would result in a reduced quenching effect of the tryptophans on the MIANS emission and, hence, also in an increased fluorescence emission without a spectral shift. Alternatively, the tryptophans only change their orientation thereby weakening the stacking between the tryptophans and the dye. Also in the MIANS-labeled LacY, the emission maximum was not significantly shifted upon ligand addition, although the fluorescence increased. This was explained with a charged residue that moves away from the dye upon substrate addition resulting, thus, in an increased fluorescence without a shift [Ron Kaback, personal communication]. This is one possible interpretation also for MelB.

The finding of the change in fluorescence intensity upon substrate binding, therefore, implies that Na^+ binding induces a conformational change in the protein, a view which is consistent with the fact that 10 mM Na^+ modify MelB affinity for its sugar substrate [Ganea et al. 2001, Mus-Veteau et al. 1995], and that loop 10-11 is involved in such a conformational change

moving to a less hydrophobic part of the protein. The finding also implies an involvement of loop 10-11 in sugar-binding induced conformational changes. This is easily acceptable taking into account a recent study proposing that loop 10-11 is a re-entrant loop in a putative aqueous channel [Ding 2004]. The dynamic aspect of loop 10-11 was recently also deduced from the change of cross-linking patterns in the absence and presence of melibiose [Ding 2004]. Further evidence for an involvement of MelB loops in conformational changes after sugar binding came from FTIR spectroscopy indicating that binding of sugar not only reduces the accessibility of MelB to solvent [Dave *et al.* 2000], but also induces a remarkable compactness of the carrier's structure, affecting mainly β-sheet domains of the transporter, which may include cytoplasmic loops 4-5 and 10-11 [Dave *et al.* 2002].

4.5.3 Melibiose Binding Induces a Slow Local Conformational Change

Stopped-flow measurements with MIANS-labeled E365C revealed that the melibiose-induced conformational change in the presence of Na^+ as determined with the MIANS fluorescence proceeds with a rate constant of ~20 s^{-1} (Figure 3-25). Since the presence of the bound label did not account for the slower kinetics of the conformational change (see above), the result suggests that the process detected by MIANS fluorescence changes does not parallel the charge translocation process and the processes detected by Trp fluorescence. Support for this contention came from the fact that the activation energy for the MIANS fluorescence (around 100 kJ/mole, Q_{10}= 3.9) is significantly different from that of the Trp or electrical data. On the other hand, the Q_{10} is similar to that determined from transport measurements (Q_{10} = 4, [Pourcher *et al.* 1990a]). The conformational change reflected by the electrical and Trp fluorescence measurements can be clearly distinguished from the process detected with the MIANS fluorescence.

It is, thus, tempting to speculate that the process detected with the MIANS label is an electroneutral slow conformational transition ($k \sim 20$ s^{-1}, Figure 4-5) following the fast electrogenic conformational change ($k \sim 50$ s^{-1}, Figure 4-5) respectively the fast conformational change reflected by the Trp fluorescence ($k \sim 65$ s^{-1}, Figure 4-5).

The simplest model for a process with two consecutive steps would be (assuming the steps are irreversible and $k_1 \neq k_2$):

$$A \xrightarrow{\ k_1\ } B \xrightarrow{\ k_2\ } C \ ,$$
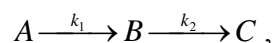
where A is the CNamel carrier, k_1 represents the rate constant of the first and k_2 of the second conformational change. B is a transient intermediate (possibly C'Namel) that appears and then disappears and C the end-product. This is solved by:

$$F(t) = A_0 \left\{ 1 + \frac{1}{k_1 - k_2} * \left(k_2 e^{-k_1(t-t_0)} - k_1 e^{-k_2(t-t_0)} \right) \right\} + Y_0 \ , \qquad \text{[Equation 10]}$$

where F(t) is the product detected with the MIANS fluorescence, A_0 is the amplitude t_0 the time when the reaction recording started (17 ms), k_1 and k_2 the rate constants of the fast and slow conformational change, respectively, t the time, and Y_0 the offset.

The melibiose induced fluorescence signal from the MIANS-labeled protein was fitted with a two-state kinetic model using a k_1 of 65s^{-1} and a k_2 of 20s^{-1}. The inset shows the residual plot indicating that the model fit suits acceptably the recorded fluorescence change. Therefore, it is reasonable to assume that after melibiose binding two different transitions take place. This is in Figure 4-5 schematically represented by an extra step, the C'Namel conformation.

Voltage clamp fluorometry applied to the rat γ–aminobutyric acid transporter rGAT1 revealed also the existence of an additional step during the transition of the transporter from the inside to the outside, which could not be detected with electrophysiological measurements, but with fluorescence studies [Li *et al.* 2000], thus supporting a kinetic model, in which multiple conformational changes occur during the transporter function. Lately, a similar observation was made for hSGLT1 demonstrating different states occurring during the reorientation of the empty carrier from the inward to the outward facing conformation [Loo *et al.* 2005]. It is, thus, reasonable to assume that in co-transporters the reorientation of the carrier from one side of the membrane to the other involves more intermediates than initially deduced from the simple one-step alternate accessible model [Jardettzky 1966]. An oxalate-bound "closed" state, an intermediate between the outwardly and inwardly "open" states, was recently also determined for the oxalate transporter (OxlT) based on the atomic structures of related transporters like LacY [Hirai & Subramaniam 2004].
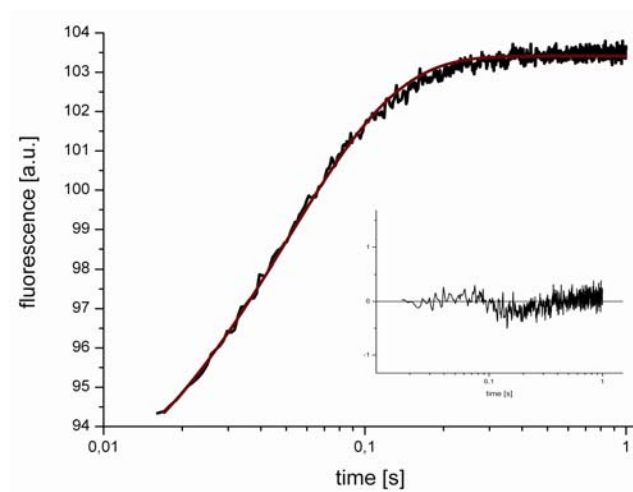
Figure 4-3. MIANS fluorescence signal fitted with a two-step model equation.
The signal was fitted with equation 4.1 using the rate constants $k_1 = 65s^{-1}$ and $k_2 = 20s^{-1}$. The inset shows the residual plot of the fit.

For soluble sugar binding proteins, conformational changes after sugar binding were subdivided into two categories: local changes, affecting only residues in and around the binding site region, and large changes, often requiring relative movements between domains [Quiocho 1986]. This latter motion buries the sugar molecule, and presumably excludes water molecules from the binding site corresponding, thus, probably to the so-called "closed" state as described above for the OxlT. For example, the refined structure of the complex of the arabinose-binding protein with L-arabinose clearly shows an almost enclosed substrate molecule, and the bound sugar cannot leave without a further conformational change [Quiocho 1986]. It is tempting to speculate that the intermediate state (state C'melNa in the model in Figure 4-5) is such a closed-state in MelB.

4.5.4 Loop 10-11 Participates in Substrate Translocation of Na$^+$-Coupled Co-transporters

The high sequence conservation in interhelix loop 10-11 is a feature of members of the GPH family (Figure 4-4 and [Poolman *et al.* 1996]). Glu-365 of MelB is the equivalent of Glu-379 in LacS, a protein of the GPH family sharing around 25% identity with MelB [Poolman *et al.* 1996]. E379A and E379Q mutants of LacS are completely defective in sugar-H$^+$ symport, although some coupled transport can be observed at low pH [Poolman *et al.* 1995]. On the other hand, the LacY is not homologous to members of the GPH family, but part of LacY bears some resemblance to a stretch of about 20 amino acids of the LacS members of the GPH family (sequence motif Lys-x-x-His-x-x-Glu [Poolman *et al.* 1992, Poolman *et al.* 1995]). In MelB$_{EC}$, this sequence motif is slightly modified to Lys-x-His-x-x-x-Glu (Figure 4-4). Whereas within the GPH family this motif is located in loop 10-11, it is found in the middle of helix X of LacY [Calamia & Manoil 1990]. Among the conserved residues are a His (322 in LacY, 376 in LacS, 361 in MelB) and a Glu residue (325 in LacY, 379 in LacS, and 365 in MelB). Whereas none of the histidines in MelB is important for the coupled transport of sugars [Pourcher *et al.* 1990a, Pourcher *et al.* 1992], the H376Q substitution in interhelix loop 10-11 of LacS results in a lowering of the coupling efficiency of the transporter. His-322 of LacY couples together with Glu-269 proton translocation and substrate binding. Substituting Glu-325 of LacY to a neutral amino acids inactivates galactoside-coupled proton translocation [Carrasco *et al.* 1986, Carrasco *et al.* 1989]. Whereas the role of this His varies, the conserved Glu seems to be important for substrate translocation in Na$^+$-coupled transporters of different families.

As inferred from MIANS labeling experiments of the single Cys mutant K373C, local conformational changes upon ligand binding take also place in loop 10-11 of LacS [Knol *et al.* 1999b]. As depicted in Figure 4-4, this residue is homologue to Lys-359 in MelB, a residue that is not essential for MelB functioning [Ding 2003, 2004, Séry 2002], but was not yet investigated with respect to conformational changes.

In this context it is interesting to note that functional re-entrant loop structures, as also loop 10-11 of MelB is one [Ding 2004], have been proposed for both intracellular and extracellular loops in a number of membrane proteins, including loop 10-11 of LacS [Spooner *et al.* 1999, Veenhoff *et al.* 2000], type IIa Na+/Pi co-transporter [Kohler *et al.* 2002, Lambert *et al.* 2001], glutamate transporters[Grunewald & Kanner 2000, Slotboom *et al.* 1999, 2001], SGLT [Lo & Silverman 1998], and human sodium/proton exchanger isoform 1 [Wakabayashi *et al.*

2000]. In aquaporin-1 [Murata *et al.* 2000] and potassium channel [Doyle *et al.* 1998], re-entrant loops were revealed by crystallography. Re-entrant loops in water-filled transport pathways are emerging as a common motif among transport proteins possibly because of their architectural flexibility in comparison with α-helical or β-sheet structures, and by allowing accessibility to backbone chain atoms for substrate or ligand coordination within the hydrophobic transmembrane region [MacKinnon 1995]. Such structure may form the basis for the postulated mechanism of Na$^+$-coupled transport whereby an alternating exposure of the substrate binding site to the periplasmic and cytoplasmic sides of the membrane drives the transport cycle.

```
MelB_Escherichia coli             IMVADIVDYGEYKLHVRCESIAYSVQTMVVKG 378

MelB_Shigella flexneri            IMVADTVDYGEYKLHVRCESIAYSVQTMVVKG 386

MelB_Salmonella typhimurium       IMVADTVDYGEFKLNIRCESIAYSVQTMVVKG 378

MelB_Klebsiella pneumoniae        IMVADTVDYGEYTMNIRCESIAYSVQTLVVKA 378

MelB_Enterobacter aerogenes       IMVADTVDYGEYTMNIRCESIAYSVQTLVVKA 378

MelB_Vibrio vulnificus            VMLADVVDYGEHKTGRRSESVIFSVQTMLVKF 378

GusB_Escherichia coli             ALEADTVEYGEYLTGVRIEGLTYSLFSFTRKC 373

XylP_Lactobacillus pentosus       VMLADSVDYGEWKNGVRAEGIVTSFSSFSAKF 397

LacS_Streptococcus thermophilus   MIISDSVEYGQWKTGHRDESLTLSVRPLIDKL 392

RafP_Pediococcus pentosaceus      MVITDSVEYGQLKLGHRDESLALSVRPLIDKF 394

MelB_Synechocystis sp.            SMIPDVVDLDELNTGKRREGFFYAFMVLLQKV 461

MelB_Fusobacterium nucleatum      AMLSEISTQISEDSGARIEGISFGIQGFFMKT 380


LacY_Escherichia                  FLLVGCFKYITSQFEVRFSATIYLVCFCFFK- 358

PutP_Escherichia                  AFLRKHASQKELVWVGRVMVLVVALVAIALAA 392
```

Figure 4-4. Sequence alignement of loop 10-11 of different members of the GPH transport family and LacY and PutP of the major-facilitator superfamily.

Alignement and labeling are as described for Figure 4-3.

125

4.6   A Mechanism for Substrate Translocation in MelB

The kinetic scheme, which is developed to describe and explain the observed electrical and fluorescence characteristics of the transport cycle, is based on a previously proposed six-state model (Figure 1-9 derived from [Bassilana *et al.* 1987, Damiano-Forano *et al.* 1986, Pourcher *et al.* 1990a]), which is similar to that proposed by Parent to describe the steady and pre-steady state behavior of SGLT [Parent *et al.* 1992a, b]. It is based on a 'single site alternate accessibility' mechanism that requires only a single site for each substrate, which is alternatively made accessible to the cytoplasmic or to the periplasmic side of the membrane. This model essentially agrees with P. Mitchell's concept of a "mobile osmotic barrier" [Mitchell 1990] and has already been used for describing the electrical behavior of GAT1 [Hilgemann & Lu 1999, Lu & Hilgemann 1999] and other transporters (e.g., Na^+-alanine transporter, [Jauch & Lauger 1988], SGLT1 [Loo *et al.* 1993a, Parent *et al.* 1992a, b], EAAC1 [Grewer *et al.* 2001, Watzke *et al.* 2000], and NaPi co-transporter [Forster *et al.* 2002]). Although this model has found support by structure determination of LacY and GlpT [Abramson *et al.* 2003b, Huang *et al.* 2003], recent analysis of OxlT crystals at 6.5 Å by cryo electron microscopy revealed, in addition to the two "open" conformations, a distinct "closed" state, in which the central cavity is tapers to a narrower opening at both periplasmic and cytoplasmic ends [Hirai & Subramaniam 2004]. A similar intermediate or "occluded state" has already been proposed earlier for the Na,K-ATPase [Glynn & Karlish 1990]. The most recent model proposes, therefore, at least three distinct conformations for a symporter: one state opened to the outside, one occluded or closed state, and one opened to the inside. Switches between the three states are proposed to proceed only in the presence or absence of the two substrates [Hirai & Subramaniam 2004]

Detailed characterization of pre-steady state relaxations carried out in this work on the Na^+/melibiose co-transporter allows now to reformulate the initial six-state kinetic model and to assign rate constants to individual reactions in the transport cycle. Furthermore, the knowledge about the orientation of the protein in the liposomal membrane allows the assignment of the electrical and fluorescent signals to reactions occurring after substrate binding at the intracellular side of MelB. Thus, in the extended six-state kinetic model shown in Figure 4-5 the intracellular binding sites (C_{in}) are exposed to the outside of the liposome, and the rate constants determined in this work assigned to intracellular substrate binding and subsequent reactions. The main features of this new model combining the knowledge

obtained from steady (review in [Pourcher *et al.* 1990a]) and pre-steady state ([Ganea *et al.* 2001] and this work) measurements are summarized as follows:

1.) In agreement with an ordered binding model, co-substrate binding to the permease facing the outer medium is sequential (Na^+/H^+ binding first, melibiose last) as proposed on the basis of α-NPG binding studies [Pourcher *et al.* 1990a]. According to a mirror type kinetic model, release of the substrates into the cell is sequential, but occurring in the reverse order (melibiose first, Na^+ last). This has been deduced from sugar exchange experiments where Na^+ is occluded from the melibiose exchange reaction (involved are only steps 5 ↔ 4 ↔ 3 ↔ 2). Electrical [Ganea *et al.* 2001] experiments, recorded on ISO oriented proteoliposomes, showed an allosteric effect of Na^+ on melibiose binding, as the $K_{0.5}^{mel}$ significantly decreased in the presence of Na^+ (20 vs 3 mM, respectively), and vise versa a decrease of $K_{0.5}^{Na}$ in the presence of melibiose (2.1 vs. 0.6 mM, [Ganea *et al.* 2001]). However, these electrical measurements are not enough to distinguish between an ordered or random binding model [Yamato 1992].

2.) MelB can also function in the reverse mode as previously shown by counterflow and exchange experiments. This is now confirmed by electrical measurements on ISO proteoliposomes, as a stationary transport component was detected. Direct evidence for the existence of an inverse transport mode behavior has also been reported using the giant excised patch clamp technique applied to Xenopus oocytes expressing SGLT1 [Sauer *et al.* 2000].

3.) Two transitions are so-called "mobile" forms, i.e., they involve a reorientation of the transporter from the outward to inward facing conformation or vice versa. The empty and the fully loaded carrier are able to re-orient their binding sites to the other side of the membrane (6 ↔ 1 and 3*↔ 4). A Na^+ leak or slippage as reported for other Na^+-dependent co-transporters (see above) has, thus far, not been detected in MelB.

4.) Pre-steady state charge movements are observed in two transitions. First, binding of Na^+ (2' ↔ 2) involves the movement of charge through most of the transmembrane electrical field. In addition, this pre-steady state charge movement can potentially be brought about by a conformational change of a charged empty transporter, or by a conformational change following the Na^+ binding reaction. The pre-steady state current decays with a $\tau_1 \sim 15$ ms ($k > 50 s^{-1}$), and is insensitive to treatment with NEM suggesting that it is not related to MelB turnover. Likewise, binding of Na^+ in the presence of melibiose causes pre-steady-state charge movements ($\tau_1 \sim 15$ ms ($k > 50 s^{-1}$)). This step was suggested to be transition 3' ↔ 3*.

Since a similar time constant after a Na^+ concentration jump was found when MelB was pre-incubated with the fluorescence sugar analog Dns^2-S-Gal ($\tau_1 \sim 18$ ms, $k \sim 55$ s^{-1}), which shows the rate of modification of the sugar binding site after Na^+ binding, it is suggested that the process detected by fluorescence parallels this latter charge translocation process.
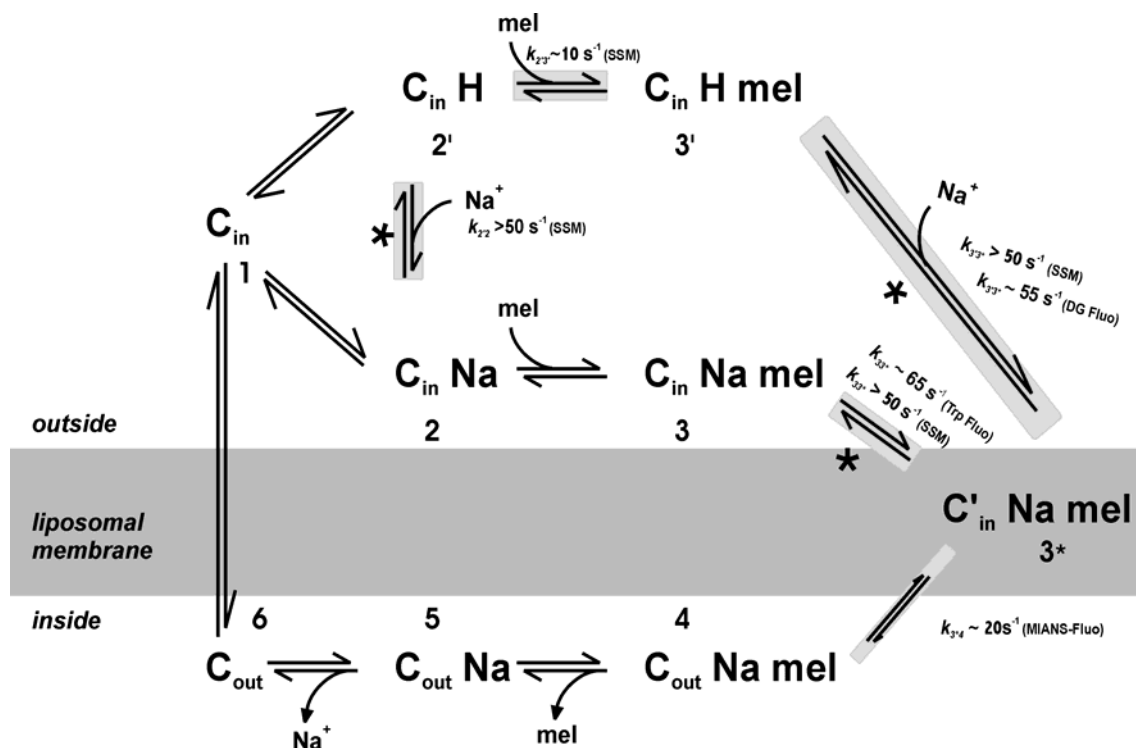

Figure 4.5. Extended 6-state kinetic model for the backward running MelB transporter.

State 1 (C_{in}) corresponds to the empty carrier set with its cytoplasmic binding sites exposed to the solution outside of the proteoliposomes. Na^+ and melibiose binding are sequential, Na^+ being first and melibiose last (states $1 \leftrightarrow 2 \leftrightarrow 3$). Alternatively, Na^+ can be substituted by H^+ (states $1 \leftrightarrow 2' \leftrightarrow 3'$). As suggested, an extra step ($3 \leftrightarrow 3^*$) preceding the general carriers' reorientation ($3^* \leftrightarrow 4$) that accounts for an electrogenic conformational change takes place immediately after melibiose binding [Meyer-Lipp *et al.* 2004]. After release of melibiose ($4 \leftrightarrow 5$) and Na^+ ($5 \leftrightarrow 6$) into the inner liposome compartment, MelB cycling ends by a return of the empty carrier towards the outer surface ($6 \leftrightarrow 1$). The asterisks indicate transitions that were found to be electrogenic [Ganea *et al.* 2001, Meyer-Lipp *et al.* 2004] with their respective rate constants k determined with the SSM method. Transitions found to involve conformational changes are underlined grey. Rate constants determined with fluorescence methods are also assigned to steps in the reaction cycle. Indicated are also the methods with what the rate constants were determined. Fluo: fluorescence; DG: DNs^2-S-Gal fluorescence.

Second, melibiose binding in the presence of Na^+ induces a transient current decaying with a $\tau_1 \sim 20$ ms ($k > 50$ s^{-1}), which was assigned to an electrogenic conformational transition (see above). Stopped-flow measurements revealed a similar time constant for the melibiose induced Trp fluorescence signal (τ_1 ca. 15 ms, $k \sim 65$ s^{-1}) suggesting that the change of the Trp fluorescence signal after melibiose binding reflects the same transition as the electrogenic transient signal. The electrogenic conformational change was suggested to be a separate step ($3 \leftrightarrow 3^*$) following melibiose binding and preceding the general reorientation ($3^* \leftrightarrow 4$). Comparison of the electrical and spectroscopic properties of R141C and E142C with the NEM-inhibited wild-type allows a speculation about this suggestion. Since both mutants and the NEM-inhibited wild-type show the same phenotype, i.e., binding of melibiose is possible but substrate translocation is impaired, one would have expected similar charge translocation and Trp fluorescence properties after melibiose binding. This is, however, not the case, as the mutants show, in contrast to the NEM-inhibited wild-type, neither a significant charge translocation nor a Trp fluorescence change. It is, thus, tempting to speculate that the defects caused by the mutation interrupt the cycle at a different state ($3 \leftrightarrow 3^*$) than when NEM is added to the wild-type ($3^* \leftrightarrow 4$). Recently, different conformational states occurring during the reorientation of the empty carrier from the inward to the outward facing conformation were demonstrated for hSGLT1 by voltage-jump experiments [Loo *et al.* 2005]. It is, thus, reasonable to assume that in co-transporters the reorientation of the carrier from one side of the membrane to the other side involves more intermediates than initially deduced from the simple one-step alternate access model.

5.) Pre-steady-state relaxations were also measured by MIANS fluorescence reflecting essentially a conformational change after melibiose binding ($\tau_1 \sim 43$ ms, $k \sim 23$ s^{-1}). According to the arguments given above, this transition could represent an electro-neutral step following the electrogenic melibiose binding reaction representing probably the reorientation itself ($3^* \leftrightarrow 4$). It is, consequently, proposed that at least one intermediate state, i.e., C'Namel between the two open forms exists in MelB.

6.) Conformational changes proceed at different steps in the transport cycle. The alternating access model predicts conformational changes associated to the return of the empty and the reorientation of the fully loaded carrier. Conformational changes follow also binding of Na^+ to MelB as deduced by proteolysis experiments [Gwizdek *et al.* 1997], quenching of Trp fluorescence [Mus-Veteau *et al.* 1995], affinity increase for melibiose [Ganea *et al.* 2001], modification of the sugar binding site environment [Maehrel *et al.* 1998], and FTIR

spectroscopy [Leon *et al.* 2005]. Once, melibiose is bound to the transporter in the presence of Na^+, a fast conformational change takes place (as deduced from Trp fluorescence and electrical measurements [Dave *et al.* 2002, Meyer-Lipp *et al.* 2004, Mus-Veteau *et al.* 1995] and this thesis) followed by a slow conformational change (represented by the MIANS fluorescence change, see above). Ligand-induced conformational changes have been discussed for many membrane transporters, e.g., the glutamate transporter [Larsson *et al.* 2004], Na,K-ATPase [Geibel *et al.* 2003], and SGLT1 [Veenstra *et al.* 2004]

An alternative to the widely applied model of alternating access is the multi-substrate single-file transport model [Su *et al.* 1996]. In this scheme, substrates are proposed to move through the protein in a single file by hopping between a series of binding sites. Unlike a strict alternating access model, this scheme does not require major conformational changes to effect compartimentalization of substrates. The hopping model can account for some features of transporters, as, e.g., for leakage currents. Simulations showed also that this model can account for the electrogenic properties of the GABA and SGLT co-transporters [Su *et al.* 1996]. Ionic currents detected in the human serotonin transporter revealed also inconsistence with the alternating access model [Adams 2003]. Detailed analysis of GAT1 by Lu and Hilgeman [Hilgemann & Lu 1999, Lu & Hilgemann 1999], revealed, however, that best agreement of the kinetic constants was obtained for the alternating access scheme. It is reasonable to assume that future models may incorporate aspects of both, the alternating access and the hopping models. The data obtained in this study, however, do not favor one of the two models as mechanism for substrate translocation in MelB.

4.7 Perspectives

In summary, the data presented above provide new insights into the structure-function relationship of MelB and the kinetics of intracellular substrate binding and related processes. Especially for the transitions after melibiose binding progress has been made in this work, but several transitions remain kinetically uncharacterized. The application of different electrophysiological techniques, i.e., patch clamp or voltage clamp of cut-open oocytes, or the construction of RSO proteoliposomes would allow the access to the cytoplasmic side of the protein, thus providing necessary information for the kinetic characterization of the remaining steps. Another approach to characterize the RSO fraction of the transporters could be the adsorption of the solubilized protein with the his tag directly to a lipid layer containing Ni^{2+}-lipids, which would favor the right-side-out orientation of the proteins, and to reconstitute the protein directly on the membrane. For all these approaches, different hindrances have to be overcome, e.g., the expression of bacterial proteins in oocytes or the controlled reconstitution of proteins in the RSO orientation is not straightforward. Also, direct reconstitution of proteins on the lipid membrane has never been tried, and the effect of the detergent on the membrane remains unclear. The easiest approach to overcome this problem would be the use of RSO membrane vesicles from *E.coli* directly on the SSM and compare its properties with those from inverted membrane vesicles. Furthermore, it is recommended to apply an assay determining more precisely the orientation of the proteins in the liposomes, i.e., the quantitative assay proposed in the first part of this thesis.

Although the reactions following melibiose binding to the transporter have been investigated in detail, reactions after Na^+ binding have not been fully characterized yet. Interestingly, a strong quenching after Na^+ addition was observed in the ThioGlo3 labeled G117C mutant, which could serve in the future for detailed analysis with the stopped-flow technique. Labeling of the solubilized protein, removal of the unbound bye by dialysis, and subsequent reconstitution could, thereby, help to minimize the high fluorescence background.

Additionally, the introduction of methods that allow resolving faster kinetics would provide new insights into reactions, which were not sufficiently resolved by the SSM. It is, additionally, advisable to improve the time resolution of the SSM system. One interesting step in the direction of measuring fast reactions has been undertaken by measuring fluorescence changes with the stopped-flow technique with a resolution of up to 1 ms. It would be interesting for the future, to analyze R141C and E142C, which are functionally and

electrically well characterized, with the stopped-flow method by adding, e.g., MIANS to the single Cys mutants. Additionally, the double mutant R141Q/E365C could be potentially interesting to investigate, as R141Q has the same defect as R141C [Abdel-Dayem *et al.* 2003], but carries an additional Cys at position 365 for the attachment of MIANS. Finally, the slow component obtained in Trp, Dns²-S-Gal, and MIANS fluorescence stopped-flow experiments could not be assigned to a specific reaction. Probably, the addition of NEM to the wild-type and the recording of the Trp and Dns²-S-Gal signal could help to overcome this problem.

Although simultaneous measurements of electrogenic activity and changes in fluorescence could not be performed, reaction rate constants determined by these two techniques could be correlated. This overcomes two inherent problems with exclusively electrical measurements: first, electroneutral transitions are not directly detected, and second, pre-steady state charge movements are most likely the result of global effects of many charges moving through small fractions of the transmembrane electrical field, while fluorescence techniques can provide insides into local activity of proteins. The combination of these two real-time techniques, therefore, offers considerable potential for correlating charge movement with conformational changes at selected sites within the protein, by discriminating electrogenic from electroneutral conformational changes, and resolving intermediate states that cannot be detected by electrophysiology. In the end it should be mentioned that also resolving the three dimensional structure of MelB is an extremely important task for the future helping to better assign electrical and fluorescence signals to specific parts of the protein.

5. Summaries

5.1 Summary

The melibiose permease (MelB) of *E.coli* functions as a secondary-active symporter by using the electrochemical H^+, Na^+, or Li^+ gradient to accumulate, e.g., melibiose [review in Pourcher *et al.* 1990a]. The global and primary objective of this thesis was to apply pre-steady state methods for the investigation of reaction rates of individual steps in the cycle of MelB. Especially the melibiose binding induced transition was investigated by the solid-supported membrane (SSM) technique [Seifert *et al.* 1993] in combination with a rapid solution exchange system [Pintchovius and Fendler 1999] and with the Stopped-flow technique [Roughton 1934]. To approach this goal, either wild-type or mutated MelB were purified and reconstituted into liposomes as described [Pourcher *et al.* 1995].

Although the orientation of the proteins is a critical factor for the activity of MelB, it was, so far, unknown. To determine the orientation of the proteins in the liposomes, single Cys mutants R139C and R141C [Abdel-Dayem *et al.* 2003] were selectively labeled with 3-(N-maleimidylpropionyl)biocytin (MPB) and analyzed by SDS-PAGE and Western Blot. The assay indicated that most of the proteins are inside-out (ISO) oriented permitting to relate the pre-steady state electrical and fluorescence signals to the reverse transport activity of MelB.

The melibiose induced electrical signal was investigated in wild-type MelB with the SSM technique. The transporter was activated by a substrate concentration jump, and transient currents were measured. When the transporter was preincubated with Na^+ at saturating concentrations, a charge translocation in the protein upon melibiose binding could still be observed. This result demonstrates that binding of the uncharged substrate melibiose triggers a charge displacement in the protein. Further analysis showed that the charge displacement is neither related to extra Na^+ binding to the transporter, nor to the displacement of already bound Na^+ within MelB. Electrogenic melibiose binding is explained by a conformational change with concomitant displacement of charged amino acid side chains and/or a reorientation of helix dipoles. A kinetic model is suggested, in which Na^+ and melibiose binding are distinct electrogenic processes associated with approximately the same charge displacement. Melibiose binding is fast in the presence of Na^+ ($k > 50$ s^{-1}).

Furthermore, two previously identified transport deficient mutants of loop 4-5, R141C and E142C [Abdel-Dayem *et al.* 2002, Séry 2002], were purified and extensively studied with the

SSM. Whereas the electrical signals from control cysteine-less mutant showed a bi-exponential time course of decay, those from R141C or E142C consisted of only a single fast exponential component, and the slow decaying component associated with substrate translocation was missing. The electrical signals evoked by a melibiose concentration jump in the presence of Na^+ were much smaller than the corresponding signals in C-less MelB. Furthermore, R141C lost the stimulating effect of melibiose on Na^+ binding. Steady-state Trp fluorescence spectroscopy revealed impaired conformational changes after melibiose binding in the mutants and fluorescence resonance energy transfer (FRET) measurements indicated that the mutants still show cooperative modification of their sugar binding sites by Na^+. These data suggest that loop 4-5 contributes to the coordinated interactions between the ion- and sugar binding site and participates in conformational changes after melibiose binding that are essential for the subsequent obligatory coupled translocation of substrates.

By using the Stopped-flow technique, three different approaches were followed. First, the intrinsic Trp fluorescence of MelB, known to increase upon melibiose binding [Mus-Veteau et al. 1995], revealed a signal with a τ_1 of ~15 ms in C-less. This time constant is of the same order of magnitude as that determined with the SSM method suggesting that Trp fluorescence and electrical signal are related processes. Conformation for this assumption came from the fact that the activation energies E_a for both processes are similar (around 45 KJ/mol). Second, by using the fluorescent sugar analog Dns^2-S-Gal, which monitors events close to the sugar binding site [Maehrel et al. 1998], a signal with a τ_1 of ~18 ms was recorded upon Na^+ addition. Finally, the fluorescent dye MIANS was used to selectively label the single Cys mutant E365C of loop 10-11. Stopped-flow measurements revealed a melibiose-induced fluorescent signal with a τ_1 of 45 ms. Since electrical measurements with the MIANS-labeled E365C excluded the possibility that the label is responsible for the slower kinetics, the conformational change detected by the MIANS fluorescence was assigned to a slow transition in the cycle of MelB after melibiose binding. E_a was determined to be 96 KJ/mol corroborating, thus, the hypothesis of a different process.

In conclusion, it was possible to correlate the electrical and fluorescence signals to partial reactions of the transport cycle and to determine their rate constants. According to this new model, the melibiose-induced signal detected with the Trp and electrical measurements corresponds to a step preceding the carriers' reorientation ($3 \leftrightarrow 3^*$, $k \sim 65s^{-1}$), and the melibiose-induced signal detected with the MIANS fluorescence to the reorientation itself ($3^* \leftrightarrow 4$, $k \sim 20s^{-1}$).

5.2 Zusammenfassung

Um die Aufnahme und Abgabe von organischen Substraten und Ionen in die Zelle zu ermöglichen, besitzt die Plasmamembran eine Reihe von verschiedenen Transportsystemen. Die Melibiose Permease (MelB) in der zytoplasmatischen Membran von *Escherichia Coli* ist ein solches Transportsystem und gehört zur Familie der Glykosid-Pentosid-Hexuronid-Transporter. MelB besteht aus 473 Aminosäuren und hat ein Molekulargewicht von 53 kDa. Das Protein ist sehr hydrophob (70% apolar) und hat zwölf Transmembrandomänen mit α-helikaler Konformation [Botfield *et al.* 1992, Gwizdek *et al.* 1997, Hacksel *et al.* 2002, Pourcher *et al.* 1990a]. Der Transport verschiedenster Substrate durch biologische Membranen ist an bereits existierende Gradienten anderer Substrate oder Ionen gekoppelt (sekundärer Transport). So nutzt zum Beispiel MelB den durch andere Systeme geschaffenen elektrochemischen Natriumgradienten, um akkumulierend ein Substrat (zum Beispiel α-Galaktoside wie Melibiose oder β-Galaktoside wie Methyl-1-thio-β-D-galaktopyranosid) in die Zelle zu befördern. MelB kann als kotransportierende Ionen neben Natrium auch Lithium und Protonen verwenden [Bassilana *et al.* 1985, Lopilato *et al.* 1978, Pourcher *et al.* 1995, Tsuchiya *et al.* 1978, Tsuchiya *et al.* 1980, Tsuchiya *et al.* 1983, Tsuchiya & Wilson 1978, Wilson & Wilson 1987]. Die Kosubstrate binden an den Transporter mit einer Stoichiometrie von 1:1. Des weiteren erhöht die Bindung des Kations die Affinität des Transporters für den Zucker, wobei Na^+ und Li^+ bessere Aktivatoren als H^+ sind. MelB katalysiert die gekoppelte Translokation von Na^+ (H^+ oder Li^+) und Zuckern ebenfalls mit einer Stoichiometrie von 1:1. Die Substratbindung an der Außenseite und die Substratdissoziation ins Zytoplasma erfolgen geordnet, d. h. Na^+ bindet zuerst gefolgt von Zucker, wohingegen der Zucker zuerst dissoziiert gefolgt von Na^+ [Bassilana *et al.* 1987, Damiano-Forano *et al.* 1986, 1988, Pourcher *et al.* 1990a]. Dabei erhöht das Membranepotential den aktiven Transport, indem es die Rate der Na^+-Dissoziation in das Zytoplasma erhöht. Wenn Melibiose in der Zelle ist, wird es von der α-Galaktosidase in Glukose und Galaktose gespalten, die beide von der Zelle verstoffwechselt werden und der Energieproduktion dienen.

MelB ist ein besonders interessantes Protein für die Untersuchung des Transport-mechanismus, da es verschiedene Zucker und Kationen als Substrate nutzt. Außerdem läßt das Protein sich in großen Mengen herstellen, aufreinigen und in Liposomen rekonstituieren [Pourcher *et al.* 1995]. Die Melibiose Permease besitzt strukturelle und funktionelle Homologie zu anderen Na^+-/Substrat-Kotransportern, die bei biologisch und medizinisch

relevanten Prozessen wichtige Funktionen einnehmen. Trotz ihrer Bedeutung sind die Kenntnisse zur Struktur und Funktionsweise dieser Transportproteine sehr begrenzt und deren Aufklärung bleibt weiterhin eine große Herausforderung. MelB dient dabei als Modell, die zugrundeliegenden molekularen Mechanismen sekundär aktiver Na$^+$-Kotransporter besser zu verstehen. Damit können generelle Prinzipien zur Funktionsweise formuliert werden, die auch auf eukaryotische Transporter angewandt werden können, die bei pathophysiologischen Prozessen eine Rolle spielen.

Bisher wurden hauptsächlich stationäre Messungen durchgeführt, die einen Einblick in den Gesamtreaktionsmechanismus von MelB gegeben haben [Pourcher *et al.* 1990a]. Vor kurzem wurden elektrogene Vorgänge, die durch die Aktivität von MelB verursacht worden sind, zum ersten Mal untersucht [Ganea *et. al.* 2001]. Hierzu wurden Proteoliposomen, die den gereinigten MelB-Transporter enthielten, auf eine festkörperunterstützte Membran (SSM) adsorbiert. Diese Technik ist besonders interessant, da mit Hilfe eines schnellen Lösungs-wechsels Konzentrationssprünge von nahezu jedem beliebigen Substrat an der SSM durchgeführt werden können. Bei dieser ersten Charakterisierung wurde festgestellt, daß die Na$^+$-Bindung an MelB eine Ladungsverschiebung innerhalb des Proteins auslöst, die sich in einer schnell abfallenden Komponente eines transienten Stromsignals widerspiegelt.

Mehrere Zwischenschritte innerhalb des Reaktionszyklus wurden bisher nicht oder nur ungenügend charakterisiert. Deswegen bestand die grundlegende Zielsetzung dieser Arbeit darin, vorstationäre, oder *pre-steady state* Methoden, zur Untersuchung einzusetzen. Diese erlauben es, Reaktionsgeschwindigkeitskonstanten von einzelnen Schritten im Reaktions-zyklus von MelB aufzulösen. Um dieses Ziel zu erreichen, wurden der Wildtyp und verschiedene mutierte Transporter solubilisiert, aufgereinigt und anschließend in Liposomen rekonstituiert, wie es bereits für MelB beschrieben worden ist [Pourcher *et al.* 1995, Rigaud *et al.* 1995]. Die Methode der Aufreinigung und Rekonstitution hat den Vorteil, daß man ohne Wechselwirkung mit anderen zellulären Proteinen die Eigenschaften von MelB untersuchen kann. Die Proteoliposomen wurden in dieser Arbeit hauptsächlich mit der SSM und der Stopped-Flow-Technik untersucht.

Die Orientierung des Transporters in den Liposomen war bisher nicht bekannt. Sie spielt jedoch eine kritische Rolle für seine Aktivität, da die Kinetiken für Substratbindung und Translokation auf beiden Seiten der Membran und damit in beide Transportrichtungen verschieden sind [Pourcher *et al.* 1990a]. Um die Orientierung des Transporters in den Liposomen zu bestimmen, wurden die Mutanten R139C und R141C, die beide auf der Basis

der cysteinlosen Mutante hergestellt worden sind [Abdel-Dayem *et al.* 2003] aufgereinigt und in Liposomen rekonstitutiert. R139C funktioniert ähnlich wie der Wildtyp, wohingegen R141C Substrate binden, aber nicht transportieren kann [Abdel-Dayem *et al.* 2003]. Die Zugänglichkeit der einzelnen Cysteine wurde mit Hilfe von SH-Reagenzien untersucht. Die Proteine wurden mit der SDS-PAGE aufgetrennt und ein Streptavidin-Alkalische-Phosphatase-Konjugat wurde benutzt, um die Markierung mit 3-(N-Maleimidylpropionyl)-biocytin (MPB) zu testen. Stilbene-disulfonat, das nicht durch die Membran dringen kann, wurde dabei benutzt, um die Cysteine, die von außen her zugänglich waren, zu blockieren. Wurde daraufhin das membranundurchlässige MPB dazugegeben und Gefrier-Tau-Beschallzyklen angewandt, so wurden nur diejenigen Cysteine markiert, die nicht durch Stilbene-disulfonat blockiert worden waren, d. h. diejenigen, die dem Inneren der Liposomen zugewandt waren. Unter diesen Bedingungen wurden sowohl R139C als auch R141C fast komplett durch MPB blockiert. Das bedeutet, daß nur eine ganz kleine Anzahl Transporter physiologisch orientiert ist (*right-side out* Orientierung), da beide Mutanten unter nativen Bedingungen dem Zytoplasma zugewandt sind. Im Gegensatz dazu führte die Markierung mit MPB ohne die Vorinkubation mit Stilbene-disulfonat zu sehr starken Signalen, welche die gleiche Intensität aufwiesen wie die Kontrolliposomen, bei denen alle Transporter markiert werden sollten. Der Orientierungs-Test zeigte, daß die meisten Proteine im Liposomen mit der Innenseite nach außen (*inside-out*) orientiert sind. Dieses Resultat ermöglicht, die transienten Signale, die mit elektrischen und Fluoreszenzmethoden generiert wurden, speziell der Rückwärtstranportaktiviät von MelB zuzuordnen.

Weiterhin wurde das elektrische Signal untersucht, das durch die Bindung von Melibiose an MelB in der Gegenwart von Natriumionen ausgelöst wird. Es war von besonderem Interesse zu sehen, daß das neutrale Substrat Melibiose in der Lage ist, ein elektrisches Signal hervorzurufen. Melibiose Konzentrationssprünge führten auch dann noch zu einem schnell abfallenden transienten Signal, wenn der Transporter vorher mit Natriumionen gesättigt wurde. Das Signal wurde also nicht durch eine erhöhte Affinität von MelB gegenüber Natrium in Gegenwart von Zucker und damit durch eine zusätzliche Natriumbindung hervorgerufen. Dieses transiente Signal rührte auch nicht von dem Transportprozeß selbst her, da es immer noch beobachtet wurde, wenn der Transport durch N-Ethylmaleimid (NEM) blockiert worden war. Im Gegensatz dazu war die langsam abfallende Komponente, die auch Transportkomponente genannt wird, unterdrückt. Zusammenfassend zeigen diese Ergebnisse, daß die schnell abfallende Komponente des elektrischen Signals eher mit der Melibiose

Bindung als mit dem Transport der Substrate assoziiert ist. Weiterhin zeigen die Ergebnisse, daß eine zusätzliche elektrogene Natriumbindung in einem folgenden Reaktionszyklus von MelB auch nicht für das Melibiose-induzierte Signal verantwortlich ist. Da das elektrische Signal auch nicht von der Verschiebung von schon gebundenem Natrium (oder Protonen) herrührt, muß es durch eine Konformationsänderung des Proteins verursacht werden, wobei geladene Aminosäuren verschoben werden oder elektrische Dipole sich neu ausrichten. Es wird ein kinetisches Modell vorgeschlagen, bei dem die Na^+- und Melibiosebindung unterschiedliche elektrogene Prozesse sind, die jeweils mit etwa der gleichen Ladungstranslokation einhergehen. Dabei sind die Bindungsreaktionen in Gegenwart des anderen Kosubstrats schnell ($k > 50$ s^{-1}).

Um ein detailliertes Verständnis der molekularen Funktionsweise und der Ladungsverschiebung von MelB zu erhalten, ist es unabdingbar, einzelne Aminosäuren zu identifizieren, die während der Substratbindung oder Translokation eine Rolle spielen. Deswegen wurden zwei Mutanten aus der Schleife 4–5 untersucht, die eine kritische Rolle bei der Substrattranslokation spielen [Abdel-Dayem *et al.* 2002, Séry 2002]. Die beiden Mutanten R141C und E142C basieren auf der cysteinlosen Mutante und wurden in der vorliegenden Arbeit aufgereinigt und umfangreich mit der SSM untersucht. Als Kontrolle diente dabei die cysteinlose Mutante, die ähnlich wie der Wildtyp funktioniert [Weissborn *et al.* 1997]. Während bei der cysteinlosen Mutante Konzentrationssprünge transiente Signale mit einem biexponentiellen Abfall generierten, führten sie bei R141C und E142C zu monoexponentiell abfallenden Signalen. Es war interessant zu sehen, daß ein Melibiose Konzentrationssprung in der Gegenwart von Natrium in den zwei Mutanten sehr viel kleiner ist als das entsprechende Signal in der cysteinlosen Mutante. Das legt die Interpretation nahe, daß R141C und E142 an der elektrogenen Konformationsänderung nach der Melibiose Bindung teilhaben. Tryptophanfluoreszenz-Spektroskopie lieferte weitere Beweise, daß es sich tatsächlich um eine beeinträchtige Konformationsänderung nach der Melibiosebindung handelt. Elektrische Messungen zeigten weiterhin, daß R141C den stimulierenden Effekt, den Melibiose normalerweise auf die Natriumbindung hat, verloren hat. Zusammenfassend läßt sich sagen, daß Schleife 4–5 zu den Interaktionen zwischen der Zucker- und Ionenbindungsstelle beiträgt. Weiterhin nimmt sie an Konformationsänderungen nach der Melibiosebindung teil , die essentiell sind für die gekoppelte Translokation beider Kosubstrate. Der Vergleich von R141C/E142C mit dem Wildtyp, der mit NEM inhibiert worden ist, legt den Schluß nahe, daß die elektrogene Konformationsänderung nach der Melibiosebindung einen zusätzlichen,

bisher nicht detektierten, Schritt darstellt, der vor der generellen Reorientierung des beladenen Transporters stattfindet. Die Analyse von Mutanten kann damit nicht nur dazu beitragen, die Beteiligung einzelner Aminosäuren an Bindungs- und Translokationsreaktionen zu evaluieren, sondern auch das kinetische Modell weiterzuentwickeln.

Die Stopped-Flow-Methode kann die Kinetiken von Konformationsänderungen mit einer Zeitauflösung von 1 ms detektieren, auch wenn diese elektroneutral sind. Sie wurde in dieser Arbeit als zweite Methode angewandt, um die Melibioseinduzierten Reaktionsschritte zu beschreiben. Drei verschiedene Ansätze kamen dabei zum tragen. Zum einen wurde die intrinsische Tryptophanfluoreszenz von MelB genutzt, von der bekannt ist, daß sie ansteigt, wenn Melibiose an den Transporter bindet [Mus-Veteau *et al.* 1995]. Das Signal, gemessen in der cysteinlosen Mutante, hatte eine Zeitkonstante τ_1 von ~ 15 ms. Interessanterweise ist diese Zeitkonstante von der gleichen Größenordnung wie die, die mit der SSM-Methode bestimmt wurde. Dies legt den Schluß nahe, daß die Prozesse, die mit der Tryptophanfluoreszenz und der SSM detektiert werden, miteinander in Verbindung stehen. Eine weitere Bestätigung für diese Behauptung lieferten weitere Messungen, bei denen die Aktivierungsenergie beider Prozesse mit ~ 45 KJ/mol bestimmt wurde. Zweitens wurde das fluoreszente Zuckeranalogon Dns^2-S-Gal für Stopped-Flow-Messungen eingesetzt. Das bei Na$^+$-Zugabe ansteigende Signal konnte mit einer Zeitkonstante τ_1 von ~ 18 ms angepaßt werden. Es ist bekannt, daß Dns^2-S-Gal Ereignisse direkt an oder in der Nähe der Zuckerbindungsstelle detektiert [Maehrel *et al.* 1998]. Drittens wurde der Fluoreszenzfarbstoff MIANS eingesetzt, der erst fluoreszierend wird, wenn er an ein Cystein in hydrophober Umgebung gebunden hat. In der Mutante E365C in Schleife 10–11 wurde dabei gezielt das einzig vorhandene Cystein markiert. E365C funktioniert ähnlich wie der Wildtyp, und elektrische Messungen zeigten, daß MIANS keinen Einfluß auf das elektrische Signal hatte. *Steady-state* Messungen zeigten, daß die Melibiosebindung eine Konformationsänderung induziert, die in der Nähe der intrazellulären Schleife 10-11 stattfindet. Zeitaufgelöste Stopped-Flow-Messungen zeigten im folgenden, daß dieses melibioseinduzierte Signal mit einer Zeitkonstante von ~ 45 ms abklingt. Diese Konformationsänderung konnte einem langsamen Übergang innerhalb des Reaktionszyklus zugeordet werden. Auch die Aktivierungsenergie, die für diesen Prozeß mit 96 KJ/mol bestimmt wurde, unterstützt die Annahme, daß es sich hierbei um einen anderen Prozeß handelt, als der mit Tryptophanfluoreszenz nachgewiesene.

Als Fazit läßt sich festhalten, daß es möglich war, die elektrischen und fluoreszenten Signale einzelnen Reaktionsschritten im Zyklus von MelB zuzuordenen und individuelle Reaktionsgeschwindigkeitskonstanten zu bestimmen (siehe Abbildung). In diesem neuen Modell wurde das melibioseinduzierte Signal, das mit der Tryptophanfluoreszenz und mit der SSM detektiert wurde, einem Schritt zugeordnet, der vor der allgemeinen Reorientierung des Transporters stattfindet ($3 \leftrightarrow 3^*$, $k \sim 65 s^{-1}$). Das melibioseinduzierte Signal hingegen, das mit der MIANS-Fluoreszenz detektiert wurde, ist vermutlich die Reorientierung selbst ($3^* \leftrightarrow 4$, $k \sim 20 s^{-1}$).
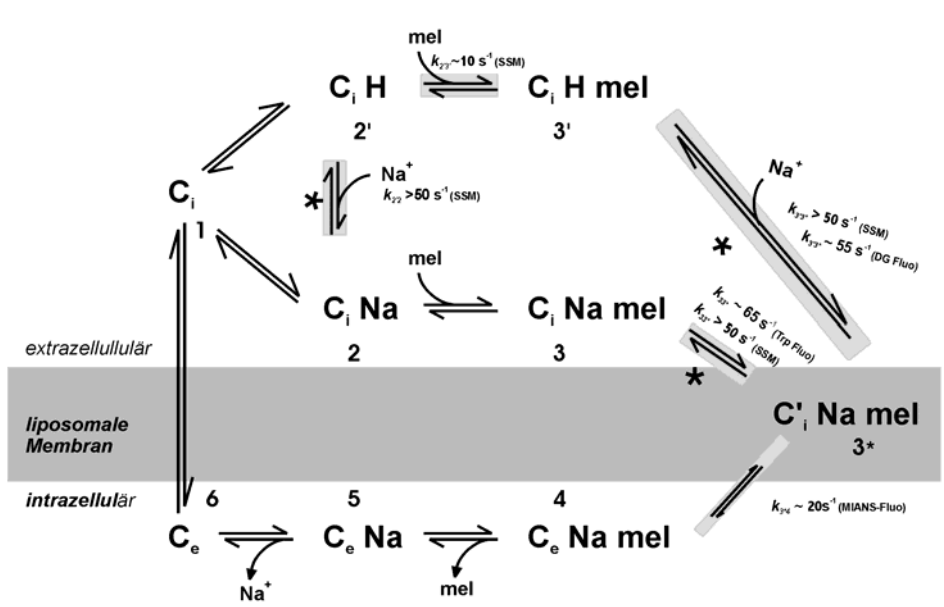

Abbildung. Erweitertes kinetisches Modell für die Melibiose Permease.

Zustand 1 (C_{in}) entspricht dem leeren Transporter, der seine zytoplasmatischen Bindungsseiten zu den Lösungen außen von den Proteoliposomen orientiert hat. Die Na^+- und Melibiosebindung erfolgen geordnet, d.h. Na^+ bindet zuerst und melibiose danach ($1\leftrightarrow2\leftrightarrow3$). Alternativ kann Na^+ durch Protonen substituiert werden (Zustände $1\leftrightarrow2'\leftrightarrow3'$). Es wurde vorgeschlagen [Meyer-Lipp *et al.* 2004] daß ein extra Schritt, der vor der generellen Reorientierung des Transporters stattfindet, der elektrogenen Konformationsänderung entspricht ($3\leftrightarrow3^*$). Danach dissoziiert Melibiose ($4\leftrightarrow5$) und dann Na^+ ($5\leftrightarrow6$) in das Innere liposomale Kompartement. Der Zyklus endet mit der Reorientierung des leeren Transporters nach außen ($6\leftrightarrow1$). Die Sterne zeigen elektrogene Übergänge an und die dazugehörigen Reaktionsgeschwindigkeitskonstanten k [bestimmt mit der SSM, Ganea *et al.* 2001, Meyer-Lipp *et al.* 2004]. Die grau unterlegten Reaktionen deuten Konformationsänderungen an. Geschwindigkeitskonstanten, die mit der Stopped-Flow-Technik bestimmt wurden, sind auch gezeigt. Erwähnt sind ebenfalls die Methoden, mit denen die Reaktionsgeschwindigkeitskonstanten bestimmt worden sind. Fluo: Fluoreszenz; DG: Dns²-S-Gal Fluoreszenz.

5.3 Résumé

Pour fournir l'énergie et les matières premières nécessaires à la machinerie cellulaire, la cellule doit élaborer des stratégies lui permettant d'accumuler certains solutés extracellulaires. La membrane biologique présentant une perméabilité sélective, elle a donc besoin de mécanismes spécifiques pour le passage de ces substances. Les transporteurs représentent un groupe de protéines membranaires responsables de l'accumulation de certains solutés. La mélibiose perméase (MelB) appartenant à la famille des transporteurs cation/glycoside-pentoside-héxuronide [Poolman et al. 1996], est un co-transporteur exprimé au niveau de la membrane interne d'*Escherichia coli*. Ce symporteur est constitué de 473 acides aminés dont 70 % sont apolaires et possède un poids moléculaire apparent de 52 kDa. La protéine possède 12 domaines transmembranaires en hélices-α interrompus par des boucles extracellulaires et intracellulaires [Botfield *et al.* 1992, Gwizdek *et al.* 1997, Hacksell *et al.* 2002, Pourcher *et al.* 1990a]. MelB utilise les ions Na^+, Li^+ ou H^+ pour le transport couplé de sucres (les α-galactosides comme le mélibiose ou les β-galactosides comme méthyl-1-thio-β-D-galactopyranoside). Alors que l'ion est transporté selon son gradient électrochimique, le sucre est accumulé contre son gradient chimique [Bassilana *et al.* 1985, Lopilato *et al.* 1978, Pourcher *et al.* 1995, Tsuchiya *et al.* 1978, 1980, 1983, Tsuchiya & Wilson 1978, Wilson & Wilson 1987]. Les résultats de l'analyse détaillée de MelB suggèrent que les substrats se fixent, et sont transportés, avec un ratio 1:1. De plus, selon le modèle cinétique établit, la fixation d'un substrat du côté externe de la perméase augmenterait son affinité pour l'autre substrat [Bassilana *et al.* 1987, Damiano-Forano *et al.* 1986, Pourcher *et al.* 1990a]. Ce modèle propose également que la fixation des substrats sur le côté externe de la perméase ainsi que la dissociation de ces mêmes co-substrats vers le cytoplasme sont des étapes ordonnées (fixation du côté externe du Na^+ d'abord puis du sucre; dissociation vers le cytoplasme d'abord du sucre puis du Na^+). Le potentiel augment le transport active par l'augmentation de la vitesse de la dissociation de Na^+ vers le cytoplasme. Le mélibiose, une fois dans la cellule, est hydrolysé par l'α-galactosidase en glucose et galactose, qui sont alors utilisés pour fournir de l'énergie.

MelB est une protéine particulièrement intéressante pour l'étude des mécanismes de transport. En effet, tout d'abord parce qu'elle utilise divers cations et sucres comme substrats mais aussi parce que MelB est facilement disponible en grande quantité sous forme purifiée et reconstituée dans des liposomes [Pourcher *et al.* 1995]. La mélibiose perméase partage

plusieurs caractéristiques structurales et fonctionnelles avec des co-transporteurs impliqués dans d'importants processus physiologiques et pathologiques. Même si les systèmes de transports sont très important, la connaissance de son mécanisme de réaction est restreints, et comprendre la relation structure fonction reste importante. L'intérêt de l'étude de MelB est de mieux comprendre son mécanisme de transport et l'acquisition de connaissances aidera alors à formuler des principes généraux applicables aux nombreux transporteurs eucaryotes aux rôles physiologiques importants.

Jusqu'à présent, les propriétés cinétiques de MelB ont principalement été caractérisées par des mesures réalisées à l'état stationnaire (voir pour revue [Pourcher *et al.* 1990a]). Récemment, l'étude de MelB a été effectuée avec de la protéine purifiée et reconstituée dans des liposomes et adsorbés sur un support membranaire solide (SSM) [Ganea *et al.* 2001]. Un système de mélange rapide de solutions est utilisé pour imposer des variations brutales de concentration des substrats à la surface de ces protéoliposomes [Pintchovius & Fendler 1999]. Cette technique est une stratégie utile pour l'analyse des événements électrogeniques survenant, au sein de protéoliposomes contenant MelB purifié, en réponse à des variations de substrats permettant d'établir leur correspondance avec des étapes partielles du cycle de la réaction de co-transport [Ganea *et al.* 2001]. Ainsi, des courants électriques transitoires, correspondant à un mouvement entrant de charges positives, ont été enregistrés lors de l'imposition de variations de concentrations individuelles ou concomitantes des deux substrats. La composante rapide du signal transitoire obtenu reflète la fixation de Na^+ sur MelB [Ganea *et al.* 2001].

Plusieurs étapes intermédiaires du cycle de transport restent quant à elles mal caractérisées. Aussi, le premier objectif de ce travail a été d'appliquer les méthodes de mesure à l'état pré-stationnaire afin de déterminer les constantes de vitesse de réaction de chaque étape du cycle de transport. Dans ce but, MelB sauvage ou muté ont été solubilisé, purifié et reconstitué dans des liposomes [Pourcher *et al.* 1995, Rigaud *et al.* 1995]. Ceci permet d'étudier les propriétés de MelB en s'affranchissant de l'éventuelle interférence d'autres protéines membranaires. Au cours de mon travail de thèse, MelB purifié et reconstitué en protéoliposomes a été analysé principalement par les deux approches que sont la méthode SSM et stopped-flow.

L'orientation que prennent les transporteurs lors de la reconstitution en liposomes était inconnue, or la définition de ce paramètre était importante pour l'étude de l'activité de la protéine. En effet, les cinétiques de fixation et de translocation des substrats diffèrent entre les côtés externe et interne de MelB par rapport à la membrane [Pourcher *et al.* 1990a]. Pour

déterminer l'orientation des protéines MelB dans les protéoliposomes, les mutants R139C et R141C, obtenus par mutagenèse dirigée et réalisés à partir de protéine MelB dépourvue de cystéine (cysteine-less) [Abdel-Dayem *et al.* 2003], ont été purifiés et reconstitués dans des liposomes. Tandis que le mutant R139C possède des propriétés comparables à celle de MelB sauvage, le mutant R141C a perdu toute activité de transport en conservant cependant ses propriétés de fixation des substrats [Abdel-Dayem *et al.* 2003]. L'accessibilité des cystéines introduites a été analysée grâce à l'utilisation de réactifs spécifiques des fonctions -SH. Ainsi, les protéines sont d'abord mis en interaction avec le 3-(N-maleimidylpropionyl)biocytin (MPB), puis séparées en SDS-PAGE et le marquage obtenu est révélé par utilisation d'un second réactif streptavidine conjuguée à de la phosphatase alkaline. Le réactif stilbene disulfonate, qui n'est pas capable de passer la membrane biologique, a été ajouté pour bloquer les cystéines accessibles depuis le milieu extérieur. Le traitement avec le réactif –SH MPB non perméant, et la réalisation de plusieurs cycles de congélation–décongelation suivis de processus de sonication engendrent un marquage uniquement des cystéines qui ne sont pas protégées par le réactif stilbene disulfonate, c'est à dire engendrent le marquage des cystéines présentes uniquement au niveau de la surface interne de MelB. Dans ces conditions, les expériences menées avec les mutants R139C et R141C ont montré que la quasi-totalité du marquage au MPB est bloquée par le traitement au stilbene disulfonate. Ces résultats suggèrent que seule une très faible proportion des protéines possède une orientation correspondant à l'orientation physiologique (right-side out). De plus, les expériences réalisées en absence de stilbene disulfonate ont donné de forts marquages dont l'intensité des signaux est comparable à celle obtenue après application de cycles de congélation-décongélation-sonication. Ce résultat confirme que la plupart des protéines est orientée avec la face cytoplasmique du côté externe (inside-out) du protéoliposome. C'est la raison pour laquelle on peut concerner les signaux pré-stationnaires obtenue avec des méthodes électriques et fluorescent à des transporteurs qui fonctionnent en arrière. Le signal électrique correspondant à l'étape de fixation du mélibiose sur la protéine MelB a déjà été étudié par la méthode de SSM. Les résultats alors obtenus sont particulièrement intéressants car ils ont montré que le processus de fixation d'un substrat non chargé tel que le sucre mélibiose, engendre un signal électrique. En effet, lorsque le transporteur est d'abord pré-incubé avec du Na^+, puis mis en présence de mélibiose, grâce à un changement rapide de solution (ou saut de concentration), cela induit alors un courant transitoire dont le signal correspondant décroît de façon bi-exponentielle (saut dit Δmel(Na)). Il faut noter que la composante rapide de ce signal, correspondant à la fixation du substrat, est observée en présence d'une concentration saturante

de Na$^+$. Ceci exclut donc l'association de ce signal à tout processus de fixation additionnel de Na$^+$. De plus, lorsque le transporteur est pré-incubé avec le réactif N-ethyl-maleimide (NEM), qui bloque la réaction de transport des substrats, un saut Δmel(Na) (à 100 mM de Na$^+$) induit alors un signal transitoire comprenant une composante rapide. Par contre, la composante lente, associée à l'étape de translocation des substrats, est supprimée. Ce résultat montre que le signal électrique rapide peut effectivement être associé à l'étape de fixation du mélibiose et non pas à celle de translocation des substrats. Ce résultat exclut également l'éventuelle contribution de toute fixation additionnelle de sodium lors d'un deuxième cycle de transport. Des expériences supplémentaires ont également suggéré que le signal électrique obtenu n'est pas provoqué par le déplacement d'ion Na$^+$ ou H$^+$ déjà fixé sur MelB, mais plutôt par un changement de conformation de la protéine déplaçant alors des acides aminés chargés ou des dipôles électriques. Un modèle cinétique a donc été proposé, selon lequel les fixations de Na$^+$ et de mélibiose sont des processus électrogéniques distincts associés avec approximative le même quantité de translocation de charge. De plus, en présence des co-substrats, les réactions de fixation des substrats sont rapides ($k > 50$ s^{-1}).

L'analyse de mutants apporterait des informations détaillées concernant la réaction de transport et les mécanismes de translocation de charges survenant au sein de la protéine MelB. Deux acides aminés, R141 et E142, situés dans la boucle 4-5, sont connus pour jouer un rôle crucial dans le processus de translocation des substrats de MelB [Abdel-Dayem *et al.* 2002, Séry 2002]. Les mutants R141C et E142C ont été purifiés, reconstitués en protéoliposomes et extensivement analysés par SSM. Les résultats obtenus avec la protéine contrôle cystéine-less (dont les propriétés sont comparables à celles de la protéine sauvage [Weissborn *et al.* 1997]) montrent des signaux présentant une courbe de décroissance bi-exponentielle. Par contre, les signaux obtenus avec les mutants R141C et E142C ne possèdent qu'une seule composante exponentielle rapide, la composante associée à l'étape de translocation est donc supprimée. De façon intéressante, avec les deux mutants, les signaux électriques obtenus suite à un saut de concentration de mélibiose appliqué en présence de Na$^+$ sont de plus faible amplitude que ceux obtenus avec la protéine cystéine-less. Ceci suggère que les résidus R141 et E142 participent à des changements de conformation électrogéniques qui surviennent après la fixation de mélibiose. La détérioration des changements de conformation survenant après la fixation de mélibiose obtenues pour ces deux mutants a également été observée à l'état stationnaire par spectroscopie de fluorescence des tryptophanes. De plus, des mesures électriques montrent la perte des phénomènes coopératifs

des substrats au sein du mutant R141C. L'ensemble de ces données indique que la boucle 4-5 contribue à la coordination d'interactions entre de site de fixation de l'ion et celui du sucre et participe à un changement de conformation survenant après la fixation du mélibiose, processus essentiel à l'étape successive de translocation obligatoirement couplée des substrats. Enfin, la comparaison des mutants R141C et E142C avec MelB sauvage, dont le transport est inhibé par la NEM, a permis d'attribuer le changement de conformation électrogénique, survenant après fixation du mélibiose, à une étape supplémentaire précédant la ré-orientation du transporteur. Ainsi une analyse par mutagenèse permet non seulement d'élucider l'implication d'acides aminés dans les processus de fixation et/ou translocation des substrats, mais aussi de préciser le modèle cinétique du cycle de transport de MelB.

La technique de stopped-flow permet d'analyser les cinétiques des changements de conformation avec une résolution inférieure à 1 ms. Cette autre méthode a également été utilisée pour l'étude des phases de transitions intervenant lors du processus de transport. Ainsi, trois approches ont été utilisées: Premièrement, l'étude de la fluorescence intrinsèque des tryptophanes de MelB, connue pour être augmentée lors de la fixation du mélibiose [Mus-Veteau *et al.* 1995], révèle un signal avec un temps de relaxation τ_1 d'environ 15 ms (protéine cystéine-less). Cette constante de temps est du même ordre de grandeur que celui déterminé par la méthode de SSM suggérant que la fluorescence des Trp et les signaux électriques sont des processus liés. Un conformation pour cette supposition vient du fait que les énergies d'activation de ces deux processus sont similaires (environ 45 KJ/mol). Deuxièmement, l'utilisation de la sonde de fluorescence analogue du sucre Dns[2]-S-Gal a permis d'enregistrer un signal avec un constant τ_1 d'environ 18 ms suite à l'ajout de Na^+. Le réactif est connu pour refléter les événements survenant à proximité ou au niveau du site de fixation du sucre [Maehrel et al. 1998]. Enfin, le colorant fluorescent MIANS, qui reste principalement non-fluorescent jusqu'à ce qu'il ait réagit avec une cystéine dans un environnement hydrophobes, a été utilisé pour marquer sélectivement l'unique résidu Cys du mutant E365C (mutation située dans la boucle 10-11). Par des mesures d'activité de transport et par des mesures électriques, il a été montré dans cette thèse, que le mutant E365C présente des caractéristiques similaires à celles du sauvage. Des mesures de fluorescence effectuées à l'état stationnaire ont montré que l'intensité de fluorescence augmente lors de la fixation du mélibiose. Ceci indique que les changements de conformation intervenant lors du co-transport de Na^+ et de mélibiose ont lieu à proximité ou au niveau du domaine intracellulaire reliant les hélices 10 et 11. De façon intéressante, les mesures de stopped-flow ont révélé un signal de fluorescence induit par

le mélibiose avec un temps de relaxation τ_1 d'environ 45 ms. Depuis que les mesures électriques effectuées avec le mutant E365C marqué avec le réactif MIANS ont exclu la possibilité que le marquage soit responsable de l'obtention de cinétiques plus lentes, les changements de conformation détectés par la fluorescence du MIANS ont été assignés à une étape lente de transition dans le cycle de transport de MelB survenant après la fixation du mélibiose. Par rapport aux signaux électriques et à la fluorescence des Trp, la valeur d'énergie d'activation de ce processus a été déterminée à 96 KJ/mol ce qui confirme un processus différent.

Pour conclure, les signaux électriques et ceux obtenus en fluorescence peuvent donc être corrélés à des étapes partielles du cycle de transport dont la valeur de constante cinétique peut être déterminée (voir figure ci-dessous). Ainsi, selon ce nouveau modèle, les signaux induits par le mélibiose et détectés par analyse de la fluorescence des Trp et par des mesures électriques correspondent à une étape précédant la ré-orientation du transporteur ($3\rightarrow3^*$, $k \sim 65s^{-1}$) tant dis que le signal induit par le mélibiose et détecté par l'utilisation du réactif MIANS correspond à l'étape de réorientation en elle même ($3^*\rightarrow4$, $k \sim 20s^{-1}$).
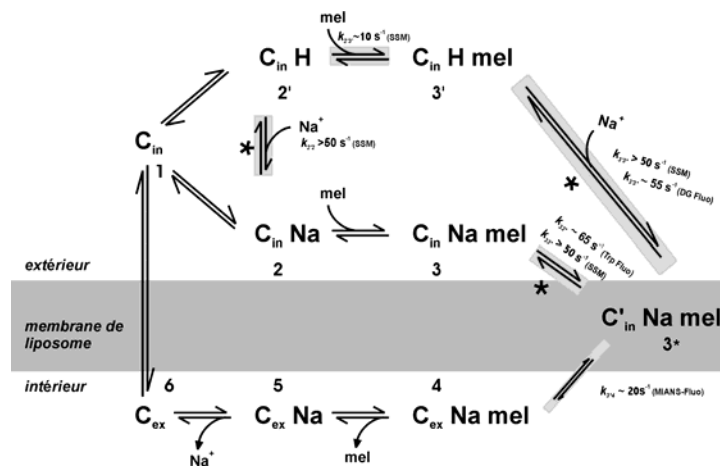
L'état 1 (Cin) correspond au transporteur sans substrats dont les sites de fixation cytoplasmiques sont orientés du côté extérieur des protéoliposomes. Les fixations de Na^+ et de mélibiose ont lieu successivement ($1\leftrightarrow2\leftrightarrow3$). Alternativement, H^+ peut substituer Na^+ (états $1\leftrightarrow2'\leftrightarrow3'$). Il a été suggéré [Meyer-Lipp et al. 2004] qu'une étape additionnelle a lieu avant la ré-orientation générale du transporteur correspondant à un changement conformationel électrogenique ($3\leftrightarrow3^*$). Ensuite, le mélibiose ($4\leftrightarrow5$) puis le Na^+ ($5\leftrightarrow6$) se dissocient vers l'intérieur des liposomes. Le cycle se termine par la ré-orientation du transporteur vers l'extérieur. ($6\leftrightarrow1$). Les étoiles indiquent les transitions électrogeniques et k le constant de vitesse de la réaction (déterminé par SSM [Ganea *et al.* 2001, Meyer Lipp *et al.* 2004]). Les réactions en gris indiquent les changements conformationels et leurs constant de vitesse de réaction déterminé par stopped-flow. Fluo: fluorescence; DG: Dns^2-S-Gal.

146

6 References

Abdel-Dayem M, Basquin C, Pourcher T, Cordat E, and Leblanc G (2003). Cytoplasmic loop connecting helices IV and V of the melibiose permease from *Escherichia coli* is involved in the process of Na$^+$-coupled sugar translocation. *J. Biol. Chem.* **278,** 1518-24.

Abramson J, Smirnova I, Kasho V, Verner G, Iwata S, and Kaback HR (2003a). The lactose permease of *Escherichia coli*: overall structure, the sugar-binding site and the alternating access model for transport. *FEBS Lett.* **555,** 96-101.

Abramson J, Smirnova I, Kasho V, Verner G, Kaback HR, and Iwata S (2003b). Structure and mechanism of the lactose permease of *Escherichia coli*. *Science* **301,** 610-05.

Adams SV and DeFelice LJ (2003). Ionic currents in the human serotonin transporter reveal inconsistencies in the alternating access hypothesis. *Biophys. J.* **85,** 1548-59.

Allen TM, Romans AY, Kercret H, and Segrest JP (1980). Detergent removal during membrane reconstitution. *Biochim. Biophys. Acta* **601,** 328-42.

Ambroise Y, Leblanc G, and Rousseau B (2000). Active-site-directed photolabeling of the melibiose permease of *Escherichia coli*. *Biochemistry* **39,** 1338-45.

Bamberg E, Apell H-J, Dencher NA, Sperling W, Stieve H, and Läuger P (1979). Photocurrents generated by bacteriorhodopsin on planar bilayer membranes. *Biophys. Struct. Mech.* **5,** 277-92.

Bamberg E, Butt HJ, Eisenrauch A, and Fendler K (1993). Charge transport of ion pumps on lipid bilayer membranes. *Q. Rev. Biophys.* **26,** 1-25.

Bamberg E, Clarke RJ, and Fendler K (2001). Electrogenic properties of the Na$^+$,K$^+$-ATPase probed by presteady state and relaxation studies. *J. Bioenerg. Biomembr.* **33,** 401-5.

Bartolommei G, Buoninsegni FT, and Moncelli MR (2004). Calcium transport by sarcoplasmic reticulum Ca-ATPase can be investigated on a solid-supported membrane. *Bioelectrochemistry* **63,** 157-60.

Basquin C (2001). Etude de la contribution relative des domaines intra et extra-membranaires au transport Na$^+$/sucre par la Melibiose Permease d' *Escherichia coli*. DEA. Université de Nice Sophia-Antipolis.

Bassilana M, Damiano-Forano E, and Leblanc G (1985). Effect of membrane potential on the kinetic parameters of the Na$^+$ or H$^+$ melibiose symport in *Escherichia coli* membrane vesicles. *Biochem. Biophys. Res. Commun.* **129,** 626-31.

Bassilana M, Pourcher T, and Leblanc G (1987). Facilitated diffusion properties of melibiose permease in *Escherichia coli* membrane vesicles. Release of co-substrates is rate limiting for permease cycling. *J. Biol. Chem.* **262,** 16865-70.

Bassilana M, Pourcher T, and Leblanc G (1988). Melibiose permease of *Escherichia coli*. Characteristics of co-substrates release during facilitated diffusion reactions. *J. Biol. Chem.* **263,** 9663-7.

Bayer EA, Zalis MG, and Wilchek M (1985). 3-(N-Maleimido-propionyl)biocytin: a versatile thiol-specific biotinylating reagent. *Anal. Biochem.* **149,** 529-36.

Bicho A and Grewer C (2005). Rapid Substrate-Induced Charge Movements of the GABA Transporter GAT1. *Biophys. J.* Epub ahead of print.

Botfield MC (1989). Structure/function correlations of the melibiose carrier of *Escherichia coli*. Thesis, Harvard University.

Botfield MC and Wilson TH (1988). Mutations that simultaneously alter both sugar and cation specificity in the melibiose carrier of *Escherichia coli*. *J. Biol. Chem.* **263,** 12909-15.

Botfield MC and Wilson TH (1989). Peptide-specific antibody for the melibiose carrier of *Escherichia coli* localizes the carboxyl terminus to the cytoplasmic face of the membrane. *J. Biol. Chem.* **264,** 11649-52.

Botfield MC, Naguchi K, Tsuchiya T, and Wilson TH (1992). Membrane topology of the melibiose carrier of *Escherichia coli*. *J. Biol. Chem.* **267,** 1818-22.

Boyer PD (1988). Bioenergetic coupling to protonmotive force: should we be considering hydronium ion coordination and not group protonation? *Trends Biochem. Sci.* **13,** 5-7.

Brandolin G, Doussiere J, Gulik A, Gulik-Krzywicki T, Lauquin GJ, and Vignais PV (1980). Kinetic, binding and ultrastructural properties of the beef heart adenine nucleotide carrier protein after incorporation into phospholipid vesicles. *Biochim. Biophys. Acta* **592,** 592-614.

Brands JF, Herbert R, and Halvorson MB (1975). Consideration of the possibility that the slow step in protein denaturation reactions is due to cis-trans isomerism of proline residues. *Biochemistry* **14,** 4953-63.

Buoninsegni FT, Bartolommei G, Moncelli MR, Inesi G, and Guidelli R (2004). Time-resolved charge translocation by sarcoplasmic reticulum Ca-ATPase measured on a solid supported membrane. *Biophys. J.* **86,** 3671-86.

Burzik C, Kaim G, Dimroth P, Bamberg E, and Fendler K (2003). Charge displacements during ATP-hydrolysis and synthesis of the Na^+-transporting F_0F_1-ATPase of *Ilyobacter tartaricus*. *Biophys. J.* **85,** 2044-54.

Calamia J and Manoil C (1990). lac permease of *Escherichia coli*: topology and sequence elements promoting membrane insertion. *Proc. Natl. Acad. Sci. U. S. A.* **87,** 4937-41.

Carrasco N, Antes LM, Poonian MS, and Kaback HR (1986). lac permease of *Escherichia coli*: histidine-322 and glutamic acid-325 may be components of a charge-relay system. *Biochemistry* **25,** 4486-8.

Carrasco N, Puttner IB, Antes LM, Lee JA, Larigan JD, Lolkema JS, Roepe PD, and Kaback HR (1989). Characterization of site-directed mutants in the lac permease of *Escherichia coli*. 2. Glutamate-325 replacements. *Biochemistry* **28,** 2533-9.

Champeil P, Henao F, and de Foresta B (1997). Dissociation of Ca^{2+} from sarcoplasmic reticulum Ca^{2+}-ATPase and changes in fluorescence of optically selected Trp residues. Effects of KCl and NaCl and implications for substeps in Ca^{2+} dissociation. *Biochemistry* **36,** 12383-93.

Chen XZ, Coady MJ, Jalal F, Wallendorff B, and Lapointe JY (1997). Sodium leak pathway and substrate binding order in the Na^+-glucose cotransporter. *Biophys. J.* **73,** 2503-10.

Chenna R, Sugawara H, Koike T, Lopez R, Gibson TJ, Higgins DG, and Thompson JD (2003). Multiple sequence alignment with the Clustal series of programs. *Nucleic Acids Res.* **31,** 3497-500.

Clarke RJ, Humphrey PA, Lupfert C, Apell HJ, and Cornelius F (2003). Kinetic investigations of the mechanism of the rate-determining step of the Na^+,K^+-ATPase pump cycle. *Ann. N. Y. Acad. Sci.* **986,** 159-62.

Clarke RJ, Kane DJ, Apell HJ, Roudna M, and Bamberg E (1998). Kinetics of Na^+-dependent conformational changes of rabbit kidney Na^+,K^+-ATPase. *Biophys. J.* **75,** 1340-53.

Cohn DE and Kaback HR (1980). Mechanism of the melibiose porter in membrane vesicles of *Escherichia coli*. *Biochemistry* **19,** 4237-43.

Cordat E, Leblanc G, and Mus-Veteau I (2000). Evidence for a role of helix IV in connecting cation- and sugar-binding sites of *Escherichia coli* melibiose permease. *Biochemistry* **39,** 4493-9.

Cordat E, Mus-Veteau I, and Leblanc G (1998). Structural studies of the melibiose permease of *Escherichia coli* by fluorescence resonance energy transfer - II. Identification of the tryptophan residues acting as energy donors. *J. Biol. Chem.* **273,** 33198-202.

Damiano-Forano E, Bassilana M, and Leblanc G (1986). Sugar binding properties of the melibiose permease in *Escherichia coli* membrane vesicles. Effects of Na^+ and H^+ concentrations. *J. Biol. Chem.* **261,** 6893-9.

Dave N, Lorenz-Fonfria VA, Villaverde J, Lemonnier R, Leblanc G, and Padros E (2002). Study of amide-proton exchange of *Escherichia coli* melibiose permease by attenuated total reflection-Fourier transform infrared spectroscopy: evidence of structure modulation by substrate binding. *J. Biol. Chem.* **277,** 3380-7.

Dave N, Troullier A, Mus-Veteau I, Dunach M, Leblanc G, and Padros E (2000). Secondary structure components and properties of the melibiose permease from *Escherichia coli*: A Fourier transform infrared spectroscopy analysis. *Biophys. J.* **79,** 747-55.

Deguchi Y, Yamato I, and Anraku Y (1990). Nucleotide sequence of gltS, the Na^+/glutamate symport carrier gene of *Escherichia coli* B. *J. Biol. Chem.* **265,** 21704-8.

Dempski RE, Friedrich T, and Bamberg E (2005). The β Subunit of the Na$^+$,K$^+$-ATPase Follows the Conformational State of the Holoenzyme. *J. Gen. Physiol.* **125,** 505-20.

Dills SS, Apperson A, Schmidt MR, and Saier MH, Jr. (1980). Carbohydrate transport in bacteria. *Microbiol. Rev.* **44,** 385-418.

Dimroth P (1997). Primary sodium ion translocating enzymes. *Biochim. Biophys. Acta* **1318,** 11-51.

Ding PZ (2003). An investigation of cysteine mutants on the cytoplasmic loop X/XI in the melibiose transporter of *Escherichia coli* by using thiol reagents: implication of structural conservation of charged residues. *Biochem. Biophys. Res. Commun.* **307,** 864-9.

Ding PZ (2004). Loop X/XI, the largest cytoplasmic loop in the membrane-bound melibiose carrier of *Escherichia coli*, is a functional re-entrant loop. *Biochim. Biophys. Acta* **1660,** 106-17.

Ding PZ and Wilson TH (2000a). Physiological evidence for an interaction between helix XI and helices I, II, and V in the melibiose carrier of *Escherichia coli. Biochem. Biophys. Res. Commun.* **268,** 409-13.

Ding PZ and Wilson TH (2000b). The melibiose carrier of *Escherichia coli*: Cysteine substitutions for individual residues in helix XI. *J. Membr. Biol.* **174,** 135-40.

Ding PZ and Wilson TH (2001a). Cysteine mutagenesis of the amino acid residues of transmembrane helix I in the melibiose carrier of *Escherichia coli. Biochemistry* **40,** 5506-10.

Ding PZ and Wilson TH (2001b). The Effect of Modifications of the Charged Residues in the Transmembrane Helices on the Transport Activity of the Melibiose Carrier of *Escherichia coli. Biochem. Biophys. Res. Commun.* **285,** 348-54.

Ding PZ and Wilson TH (2001c). The proximity between helix I and helix XI in the melibiose carrier of *Escherichia coli* as determined by cross-linking. *Biochim. Biophys. Acta* **1514,** 230-8.

Ding PZ, Botfield MC, and Wilson TH (2000). Sugar recognition mutants of the melibiose carrier of *Escherichia coli*: possible structural information concerning the arrangement of membrane-bound helices and sugar/cation recognition site. *Biochim. Biophys. Acta* **1509,** 123-30.

Ding PZ, Weissborn AC, and Wilson TH (2001). Cysteine substitutions for individual residues in helix VI of the melibiose carrier of *Escherichia coli. J. Membr. Biol.* **183,** 33-8.

Doyle DA, Morais Cabral J, Pfuetzner RA, Kuo A, Gulbis JM, Cohen SL, Chait BT, and MacKinnon R (1998). The structure of the potassium channel: molecular basis of K$^+$ conduction and selectivity. *Science* **280,** 69-77.

Eskandari S, Loo DD, Dai G, Levy O, Wright EM, and Carrasco N (1997). Thyroid Na$^+$/I$^-$ symporter. Mechanism, stoichiometry, and specificity. *J. Biol. Chem.* **272,** 27230-8.

Fang G, Friesen R, Lanfermeijer F, Hagting A, Poolman B, and Konings WN (1999). Manipulation of activity and orientation of membrane-reconstituted di-tripeptide transport protein DtpT of *Lactococcus lactis. Mol. Membr. Biol.* **16,** 297-304.

Fendler K, Grell E, and Bamberg E (1987). Kinetics of pump currents generated by the Na$^+$,K$^+$-ATPase. *FEBS Lett.* **224,** 83-8.

Fendler K, Grell E, Haubs M, and Bamberg E (1985). Pump currents generated by the purified Na$^+$,K$^+$-ATPase from kidney on black lipid membranes. *EMBO J.* **4,** 3079-85.

Fendler K, Jaruschewski S, Hobbs A, Albers W, and Froehlich JP (1993). Pre-steady-state charge translocation in NaK-ATPase from eel electric organ. *J. Gen. Physiol.* **102,** 631-66.

Ferguson N and Fersht AR (2003). Early events in protein folding. *Curr. Opin. Struct. Biol.* **13,** 75-81.

Florin EL and Gaub HE (1993). Painted supported lipid membranes. *Biophys. J.* **64,** 375-83.

Forster I, Hernando N, Biber J, and Murer H (1998). The voltage dependence of a cloned mammalian renal type II Na$^+$/Pi cotransporter (NaPi-2). *J. Gen. Physiol.* **112,** 1-18.

Forster IC, Kohler K, Biber J, and Murer H (2002). Forging the link between structure and function of electrogenic cotransporters: the renal type IIa Na$^+$/Pi cotransporter as a case study. *Prog. Biophys. Mol. Biol.* **80,** 69-108.

Franco PJ and Wilson TH (1996). Alteration of Na$^+$-Coupled Transport in Site-Directed Mutants of the Melibiose Carrier of *Escherichia Coli. Biochim. Biophys. Acta* **1282,** 240-8.

Franco PJ and Wilson TH (1999). Arg-52 in the melibiose carrier of *Escherichia coli* is important for cation-coupled sugar transport and participates in an intrahelical salt bridge. *J. Bacteriol.* **181,** 6377-86.

Franco PJ, Jena AB, and Wilson TH (2001). Physiological evidence for an interaction between helices II and XI in the melibiose carrier of *Escherichia coli. Biochim. Biophys. Acta* **1510,** 231-42.

Frankel DG (1987). Glycolysis, Pentose Phosphate Pathway, and Enter-Doudoroff Pathway. In: Neidhardt FC, Ingraham JL, Low JKB, Magasanik B, Schaechter M and Umbarger HE (eds.): *Escherichia Coli* and *Salmonella Typhimurium* - Cellular and Molecular Biology. American Society for Microbiology, Washington, D.C.

Friedrich T, Bamberg E, and Nagel G (1996). Na$^+$,K$^+$-ATPase pump currents in giant excised patches activated by an ATP concentration jump. *Biophys. J.* **71,** 2486-500.

Frillingos S, Gonzalez A, and Kaback HR (1997). Cysteine-scanning mutagenesis of helix IV and the adjoining loops in the lactose permease of *Escherichia coli*: Glu126 and Arg144 are essential off. *Biochemistry* **36,** 14284-90.

Ganea C, Pourcher T, Leblanc G, and Fendler K (2001). Evidence for intraprotein charge transfer during the transport activity of the melibiose permease from *Escherichia coli. Biochemistry* **40,** 13744-52.

Geibel S, Kaplan JH, Bamberg E, and Friedrich T (2003). Conformational dynamics of the Na$^+$/K$^+$-ATPase probed by voltage clamp fluorometry. *Proc. Natl. Acad. Sci. U. S. A.* **100,** 964-9.

Gershoni JM and Palade GE (1982). Electrophoretic transfer of proteins from sodium dodecyl sulfate-polyacrylamide gels to a positively charged membrane filter. *Anal. Biochem.* **124,** 396-405.

Glynn IM and Karlish SJ (1990). Occluded cations in active transport. *Annu. Rev. Biochem.* **59,** 171-205.

Goswitz VC and Brooker RJ (1995). Structural features of the uniporter/symporter/antiporter superfamily. *Protein Sci.* **4,** 534-7.

Grewer C, Madani Mobarekeh SA, Watzke N, Rauen T, and Schaper K (2001). Substrate translocation kinetics of excitatory amino acid carrier 1 probed with laser-pulse photolysis of a new photolabile precursor of D-aspartic acid. *Biochemistry* **40,** 232-40.

Gropp T, Brustovetsky N, Klingenberg M, Muller V, Fendler K, and Bamberg E (1999). Kinetics of electrogenic transport by the ADP/ATP carrier. *Biophys. J.* 77, 714-26.

Grunewald M and Kanner BI (2000). The accessibility of a novel reentrant loop of the glutamate transporter GLT-1 is restricted by its substrate. *J. Biol. Chem.* **275,** 9684-9.

Gwizdek C, Leblanc G, and Bassilana M (1997). Proteolytic Mapping and Substrate Protection of the *Escherichia Coli* Melibiose Permease. *Biochemistry* **36,** 8522-9.

Hacksell I, Rigaud JL, Purhonen P, Pourcher T, Hebert H, and Leblanc G (2002). Projection structure at 8 Å resolution of the melibiose permease, a Na-sugar co-transporter from *Escherichia coli. EMBO J.* **21,** 3569-74.

Hama H and Wilson TH (1992). Primary structure and characteristics of the melibiose carrier of *Klebsiella pneumoniae. J. Biol. Chem.* **267,** 18371-6.

Hama H and Wilson TH (1993). Cation-coupling in chimeric melibiose carriers derived from *Escherichia coli* and *Klebsiella pneumoniae*. The amino-terminal portion is crucial for Na$^+$ recognition in melibiose transport. *J. Biol. Chem.* **268,** 10060-5.

Hama H and Wilson TH (1994). Replacement of alanine 58 by asparagine enables the melibiose carrier of *Klebsiella pneumoniae* to couple sugar transport to Na$^+$. *J. Biol. Chem.* **269,** 1063-7.

Hamill OP, Marty A, Neher E, Sakmann B, and Sigworth FJ (1981). Improved patch-clamp techniques for high-resolution current recording from cells and cell-free membrane patches. *Pflugers Arch.* **391,** 85-100.

Hanatani M, Yazyu H, Shiota-Niiya S, Moriyama Y, Kanazawa H, Futai M, and Tsuchiya T (1984). Physical and genetic characterization of the melibiose operon and identification of the gene products in *Escherichia coli. J. Biol. Chem.* **259,** 1807-12.

Hartung K, Froehlich JP, and Fendler K (1997). Time-resolved charge translocation by the Ca-ATPase from sarcoplasmic reticulum after an ATP concentration jump. *Biophys. J.* **72,** 2503-14.

Hazama A, Loo DD, and Wright EM (1997). Presteady-state currents of the rabbit Na$^+$/glucose cotransporter (SGLT1). *J. Membr. Biol.* **155,** 175-86.

Henderson PJ (1990). Proton-linked sugar transport systems in bacteria. *J. Bioenerg. Biomembr.* **22,** 525-69.

Hertzberg EL and Hinkle PC (1974). Oxidative phosphorylation and proton translocation in membrane vesicles prepared from *Escherichia coli*. *Biochem. Biophys. Res. Commun.* **58,** 178-84.

Heymann JA, Hirai T, Shi D and Subramaniam S (2003). Projection structure of the bacterial oxalate transporter OxlT at 3.4Å resolution. *J. Struct. Biol.* **144,** 320-6.

Heymann JA, Sarker R, Hirai T, Shi D, Milne JL, Maloney PC, and Subramaniam S (2001). Projection structure and molecular architecture of OxlT, a bacterial membrane transporter. *EMBO J.* **20,** 4408-13.

Higuchi R, Krummel B, and Saiki RK (1988). A general method of in vitro preparation and specific mutagenesis of DNA fragments: study of protein and DNA interactions. *Nucleic Acids Res.* **16,** 7351-67.

Hilgemann DW and Lu CC (1999). GAT1 (GABA:Na$^+$:Cl$^-$) cotransport function. Database reconstruction with an alternating access model. *J. Gen. Physiol.* **114,** 459-75.

Hirai T and Subramaniam S (2004). Structure and transport mechanism of the bacterial oxalate transporter OxlT. *Biophys. J.* **87,** 3600-7.

Hirai T, Heymann JA, Shi D, Sarker R, Maloney PC, and Subramaniam S (2002). Three-dimensional structure of a bacterial oxalate transporter. *Nat. Struct. Biol.* **9,** 597-600.

Hiratsuka T (1992). Movement of Cys-697 in myosin ATPase associated with ATP hydrolysis. *J. Biol. Chem.* **267,** 14941-8.

Höfer M (1981). Transport Across Biological Membranes. Pitman Publishing Ltd., Bath.

Hogland RP (2002). Handbook of Fluorescent Probes and Research Products. Eugene, OR.

Honig BH and Hubbell WL (1984). Stability of "salt bridges" in membrane proteins. *Proc. Natl. Acad. Sci. U. S. A.* **81,** 5412-6.

Huang C and Mason JT (1978). Geometric packing constraints in egg phosphatidylcholine vesicles. *Proc. Natl. Acad. Sci. U. S. A.* **75,** 308-10.

Huang Y, Lemieux MJ, Song J, Auer M, and Wang DN (2003). Structure and mechanism of the glycerol-3-phosphate transporter from *Escherichia coli*. *Science* **301,** 616-20.

Huber RE, Lytton J, and Fung EB (1980). Efflux of beta-galactosidase products from *Escherichia coli*. *J. Bacteriol.* **141,** 528-33.

Jardettzky O (1966). Simple allosteric model for membrane pumps. *Nature* **5052,** 969-70.

Jauch P and Lauger P (1986). Electrogenic properties of the sodium-alanine cotransporter in pancreatic acinar cells: II. Comparison with transport models. *J. Membr. Biol.* **94,** 117-27.

Jung H (2001). Towards the molecular mechanism of Na$^+$/solute symport in prokaryotes. *Biochim. Biophys. Acta* **1505,** 131-43.

Jung H, Tebbe S, Schmid R, and Jung K (1998). Unidirectional reconstitution and characterization of purified Na$^+$/proline transporter of *Escherichia coli*. *Biochemistry* **37,** 11083-8.

Kaback HR (1988). Site-directed mutagenesis and ion-gradient driven active transport: on the path of the proton. *Annu. Rev. Physiol.* **50,** 243-56.

Kaback HR (1997). A molecular mechanism for energy coupling in a membrane transport protein, the lactose permease of *Escherichia coli*. *Proc. Natl. Acad. Sci. U. S. A.* **94,** 5539-43.

Kaback HR, Sahin-Toth M, and Weinglass AB (2001). The kamikaze approach to membrane transport. *Nat. Rev. Mol. Cell Biol.* **2,** 610-20.

Kane DJ, Fendler K, Grell E, Bamberg E, Taniguchi K, Froehlich JP, and Clarke RJ (1997). Stopped-flow kinetic investigations of conformational changes of pig kidney Na$^+$,K$^+$-ATPase. *Biochemistry* **36,** 13406-20.

Kawakami T, Akizawa Y, Ishikawa T, Shimamoto T, Tsuda M, and Tsuchiya T (1988). Amino acid substitutions and alteration in cation specificity in the melibiose carrier of *Escherichia coli*. *J. Biol. Chem.* **263,** 14276-80.

REFERENCES

Knol J, Fekkes P, Bron J, and Poolman B (1999a). The Role of Amphiphatic α-Helix-II in Proton Coupled Transport by the Galactoside Transport System of *Streptococcus Thermophilus*. In: Knol J: Membrane Reconstitution and Functional Analysis of a Sugar Transport System. PrintPartners Ipskamp, Enschede, Thesis, Groningen.

Knol J, Friesen RHE, Sjollema K, Klunder B, and Poolman B (1999b). Membrane Reconstitution Mediated by DDM or Triton X-100: Lipid to Protein Ratios. In: Knol J: Membrane Reconstitution and Functional Analysis of a Sugar Transport System. PrintPartners Ipskamp, Enschede, Thesis, Groningen.

Knol J, Sjollema K, and Poolman B (1998). Detergent-mediated reconstitution of membrane proteins. *Biochemistry* **37,** 16410-5.

Knol J, Veenhoff L, Liang WJ, Henderson PJ, Leblanc G, and Poolman B (1996). Unidirectional reconstitution into detergent-destabilized liposomes of the purified lactose transport system of *Streptococcus thermophilus. J. Biol. Chem.* **271,** 15358-66.

Kohler K, Forster IC, Stange G, Biber J, and Murer H (2002). Identification of functionally important sites in the first intracellular loop of the NaPi-IIa cotransporter. *Am. J. Physiol. Renal Physiol.* **282,** F687-96.

Kuroda M, de Waard S, Mizushima K, Tsuda M, Postma P, and Tsuchiya T (1992). Resistance of the melibiose carrier to inhibition by the phosphotransferase system due to substitutions of amino acid residues in the carrier of *Salmonella typhimurium. J. Biol. Chem.* **267,** 18336-41.

Kuroda M, Wilson TH, and Tsuchiya T (2001). Regulation of galactoside transport by the PTS. *J. Mol. Microbiol. Biotechnol.* **3,** 381-4.

Kushner SR (1978). An improved method for transformation of *Escherichia coli* with ColEl-derived plasmids. In: Boyer HW and Nicosia S (eds.): Genetic engineering. Elsevier/North-Holland Publishing Co., Amsterdam.

Laemmli UK (1970). Cleavage of structural proteins during the assembly of the head of bacteriophage T4. *Nature* **227,** 680-5.

Lambert G, Forster IC, Stange G, Kohler K, Biber J, and Murer H (2001). Cysteine mutagenesis reveals novel structure-function features within the predicted third extracellular loop of the type IIa Na^+/P_i cotransporter. *J. Gen. Physiol.* **117,** 533-46.

Langmuir, M. E., Yang, J.-R., Moussa, A. M., Laura, R., and LeCompte, K. A. (1995). New naphthopyranone based fluorescent thiol probes, *Tetrahedron Lett. 36,* 3989-3992.

Larsson HP, Tzingounis AV, Koch HP, and Kavanaugh MP (2004). Fluorometric measurements of conformational changes in glutamate transporters. *Proc. Natl. Acad. Sci. U. S. A.* **101,** 3951-6.

Läuger P (1991). Electrogenic Ion Pumps. Sinauer Associates, Inc., Sunderland, Massachusetts.

Leblanc G, Bassilana M, Pourcher T (1988). Na^+, H^+, or Li^+-coupled melibiose symport in *E.coli*. In: Palmieri F Quagliariello E (eds.): Molecular basis of biomembrane transport. Elsevier Science Publishers B.V., Amsterdam.

Leblanc G, Pourcher T, and Zani ML (1993). The melibiose permease of *Escherichia coli*: importance of the NH_2-terminal domains for cation recognition by the Na^+/sugar cotransporter. *Soc. Gen. Physiol. Ser.* **48,** 213-27.

Leon X, Lorenz-Fonfria VA, Lemonnier R, Leblanc G, and Padros E (2005). Substrate-Induced Conformational Changes of Melibiose Permease from *Escherichia coli* Studied by Infrared Difference Spectroscopy. *Biochemistry* **44,** 3506-14.

Levy D, Gulik A, Bluzat A, and Rigaud JL (1992). Reconstitution of the sarcoplasmic reticulum Ca^{2+}-ATPase: mechanisms of membrane protein insertion into liposomes during reconstitution procedures involving the use of detergents. *Biochim. Biophys. Acta* **1107,** 283-98.

Li M, Farley RA, and Lester HA (2000). An intermediate state of the gamma-aminobutyric acid transporter GAT1 revealed by simultaneous voltage clamp and fluorescence. *J. Gen. Physiol.* **115,** 491-508.

Li M and Lester HA (2002). Early fluorescence signals detect transitions at mammalian serotonin transporters. *Biophys. J.* **83,** 206-18.

Lin ECC (1987). Dissimilatory Pathways for Sugars, Polyols, and Carboxylates. In: Neidhardt FC, Ingraham JL, Low JKB, Magasanik B, Schaechter M and Umbarger HE (eds.): *Escherichia Coli* and *Salmonella Typhimurium*- Cellular and Molecular Biology. American Society for Microbiology, Washington, D.C.

Liu JY, Miller PF, Gosink M, and Olson ER (1999a). The identification of a new family of sugar efflux pumps in *Escherichia coli*. *Mol. Microbiol.* **31,** 1845-51.

Liu JY, Miller PF, Willard J, and Olson ER (1999b). Functional and biochemical characterization of *Escherichia coli* sugar efflux transporters. *J. Biol. Chem.* **274,** 22977-84.

Lo B and Silverman M (1998). Cysteine scanning mutagenesis of the segment between putative transmembrane helices IV and V of the high affinity Na^+/Glucose cotransporter SGLT1. Evidence that this region participates in the Na^+ and voltage dependence of the transporter. *J. Biol. Chem.* **273,** 29341-51.

Loo DD, Hazama A, Supplisson S, Turk E, and Wright EM (1993). Relaxation kinetics of the Na^+/glucose cotransporter. *Proc. Natl. Acad. Sci. U. S. A.* **90,** 5767-71.

Loo DD, Hirayama BA, Cha A, Bezanilla F, and Wright EM (2005). Perturbation analysis of the voltage-sensitive conformational changes of the Na^+/glucose cotransporter. *J. Gen. Physiol.* **125,** 13-36.

Loo TW and Clarke DM (1995). Membrane topology of a cysteine-less mutant of human P-glycoprotein. *J. Biol. Chem.* **270,** 843-8.

Lopilato J, Tsuchiya T, and Wilson TH (1978). Role of Na^+ and Li^+ in thiomethylgalactoside transport by the melibiose transport system of *Escherichia coli*. *J. Bacteriol.* **134,** 147-56.

Lowry OH, Rosebrough NJ, Farr AL, and Randall RJ (1951). Protein measurement with the Folin phenol reagent. *J. Biol. Chem.* **193,** 265-75.

Lu CC and Hilgemann DW (1999). GAT1 (GABA:Na^+:Cl^-) cotransport function. Kinetic studies in giant *Xenopus* oocyte membrane patches. *J. Gen. Physiol.* **114,** 445-57.

MacKinnon R (1995). Pore loops: an emerging theme in ion channel structure. *Neuron* **14,** 889-92.

Maehrel C, Cordat E, Mus-Veteau I, and Leblanc G (1998). Structural studies of the melibiose permease of *Escherichia coli* by fluorescence resonance energy transfer - I. Evidence for ion-induced conformational change. *J. Biol. Chem.* **273,** 33192-7.

Mandel M and Higa A (1970). Calcium-dependent bacteriophage DNA infection. *J. Mol. Biol.* **53,** 159-62.

Mannuzzu LM, Moronne MM, and Isacoff EY (1996). Direct physical measure of conformational rearrangement underlying potassium channel gating. *Science* **271,** 213-6.

Marmé N, Knemeyer JP, Sauer M, and Wolfrum J (2003). Inter- and intramolecular fluorescence quenching of organic dyes by tryptophan. *Bioconjug. Chem.* **14,** 1133-9.

Martin GE, Rutherford NG, Henderson PJ, and Walmsley AR (1995). Kinetics and thermodynamics of the binding of forskolin to the galactose-H^+ transport protein, GalP, of *Escherichia coli*. *Biochem. J.* **308 (Pt 1),** 261-8.

Matsuzaki S, Weissborn AC, Tamai E, Tsuchiya T, and Wilson TH (1999). Melibiose carrier of *Escherichia coli*: use of cysteine mutagenesis to identify the amino acids on the hydrophilic face of transmembrane helix 2. *Biochim. Biophys. Acta* **1420,** 63-72.

Meinild AK, Hirayama BA, Wright EM, and Loo DD (2002). Fluorescence studies of ligand-induced conformational changes of the Na^+/glucose cotransporter. *Biochemistry* **41,** 1250-8.

Meyer-Lipp K, Ganea C, Pourcher T, Leblanc G, and Fendler K (2004). Sugar binding induced charge translocation in the melibiose permease from *Escherichia coli*. *Biochemistry* **43,** 12606-13.

Mitchell P (1961). Coupling of phosphorylation to electron and hydrogen transfer by a chemi-osmotic type of mechanism. *Naturwissenschaften* **191,** 144-8.

Mitchell P (1966). Chemiosmotic coupling in oxidative and photosynthetic phosphorylation. *Biol. Rev. Camb. Philos. Soc.* **41,** 445-502.

Mitchell P (1967). Proton-translocation phosphorylation in mitochondria, chloroplasts and bacteria: natural fuel cells and solar cells. *Fed. Proc.* **26,** 1370-9.

Mitchell P (1990). Osmochemistry of solute translocation. *Res. Microbiol.* **141,** 286-9.

Mitchell P and Moyle J (1967). Chemiosmotic hypothesis of oxidative phosphorylation. *Nature* **213,** 137-9.

Mizushima K, Awakihara S, Kuroda M, Ishikawa T, Tsuda M, and Tsuchiya T (1992). Cloning and sequencing of the melB gene encoding the melibiose permease of *Salmonella typhimurium* LT2. *Mol. Gen. Genet.* **234,** 74-80.

Moniruzzaman M, Lai X, York SW, and Ingram LO (1997). Extracellular melibiose and fructose are intermediates in raffinose catabolism during fermentation to ethanol by engineered enteric bacteria. *J. Bacteriol.* **179,** 1880-6.

Murata K, Mitsuoka K, Hirai T, Walz T, Agre P, Heymann JB, Engel A, and Fujiyoshi Y (2000). Structural determinants of water permeation through aquaporin-1. *Nature* 407, 599-605.

Musafia B, Buchner V, and Arad D (1995). Complex salt bridges in proteins: statistical analysis of structure and function. *J. Mol. Biol.* **254,** 761-70.

Mus-Veteau I and Leblanc G (1996). Melibiose Permease of *Escherichia Coli* - Structural Organization of Cosubstrate Binding Sites as Deduced from Tryptophan Fluorescence Analyses. *Biochemistry* **35,** 12053-60.

Mus-Veteau I, Pourcher T, and Leblanc G (1995). Melibiose permease of *Escherichia coli*: substrate-induced conformational changes monitored by tryptophan fluorescence spectroscopy. *Biochemistry* **34,** 6775-83.

Niiya S, Moriyama Y, Futai M, and Tsuchiya T (1980). Cation coupling to melibiose transport in *Salmonella typhimurium*. *J. Bacteriol.* **144,** 192-9.

Niiya S, Yamasaki K, Wilson TH, and Tsuchiya T (1982). Altered cation coupling to melibiose transport in mutants of *Escherichia coli*. *J. Biol. Chem.* **257,** 8902-6.

Nikaido H and Saier MH, Jr. (1992). Transport proteins in bacteria: common themes in their design. *Science* **258,** 936-42.

Okazaki N, Jue XX, Miyake H, Kuroda M, Shimamoto T, and Tsuchiya T (1997a). A melibiose transporter and an operon containing its gene in *Enterobacter cloacae*. *J. Bacteriol.* **179,** 4443-5.

Okazaki N, Jue XX, Miyake H, Kuroda M, Shimamoto T, and Tsuchiya T (1997b). Sequence of a melibiose transporter gene of *Enterobacter cloacae*. *Biochim. Biophys. Acta* **1354,** 7-12.

Okazaki N, Kuroda M, Shimamoto T, and Tsuchiya T (1997c). Characteristics of the melibiose transporter and its primary structure in *Enterobacter aerogenes*. *Biochim. Biophys. Acta* **1326,** 83-91.

Pardee AB (1957). An inducable mechanism for accumulation of melibiose in *Escherichia coli*. *J. Bacteriol.* **73,** 376-85.

Parent L, Supplisson S, Loo DD, and Wright EM (1992a). Electrogenic properties of the cloned Na^+/glucose cotransporter: I. Voltage-clamp studies. *J. Membr. Biol.* **125,** 49-62.

Parent L, Supplisson S, Loo DD, and Wright EM (1992b). Electrogenic properties of the cloned Na^+/glucose cotransporter: II. A transport model under nonrapid equilibrium conditions. *J. Membr. Biol.* **125,** 63-79.

Paulsen IT. Transport DB. At: http://www.membranetransport.org, access from 03.03.05.

Paulsen IT, Nguyen L, Sliwinski MK, Rabus R, and Saier MH, Jr. (2000). Microbial genome analyses: comparative transport capabilities in eighteen prokaryotes. *J. Membr. Biol.* **301,** 75-100.

Phair RD. Integrative Bioinformatics: Practical Kinetic Modeling of Large Scale Biological Systems. At: http://www.bioinformaticsservices.com/bis/resources/cybertext/IBcont.html, access from: 03.03.05.

Pintschovius J and Fendler K (1999). Charge translocation by the Na^+/K^+-ATPase investigated on solid supported membranes: rapid solution exchange with a new technique. *Biophys. J.* **76,** 814-26.

Pintschovius J, Fendler K, and Bamberg E (1999). Charge translocation by the Na^+/K^+-ATPase investigated on solid supported membranes: cytoplasmic cation binding and release. *Biophys. J.* **76,** 827-36.

Poolman B and Konings WN (1993). Secondary solute transport in bacteria. *Biochim. Biophys. Acta* **1183,** 5-39.

Poolman B, Knol J, van der Does C, Henderson PJ, Liang WJ, Leblanc G, Pourcher T, and Mus-Veteau I (1996). Cation and sugar selectivity determinants in a novel family of transport proteins. *Mol. Microbiol.* **19,** 911-22.

Poolman B, Knol J, Lolkema JS (1995). Kinetic analysis of lactose and proton coupling in Glu379 mutants of the lactose transport protein of *Streptococcus thermophilus. J. Biol. Chem.* **270,** 12995-3003.

Poolman B, Modderman R, and Reizer J (1992). Lactose transport system of *Streptococcus thermophilus.* The role of histidine residues. *J. Biol. Chem.* **267,** 9150-7.

Pourcher T, Bassilana M, Sarkar HK, Kaback HR, and Leblanc G (1990a). The melibiose/Na$^+$ symporter of *Escherichia coli*: kinetic and molecular properties. *Philos. Trans. R. Soc. Lond. B. Biol. Sci.* **326,** 411-23.

Pourcher T, Bassilana M, Sarkar HK, Kaback HR, and Leblanc G (1992). Melibiose permease of *Escherichia coli*: mutation of histidine-94 alters expression and stability rather than catalytic activity. *Biochemistry* **31,** 5225-31.

Pourcher T, Bibi E, Kaback HR, and Leblanc G (1996). Membrane Topology of the Melibiose Permease of *Escherichia Coli* Studied By Melb-Phoa Fusion Analysis. *Biochemistry* **35,** 4161-8.

Pourcher T, Deckert M, Bassilana M. and Leblanc G (1991). Melibiose permease of *Escherichia coli*: mutation of aspartic acid 55 in putative helix II abolishes activation of sugar binding by Na$^+$ ions. *Biochem. Biophys. Res. Commun.* **178,** 1176-81.

Pourcher T, Leclercq S, Brandolin G, and Leblanc G (1995). Melibiose permease of *Escherichia coli*: large scale purification and evidence that H$^+$, Na$^+$, and Li$^+$ sugar symport is catalyzed by a single polypeptide. *Biochemistry* **34,** 4412-20.

Pourcher T, Sarkar HK, Bassilana M, Kaback HR, and Leblanc G (1990b). Histidine-94 is the only important histidine residue in the melibiose permease of *Escherichia coli. Proc. Natl. Acad. Sci. U. S. A.* **87,** 468-72.

Pourcher T, Zani ML, and Leblanc G (1993). Mutagenesis of acidic residues in putative membrane-spanning segments of the melibiose permease of *Escherichia coli*. I. Effect on Na$^+$-dependent transport and binding properties. *J. Biol. Chem.* **268,** 3209-15.

Postma PW, Lengeler JW, and Jacobson GR (1993). Phosphoenolpyruvate:carbohydrate phosphotransferase systems of bacteria. *Microbiol. Rev.* **57,** 543-94.

Prestidge LS and Pardee AB (1965). A second permease for methyl-thio-β-D-galactoside in *Escherichia coli. Biochim. Biophys. Acta* **100,** 591 - 3.

Quick M and Jung H (1998). A conserved aspartate residue, Asp187, is important for Na$^+$-dependent proline binding and transport by the Na$^+$/proline transporter of *Escherichia coli. Biochemistry* **37,** 13800-6.

Quiocho FA (1986). Carbohydrate-binding proteins: tertiary structures and protein-sugar interactions. *Annu. Rev. Biochem.* **55,** 287-315.

Quiocho FA (1988). Molecular features and basic understanding of protein-carbohydrate interactions: the arabinose-binding protein-sugar complex. *Curr. Top. Microbiol. Immunol.* **139,** 135-48.

Reenstra WW, Patel L, Rottenberg H, and Kaback HR (1980). Electrochemical proton gradient in inverted membrane vesicles from *Escherichia coli. Biochemistry* **19,** 1-9.

Reinders A and Ward JM (2001). Functional characterization of the alpha-glucoside transporter Sut1p from *Schizosaccharomyces pombe*, the first fungal homologue of plant sucrose transporters. *Mol. Microbiol.* **39,** 445-54.

Reizer J, Reizer A, and Saier MH, Jr. (1994). A functional superfamily of sodium/solute symporters. *Biochim. Biophys. Acta* **1197,** 133-66.

Richard P, Rigaud JL, and Graber P (1990). Reconstitution of F$_0$F$_1$ into liposomes using a new reconstitution procedure. *Eur. J. Biochem.* **193,** 921-5.

Rigaud JL, Paternostre MT, and Bluzat A (1988). Mechanisms of membrane protein insertion into liposomes during reconstitution procedures involving the use of detergents. 2. Incorporation of the light-driven proton pump bacteriorhodopsin. *Biochemistry* **27,** 2677-88.

Rigaud JL, Pitard B, and Levy D (1995). Reconstitution of membrane proteins into liposomes: application to energy-transducing membrane proteins. *Biochim. Biophys. Acta* **1231,** 223-46.

Roughton FJW (1934). The Kinetics of Haemoglobin IV - The Competition of Carbon Monoxide and Oxygen for Haemoglobin. *Proc. R. Soc. London, B* **115,** 473-6.

REFERENCES

Saier MH, Jr. (1989). Protein phosphorylation and allosteric control of inducer exclusion and catabolite repression by the bacterial phosphoenolpyruvate: sugar phosphotransferase system. *Microbiol. Rev.* **53,** 109-20.

Saier MH, Jr. (2000a). A functional-phylogenetic classification system for transmembrane solute transporters. *Microbiol. Mol. Biol. Rev.* **64,** 354-411.

Saier MH, Jr. (2000b). Families of transmembrane sugar transport proteins. *Mol. Microbiol.* **35,** 699-710.

Saier MH, Jr., Novotny MJ, Comeau-Fuhrman D, Osumi T, and Desai JD (1983). Cooperative binding of the sugar substrates and allosteric regulatory protein (enzyme IIIGlc of the phosphotransferase system) to the lactose and melibiose permeases in *Escherichia coli* and *Salmonella typhimurium*. *J. Bacteriol.* **155,** 1351-7.

Saier MH, Jr., Beatty JT, Goffeau A, Harley KT, Heijne WH, Huang SC, Jack DL, Jahn PS, Lew K, Liu J, Pao SS, Paulsen IT, Tseng TT, and Virk PS (1999). The major facilitator superfamily. *J. Mol. Microbiol. Biotechnol.* 1, 257-79.

Sanger F and Coulson AR (1978). The use of thin acrylamide gels for DNA sequencing. *FEBS Lett.* **87,** 107-10.

Sanger F, Nicklen S, and Coulson AR (1977). DNA sequencing with chain-terminating inhibitors. *Proc. Natl. Acad. Sci. U. S. A.* **74,** 5463-7.

Sauer GA, Nagel G, Koepsell H, Bamberg E, and Hartung K (2000). Voltage and substrate dependence of the inverse transport mode of the rabbit Na$^+$/glucose cotransporter (SGLT1). *FEBS Lett.* **469,** 98-100.

Seal RP, Leighton BH, and Amara SG (1998). Transmembrane topology mapping using biotin-containing sulfhydryl reagents. *Methods Enzymol.* **296,** 318-31.

Seifert K, Fendler K, and Bamberg E (1993). Charge transport by ion translocating membrane proteins on solid supported membranes. *Biophys. J.* **64,** 384-91.

Séry N (2002). Roles fonctionnelles des boucles cytoplasmique d'un co-transporteur Na+/sucre d'*Escherichia coli*, la mélibiose perméase. DEA, Université de Nice-Sophia Antipolis.

Shimamoto T, Xu XJ, Okazaki N, Kawakami H, and Tsuchiya T (2001). A cryptic melibiose transporter gene possessing a frameshift from *Citrobacter freundii*. *J. Biochem. (Tokyo).* **129,** 607-13.

Slotboom DJ, Sobczak I, Konings WN, and Lolkema JS (1999). A conserved serine-rich stretch in the glutamate transporter family forms a substrate-sensitive reentrant loop. *Proc. Natl. Acad. Sci. U. S. A.* **96,** 14282-7.

Slotboom DJ, Konings WN, and Lolkema JS (2001). The structure of glutamate transporters shows channel-like features. *FEBS Lett.* **492,** 183-6.

Spooner PJ, Veenhoff LM, Watts A, and Poolman B (1999). Structural information on a membrane transport protein from nuclear magnetic resonance spectroscopy using sequence-selective nitroxide labeling. *Biochemistry* **38,** 9634-9.

Stengelin M, Fendler K, and Bamberg E (1993). Kinetics of transient pump currents generated by the (H,K)-ATPase after an ATP concentration jump. *J. Membr. Biol.* **132,** 211-27.

Stock J and Roseman S (1971). A sodium-dependent sugar co-transport system in bacteria. *Biochem. Biophys. Res. Commun.* **44,** 132-8.

Su A, Mager S, Mayo SL, and Lester HA (1996). A multi-substrate single-file model for ion-coupled transporters. *Biophys. J.* **70,** 762-77.

Tadini-Buoninsegni F, Nassi P, Nediani C, Dolfi A, and Guidelli R (2003). Investigation of Na$^+$,K$^+$-ATPase on a solid supported membrane: the role of acylphosphatase on the ion transport mechanism. *Biochim. Biophys. Acta* **1611,** 70-80.

Tanaka K, Niiya S, and Tsuchiya T (1980). Melibiose transport of *Escherichia coli*. *J. Bacteriol.* **141,** 1031-6.

Tokuda H and Kaback HR (1977). Sodium-dependent methyl 1-thio-beta-D-galactopyranoside transport in membrane vesicles isolated from *Salmonella typhimurium*. *Biochemistry* **16,** 2130-6.

Tokuda H and Kaback HR (1978). Sodium-dependent binding of p-nitrophenyl alpha-D-galactopyranoside to membrane vesicles isolated from *Salmonella typhimurium*. *Biochemistry* **17,** 698-705.

Towbin H, Staehelin T, and Gordon J (1979). Electrophoretic transfer of proteins from polyacrylamide gels to nitrocellulose sheets: procedure and some applications. *Proc. Natl. Acad. Sci. U. S. A.* **76,** 4350-4.

Tsuchiya T and Wilson TH (1978). Cation-sugar cotransport in the melibiose transport system of *Escherichia coli*. *Membr. Biochem.* **2,** 63-79.

Tsuchiya T, Lopilato J, and Wilson TH (1978). Effect of lithium ion on melibiose transport in *Escherichia coli*. *J. Membr. Biol.* **42,** 45-59.

Tsuchiya T, Oho M, and Shiota-Niiya S (1983). Lithium ion-sugar cotransport via the melibiose transport system in *Escherichia coli*. Measurement of Li^+ transport and specificity. *J. Biol. Chem.* **258,** 12765-7.

Tsuchiya T, Raven J, and Wilson TH (1977). Co-transport of Na^+ and methyl-beta-D-thiogalactopyranoside mediated by the melibiose transport system of *Escherichia coli*. *Biochem. Biophys. Res. Commun.* **76,** 26-31.

Tsuchiya T, Takeda K, and Wilson TH (1980). H^+ -substrate cotransport by the melibiose membrane carrier in *Escherichia coli*. *Membr. Biochem.* **3,** 131-46.

Veenhoff LM, Heuberger EH, and Poolman B (2001). The lactose transport protein is a cooperative dimer with two sugar translocation pathways. *EMBO J.* **20,** 3056-62.

Veenstra M, Lanza S, Hirayama BA, Turk E, and Wright EM (2004). Local conformational changes in the Vibrio Na^+/galactose cotransporter. *Biochemistry* **43,** 3620-7.

Wadiche JI, Arriza JL, Amara SG, and Kavanaugh MP (1995). Kinetics of a human glutamate transporter. *Neuron* **14,** 1019-27.

Wakabayashi S, Pang T, Su X, and Shigekawa M (2000). A novel topology model of the human Na^+/H^+ exchanger isoform 1. *J. Biol. Chem.* **275,** 7942-9.

Wallin E and von Heijne G (1998). Genome-wide analysis of integral membrane proteins from eubacterial, archaean, and eukaryotic organisms. *Protein Sci.* **7,** 1029-38.

Walmsley AR, Martin GE, McDonald TP, and Henderson PJ (1994). The pre-steady-state kinetics of conformational changes in sugar transporters. *Biochem. Soc. Trans.* **22,** 650-4.

Wang YF, Dutzler R, Rizkallah PJ, Rosenbusch JP, and Schirmer T (1997). Channel specificity: structural basis for sugar discrimination and differential flux rates in maltoporin. *J. Mol. Biol.* **272,** 56-63.

Watzke N, Bamberg E, and Grewer C (2001). Early intermediates in the transport cycle of the neuronal excitatory amino acid carrier EAAC1. *J. Gen. Physiol.* **117,** 547-62.

Watzke N, Rauen T, Bamberg E, and Grewer C (2000). On the mechanism of proton transport by the neuronal excitatory amino acid carrier 1. *J. Gen. Physiol.* **116,** 609-22.

Webster C, Gardner L, and Busby S (1989). The *Escherichia coli* melR gene encodes a DNA-binding protein with affinity for specific sequences located in the melibiose-operon regulatory region. *Gene* **83,** 207-13.

Webster C, Gaston K, and Busby S (1988). Transcription from the *Escherichia coli* melR promoter is dependent on the cyclic AMP receptor protein. *Gene* **68,** 297-305.

Webster C, Kempsell K, Booth I, and Busby S (1987). Organisation of the regulatory region of the *Escherichia coli* melibiose operon. *Gene* **59,** 253-63.

Weissborn AC, Botfield MC, Kuroda M, Tsuchiya T, and Wilson TH (1997). The Construction of a Cysteine-Less Melibiose Carrier from E-Coli. *Biochim. Biophys. Acta* **1329,** 237-44.

West IC and Mitchell P (1974). Proton/sodium ion antiport in *Escherichia coli*. *Biochem. J.* **144,** 87-90.

Wilson DM and Wilson TH (1987). Cation specificity for sugar substrates of the melibiose carrier in *Escherichia coli*. *Biochim. Biophys. Acta* **904,** 191-200.

Wilson DM and Wilson TH (1992). Asp-51 and Asp-120 are important for the transport function of the *Escherichia coli* melibiose carrier. *J. Bacteriol.* **174,** 3083-6.

Wilson DM and Wilson TH (1994). Transport properties of Asp-51→Glu and Asp-120→Glu mutants of the melibiose carrier of *Escherichia coli*. *Biochim. Biophys. Acta* **1190,** 225-30.

Wilson TH and Wilson DM (1998). Evidence for a Close Association between Helix Iv and Helix Xi in the Melibiose Carrier of *Escherichia Coli*. *Biochim. Biophys. Acta* **1374,** 77-82.

REFERENCES

Wilson DM, Hama H, and Wilson TH (1995). Gly113→Asp Can Restore Activity to the Asp51→Ser Mutant in the Melibiose Carrier of *Escherichia Coli*. *Biochem. Biophys. Res. Commun.* **209,** 242-9.

Wilson DM, Tsuchiya T, and Wilson TH (1986). Methods for the study of the melibiose carrier of *Escherichia coli*. *Methods Enzymol.* **125,** 377-87.

Yamato I and Anraku Y (1993). Na$^+$/substrate symport in prokaryotes. In: Bakker EP (ed.): Alkali cation transport systems in prokaryotes. CRC Press, Boca Raton.

Yan RT and Maloney PC (1995). Residues in the pathway through a membrane transporter. *Proc. Natl. Acad. Sci. U. S. A.* **92,** 5973-6.

Yazyu H, Shiota S, Futai M, and Tsuchiya T (1985). Alteration in cation specificity of the melibiose transport carrier of *Escherichia coli* due to replacement of proline 122 with serine. *J. Bacteriol.* **162,** 933-7.

Yazyu H, Shiota-Niiya S, Shimamoto T, Kanazawa H, Futai M, and Tsuchiya T (1984). Nucleotide sequence of the melB gene and characteristics of deduced amino acid sequence of the melibiose carrier in *Escherichia coli*. *J. Biol. Chem.* **259,** 4320-6.

Zani ML, Pourcher T, and Leblanc G (1993). Mutagenesis of acidic residues in putative membrane-spanning segments of the melibiose permease of *Escherichia coli*. II. Effect on cationic selectivity and coupling properties. *J. Biol. Chem.* **268,** 3216-21.

Zani ML, Pourcher T, and Leblanc G (1994). Mutation of polar and charged residues in the hydrophobic NH$_2$-terminal domains of the melibiose permease of *Escherichia coli*. *J. Biol. Chem.* **269,** 24883-9.

Zeng H, Parthasarathy R, Rampal AL, and Jung CY (1996). Proposed structure of putative glucose channel in GLUT 1 facilitative glucose transporter. *Biophys. J.* **70,** 14-21.

Zhou A, Wozniak A, Meyer-Lipp K, Nietschke M, Jung H, and Fendler K (2004). Charge Translocation During Cosubstrate Binding in the Na$^+$/Proline Transporter of *E.coli*. *J. Mol. Biol.* **343,** 931-42.

Acknowledgements

List of Publications

Meyer K, Rosa C, Hischenhuber C, Meyer R (2001): Determination of Locust Bean Gum and Guar Gum by Polymerase Chain Reaction and Restriction Fragment Length Polymorphism Analysis. *Journal of AOAC International* **84**, 89-99.

Meyer-Lipp K, Ganea C, Pourcher T, Leblanc G, Fendler K (2004): Sugar binding induced charge translocation in the melibiose permease from *Escherichia coli. Biochemistry* **43**, 12606-12613.

Zhou A, Wozniak A, **Meyer-Lipp K**, Nietschke M, Jung H, Fendler K (2004): Charge translocation during cosubstrate binding in the Na$^+$/proline transporter of *E.coli*. *Journal of Molecular Biology* **343**, 931-942.

Curriculum Vitae

PERSONAL DETAILS

Dipl. oec. troph. Kerstin Meyer-Lipp

Tulpenweg 1

61231 Bad Nauheim, Germany

Date of birth: 15.02.1974 in Hamburg

Married, 1 child (Jonas, 30.12.02)

UNIVERSITY STUDIES

since 02/01	PhD in Biochemistry ("Cotutelle de thèse"):
	Max-Planck Institute of Biophysics, Frankfurt, Germany (Advisors: Prof. Dr. Ernst Bamberg, Prof. Dr. Klaus Fendler)
	Université de Nice Sophia-Antipolis, Nice, France (Advisor: Dr. Gérard Leblanc)
11/02 - 09/03	Maternity leave

10/94 - 04/00	Diploma degree in Nutritional Sciences and Home Economics
	Justus-Liebig University (JLU), Giessen, Germany
10/95 - 01/00	Additional examination in Quality Management, JLU, Giessen, Germany
04/97 - 02/00	Additional examination in Educational Sciences, JLU, Giessen, Germany
03/99 - 08/99	Diploma thesis, Nestlé Research Centre, Vers-chez-les-Blanc, Switzerland
	"Authenticity Assessment of Locus Bean Gum and Guar Gum Using Polymerase Chain Reaction and Restriction Fragment Length Polymorphism" (Advisors: Dr. Rolf Meyer and Prof. Dr. Birgit Arnholdt-Schmitt)

APPRENTICESHIPS

08/90 - 01/94	Apprenticeship as chemical-technical assistant, Hamburg, Germany
09/91 - 10/93	Apprenticeship as church musician (D and C), Hannover, Germany

SCHOOL

1984- 1993	Friedrich-Ebert-Gymnasium, Hamburg, Germany
1980 - 1984	Elementary school, Am Falkenberg, Hamburg

SCHOLARSHIPS

10/01 - 12/01	Boehringer Ingelheim Fonds
09/02 - 10/02	German Academic Exchange Service (DAAD)